Characterising heterogeneous TRAIL responsiveness and overcoming TRAIL resistance in multicellular tumour spheroids

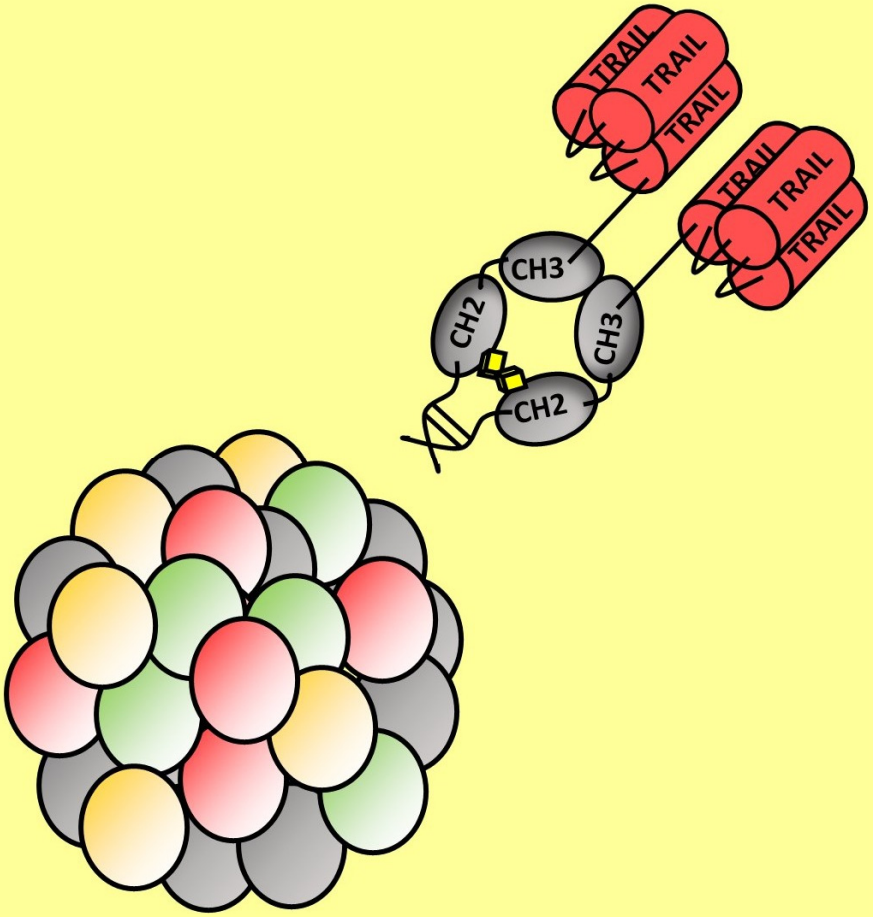

Dissertation

Daniela Stöhr

-2018-

Characterising heterogeneous TRAIL responsiveness and overcoming TRAIL resistance in multicellular tumour spheroids

Von der Fakultät Energie-, Verfahrens- und Biotechnik der Universität Stuttgart
sowie dem Stuttgart Research Centre for Simulation Technology
zur Erlangung der Würde eines
Doktors der Naturwissenschaften (Dr. rer. nat.) genehmigte Abhandlung

Vorgelegt von

Daniela Stöhr

aus Winnenden

Hauptberichter: Prof. Dr. Peter Scheurich
Mitberichter: Prof. Dr. Markus Morrison
Mitberichter: Prof. Dr. Nicole Radde

Tag der mündlichen Prüfung: 22.10.2018

Institut für Zellbiologie und Immunologie der Universität Stuttgart

2018

"*Research is formalized curiosity.*

It is poking and prying with a purpose."

Zora Neale Hurston

Diese Arbeit widme ich meinem Vater Harald Stöhr,
der es geschafft hat nicht nur in mir die Liebe zur Biologie wachsen zu lassen,
sondern auch nie müde wurde in anderen Neugier und Faszination zu wecken,
und so unser aller Leben zu bereichern.

Table of contents

Abbreviations

AA	arachidonic acid
ADP	adenosine diphosphate
AP1	activator protein 1
Apaf-1	protease activating factor-1
ATF3	cyclic AMP (adenosine monophosphate)-dependent transcription factor 3
Atg5	autophagy related 5
ATP	adenosine triphosphate
AU	arbitrary units
BAD	Bcl-2 antagonist of cell death
Bak	Bcl-2 antagonist or killer
Bax	Bcl-2 associated X protein
Bcl-2	B cell lymphoma-2
Bcl-xl	Bcl-extra large
BH3	Bcl-2 homology 3
Bid	Bcl2-homology (BH3)-only protein
Bim	Bcl-2-interacting mediator of cell death
BIP	chaperon binding immunoglobulin protein
BIR	baculovirus IAP repeat
BLAST	basic local alignment search tool
BSA	bovine serum albumin
CAD	caspase-activated DNase
cAMP	cyclic adenosine monophosphate
CARD	caspase activation and recruitment domain
Caspase	aspartate-specific cysteine protease
CD44	cluster of differentiation 44
CDI	coefficient of drug interaction
CDK	cyclin-dependent kinase
cDNA	complementary DNA
cFlip	cellular FLICE-like inhibitory protein
cFlip-L	cFlip-long
cFlip-R	cFLip-Raji
cFlip-S	cFLip-short

CH	constant domain of the heavy chain
CHOP	C/EBP homologous protein
cIAP-1	cellular IAP-1
cIAP-2	cellular IAP-2
COX	cyclooxygenase
COX I	cyclooxygenase I
COX II	cyclooxygenase II
CRD	cysteine rich domain
CRISPR/Cas9	clustered regularly interspaced short palindromic repeats/CRISPR associated 9
Ctrl	control
CYP1B1	monooxygenase cytochrome P450 1B1
DAMPs	damage-associated molecular patterns
DAPI	4',6-diamidin-2-phenylindol
dATP	deoxyadenosine triphosphate
Db	diabody
DD	death domain
ddH_20	bidistilled water
DED	death effector domain
DISC	death inducing signalling complex
DMSO	dimethyl sulfoxide
DNA	deoxyribonucleic acid
DNMT-1	DNA methyltransferase-1
DTT	dithiothreitol
EBP	enhancer binding protein
EC_{50}	half-maximal effective concentration
ECM	extracellular matrix
EDTA	ethylenediaminetetraacetic acid
e.g.	*exempli gratia* (for example)
EGFP	enhanced green fluorescent protein
EGFR	epidermal growth factor receptor
eIF2α	eukaryotic translation initiation factor 2α
Elk1	ETS (E26 transformation-specific)-like transcription factor 1
EMT	epithelial to mesenchymal transition
EP1	prostaglandin E_1 receptor

ER	endoplasmic reticulum
ERAD	ER associated degradation
ERK	extracellular-signal regulated kinase
et al.	*et alii* (and others)
Eq.	equation
FADD	Fas-associated protein with death domain
FasL	Fas ligand
Fc	fragment crystallizable
FCS	fetal calf serum
FISH	fluorescence *in situ* hybridisation
FITC	fluorescein isothiocyanate
FLAG-tag	DYKDDDDK-tag
FLICE	FADD-like interleukin-1β-converting enzyme
FOXO3a	forkhead-box-protein O3a
Fv	single-chain fragment variable
GAPDH	glycerinaldeyd-3-phosphat-dehydrogenase
GPI	glycosylphosphatidylinositol
Hif-1α	hypoxia-inducible factor-1α
His	hexahistidine
HRP	horse radish peroxidase
Hsp	heat shock protein
HuR	Hu antigen R
IAP	inhibitor of apoptosis
IHC	immunohistochemistry
Ig	immunoglobulin
IRE1α	inositol-requiring protein 1α
IZI	Institute of Cell Biology and Immunology
JAK	Janus kinase
JNK	c-Jun N-terminal kinase
kDa	kilo Dalton
KO	knockout
LC3-I	microtubule-associated protein light chain 3-I
LC3-II	microtubule-associated protein light chain 3-II
LUBAC	linear ubiquitin chain assembly complex
MAPK	mitogen-activated protein kinase

Mcl-1	myeloid cell leukemia-1
MCTS	multicellular tumour spheroid
miRNA	micro RNA
MLKL	mixed lineage kinase domain like pseudokinase
MOMP	mitochondrial outer membrane permeabilisation
mRNA	messenger RNA
NEMO	NF-κB essential modulator
NF-κB	nuclear factor 'kappa-light-chain-enhancer' of activated B-cells
NK	natural killer
NOD	nucleotide-binding oligomerisation domain
NSAID	non-steroidal anti-inflammatory drug
NSCLC	non-small-cell lung cancer
OPG	Osteoprotegerin
PAGE	polyacrylamide gel electrophoresis
PARP	poly (ADP-ribose) polymerase
PARP13	poly (ADP-ribose) polymerase 13
PBA	PBS containing BSA and sodium azide
PBS	phosphate buffered saline
PERK	protein kinase RNA-like endoplasmic reticulum kinase
PFA	paraformaldehyde
PGD_2	prostaglandin D_2
PGE_2	prostaglandin E_2
PGF_{2a}	prostaglandin F_{2a}
PGG_2	prostaglandin G_2
PGH_2	prostaglandin H_2
PGI_2	prostaglandin I_2
PI3K	phosphatidylinositol-4,5-bisphosphate 3-kinase
PIK3CA	phosphatidylinositol-4,5-bisphosphate 3-kinase, catalytic subunit α
PLAD	pre-ligand binding assembly domain
PP1	protein phosphatase 1
pRb	phosphorylated Rb
PS	Phosphatidylserine
Puma	p53 upregulated modulator of apoptosis
pVHL	Hippel-Lindau tumour suppressor

qPCR	quantitative polymerase chain reaction
QVD	Q-VD-OPh
RANKL	receptor activator of NF-κB ligand
Rb	retinoblastoma protein
RIDD	IRE1α-dependent decay of mRNAs
RING	really interesting new gene
RIPA	radioimmunoprecipitation assay
RIPK1	receptor-interacting serine/threonine protein kinase 1
RIPK3	receptor-interacting serine/threonine protein kinase 3
RNA	ribonucleic acid
RPMI	Roswell Park Memorial Institute
RSK	ribosomal protein S6 kinase
RT	room temperature
scFv	single-chain fragment variable
scTRAIL	single-chain TRAIL
SD	standard deviation
SDS	sodium deoxycholate
SEM	standard error of the mean
SERCA	sarco/endoplasmic reticulum Ca^{2+} APTase
sKO	surface knockout
SMAC	second mitochondria-derived activator of caspases
SP1	specificity protein 1
STAT3	signal transducer and activator of transcription 3
TALEN	transcription activator-like effector nuclease
TAPE	region rich in threonine, alanine, proline and glutamine
tBid	truncated Bid
TBS	tris buffered saline
TBST	TBS with Tween-20
THD	TNF homology domain
TK1	thymidine kinase 1
TNF	tumour necrosis factor
TNFR1	TNF receptor 1
TRAF2	TNF receptor-associated factor 2
TRAIL	TNF-related apoptosis inducing ligand
TRAILR1; T1	TRAIL receptor 1

TRAILR2; T2	TRAIL receptor 2
TRAILR2-L	TRAILR2-long
TRAILR2-S	TRAILR2-short
TRAILR3; T3	TRAIL receptor 3
TRAILR4; T4	TRAIL receptor 4
Tris	Tris-(hydroxymethyl)-aminomethane
TxA_2	thromboxane A_2
UBA	ubiquitin-associated
UPR	unfolded protein response
ut ctrl	untreated control
UTR	untranslated region
v/v	volume/volume
VEGF	vascular endothelial growth factor
V_H	variable domain of the heavy chain
V_L	variable domain of the light chain
w/v	weight/volume
WT	Wildtype
XBP-1	X box-binding protein-1
XIAP	X-linked inhibitor of apoptosis protein
YY1	Yin Yang 1

Abstract

The cytokine tumour necrosis factor (TNF)-related apoptosis-inducing ligand (TRAIL) is a member of the large TNF superfamily that can trigger apoptosis in transformed or infected cells by binding and activating two receptors, TRAIL receptor 1 (TRAILR1) and TRAIL receptor 2 (TRAILR2). Compared to other death ligands of the same family, TRAIL exclusively induces apoptosis in malignant cells while sparing normal tissue and has been therefore extensively investigated for its suitability as an anti-cancer agent, however, to date with only limited success. Alongside insufficient activity of generated TRAILR agonists, this failure can also be attributed to many tumour types being inherently TRAIL-resistant. Thereby, it was shown that resistance is not only mediated by pro-tumourigenic mutations but that at the same time also adverse conditions such as hypoxia and nutrient starvation, typically occurring in poorly vascularised tumours, can change protein expression and affect the cell cycle status of single cells thus rendering them TRAIL-resistant.

To investigate the underlying mechanisms in more detail, multicellular tumour spheroids (MCTSs) were utilised in this study as they better resemble the architecture of poorly-vascularised solid tumours and micrometastases in the human body than cultivating cancer cells in standard 2D cultures. Similar to the zonation in a tumour, MCTSs comprise not only of proliferative but, due to undersupply with nutrients and oxygen, also quiescent and dead cells. By stimulating the MCTSs, generated from genetically identical cancer cells, with improved 2nd generation TRAILR agonists it was shown that a layer of TRAIL-resistant cells surrounded and thus protected highly TRAIL-sensitive cells further inside from TRAIL-induced apoptosis, resulting in an overall increased treatment resistance. Interestingly, this heterogenous TRAIL sensitivity of MCTS-forming cells could be attributed to localisation-dependent TRAILR1/R2 expression within MCTSs. It was found that solely proliferative cells expressed high amounts of TRAILR1 whereas in quiescent cells the expression of the receptor was only weak or completely absent. Furthermore, cells with strong expression of TRAILR2 were, similar to TRAILR1, found at the spheroid surface but additionally in a layer close to the necrotic core. Notably, in quiescent cells a large amount of TRAILR2 was localised intracellularly. After knockout of TRAILR2 in spheroid-forming cells, the highly sensitive phenotype disappeared, indicating that large amounts of intracellular TRAILR2 sensitised quiescent cells close to the necrotic core to TRAIL-induced apoptosis by a so far unknown mechanism. The observed localisation-dependent TRAILR1/R2 expression within MCTSs was found to be most likely a consequence of hypoxia and nutrient deprivation experienced within MCTSs, as recreating such conditions in 2D-cultured cells was shown to

influence the amounts of TRAILR1 and TRAILR2. More precisely, oxygen and glucose withdrawal both increased the expression of TRAILR2, while hypoxia reduced the amounts of TRAILR1 in the investigated cells. In the last part of this thesis, attempts were made to restore TRAILR expression in intermediate TRAIL-resistant layers of MCTSs to enhance the overall treatment response. Thereby, it was found that stimulation with inhibitors of the enzyme cyclooxygenase II sensitised MCTSs to TRAIL-induced apoptosis, most likely by upregulating TRAILR2 expression. In conclusion, this study provides new insights into TRAILR expression regulation in solid tumours and the consequent emergence of a novel mechanism of TRAIL resistance. Furthermore, overcoming the observed protection of TRAIL-sensitive cells by a barrier of TRAIL-resistant cells, was shown to be a potential beneficial strategy in improving TRAIL efficacy for the treatment of solid tumours and micrometastases.

Zusammenfassung

Das Zytokin Tumornekrosefaktor-verwandter Apoptose-induzierender Ligand (*tumor necrosis factor-related apoptosis-inducing ligand*, TRAIL) gehört zur großen TNF Superfamilie und kann durch Aktivierung zweier Rezeptoren, TRAIL Rezeptor 1 (TRAILR1) und TRAIL Rezeptor 2 (TRAILR2), Apoptose in transformierten und infizierten Zellen auslösen. Im Vergleich zu anderen Todesliganden dieser Familie führt TRAIL nur in verändertem, jedoch nicht in gesundem, Gewebe zum Zelltod und wurde aus diesem Grund bereits ausführlich hinsichtlich seiner Tauglichkeit in der Tumortherapie untersucht. Ergebnisse dieser Studien waren bisher jedoch ernüchternd, da eine solche Behandlung nur in Einzelfällen eine vorteilhafte Wirkung zeigte. Dies ist, neben einer unzureichenden Bioaktivität der hergestellten TRAILR Agonisten, vor allem auf eine initiale Resistenz der Krebszellen gegenüber TRAIL zurückzuführen. Jene Resistenz ist hierbei nicht nur das Ergebnis tumorfördernder Mutationen, sondern kann auch durch Nährstoff- und Sauerstoffmangel in schlecht durchbluteten Tumorregionen ausgelöst werden. Solche Bedingungen reduzieren die TRAIL Sensitivität der Krebszellen nicht durch Modifizierung der DNA, sondern durch Veränderung der Proteinexpression und des Zellzyklusstatus.

Um die zugrundeliegenden Mechanismen besser zu verstehen, wurden in dieser Arbeit so genannte multizelluläre Tumorsphäroide (*multicellular tumour spheroids,* MCTSe) als *in vitro* Modell für solide Tumore und Mikrometastasen verwendet. Durch ihre Zusammensetzung aus proliferierenden und, durch Nährstoff-/Sauerstoffmangel, quieszenten bzw. nekrotischen Zellen ähneln diese Zellaggregate mehr der Architektur eines schlecht durchbluteten Tumors als normale 2D Zellkulturen. In Versuchen mit verbesserten TRAILR Agonisten stellte sich heraus, dass eine TRAIL-resistente Zellschicht, TRAIL-sensitive Zellen im Inneren der Sphäroide umschloss, was zu einer insgesamt verstärkten TRAIL Resistenz der MCTSe führte. Interessanterweise konnte diese heterogene TRAIL Sensitivität auf eine lokalisationsbedingte Expression der TRAIL Rezeptoren zurückgeführt werden. Tatsächlich exprimierten innerhalb der MCTSe ausschließlich proliferierende Zellen an der Sphäroid-Oberfläche große Mengen an TRAILR1, während in quieszenten Zellen nur niedrige Level dieses Rezeptors nachweisbar waren. Des Weiteren wurde TRAILR2 nicht nur vermehrt in äußeren Zellschichten gefunden, sondern auch in Regionen nahe dem nekrotischen Kern, wobei in diesen quieszenten Zellen der Hauptteil des Rezeptors nicht an der Zelloberfläche, sondern innerhalb der Zelle lokalisiert war. Es kann davon ausgegangen werden, dass eine große Menge an intrazellulärem TRAILR2 die Sensitivität von Zellen im Inneren der MCTSe durch einen bisher unbekannten Mechanismus gegenüber TRAIL erhöht, da nach einem Knockout dieses Rezeptors die zuvor beschriebene, stark TRAIL-sensitive Zellpopulation nicht

mehr vorhanden war. Darüber hinaus deuten Ergebnisse an, dass die lokalisationsbedingte, erhöhte TRAILR Expression durch Unterversorgung der Zellen mit Sauerstoff und Nährstoffen zustande kam, da eine Nachbildung dieser Konditionen mit 2D kultivierten Zellen die Expression der beiden Rezeptoren stark beeinflusste. Während Sauerstoffentzug zu einer Reduktion der TRAILR1 Menge führte, induzierten Sauerstsoff- sowie Glucosemangel die vermehrte Expression von TRAILR2. Im letzten Teil dieser Arbeit wurden Anstrengungen unternommen die TRAILR Expression in den mittleren Schichten der Sphäroide wiederherzustellen und damit die gesamte Sensitivität der MCTSe gegenüber TRAIL zu erhöhen. Es konnte gezeigt werden, dass eine Behandlung der Sphäroide mit Inhibitoren des Enzyms Cyclooxygenase II zu einer verstärkten TRAILR2 Expression führte, die zeitgleich mit einer Erhöhung der TRAIL Sensitivität einherging. Zusammenfassend lässt sich sagen, dass durch diese Arbeit neue Einsichten in die Regulationsmechanismen der TRAILR Expression und die damit verbundene TRAIL Resistenz solider Tumore gewonnen werden konnten. Mit der Sensitivierung der Sphäroid-bildenden Zellen durch Cyclooxygenase II Inhibitoren konnte des Weiteren ein Weg aufgezeigt werden, die Effektivität von TRAIL als Medikament in der Behandlung solider Tumore zu erhöhen.

1 Introduction

1.1 Multicellular tumour spheroids

In 1953, HeLa, the first human cancer cell line was derived from a patient with cervical cancer and used in *in vitro* experiments. Since then, countless studies have been conducted with further cancer cell lines grown in monolayer cultures at the bottom of cell culture flasks (2D *in vitro* cell culture). However, even though 2D cell culture is a cheaper and more ethical alternative to animal experiments it is not very close to the *in vivo* situation which often makes a translation of obtained results to clinical settings difficult. For example, it was shown that in some cases radiotherapy or certain anti-cancer agents were more efficient on 2D-cultivated cells than *in vivo* (Kaaijk et al., 1997; Martin and McNally, 1980; reviewed by Santini and Rainaldi, 1999). Reasons for the observed discrepancies between the outcome of *in vitro* and *in vivo* studies can be manifold. Firstly, cells growing on artificial surfaces, do not adopt the same shape as they would display in a tumour, resulting in an altered cytoskeleton and nuclear structure which are known to influence gene expression and protein synthesis (Thomas et al., 2002; Vergani et al., 2004). Furthermore, the 3D architecture of a solid tumour increases cell-to-cell contact and communication between single cells, which were shown to influence their susceptibility towards anti-cancer agents as well as their capacity to migrate and metastasise (reviewed by Brücher and Jamall, 2014). A further difference between 2D cell culture and cancer cells within a tumour is the fact that malignant cells *in vitro* are in contact with surrounding immune cells, fibroblast, endothelial cells and the extracellular matrix. Interestingly, this was not only demonstrated to influence their potential to undergo epithelial to mesenchymal transition (EMT) but to modulate also the cells' sensitivity to anti-cancer agents (reviewed by Thoma et al., 2014). Lastly, cells within fast-growing, solid tumours are often undersupplied with oxygen and nutrients due to insufficient neovascularisation. As a consequence, such tumours are comprised of quiescent and proliferative cells that differ in their protein expression resulting in heterogenous susceptibility to anti-cancer agents. Of note, 2D-cultured cells turned out to be more susceptible to radiotherapy than tumours due to the fact that hypoxic cells are resistant to such treatment (reviewed by Horsman and Overgaard, 2016; reviewed by Rey et al., 2017). Taken together, since 2D cell culture differs in so many aspects from a tumour, it could be suggested that only animal models should be used in cancer research. However, alongside being cost-intensive and ethical questionable, it was described 2014 by Mak and colleagues that only very view findings obtained from animal experiments are later translated into successful clinical phase I studies (Mak et al., 2014). The reasons for this are most likely the

genetic, physiological and immunological differences between animals and humans, as well as wrong model choices (reviewed by Schuh, 2004).

In 1971, in an attempt to close the gap between 2D cell culture and actual cancerous diseases, Sutherland and colleagues grew Chinese hamster V79 lung cells in small aggregates, called multicellular tumour spheroids (MCTSs), for the first time (Sutherland and Mccredie, 1971). Since then, more than 380 cell lines were cultivated in 3D, which was shown to better resemble gene expression profiles of tumours tissue than 2D cultivation (reviewed by Verjans et al., 2017). Indeed, it was furthermore demonstrated in many experiments that assays based on MCTSs could better predict treatment efficacy of anti-cancer agents *in vivo* than experiments performed with 2D-cultivated cells (reviewed by Mehta et al., 2012). The reasons for the observed improved predictive power of MCTSs are firstly, that similar to a tumour, a zonation of necrotic, quiescent and proliferative cells develops in spheroids from a diameter of in average 500 µm, due to insufficient supply of nutrients and oxygen as wells accumulation of waste products such as lactate that changes the pH (reviewed by Verjans et al., 2017) (Figure 1). Furthermore, drug penetration in tumours is also better reflected in MCTSs, due to enhanced cell-to cell contact as well as heterogenous consumption of the compound by spheroid-forming cells. Of note, in order to simulate communication of tumour cells with associated cell types such as immune cells, stromal fibroblasts or endothelial cells, it is also possible to, in case of fibroblasts, co culture them as mixed MCTSs, or to grow the spheroids in the same well together with immune cells and/or an endothelial cell layer (reviewed by Friedrich, Ebner and Kunz-Schughart, 2007; reviewed by Knight and Przyborski, 2015; reviewed by Verjans et al., 2017). Methods to generate MCTSs are manifold, ranging from scaffold free systems to complex arrangements of different cells types placed in frameworks generated from synthetic or natural materials. In scaffold-free approaches, such as the hanging drop system, cells form the extracellular matrix (ECM) holding them together by itself. In contrast, structures generated from materials such as matrigel, collagen, fibrin or gelatin can also be used to allow cells grow in 3D structures. Even though scaffold free approaches are not applicable for all tumour cells types, they are superior in terms of spheroid size control and reproducibility. In the future, techniques such as the organ/body on a chip may be applied in which different cancer or non-malignant cell types can be cultivated together with immune cells, fibroblasts, endothelial cells or matrix components in a microfluid system, improving the predictive power of *in vitro* experiments (reviewed by Bhise et al., 2014). Taken together, cultivating cancer cells in 3D has been shown to be superior to 2D cell culture in terms of simulating the complex behaviour of cancer cells *in vivo*.

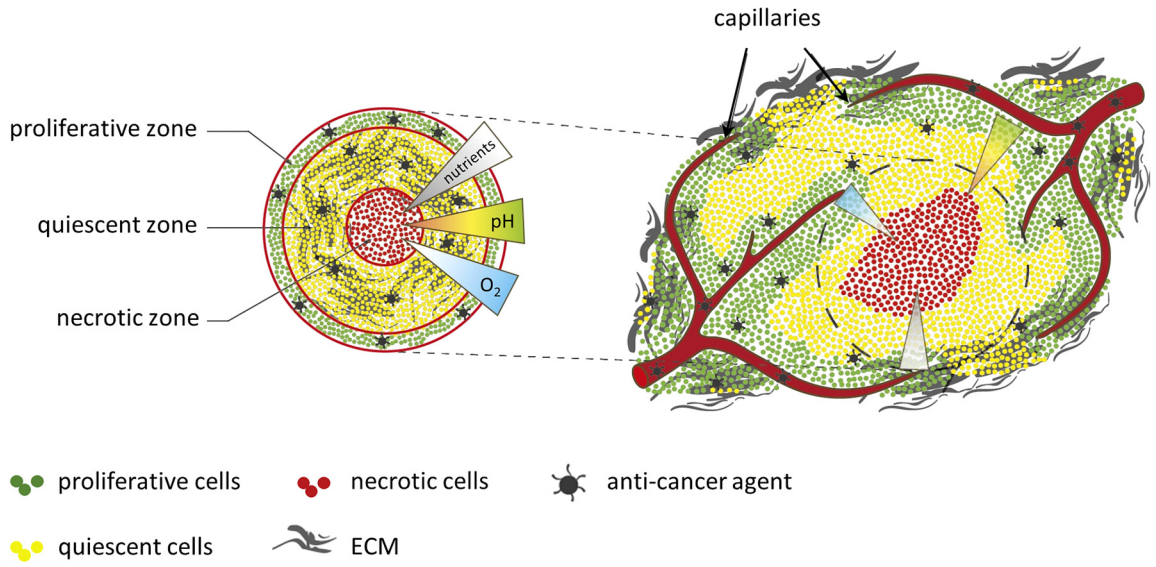

Figure 1: Schematic zonation of a MCTS (left) and a solid tumour (right)

Near blood vessels or at the surface of MCTSs, cells remain proliferative while closer to the interior, cells enter the quiescent state due to undersupply of nutrients and oxygen as well as accumulation of waste products such as lactate. As a result of persistent stress, cells in the centre undergo cell death. Image modified according to the Creative Commons Attribution 3.0 International Public License from Millard et al., 2017.

1.2 The cell cycle

In order to generate or replace tissue, cells have to undergo division. In the human body most cells only divide occasionally or not all, while some cells in highly active tissues such as the gastric mucosa, as well as matrix cells that give rise to the hair shaft, double itself after a mean cell cycle time of ~24 h (Alberts et al., 2002; Van Scott et al., 1963; Willems, 1972). Of note, this value roughly corresponds to cell cycle lengths determined for human cancer cells grown *in vitro* (Heintz et al., 1983; Pereira et al., 2017; Weber et al., 2014). The cell cycle itself is subdivided into 4 distinct phases. G_1 phase, in which the cell displays an active metabolism and grows constantly, S phase where DNA (deoxyribonucleic acid) replication takes place and G_2 phase in which growth proceeds and the cell generates many proteins to prepare itself for division in M phase. Assuming a cell cycle duration of 24 h, a cell stays approximately 11 h in G_1, 8 h in S, 4 h in G_2 and only 1 h in M phase (Cooper, 2000). Progression through the cell cycle is tightly regulated by an interplay of many different proteins, particularly cyclin-dependent kinases (CDKs), cyclins, CDK inhibitors and tumour suppressor gene products such as retinoblastoma protein (Rb). Interestingly, the protein amounts of CDKs are unchanged during the cell cycle but their activity is regulated by

binding of cyclins, of which expression strongly fluctuates depending on the distinctive cell cycle phase. Activated CDKs exert their functions in cell cycle control by subsequently phosphorylating other proteins important for successful cell cycle progression (reviewed by Vermeulen et al., 2003). In more detail, in the presence of mitogenic signalling, cyclin D binds to CDK4/6 resulting in the phosphorylation of Rb (pRb) in G_1 phase. As a consequence, pRb cannot further sequester transcription factors of the E2F family which in turn initiate the expression of cell cycle-relevant proteins such as cyclin E and A. Progression from G_1 to S phase is thereafter mediated by the CDK2/cyclin E, CDK2/cyclin A complexes. In G_2 phase of the cell cycle two complexes, CDK1/cyclin A and CDK1/cyclin B, are formed and drive cell cycle progression by phosphorylating their cognate substrates with CDK1/cyclin B finally mediating the transition from G_2 to M phase (reviewed by Asghar et al., 2015; reviewed by Vermeulen et al., 2003). At the exit from mitosis, protein phosphatase 1 (PP1) binds to and dephosphorylates pRb, thus permitting re-entry into the cell cycle (Vietri et al., 2006). As mentioned previously in this thesis, not all cells in the human body actively proliferate but some, such as fibroblasts, adult stem cells and epithelial cells, are in a reversible dormant state that is only exited if the conditions require it (reviewed by Yao, 2014)(Figure 2). Furthermore, this status of quiescence, or G_0 phase, can also be induced by adverse conditions such as hypoxia, nutrient starvation, or contact inhibition not only in healthy tissue but also in malignant cells (Coller et al., 2006; Eliasson et al., 2010; Horree et al., 2008; Wang et al., 2018; Yang and Chi, 2015). Cells in G_0 phase are mostly characterised by a reduced metabolism, reflected by a lower ribonucleic acid (RNA) content, as well as an enhanced expression of the protein p27, an inhibitor of CDKs (Baisch, 1988; Hüttmann et al., 2001; reviewed by Valcourt et al., 2012). In the past it was thought that quiescent cells simply stop cell cycle progression and passively stay in this state until the conditions improve. However recently it was shown that cells actively maintain this dormancy by enhancing the expression of distinct genes, including those that are responsible for the reversibility of the status (Coller et al., 2006). Furthermore, the fact that different stimuli are able to activate slightly different profiles of genes, including some genes common to all, points to quiescence as being a heterogenous collection of many states (Coller et al., 2006). This is further supported by the finding of different grades of quiescence. It was shown that cells can be, dependent on the extent of stimulus, in a status where re-entering cell cycle progression is easier or takes more time (Rodgers et al., 2014; Yao, 2014). Interestingly, most cells leave cell cycle in G_1 phase, however especially in yeast but also in some human cell lines exit in other cell cycle phases has been observed (Baisch, 1988; reviewed by Daignan-Fornier and Sagot, 2011; Drewinko et al., 1984; Laporte et al., 2011)(Figure 2). Whether the preferential leaving in G_1 has a selective advantage or is simply the result of a prolonged G_1 phase during adverse conditions, has yet to be investigated. As mentioned previously in this

thesis, tumour-forming cells deprived of nutrients and oxygen, can also adopt a quiescent state. Consequently, conventional chemotherapeutics that exert their function via disturbing cell cycle progression fail in eradicating these cells (Chen, Dong, et al., 2016). Furthermore, hypoxia and nutrient starvation were also shown to render cells resistant against treatment with apoptosis-inducing ligands such as TRAIL (Park et al., 2002; reviewed by Trivedi and Mishra, 2015). To overcome the observed drug resistance of quiescent cancer cells it is desirable to either force them to re-enter cell cycle, lock them in their status to prevent future proliferation, or eradicate them in their dormant state. However, a better understanding of quiescence is a prerequisite to maintain control of the desired treatment method.

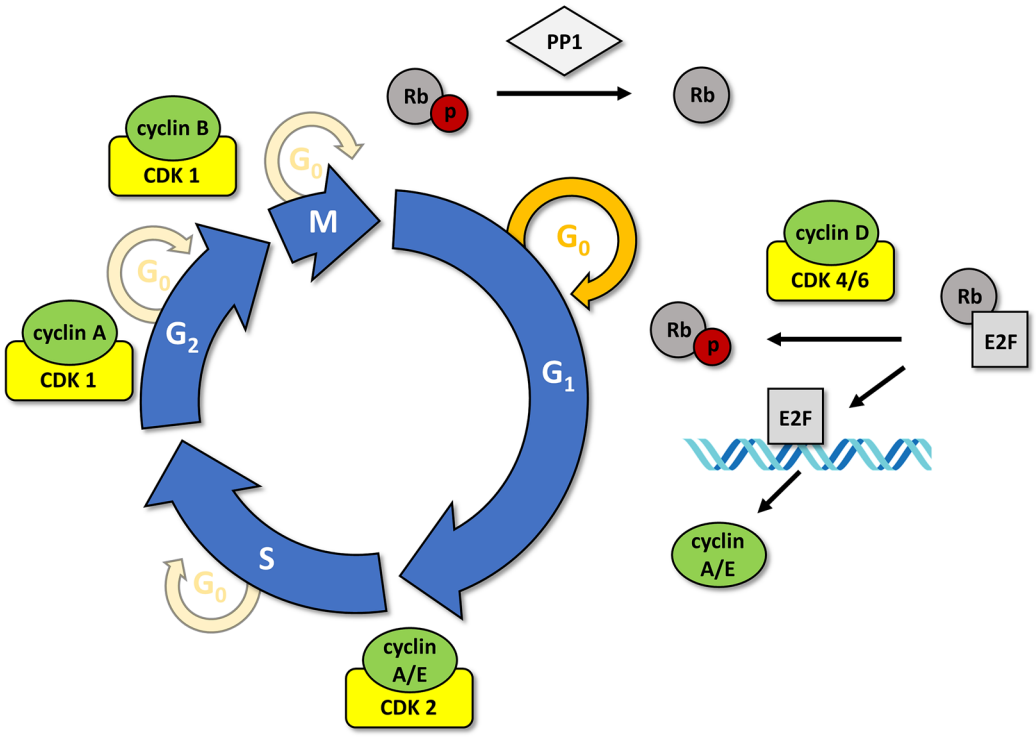

Figure 2: Schematic of the cell cycle

Cell cycle progression is regulated by an interplay of different cyclins, CDKs and CDK substrates such as Rb that induces in its phosphorylated state the expression of cell cycle-related proteins by releasing transcription factors of the E2F family.

1.3 Apoptosis

Approximately 1 million damaged or overaged cells die in the human body every second to ensure tissue homeostasis (Green, 2011). In contrast to necrosis, a form of uncontrolled cell lysis that occurs in response to physical damage, infection or adverse conditions such as hypoxia, this process is highly regulated to ensure that selected cells are removed without harming the surrounding tissue by the release of cellular components. The basic concept of programmed cell death has been known since 1842, however only in 1972 was it referred to for the first time with the word apoptosis, which means leaves falling off from trees in ancient Greek, by Kerr and co-workers (Kerr et al., 1972; Vogt, 1842). Gradually it was found that apoptosis is not only involved in tissue homeostasis in the adult human body but that it also plays an important role in the development of human and all other metazoan embryos. Examples are numerous, ranging from the depletion of surplus neurons in brain development and the elimination of connecting tissue between fingers and toes in the formation of extremities to the removal of the tadpole tail during their metamorphosis to frogs (Kerr et al., 1974); (Mori et al., 1995; reviewed by Yuan and Yanker, 2000). Apoptotic cells die in a characteristic way, starting with the adoption of a round shape and simultaneously shrinking, which is followed by condensation of chromatin and fragmentation of DNA. During the whole process, the cell membrane stays intact, preventing the release of damage-associated molecular patterns (DAMPs) that lead to inflammation as observed after necrotic cell death. In contrast to rupturing necrotic cells, apoptotic cells disintegrate into smaller apoptotic bodies that are engulfed by e.g. macrophages due to their emission of “find me” and “eat me signals”. In apoptosis, but not necrosis, phosphatidylserine (PS) translocates from the inner layer of the cell membrane to the cell surface, thus allowing facile detection of apoptotic cell death by flow cytometry due to binding of PS to fluorescently labelled Annexin V (reviewed by Arandjelovic and Ravichandran, 2015; Kerr et al., 1972; reviewed by Kiraz et al., 2016). Alongside being involved in tissue renewal and embryonic development, apoptosis also represents a barrier against the formation of cancer. Normally, DNA damage, withdrawal of survival signals or enhanced expression of oncoproteins is sensed within the cell, resulting in its elimination by apoptosis. Furthermore, leukocytes can also induce apoptosis in tumour cells by activating death receptors on their surfaces. However, during the development of malignancies, cells often acquire resistance against this form of programmed cell death by loss of function of the sensor proteins as well as downregulation of proteins that promote apoptosis and/or conversely upregulation of cell death inhibitors. Therefore, apoptosis inducing anti-cancer agents often turn out to be solely effective when applicated together with sensitisers that

impede the function of apoptosis inhibitors or change the expression, thus the ratio between pro- and anti-apoptotic proteins.

Apoptotic cell death can be executed via the extrinsic and the intrinsic pathway. External and internal stimuli such as irradiation, genotoxic agents, viral infection, formation of reactive oxygen species, growth factor withdrawal or endoplasmic reticulum (ER) stress can induce the intrinsic pathway of apoptosis in which mitochondrial outer membrane permeabilisation (MOMP) plays a central role. In addition, ligands that belong to the tumour necrosis factor (TNF) receptor superfamily such TNF, TNF-related apoptosis-inducing ligand (TRAIL) and Fas ligand (FasL) can bind to their cognate receptors, TNF receptor 1 (TNFR1), TRAIL receptor 1/2 (TRAILR1/2) and Fas, activating the extrinsic pathway of apoptosis (reviewed by Redza-Dutordoir and Averill-Bates, 2016; reviewed by Roos and Kaina, 2006; reviewed by Ichim and Tait, 2016; reviewed by Takuma et al., 2005; reviewed by Thomson, 2001). In both signalling cascades, cell death is executed via an interplay between initiator and effector aspartate-specific cysteine proteases (caspases) that activate each other, resulting finally in the proteolytic cleavage of numerous substrates such as anti-apoptotic key players, structural proteins like tubulin and actin, DNA repair poly ADP (adenosine diphosphate)-ribose polymerase (PARP) and different cyclins and kinases such as protein kinase B/Akt. Furthermore, effector caspases also activate the caspase-activated DNase (CAD), resulting in the fragmentation of DNA (Fischer et al., 2003; Ichim and Tait, 2016; Kiraz et al., 2016; Nagata, 2000). All caspases are synthesised in the cell as inactive precursors (zymogens) that consist out of a N-terminal prodomain and a C-terminal protease domain. The prodomain of initiator caspase 8 and 10 contains two death effector domains (DEDs) that enable their recruitment to the death inducing signalling complex (DISC) and binding of further proteins. In contrast to that, the prodomain of initiator caspase 9 is comprised of a caspase activation and recruitment domain (CARD) which is necessary for its binding to the apoptosome, a complex of different proteins that causes its activation. If initiator caspases come into close proximity to each other within their respective complexes, their protease domains dimerise, resulting in proteolytic cleavage and activation (reviewed by Creagh, 2014). However, only recently it was shown that procaspase 9 can also be activated when forming a heterodimer with the apoptosome without the requirement for proteolytic cleavage (Wu, Lee, et al., 2016). In contrast to initiator caspases, the proforms of effector caspases (caspase 3, 7) are already preassembled as homodimers in non-apoptotic cells. After cleavage by active initiator caspases, they subsequently exert their function as executioner of apoptosis (reviewed by Creagh, 2014). Interestingly, it was shown that caspase 3 is able to activate procaspase 6 which in turn can cleave procaspase 8 (Cowling and Downward, 2002; Inoue et al., 2009). Even though initially thought to be a positive feedback loop, a system biology

approach suggested that this cleavage event results in caspase 8 monomers that lower the apoptotic potential due to the reduced probability of forming active caspase 8 dimers. (Würstle et al., 2010). Caspase 3 also cleaves procaspase 9 and self-cleaved caspase 9 (p35/p12) into p37/p10 and p35/p10 forms respectively, which prevents the association of the inhibitor XIAP and increases the activity of the p35/p12 fragment, forming a positive feedback loop (Denault et al., 2007).

As mentioned previously in this thesis the extrinsic pathway of apoptosis is triggered by binding of apoptosis-inducing ligands to their cognate receptors. In response to stimulation with TRAIL, receptors trimerise and the DISC is formed, containing the receptors, Fas-associated protein with death domain (FADD), cellular FLICE-like inhibitory protein (cFlip, FLICE = FADD-like interleukin-1β-converting enzyme, another name for caspase 8), procaspase 8 and procaspase 10. It has been demonstrated that FADD is recruited to the receptor trimer by death domain (DD) interactions, which are present on the intracellular domain of the death receptors and in FADD. Controversy remains as to the exact stoichiometry of FADD to death receptor, with 1 FADD per trimer and 3 FADDs per trimer having been suggested (Dickens et al., 2012; Majkut et al., 2014; Schleich et al., 2016). FADD also contains a DED, allowing it to subsequently recruit procaspase 8 via binding to its DED1. Thereafter, further procaspase 8 proteins are recruited via their DEDs forming a large filament in which their proteolytic cleavage and activation is carried out (Dickens et al., 2012; Fu et al., 2016; Schleich et al., 2016). Beside further procaspase molecules, initial procaspase 8 can also recruit cFlip, a protein that displays high similarity to caspase 8 but lacks its protease activity. Originally, it was believed that cFlip can actively compete with procaspase 8 for binding to the DED of FADD, however more recently it has been demonstrated that procaspase 8 is required for recruitment of cFlip, giving rise to a hierarchal binding model of DISC formation where procaspase 8 is first recruited to FADD to initiate the extension of the DISC. The two short isoforms of the protein, cFlip-S and cFlip-R, completely lack the protease domain and inhibit caspase 8 activation when being part of the DISC. Conversely, the role of the long isoform (cFlip-L) is not well defined. Even though cFlip-L contains an inactive protease domain, it was shown to enhance apoptosis when present in physiological concentrations. It was suggested that heterodimerisation with procaspase 8 can stabilise the catalytic domain of the caspase, allowing local catalytic activity of the protein and incomplete processing of the heterodimer. Corresponding with that hypothesis, higher concentrations of cFlip-L were shown to inhibit apoptotic-signalling probably due to its excessive presence in the DISC that prevented the formation of interactions with procaspase 8 (Hughes et al., 2016). However, it has also been suggested that this heterodimer allows a different substrate activity of caspase 8, thus altering downstream

signalling (Pop et al., 2011). Beside caspase 8, also the close homolog caspase 10 can be recruited to the filament. Only recently the current assumption of caspase 10, being similarly to caspase 8 involved in the execution of apoptosis, was challenged by the finding that, in different cell lines as well as in a cell free system, caspase 10 inhibited apoptosis and rather shifted the DISC signalling to the induction of pro-survival genes. However, whether caspase 10 inhibits apoptosis by preventing filament assembly or forming inactive heterodimers with caspase 8 has yet to be investigated (Horn et al., 2017). Taken together, DISC assembly is a highly complex cooperative and hierarchical process that comprises different proteins, shifting signalling to either pro- or anti-apoptotic outcomes (Figure 3). Alongside type I cells, in which activation of the intrinsic pathway is sufficient to induce apoptosis, type II cells need an amplification of the apoptotic signal via the intrinsic route to be eradicated (Scaffidi et al., 1998). As described previously external and internal signals can induce the formation of pores in the mitochondrial outer membrane finally resulting in the activation of effector caspases. However, at the same time also the activation of death-inducing receptors can trigger MOMP via caspase 8. After cleavage of the B cell lymphoma-2 (Bcl-2) homology (BH3)-only protein Bid by the effector caspase, truncated Bid (tBid) translocates to the mitochondrial outer membrane and initiates the formation of pores generated from two pro-apoptotic effector proteins of the Bcl-2 protein family, Bcl-2 associated X protein (Bax) and Bcl-2 antagonist or killer (Bak) (reviewed by Martinou and Youle, 2011). Alongside tBid and the two pore formation proteins, numerous other members of the Bcl-2 protein family are involved in the regulation of MOMP. Anti-apoptotic Bcl-2 family proteins such as Bcl-2, Bcl-xl and myeloid cell leukemia-1 (Mcl-1) can directly bind to Bax and/or Bak preventing pore formation. Furthermore, these proteins can be sequestered from their inhibiting function by binding to pro-apoptotic Bcl-2 family members (BH3-only proteins) such as Bcl-2 interacting mediator of cell death (Bim), antagonist of cell death (BAD), p53 upregulated modulator of apoptosis (Puma) and NOXA. Thus, the ratio between pro- and anti-apoptotic Bcl-2 family proteins dictates the fate of the cell (reviewed by Finlay et al., 2017; reviewed by Kiraz et al., 2016). After pore formation, cytochrome c is released from the mitochondrial intermembrane space and forms, together with apoptotic protease activating factor-1 (Apaf-1) and deoxyadenosine triphosphate/adenosine triphosphate (dATP/ATP), a heptameric complex that recruits procaspase 9 via interaction between the CARD domains present in both, Apaf-1 and procaspase 9. In this structure, called the apoptosome, proximity induced homodimerisation then subsequently results in the activation of bound procaspase 9 molecules which thereafter drive apoptosis by cleaving effector procaspases. As described earlier, only recently it was shown that procaspase 9 can also be activated as a monomer by binding to another domain in Apaf-1 (NOD = nucleotide-binding oligomerisation domain) resulting in conformational changes in the caspase (Wu,

Lee, et al., 2016). Similarly to members of the Bcl-2 family that control MOMP, procaspase activation is also negatively regulated by a group of proteins, called inhibitors of apoptosis (IAPs). A common feature of these proteins is the occurrence of one to three baculovirus IAP repeats (BIR) domains which appear as zinc finger folds in the molecules and are responsible for various protein-protein interactions. X-linked inhibitor of apoptosis protein (XIAP) contains three BIR domains which allows it bind to and inactivate caspase 3, 7 and 9. Furthermore, due to its additional ubiquitin-associated (UBA) domain and its really interesting new gene (RING) domain, XIAP can also target proteins for ubiquitin-dependent degradation. Two other members of the IAP family, cellular IAP-1 (cIAP-1) and cellular IAP-2 (cIAP-2), containing three BIR and one RING domain(s), also bind to caspase 3, 7 and 9, but instead of inhibiting their activity rather accelerate their degradation. Furthermore, both proteins were also shown to activate nuclear factor 'kappa-light-chain-enhancer' of activated B-cells (NF-κB) and mitogen-activated protein kinase (MAPK) signalling, thus contributing to survival signalling (reviewed by Kiraz et al., 2016). The last member of the IAP family to be described here, is the small, only one BIR domain containing protein survivin. Alongside its well described function in cell cycle control, survivin was also shown in many studies to inhibit apoptosis. However, whether it functions via direct binding to caspases, or interacts with XIAP, enhancing its anti-apoptotic activity, is still under investigation (reviewed by Altieri, 2015; Zumbrägel et al., 2017). All previously described IAPs can be sequestered from their anti-apoptotic functions by second mitochondria-derived activator of caspases (SMAC). During MOMP, SMAC is released from the mitochondria similarly to cytochrome c and binds as homodimers to IAPs resulting in the release of bound caspases (reviewed by Kiraz et al., 2016) (Figure 3).

Taken together, apoptosis is a complex, highly regulated signalling pathway that can be activated by numerous external and internal stimuli, resulting in the eradication of selected mutated or damaged cells. Consequently, genotoxic agents that activate this form of programmed cell death in proliferating cells, are already used for quite a long time in cancer therapy. However, only recently evidence raised that induction of apoptosis might be not always beneficial for cancer patients, but also harbours risks. For example, it was shown that in apoptotic cells, activation of caspases resulted in the increased production of arachidonic acid, which was subsequently converted by cyclooxygenase (COX) to prostaglandin E_2 (PGE_2). Released PGE_2 was in the following demonstrated to promote proliferation in the surrounding tissue (phoenix rising effect). Furthermore “find and eat me” signalling was demonstrated to enhance angiogenesis and attract macrophages that in some cases were able to promote cancer progression. Lastly, it has been shown that selected cells could survive low level of caspase activation, that nevertheless resulted in DNA damage and

genome instability, enhancing tumorigenesis (reviewed by Ichim and Tait, 2016). In accordance with the described findings, several tumour types are actually more sensitive to apoptosis than surrounding healthy tissue and high level of anti-apoptotic proteins correlate in some cancerous diseases with better prognosis. Thus, combining apoptosis inducing agents with drugs that prevent the described severe side effects might be a promising approach for future cancer therapy.

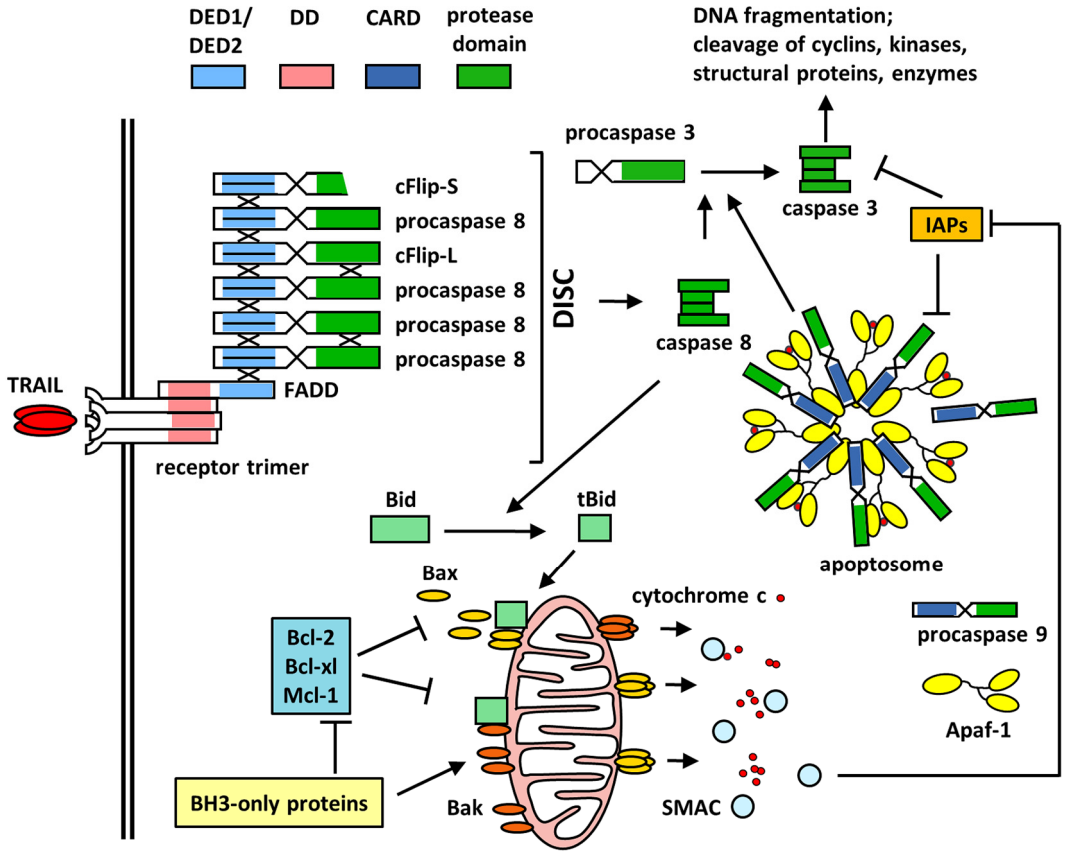

Figure 3: Schematic of TRAIL-induced apoptosis

Binding of TRAIL results in trimerisation of TRAILRs and subsequent formation of the DISC. Within this complex, procaspase 8 is activated and can proteolytically cleave and activate procaspase 3 to execute cell death. In type II cells, amplification of the apoptotic signal via the mitochondrion is necessary for the efficient transmission of the apoptotic signal. Thereby Bid, cleaved by caspase 8, facilitates pore formation in the mitochondrial outer membrane resulting in the release of cytochrome c and SMAC. Together with Apaf-1 and dATP/ATP, cytochrome c forms a platform in which procaspase 9 is activated to cleave procaspase 3. Apoptosis is further regulated by an interplay of pro- and anti-apoptotic members of the Bcl-2 family as well as IAPs. Schematic modified from the original design by Gavin Fullstone.

1.4 TRAIL as member of the TNF superfamily

The TNF superfamily comprises, to date, of 19 ligands and 29 receptors of which all of them are involved in pro-inflammatory signalling. However, as described previously, individual ligands are also able to induce apoptosis, or promote proliferation and differentiation (reviwed by Aggarwal et al., 2012). Synthesised as type II transmembrane proteins with an extracellular C-terminal domain and an intracellular N-terminus, members of the TNF superfamily activate their cognate receptors in a homotrimeric assembly mediated by the TNF homology domain (THD) located in the C-terminal end of the proteins. Even though most ligands execute signalling when bound to membranes, some TNF superfamily members can be cleaved from the cell surface by different proteases which, depending on the protein, either activate or inhibit their function (reviewed by Bodmer, Schneider and Tschopp, 2002). It was already known for quite a long time that bacterial infection-mediated inflammation was able to induce tumour regression when William Coley started to treat cancer patients in 1893 with a mixture of different bacteria (reviewed by McCarthy, 2006; Coley, 1891). However, only in 1975 it was found that the factor responsible for tumour shrinkage was not a bacterial derived endotoxin, but a compound produced by the human body in response to infection, termed TNF (Carswell et al., 1975). Finally, in the mid-1980s the tumour necrosis-inducing compound TNF was structurally identified by a group around Aggarwal (Aggarwal et al., 1985). Since then further members of the TNF superfamily were identified due to human complementary DNA (cDNA) sequence homology, with TRAIL being discovered in the 1990s by two independent groups (Pitti et al., 1996; Wiley et al., 1995). In contrast to other TNF superfamily ligands, stable trimerisation and hence activity of TRAIL monomers requires a zinc ion that connects the single proteins by binding to cysteine residue 230 (Bodmer et al., 2000; Hymowitz et al., 2000). In the human body TRAIL can bind to five TRAIL receptors (TRAILRs), TRAILR1, TRAILR2, TRAILR3, TRAILR4 and osteoprotegerin (OPG). Each receptor binding site is formed between two individual monomers of the TRAIL trimer, resulting in the trimerisation of TRAIL receptors after binding of the trimeric ligand (Hymowitz et al., 1999; reviewed by Ramamurthy et al., 2015). Mainly produced by cells of the immune system such as natural killer (NK) and T cells, this TNF superfamily member is not only involved in the elimination of infected or malignant cells by inducing apoptosis, but also influences the development of leukocytes (Collison et al., 2009; reviewed by Danish et al., 2017; reviewed by Mizrahi and Askenasy, 2014). However, beside its role in the immune system, TRAIL was also shown to regulate germ cell apoptosis and protect spermatozoa in the human testis. Furthermore, TRAIL produced by the medial smooth layer of the aorta and pulmonary arteries has been demonstrated to positively influence endothelial cell proliferation as well as survival. Additionally, exposing endothelial cells to TRAIL was shown to influence the

adhesion of leukocytes to the endothelium. Alongside the previously mentioned cell types and organs, TRAIL and its receptors were also shown to be expressed by a range of other tissues such as the colon, the lung and the kidney with their physiological function in these organs needing further investigation (reviewed by Danish et al., 2017).

1.4.1 TRAIL receptors

Receptors of the TNF superfamily are characterised by the presence of at least one cysteine rich domain (CRD) in their extracellular part which is/are responsible for ligand binding (reviewed by Bodmer, Schneider and Tschopp, 2002). Searching the human genome database for sequence homologies with TNFR1, Pan and colleagues discovered 1997 the first TRAIL-binding receptor, TRAILR1 (Pan, O'Rourke, et al., 1997). Comprised all together of 468 amino acids, the extracellular part of TRAILR1 is build up from two complete CRDs that form the ligand-binding site and one partial CRD that harbours a putative pre-ligand binding assembly domain (PLAD), allowing ligand-independent homo- and hetero-oligomerisation of TRAILRs on the cell membrane (reviewed by Chan, 2007; Clancy et al., 2005; reviewed by Danish et al., 2017; Neumann et al., 2014). As described previously in this thesis, the intracellular moiety of TRAILR1 contains a death domain that is necessary for the formation of signalling complexes. TRAILR2, the second receptor of the TRAILR family able to induce apoptosis, was described only shortly after the discovery of TRAILR1 by several independent groups (MacFarlane et al., 1997; Pan, Ni, et al., 1997; Schneider et al., 1997; Screaton et al., 1997; Walczak et al., 1997; Wu et al., 1997). Two isoforms of TRAILR2 can be found in the human body. The short isoform (TRAILR2-S) comprises of 411 amino acids that are allocated, similar to TRAILR1, on two complete and one partial CRD as well as an intracellular death domain. In contrast to TRAIL2-S, TRAILR2-L contains additional 29 amino acids close to the cell membrane prior to the first CRD. As this part of the protein is rich in threonine, alanine, proline and glutamine it is referred to as TAPE (reviewed by von Karstedt, Montinaro and Walczak, 2017; Schneider et al., 1997). In addition to previously described TRAILR1 and TRAILR2, two further TRAIL-binding receptors, TRAILR3 and TRAILR4 were discovered in the late nineties (Degli-Esposti, Dougall, et al., 1997; Degli-Esposti, Smolak, et al., 1997; Marsters et al., 1997; Mongkolsapaya et al., 1998; Pan et al., 1998). In contrast to the two apoptosis-inducing receptors, the 259 amino acids comprising TRAILR3 lacks an intracellular domain but is bound to the cell membrane via a glycosylphosphatidylinositol (GPI) anchor. Two complete and one partial CRD are connected to the anchor via five TAPE domains. Due to the lack of an intracellular domain, direct signalling via TRAILR3 is highly unlikely, although signal transduction via the GPI anchor cannot be completely excluded (reviewed by

Kimberley and Screaton, 2004). Nevertheless, the main function of TRAILR3 is highly likely that of a regulatory receptor, either inhibiting signalling via TRAILR1 and TRAILR2 by sequestering TRAIL or forming signalling-incompetent heteromeric complexes (Neumann et al., 2014). The conformation of the 386 amino acids comprising TRAILR4 is closely related to those of TRAILR1/R2, containing two complete and one partial CRD. However, in contrast to the other two receptors, TRAILR4 only comprises a truncated DD and is therefore believed to be incapable of recruiting FADD and thus inducing apoptotic signalling. Whether TRAILR4 is able to activate the NF-κB and Akt pathway, as it was suggested by different studies, is under debate and needs further investigation (Degli-Esposti, Dougall et al., 1997; Harper et al., 2001; Hu et al., 1999; Lalaoui et al., 2011; Marsters et al., 1997; Neumann et al., 2014). Similarly to TRAILR3, TRAILR4 most likely acts solely as a regulatory receptor. The fifth receptor known to bind TRAIL is OPG. OPG is a soluble protein that is mainly known for its ability to regulate osteoclast differentiation by sequestering receptor activator of NF-κB ligand (RANKL) (Boyle et al., 2003). Even though OPG binds TRAIL only with low affinity, it was shown to inhibit apoptosis induction *in vitro* (de Toni et al., 2008; Emery et al., 1998; Lane et al., 2012). However, whether this finding is of physiological relevance has yet to be investigated (Figure 4).

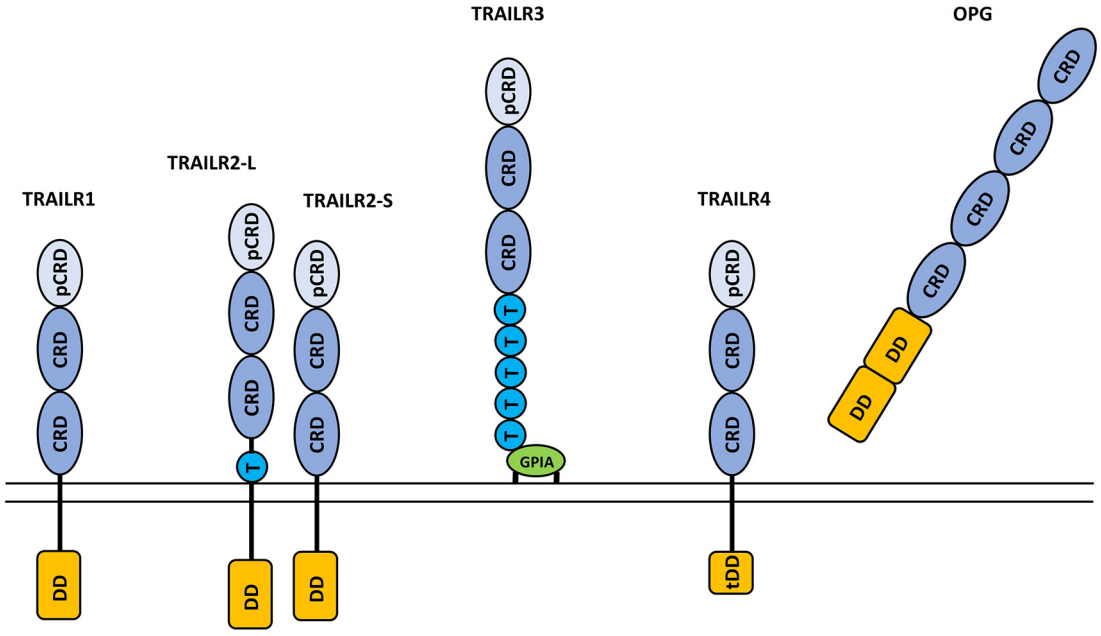

Figure 4: Structure of TRAILRs

All five TRAILRs are comprised of up to four CRDs that are necessary for ligand binding. TRAILR1/2 (S = short isoform; L = long isoform)/3/4 also contain a partial CRD that harbours the PLAD which allows ligand-independent homo- and hetero-oligomerisation of the receptors on the cell surface. Signal transduction is mediated via an intracellular DD which is truncated in TRAILR4 (tDD). TRAILR3 is bound to the cell membrane via an glycosylphosphatidylinositol anchor (GPIA). The long isoform of TRAILR2-L, as well as TRAILR3 additionally contain TAPE (T) domains, short protein moieties rich in threonine, alanine, proline and glutamine.

1.4.2 Mechanistical insight into TRAILR activation

As previously described in this thesis, ligands of the TNF superfamily such as TRAIL, form noncovalently-linked homotrimers that attach with their outside part to cognate receptors. Thereby two TRAIL monomers build together an interface in which one receptor can be bound. Currently it is presumed that TRAILRs are pre-arranged on the cell membrane as inactive antiparallel dimers, mediated by the PLAD domain located in the last CRD of the receptors. Binding of the trimeric ligand, subsequently leads to formation of large hexagonal structures of activated receptors resulting in DISC formation and execution of downstream signalling (reviewed by Vanamee and Faustman, 2018) (Figure 5). As stated earlier, TRAILR3 and TRAILR4 are not able to induce apoptosis but it was shown that their overexpression can render TRAIL-sensitive cells into a TRAIL-resistant phenotype (Degli-Esposti, Dougall, et al., 1997; Degli-Esposti, Smolak, et al., 1997). Furthermore, evidence exists that malignant and normal diploid cells can upregulate TRAILR3 and TRAILR4 expression thereby acquiring resistance against TRAIL (Bouralexis et al., 2003; Clancy et al., 2005; Davidovich et al., 2004; Riccioni et al., 2005). Earlier it was thought that both receptors simply inhibit signalling by sequestering TRAIL from binding to apoptosis-inducing TRAILR1 and TRAILR2. However, the fact that TRAILR3 and TRAILR4 display lower affinities to the ligand than TRAILR1 and TRAILR2 as well as the observation that TRAIL in excess does not abolish inhibition, argues against the theory of TRAILR3 and TRAILR4 solely being decoy receptors (Lee et al., 2005); (unpublished data, Simon Neumann). Since it was shown that at least TRAILR4 can form heteromers with TRAILR1 and TRAILR2, resulting in inhibition of apoptosis induction, the theory of mixed receptor complexes that regulate signalling capacity is much more convincing (Clancy et al., 2005; Merino et al., 2006; Neumann et al., 2014). Although the formation of heterotrimers including TRAILR3 is relatively unlikely, due to its preferential localisation in lipid rafts as well as expression of, in comparison to the other TRAILRs, a larger linker between its transmembrane domain and the ligand binding CRDs (Mongkolsapaya et al., 1998; Sharma et al., 2004; Varma and Mayor, 1998). Whether TRAILR3 nevertheless forms heterotrimers with TRAILR1/R2, inhibiting apoptosis, or acts simply as a decoy receptor has yet to investigated. Of note, as TRAILR2-S displays a linker length comparable to TRAILR1 whilst, the connecting domain in TRAILR2-L is much longer, it might be speculated that TRAILR2-L would preferentially form homotrimers due to steric effects (Screaton et al., 1997).

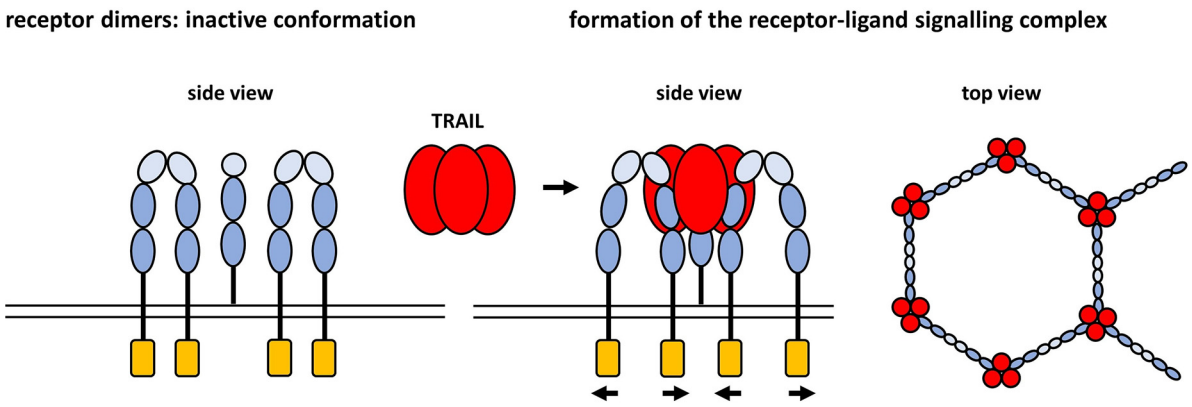

Figure 5: Hexagonal TRAILR networks on the cell surface

TRAILRs pre-assemble ligand-independently on the cell surface via a PLAD located in the first CRD (light blue). After binding of TRAIL, receptors become activated and the DISC is formed via interaction of the receptor located DD (orange) and the DED of FADD (not depicted).

1.4.3 Non-canonical TRAILR signalling

Alongside inducing DISC-dependent apoptosis, activation of TRAILR1 and TRAILR2 can also result in receptor-interacting serine/threonine protein kinase 1 (RIPK1)-dependent apoptosis, necroptotic cell death or pro-survival signalling. Under certain circumstances, such as the depletion of cIAPs or TNF receptor-associated factor 2 (TRAF2) as well as under acidic pH, stimulation with TRAIL can trigger the formation of a secondary complex that is devoid of TRAILRs but contains FADD, procaspase 8, RIPK1, TRAF2 and NF-κB essential modulator (NEMO) (reviewed by von Karstedt et al., 2017). Similar to the DISC, this complex is also able to activate procaspase 8, resulting in the execution of RIPK1-dependent apoptosis (Feoktistova et al., 2011). However, in case of blocked caspase activity, the complex can recruit the protein receptor-interacting serine/threonine protein kinase 3 (RIPK3). Activated RIPK3 can in turn bind to mixed lineage kinase domain like pseudokinase (MLKL) resulting in its oligomerisation and insertion into the cell membrane. Similarly to necrosis, components of the cell are subsequently released into the environment and induce inflammation, thus earning it the name necroptosis (reviewed by Chen, Yu, et al., 2016). In some cases, both, formation of the DISC and complex II can not only result in the execution of programmed cell death but also promote proliferation, invasion, migration and metastasis. Alongside inducing necroptosis, blocked caspase 8 activity can also lead to RIPK1-dependent activation of the transcription factor NF-κB resulting in the expression of numerous gene products involved in cell survival and proliferation. Furthermore, activation of TRAILR1 and TRAILR2 was also shown to enhance pro-survival signalling by triggering the c-Jun N-terminal kinase (JNK), MAPK and phosphatidylinositol-4,5-bisphosphate 3-kinase

(PI3K)/Akt pathways as well as to increase migration in NSCLC cell lines via the RIPK1/protein kinase SRC/signal transducer and activator of transcription 3 (STAT3) axis (reviwed by von Karstedt et al., 2017; reviewed by de Miguel et al., 2016). In TRAIL-mediated apoptosis, the first complex to be formed is always the DISC. The decision of whether a different complex is build up thereafter, is most likely the result of many factors, including concentration and presentation of the ligand, post-translational modifications of the receptors and availability of complex-forming proteins (reviewed by Flusberg and Sorger, 2015). Furthermore, only recently it was demonstrated that the linear ubiquitin chain assembly complex (LUBAC) can regulate the outcome of TRAILR activation by adding linear ubiquitin chains to RIPK1 and caspase 8, limiting apoptosis and necroptosis while promoting the induction of pro-survival genes (Lafont et al., 2017). Of note, the fact that activation of TRAILRs can result either in the induction of cell death or transcription of pro-survival genes might explain the observation of TRAILR expression not being a prognostic marker in cancer therapy.

1.4.4 Differences between TRAILR1 and TRAILR2

Interestingly, only human and chimpanzees possess two apoptosis-inducing TRAILRs while in all other vertebrates only one receptor is expressed, pointing to the evolution of non-redundant functions of these receptors in these two species. Whether ligand-induced apoptosis is equally triggered via both, TRAILR1 and TRAILR2, or mainly executed via one of the two receptors, is largely dependent on the cell type. In leukemic malignancies apoptosis is mostly induced by TRAILR1, while in solid tumours induction is either mediated via TRAILR2 or TRAILR1, but also equally contribution of both receptors has been observed (reviewed by van Roosmalen et al., 2014). Even though ER stress-induced apoptosis was suggested, alongside other mechanisms, to be mediated by accumulation of intracellular TRAILR2, evidence also exists for a contribution of TRAILR1, speaking against a unique function of TRAILR2 in this setting (Li et al., 2015; Lu et al., 2014). Taken together, the two signalling-competent TRAILRs have most likely not emerged to undertake different functions in terms of executing apoptosis but more recent findings suggest that one TRAILR, TRAILR2 is playing a superior role in pro-survival signalling. For example it was shown that TRAILR2, alongside being a membrane-bound receptor, can also be located in the nucleus where it ligand-independently promotes proliferation by inhibiting the maturation of the micro RNA (miRNA) let7 (Haselmann et al., 2014). Furthermore, Karstedt and colleagues demonstrated that cancer progression, invasion and metastasis was induced by TRAILR2 in complex with TRAIL in KRAS-mutated tumour cells (von Karstedt et al., 2015).

1.4.5 Regulation of TRAILR amounts and modulation of TRAILR signalling capacity by glycosylation

Adverse environmental conditions such as hypoxia or glucose starvation can change the amounts of TRAILRs in a cell. Thereby, expression of the receptors is not only controlled on the transcriptional level, but different messenger RNA (mRNA)-binding proteins and miRNAs also regulate the stability of mRNA transcripts. Studies demonstrated that expression of TRAILR1, TRAILR3 and TRAILR4 can be inhibited due to hypermethylation of the respective promotor regions (Bae et al., 2008; Elias et al., 2009; Horak et al., 2005; Wu, Chen, et al., 2016). Furthermore, it has been shown that in response to hypoxia or nutrient starvation, the protein Hu antigen R (HuR) can bind to TRAILR1 and TRALR2 mRNA most likely inhibiting translation, while TRAILR4 amounts were shown to be downregulated in response to binding of protein poly (ADP-ribose) polymerase 13 (PARP13) to TRAILR4 transcripts (Blanco et al., 2016; Burkhart et al., 2013; Pineda et al., 2012; Romeo et al., 2016; Todorova et al., 2015). Interestingly, alongside mRNA-binding proteins, miRNA has also been demonstrated to inhibit the expression of at least TRAILR1 (Razumilava et al., 2012). Additionally to the previously described mechanisms, TRAILR amounts are also controlled by several transcription factors that can be activated or induced in adaption to the environment. TRAILR1 and TRAILR2 are suggested to be both regulated in response to stress by NF-κB, p53, forkhead-box-protein O3a (FOXO3a), activator protein 1 (AP1) and specificity protein 1 (SP1) while the transcriptional repressor GLI3 was shown to solely inhibit TRAILR1 expression and Yin Yang 1 (YY1) to exclusively downregulate TRAILR2 (reviewed by van Roosmalen et al., 2014). Regarding the two regulating TRAILRs, TRAILR3 and TRAILR4, it was found that their expression is controlled by p53 (Liu et al., 2005; Toscano et al., 2008). Additionally, TRAILR4 has been shown to be upregulated in response to hypoxia via a hypoxia-inducible factor-1α (Hif-1α)-mediated mechanism while expression of TRAILR3 was demonstrated to be enhanced in response to NF-κB activation (Bernard et al., 2001; Pei et al., 2010). As later described in more detail in this chapter, adverse conditions can induce ER stress which, if not resolved, triggers apoptosis. Prolonged ER stress was shown to result in the induction of the transcription factor C/EBP homologous protein (CHOP), which was found to upregulate, with or without the contribution of two further transcription factors, ELK-1 and cyclic adenosine monophosphate (cAMP)-dependent transcription factor 3 (ATF3), the expression of TRAILR2 (Edagawa et al., 2014; Oh et al., 2010; Yamaguchi and Wang, 2004). However, CHOP-independent TRAILR2 upregulation in response to ER stress was also demonstrated, which was mediated by further proteins involved in the ER stress-induced unfolded protein response (UPR) (Iurlaro et al., 2017; Liu et al., 2009). Although so far only the accumulation of TRAILR2 has been shown to ligand-independently provide a platform in which

procaspase 8 becomes activated, also upregulation of TRAILR1 in response to ER stress via interplay between the transcription factors CHOP and phosphorylated Jun of the AP1 complex as well as the acetyltransferase GCN5 was demonstrated (Li et al., 2015; Lu et al., 2014).

A cells' susceptibility to TRAIL is not solely regulated by its expression of TRAILRs or further apoptosis-relevant proteins, but also by posttranslational modification or enhanced/decreased degradation of those proteins. In cancer cells, glycosylation of TRAILR1 and TRAILR2 was shown to increase TRAIL sensitivity. Thereby, the sugar moieties did not enhance the affinity for the ligand, but positively influenced receptor aggregation as well as procaspase 8 recruitment and activation (reviewed by Micheau, 2018). Lastly, modulation of TRAILR amounts can also be achieved via a regulation of degradation. TRAILR1 and TRAILR2 can both be ubiquitinated by E3 ubiquitin-protein ligases which targets them for degradation via the lysosomal or proteasomal pathway. Indeed, increased expression of such ligases was shown to enhance TRAIL resistance by downregulating TRAILR surface amounts (reviewed by Mert and Sanlioglu, 2016). Taken together, in adaption to the environment, TRAILR expression and signalling within cells can be regulated on many different levels not all of which were discussed here. Therefore, it might be speculated that gradients of oxygen and nutrients, which occur in solid tumours, result in heterogenous spatial-dependent TRAILR expression and signalling, influencing the cells' susceptibility to TRAIL.

1.4.6 TRAIL as anti-cancer agent

Ligands of the TNF superfamily such as TNF, FasL or TRAIL were initially thought to be suitable anti-cancer agents with the ability to induce apoptosis independent of a cells' p53 status. However, exclusively TRAIL underwent further investigations as TNF and FasL appeared to be harmful not only for tumour cells but also against healthy tissue (Kimura et al., 1987; Ogasawara et al., 1993). Although, initial trials with early TRAIL formats showed toxicity against hepatocytes, this was attributed to formation of higher aggregates due to additional expression of FLAG- or hexahistidine (His)-tags meant for purification purposes (Ganten et al., 2006; reviewed by Koschny et al., 2007; Lawrence et al., 2001). Without the expression of such moieties, TRAIL turned out to be exclusively active against cancer cells. Underlying reasons for this observation are still not completely resolved however evidence exists that non-transformed cells acquire TRAIL resistance by high amounts of TRAILR3, cFlip, XIAP, Bcl-2 and low expression of TRAILR1 and TRAILR2 (van Dijk et al., 2013; Sheridan et al., 1997; Zhang et al., 2000).

The first generation of TRAIL based anti-cancer therapeutics comprised the soluble, recombinant human TRAIL, dulanermin, and agonistic monoclonal antibodies against TRAILR1 and TRAILR2. However unfortunately, even though well tolerated in clinical trials, overall results were largely disappointing as it turned out that only very few cancer patients profited from treatment (Camidge et al., 2010; Herbst et al., 2010; reviewed by den Hollander et al., 2013; Tolcher et al., 2007). This failure of the first wave of TRAILR activating agents can be attributed to various reasons. Alongside the problem that many tumours are initially TRAIL-resistant, dulanermin displays an *in vivo* half-life of just 30 min and fails in efficiently clustering of TRAILRs. Furthermore, due to its non-selectivity, it can also bind to the regulatory receptors TRAILR3 and TRAILR4. Even though agonistic antibodies solely bind to the death-inducing TRAILRs and display in comparison to dulanermin a much more extended half-life, they are also not able to trimerise receptors due to their dimeric format. Furthermore, agonistic antibodies can bind with their fragment crystallizable (Fc) part to cells in the blood stream which diminishes the concentration that reaches the tumour site (reviewed by von Karstedt et al., 2017).

In order to overcome these drawbacks, many efforts were made in the recent years to improve and increase stability, pharmacokinetics, targeting and valency of TRAIL receptor-binding anti-cancer agents. As agonistic TRAILR-specific antibodies failed to efficiently cluster TRAILRs due to their bivalent format, antibodies with higher valency (nanobodies) were developed (Huet et al., 2014; Papadopoulos et al., 2015). Amongst these, TAS266 was the first to enter a clinical trial, which was however ended due to strong toxicity of the compound (Papadopoulos et al., 2015). An alternative approach to increase the activity of TRAIL-specific antibodies is the generation of bispecific formats that not only attach to and activate TRAILRs but are also capable of binding to further antigens present on the tumour cells (reviewed by Kontermann, 2012; Michaelson et al., 2009). It is conceivable that in this way not only targeting of the antibodies can be improved but that simultaneous activation/inhibition of different receptor types might also enhance the bioactivity of the compound. Michaelson and colleagues, for example, developed a bispecific antibody that targeted both TRAILR2 and lymphotoxin β receptor, thereby displaying enhanced activity when compared to the respective antibodies targeting only one receptor type (Michaelson et al., 2009).

Similar to the evolution observed for TRAILR-specific antibodies, also soluble recombinant human TRAIL was further developed as an anti-cancer agent. To improve its stability, TRAIL monomers were fused to tags such as poly-histidine, FLAG epitope, leucine zipper, isoleucine zipper, the trimerisation domain of tenascin-C, human serum albumin or human adenovirus

type 5 fiber of which all of them enforce homotrimerisation (Berg et al., 2007; reviewed by von Karstedt et al., 2017; Yan et al., 2016). Alternatively, the extracellular domains of three TRAIL monomers can be connected by short peptide linkers resulting in single-chain TRAIL (scTRAIL) formats that can easily be combined with antibody moieties to further increase stability but also to allow efficient targeting to the tumour site. In 2012, Siegemund and colleagues developed an antibody TRAIL fusion protein comprised of the single-chain fragment variable (scFv) fragment of the epidermal growth factor receptor (EGFR)-binding antibody cetuximab and one scTRAIL. By reducing the linker length within the scFv fragment, non-covalent dimerisation of two scFV-scTRAIL molecules was achieved resulting in $Db_{\alpha EGFR}$-scTRAIL (Siegemund et al., 2012). Of note, recently this protein format was further improved by varying the linker lengths between the single TRAIL monomers (Siegemund et al., 2016) (Figure 6). In an alternative approach, a scTRAIL moiety was fused to the Fc part of an (immunoglobulin G) IgG antibody. Thereby, formation of disulphide bonds between two Fc parts resulted in the formation of the hexavalent TRAILR agonist, Fc-scTRAIL (or Fc-scTRAIL 1551). EGFR targeting was furthermore achieved by fusing Cetuximab derived scFv to the N-terminus of Fc-scTRAIL (Hutt et al., 2017) (Figure 6). In subsequent studies it was shown that being able to bind to the EGFR increased significantly the bioactivity of the investigated antibody TRAIL fusion proteins *in vitro*, most likely due to increased clustering of TRAILR. However, surprisingly this positive effect of targeting did not translate *in vivo*. It might be speculated that high affinity to the EGFR impaired tumour penetration and/or resulted in binding of the protein to tumour distant tissue that expressed low amounts of the receptor (Hutt et al., 2018). Taken together, although generated TRAILR agonists could so far not meet the high expectations that were initially set into them, there is still reason for legitimate hope that in the future 2nd generation compounds might catch up on them. However, as many tumours are initially TRAIL-resistant, it will be important to carefully select patients that benefit from treatment as well as to find suitable co-treatments for sensitisation.

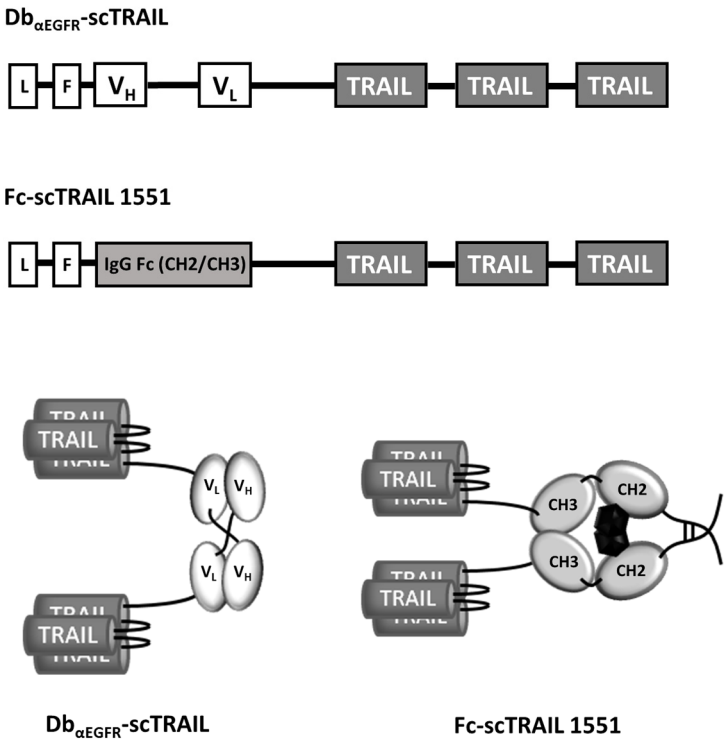

Figure 6: Structure of two 2nd generation TRAILR agonists

A scFv fragment (V_H = variable domain of the heavy chain; V_L = variable domain of the light chain) of the EGFR-binding antibody cetuximab is fused to scTRAIL which results, after non-covalent dimerisation, in the formation of Db$_{\alpha EGFR}$-scTRAIL (Siegemund et al., 2012; Siegemund et al., 2016). Fc-scTRAIL is generated by fusing the Fc part of an human IgG antibody (CH = constant domain of the heavy chain) to scTRAIL. Dimerisation is hereby achieved via disulphide bonds (Hutt, 2017). F = FLAG tag; L = Igκ chain leader sequence.

1.5 Endoplasmic reticulum stress and the unfolded protein response

In eukaryotic cells the ER is responsible for Ca^{2+} homeostasis as well as folding and transport of newly generated proteins. However, several adverse conditions are known to disturb this fragile equilibrium, causing ER stress (reviewed by Hetz, 2012; reviewed by Iurlaro and Muñoz-Pinedo, 2016; reviewed by Lindholm et al., 2017). Amongst these, especially the withdrawal of oxygen and nutrients is fatal, as it results in insufficient ATP generation to supply the energy-intensive processes of protein folding. Furthermore, oxygen is also needed for the formation of disulphide bonds while glucose is necessary for the glycosylation of proteins (Kaufman et al., 2002; Schönenberger, 2015; Sies and Bruene, 2007). Alongside hypoxia and starvation, both conditions that occur in fast proliferating, solid tumours as well as in large MCTSs, ER stress can also be induced by disturbed Ca^{2+} homeostasis, which results in the inhibition of calcium-dependent chaperons or by viral

infections that overload the cell with virus-encoded proteins (von dem Bussche et al., 2010; reviewed by Coe and Michalak, 2009; reviewed by He, 2006). In response to ER stress the UPR is induced, which in the beginning attempts to reduce the amount of unfolded and misfolded proteins by breakdown of mRNA, enlargement of the ER membrane and synthesis of protein folding chaperons, however in unresolved ER stress apoptosis is initiated (Figure 7). First, the chaperon binding immunoglobulin protein (BIP) binds to unfolded or misfolded proteins thereby allowing the activation of the three axes of the UPR. In the inositol-requiring protein 1α-X box-binding protein-1 (IRE1α-XBP-1) branch, sequestering of BIP allows the dimerisation and subsequent autophosphorylation of the protein IRE1α that possesses both kinase and endoribonuclease activity. Under low ER stress, activated IRE1α cleaves the precursor mRNA XBP-1u to XBP-1s which results in the translation of the transcription factor XBP-1 that induced the expression of the transcription factor CHOP and of proteins involved in protein quality control as well as ER associated degradation (ERAD). Furthermore, XBP-1 was also shown to influence phospholipid synthesis and thus contribute to the enlargement of the ER membrane. In cases of prolonged ER stress, XBP-1 translation is reduced and IRE1α-dependent decay of mRNAs (RIDD) plays a more important role (reviewed by Hetz, 2012; reviewed by Iurlaro and Muñoz-Pinedo, 2016; reviewed by Lindholm et al., 2017). Already under basal conditions RIDD was shown to actively contribute to ER homeostasis by regulating the translation of many proteins involved in protein folding but also in cell cycle progression and apoptosis. Furthermore, it was shown that RIDD increased with increasing ER stress and was suggested to finally overrun the ER stress resolving functions of XBP-1, inducing apoptosis by splicing mRNAs that code for anti-apoptotic proteins for example (reviwed by Maurel et al., 2014). Alongside its function as ribonuclease, IRE1α was also shown to recruit the adapter protein TRAF2 which can lead to activation of JNKs and subsequent apoptosis induction (Lee et al., 2011; Urano et al., 2000). Taken together, signalling via the IRE1α axes might be pro- or anti-apoptotic *in vivo* most likely depending on the strength and duration of the ER stress stimulus. However to date, regulation of this decision has not yet been investigated in much detail. In the second branch of the UPR, the inactive transcription factor ATF6 is transported from the ER to the Golgi apparatus during ER stress, where it is activated via two intramembranous proteases. Activated ATF6 then subsequently induces the expression of ERAD components and the transcription factors XBP-1 and CHOP as well as ER chaperons such as BIP (Baumeister et al., 2005; reviewed by Lindholm et al., 2017; Yoshida et al., 2000). Finally, in the third axis of the UPR, activation of the protein kinase RNA-like endoplasmic reticulum kinase (PERK), via detachment of BIP, results in the phosphorylation and inactivation of the eukaryotic translation initiation factor 2α (eIF2α). Without active eIF2α, translation of proteins that lack an internal site for ribosomal entry is impaired thus overall protein translation is attenuated.

However, the expression of individual proteins such as transcription factor ATF4 is even enhanced in the presence of phosphorylated eIF2α which results in the transcription of proteins that are involved in protein folding and transport or take part in the antioxidant response (Harding et al., 2003; reviewed by Iurlaro and Muñoz-Pinedo, 2016). Alongside this, ATF4, similar to XBP-1 and ATF6, also induces the expression of the transcription factor CHOP which was shown to be responsible for the execution of apoptosis during prolonged ER stress by, among other things, downregulating Bcl-2 and/or upregulating TRAILR2 amounts (Martín-Pérez et al., 2012; Mc Cullough et al., 2001; Yamaguchi and Wang, 2004). As described earlier, only very recently it was shown that high amounts of intracellular TRAILR2 can induce ligand-independently apoptosis by most likely forming a platform in which procaspase 8 becomes activated (Lu et al., 2014). The decision between the attempt to resolve ER stress and the induction of apoptosis is complex and not yet completely understood. Regarding the upregulation of TRAILR2 via CHOP it was for example shown that, in the beginning of ER stress, TRAILR2 mRNA is constantly degraded by IRE1α. However, during persistent ER stress, induction of TRAILR2 expression overruns the degradation process (Lu et al., 2014). Taken together the ER stress-induced UPR is a complex interplay of different signalling cascades that regulates ER homeostasis. Since tumour cells often grow under ER stress due to nutrient and oxygen deprivation, treatment with drugs that enhance the UPR thus inducing apoptosis, might be a promising approach in cancer therapy. Furthermore, it was already shown that ER-stressed cancer cells are more susceptible to TRAILR treatment than unstressed cells, most likely due to upregulation of TRAILRs or downregulation of anti-apoptotic proteins (Edagawa et al., 2014; Liu et al., 2004; Martín-Pérez et al., 2012; Yamanaka et al., 2006).

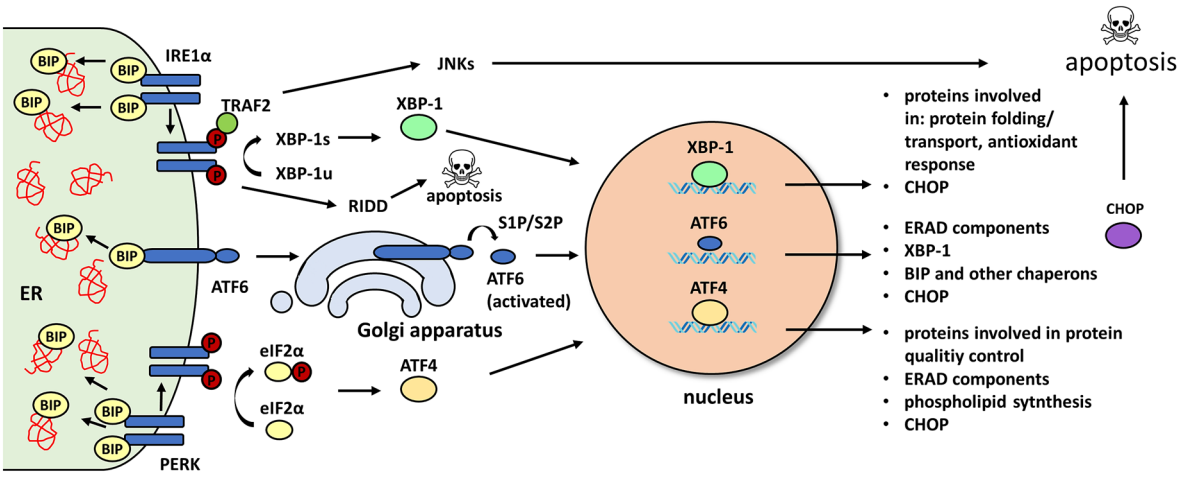

Figure 7: Schematic of the unfolded protein response

Unfolded and misfolded proteins (🔥) induce the three branches of the UPR resulting in the transcription of proteins that resolve ER stress (mild stress conditions) or induce apoptosis (persistent ER stress).

1.6 Cyclooxygenase II and Cyclooxygenase II inhibitors

Cyclooxygenases, also called prostaglandin H synthases, are part of the superfamily of myeloperoxidases and catalyse the conversion of the fatty acid arachidonic acid (AA) to prostaglandin H_2 (PGH_2) in a two-step process. First AA is oxidised to prostaglandin G_2 (PGG_2) at a catalytic site with cyclooxygenase activity before it is finally reduced to PGH_2 in a second catalytic centre with peroxidase activity. PGH_2 is then converted to prostaglandin E_2 (PGE_2), prostaglandin I_2 (PGI_2), prostaglandin D_2 (PGD_2), prostaglandin F_{2a} (PGF_{2a}) and thromboxane A_2 (TxA_2) by distinct prostaglandin synthases (reviewed by Greenhough et al., 2009). Prostaglandins and TxA_2 generated in this way are released by the cells and can exert their function in an autocrine and paracrine way via binding to different G-protein coupled receptors (reviewed by Ricciotti and Fitzgerald, 2011). In the human body two isoforms, cyclooxygenase I and II (COX I and COX II), are expressed that share 60% amino acid identity (Kurumbail et al., 1996). COX I is constitutively expressed in many tissues, such as the kidney, lung and the gastrointestinal tract as well as in platelets. In the gastrointestinal mucosa, PGE_2 and PGI_2 act cytoprotectively while TxA_2 generated in platelets induces their aggregation (reviewed by Chandrasekharan and Simmons, 2004). The second isoform of the enzyme, COX II, is also constitutively expressed in some few organs and tissues such as the brain, kidney and endothelial cells, where it is implicated in memory formation as well as learning, control of the renal blood flow and cytoprotection (reviewed by Grosser et al., 2006; reviewed by Patrignani and Patrono, 2015; reviewed by Yagami et al., 2016). However, its main function is to increase the blood flow and regulate the function of immune cells

during inflammation, when its expression is induced by different growth factors and cytokines (reviewed by Ricciotti and Fitzgerald, 2011). Furthermore, it was also shown that the expression of COX II can be upregulated under hypoxia and in response to signals released from necrotic cells (Kaidi et al., 2006; Sha et al., 2013). Interestingly, enhanced COX II expression was found in many tumours of epithelial origin, such as colon, lung, breast and prostate, correlating with a poor prognosis due to enhanced proliferation, vascularisation, invasion and metastasis (Brown and DuBois, 2005; Gupta et al., 2000; Soslow et al., 2000; Williams et al., 1999). Best investigated thus far is the function of PGE_2 as it was shown to increase tumour cell proliferation by promoting EGFR, PI3K/Akt, Src kinase, extracellular-signal regulated kinase (ERK), cAMP/protein kinase A and β-catenin signalling (Castellone and Teramoto, 2005; Leone et al., 2007; Pai et al., 2002; Pozzi et al., 2004; Sheng et al., 2001; Tessner et al., 2004). In addition, this prostaglandin was shown to upregulate the anti-apoptotic protein Bcl-2 and inhibit the translocation of Bax to the mitochondria thus protecting cells from apoptosis (Leone et al., 2007; Sheng et al., 1998). Lastly, PGE_2 was also demonstrated to enhance metastasis and induce the expression of vascular endothelial growth factor (VEGF), which is necessary for neovascularisation of growing tumours (reviewed by Gately, 2000; Kundu et al., 2014; Majima et al., 2000). Alongside the pro-tumourigenic functions of generated PGE_2, high expression of COX II was also shown to correlate with TRAIL resistance due to low expression of TRAILR1/R2 and knockdown of the enzyme as well as treatment with COX II inhibitors was found to increase expression of the receptors and enhance susceptibility *in vitro* (Chandrasekaran et al., 2014; Tang et al., 2002). However, the underlying mechanism for this observation has yet to be investigated.

Due to the previously mentioned pro-tumourigenic functions of COX II and its product PGE_2, inhibiting COX I/II activity seems to be a promising approach to prevent the development of cancer or reduce tumour progression. Furthermore, inhibition of COX enzymes might also impede the previously described phoenix rising pathway, where PGE_2 released from dying cells, promotes surrounding tissue to proliferate. Cyclooxygenase inhibitors, also called non-steroidal anti-inflammatory drugs (NSAIDs), are already used for over 100 years to treat inflammation and pain. The first compound to be developed in 1897 was the COX I selective inhibitor aspirin. Since then, many non-selective NSAIDs, such as ibuprofen, were discovered and used in the clinic. However, as prostaglandins generated by the constitutively expressed enzyme COX I are necessary in the human body to ensure housekeeping functions, such as the protection of the gastrointestinal tract, the prolonged application of non-selective NSAIDs often causes severe side effects. In order to reduce these adverse implications, much effort was put into the research for new compounds that solely inhibit the activity of COX II. Finally, this led in the nineties to the discovery of the first COX II selective drugs NS-398 and

celecoxib of which the latter was only shortly after approved for the treatment of arthritis and pain. However, even though selective COX II inhibitors were indeed shown to no longer cause destruction of the gastric mucosa, both non-selective and COX II selective NSAIDs, were only recently demonstrated to increase the risk for cardiovascular diseases such as hypertension and stroke when applicated for a longer time period (reviewed by Patrignani and Patrono, 2015). Therefore, comparable to non-selective NSAIDs, also a prolonged application of COX II specific compounds is not recommended. Since 1970, when it was realised for the first time that malignant colorectal tissue showed a higher expression of PGE_2 than surrounding healthy mucosa, numerous studies were carried out demonstrating that non-selective NSAIDs can prevent the formation of many different tumour types when used in low concentrations and for a time period longer than 5 years. Furthermore, NS-398 and celecoxib were also shown to inhibit proliferation of tumour cells both *in vitro* and *in vivo* (Grösch et al., 2001; Yao et al., 2004). Thereby, it has become apparent that the drugs do not only hinder cell cycle progression by inhibiting the production of prostaglandins, but also by regulating the expression of cell cycle-relevant proteins such as cyclin A, B, D, p27 and p21 in a COX II independent manner (Baek et al., 2007; Smith et al., 2000; Sobolewski et al., 2015; Vaish et al., 2014). Alongside their anti-proliferative capacity, NS-398 and celecoxib were also shown to induce apoptosis in different tumour types *in vivo* and *in vitro* as well as to sensitise cancer cells to TRAIL treatment. Interestingly, in many cases tumour cells were, independent of their expression of COX II, primed for apoptosis by an upregulation of TRAILR2 and/or downregulation of survivin or cFlip (Chen et al., 2007; Liu et al., 2004; Oh et al., 2010; Pyrko et al., 2006; Qiu et al., 2012; Yamanaka et al., 2006). As an underlying mechanism it was suggested that drugs like NS-398 and celecoxib can not only inhibit COX II but at the same time also induce ER stress in cancer cells, resulting in an activation of the UPR which subsequently leads to an transcriptional upregulation of TRAILR2 which, as described earlier, can result in the induction of apoptosis (Cano-González et al., 2018; Edagawa et al., 2014; reviewed by Jendrossek, 2013; Lu et al., 2014; Yamaguchi and Wang, 2004). Taken together, COX II specific NSAIDs are promising candidates for the treatment of different malignancies, with celecoxib being currently tested in several clinical trials as single treatment or in combination with other anti-cancer agents (DrugLib.com, 2006; National Cancer Institute). However, as mentioned previously in this thesis, their long term harmful effects on the cardiovascular system most likely exclude them from being used in cancer prevention.

1.7 Aim of the thesis

Due to its unique ability of inducing apoptosis solely in malignant cells while sparing normal tissue, TRAIL has been investigated extensively for a possible application in cancer therapy, however to date with only very limited success. The cause for this failure was not only the insufficient activity and poor half-life of the TRAILR agonists but also the initial TRAIL resistance of many tumour types. Interestingly, it was found that not only pro-tumourigenic mutations but also adverse conditions such as hypoxia and nutrient starvation, that occur in poorly vascularised tumours and small micrometastases, can render single cells within a tumour resistant to TRAIL. The major aim of this thesis was to investigate the effects of 2nd generation TRAIL agonists with improved bioavailability and potency on cancer cells cultivated as MCTSs, thereby uncovering the underlying mechanisms of emerging TRAIL resistance. In order to achieve this, first, MCTSs, generated from different cancer cell lines, were examined regarding their suitability as a model system for solid tumours. Solid poorly vascularised tumours are characterised by the presence of proliferative, quiescent and dead cells. Therefore, it was aimed to characterise the growth, presence and spatial distribution of such cells in MCTSs. Once the MCTSs were established as a good model system of solid tumours, they were utilised to examine the TRAIL-susceptibility of cancer cells grown in 3D. To uncover underlying reasons for the observed existence of a TRAIL-resistant cell population within MCTSs, overall expression and spatial distribution of apoptosis-relevant proteins was investigated. Furthermore, hypoxia and nutrient starvation were applied to 2D-cultivated cells in order to mimic environmental conditions encountered within MCTSs, thus examining the potential mechanisms of resistance within the spheroids. Lastly, it was looked to re-sensitise TRAIL-resistant cells within MCTSs to enhance overall treatment effectiveness by pre-incubation with COX II inhibitors. Thereby, also the potential mechanisms of synergism were investigated. Of note, as this project was part of the excellence cluster of the University of Stuttgart, SimTech, the generated data was also utilised by systems biologist and engineering collaborators for the generation and validation of models simulating the growth and drug responsiveness of micrometastases.

2 Materials

2.1 Cell lines

HCT116	human colorectal carcinoma cell line purchased from Banca Biologica e Cell Factory-IST Genova, IRCCS Azienda Ospedaliera Universitaria, San Martino
HCT116 T1 KO	human colorectal carcinoma cell line with knockout (KO) of TRAILR1 (T1, exon 1) generated by the transcription activator-like effector nuclease (TALEN) approach; kindly provided by Olivier Micheau, INSERM, UMR866, Dijon,
HCT116 T1 KO/T2 sKO	human colorectal carcinoma cell line HCT116 with knockout of TRAILR1 (exon 1) and partial knockout of TRAILR2 (exon 3, only gone from the cell surface, but high amounts to be found intracellularly) generated by the TALEN approach; kindly provided by Olivier Micheau, INSERM, UMR866, Dijon, France
HCT116 T2 KO	human colorectal carcinoma cell line purchased from Banca Biologica e Cell Factory-IST Genova, IRCCS Azienda Ospedaliera Universitaria, San Martino with knockout of TRAILR2 generated by the clustered regularly interspaced short palindromic repeats/CRISPR associated 9 (CRISPR/Cas9) approach (Alexandra Mack)
HCT116 T2 sKO	human colorectal carcinoma cell line HCT116 with partial knockout of TRAILR2 (T2, exon 3, only gone from the cell surface (sKO), but high amounts to be found intracellularly) generated by the TALEN approach; kindly provided by Olivier Micheau, INSERM, UMR866, Dijon, France
HT29	human colorectal adenocarcinoma cell line, kindly provided by the Olayioye group, Institute of Cell Biology and Immunology, University of Stuttgart, Germany

MEF-hT1	murine embryonic fibroblast stably transfected with human TRAILR1
MEF-hT2	murine embryonic fibroblast stably transfected with human TRAILR2
NCI-H460	human non-small-cell lung carcinoma cell line purchased from ATCC, Manassas, USA

2.2 Buffers, solutions and cell culture reagents

0.1% Triton X-100	0.1% (v/v) Triton X-100 in PBS
10 × trypsin/ ethylenediaminetetraacetic acid (EDTA)	Life technologies, Gibco, Karlsruhe, Germany
4% paraformaldehyde (PFA)	4% (w/v) PFA in PBS (pH 7.4); Merck, Darmstadt, Germany
5 x loading buffer	312.5 nM Tris-HCl pH 6.8, 25% (v/v) glycerine, 10% (w/v) SDS, 500 mM DTT, 0.05% (w/v)
Annexin V binding buffer (10 x concentrated)	BD Pharmingen, BD Biosciences, San Diego, USA
blocking solution	5% (v/v) FCS and 0.1% (v/v) Triton X-100 in PBS
Bolt MES SDS Running Buffer (20X)	Thermo Fisher Scientific Inc., Waltham, USA
crystal violet solution	0.5% (w/v) crystal violet powder, 20% (v/v) methanol in ddH_20
Dako target retrieval solution pH 6	Dako, Agilent Technologies, Santa Clara, USA
eosin solution	Carl Roth GmbH & Co. KG, Karlsruhe, Germany
fetal calf serum (FCS) (P30-3309)	PAN-Biotech GmbH, Aidenbach, Germany
freezing medium	10% (v/v) DMSO in FCS
haematoxylin solution	Merck KGaA, Darmstadt, Germany
Neo-Clear solution	Merck KGaA, Darmstadt, Germany
NuPAGE MES SDS Running Buffer (20x)	Thermo Fisher Scientific Inc., Waltham, USA

PBA	PBS + 0.05% (w/v) BSA + 0.02% (w/v) NaN_3 in ddH_20
phosphate buffered saline (PBS)	2.67 mM KCl, 1.47 mM KH_2PO_4, 137.9 mM NaCl, 8.06 mM Na_2HPO_4, pH 7.4
radioimmunoprecipitation assay buffer (RIPA buffer)	1% (v/v) NP-40, 0.5% (w/v) sodium deoxycholate, 1% (w/v) SDS in TBS
reverse transcriptase buffer	QuantiTect Reverse Transcriptase Kit, QIAGEN, Hilden, Germany
RPMI 1640 medium (+ 2 mM L-glutamine, 21875-034)	Life Technologies, Gibco, Karlsruhe, Germany
RPMI 1640 medium (+ 2 mM L-glutamine; without glucose, 11879-020)	Life Technologies, Gibco, Karlsruhe, Germany
sucrose solution	30% (w/v) sucrose in ddH_20
TBS with Tween-20 (TBST)	0.1% (v/v) Tween-20 in TBS
tris buffered saline (TBS)	20 mM Tris-HCl, 150 mM NaCl in ddH_20, pH 7.4
wipe out buffer	QuantiTect Reverse Transcriptase Kit, QIAGEN, Hilden, Germany

2.3 Chemicals, reagents, recombinant proteins

agarose	Carl Roth GmbH & Co. KG, Karlsruhe, Germany
Annexin V-EGFP	manufactured by Dr. Fabian Richter, Institute of Cell Biology and Immunology, University of Stuttgart
Antibody Diluent	Dako, Agilent Technologies, Santa Clara, USA
blocking reagent	Roche Diagnostics, Mannheim, Germany
bovine serum albumin (BSA)	Sigma-Aldrich, Munich, Germany
bovine serum albumin (BSA) standard	Paesel + Lorei GmbH & Co. KG, Rheinberg, Germany

bromophenol blue	Serva Electrophoresis GmbH, Heidelberg, Germany
Bradford reagent	Carl Roth GmbH & Co. KG, Karlsruhe, Germany
celecoxib	Selleckchem.com; ABSOURCE DIAGNOSTICS GmbH, Munich, Germany
crystal violet powder	Carl Roth GmbH & Co. KG, Karlsruhe, Germany
4', 6-diamidin-2-phenylindol (DAPI)	Thermo Fisher Scientific, Ulm, Germany
$Db_{\alpha EGFR}$-scTRAIL	manufactured by Dr. Martin Siegemund and Doris Götsch, Institute of Cell Biology and Immunology, University of Stuttgart
dimethyl sulfoxide (DMSO)	Carl Roth GmbH & Co. KG, Karlsruhe, Germany
dithiothreitol (DTT)	Carl Roth GmbH & Co. KG, Karlsruhe, Germany
DyNAmo ColorFlash SYBR Green (real-time quantitative polymerase chain reaction (qPCR) Mix (2 x)	DyNAmo ColorFlash SYBR Green qPCR Kit, Biozym Scientific GmbH, Hessisch Oldendorf, Germany
eosin	Carl Roth GmbH & Co. KG, Karlsruhe, Germany
ethanol	Carl Roth GmbH & Co. KG, Karlsruhe, Germany
Fc-scTRAIL 1551	manufactured by the Kontermann group, Institute of Cell Biology and Immunology, University of Stuttgart
Fluoromount-G Slide Mounting Medium	Southern Biotechnology Associates Inc., Birmingham, USA
glycerol	Carl Roth GmbH & Co. KG, Karlsruhe, Germany
Hoechst 33342	Thermo Fisher Scientific, Ulm, Germany
KCl	Carl Roth GmbH & Co. KG, Karlsruhe, Germany
KH_2PO_4	Carl Roth GmbH & Co. KG, Karlsruhe, Germany
methanol	Carl Roth GmbH & Co. KG, Karlsruhe, Germany
Na_2HPO_4	Carl Roth GmbH & Co. KG, Karlsruhe, Germany
NaCl	Carl Roth GmbH & Co. KG, Karlsruhe, Germany

Nonidet P 40 (NP-40)	Sigma-Alderich, Steinheim, Germany
Neo-Mount	Merck KGaA, Darmstadt, Germany
NS-398	Sigma-Aldrich, Munich, Germany
NuPAGE Antioxidant	Thermo Fisher Scientific Inc., Waltham, USA
peroxidase blocking reagent	Dako, Agilent Technologies, Santa Clara, USA
peroxidase labelled polymer	Dako, Agilent Technologies, Santa Clara, USA
protease inhibitor cocktail cOmplete, EDTA free	Roche Diagnostics AG, Basel, Switzerland
Pyronin Y	Sigma-Alderich, Steinheim, Germany
QVD-Oph (QVD)	Sigma-Aldrich, Munich, Germany
reverse transcriptase	QuantiTect Reverse Transcriptase Kit, QIAGEN, Hilden, Germany
reverse transcriptase primer	QuantiTect Reverse Transcriptase Kit, QIAGEN, Hilden, Germany
RNase-free water	QIAGEN, Hilden, Germany
sodium azide (NaN_3)	Carl Roth GmbH & Co. KG, Karlsruhe, Germany
sodium deoxycholate	Carl Roth GmbH & Co. KG, Karlsruhe, Germany
sodiumdodecylsulfate (SDS)	Carl Roth GmbH & Co. KG, Karlsruhe, Germany
substrate chromogen 3, 3'-diaminobenzidine 1:50 in substrate buffer e-chromogen solution	Dako, Agilent Technologies, Santa Clara, USA
sucrose	Carl Roth GmbH & Co. KG, Karlsruhe, Germany
SuperSignal West Dura Extended Duration Substrate	Pierce Protein Research Products, Thermo Fisher Scientific, Ulm, Germany
SuperSignal West Pico ECL Substrate	Pierce Protein Research Products, Thermo Fisher Scientific, Ulm, Germany
Tissue-Tek O.C.T: Compound (TTEK) (Tissue Freezing Medium)	A. Hartenstein GmbH, Wuerzburg, Germany
Tris-(hydroxymethyl)-aminomethane (Tris)	Carl Roth GmbH & Co. KG, Karlsruhe, Germany

Tris-HCl	Carl Roth GmbH & Co. KG, Karlsruhe, Germany
Triton X-100	Carl Roth GmbH & Co. KG, Karlsruhe, Germany
Tween-20	Carl Roth GmbH & Co. KG, Karlsruhe, Germany
xylene substitute Neo-Clear	Merck KGaA, Darmstadt, Germany

2.4 Instruments

-20°C freezer	Comfort NoFrost, Liebherr, Bulle, Switzerland
-80°C freezer	HT5786-A, Hettich lab technologies, Tuttlingen, Germany
bright field slide scanner	Leica SCN400, Leica Microsystems, Wetzlar, Germany
centrifuge	Eppendorf centrifuge 5415R, Hettich lab technologies, Tuttlingen Germany
centrifuge	Heraeus Multifuge 3-LR, Hettich lab technologies, Tuttlingen, Germany
centrifuge	Eppendorf centrifuge 5810R, Hettich lab technologies, Tuttlingen, Germany
cryostat	CM30505, Leica Biosystems Nussloch GmbH, Nussloch, Germany
dish centrifuge	Sprout Minizentrifuge, Biozym Scientific GmbH, Hessisch Oldendorf, Germany
ECL imager	FUSION SOLO S, Vilber Lourmat, Eberhardzell, Germany
ECL imager	Amersham Imager 600, GE Healthcare Europe GmbH, Freiburg, Germany
electrophoresis power supply	EPS 601, Amersham Pharmacia Biotech; GE Healthcare Europe GmbH, Freiburg, Germany
electrophoresis power supply	EPS 301, Amersham Pharmacia Biotech; GE Healthcare Europe GmbH, Freiburg, Germany
film developing machine	Agfa Curix60, Agfa HealthCare GmbH, Cologne, Germany

flow cytometer	MACSQuant Analyser 10, Militneyi Biotec, Bergisch Gladbach, Germany
flow cytometer	LSRFortessa, BD Biosciences, San Diego, USA
heat block	HBT-1-131, Haep Labor Consult, Bovenden, Germany
heat block	Eppendorf Thermomixer compact, Merck KGaA, Darmstadt, Germany
hypoxia chamber	0_2 Control inVitro Glove Box, Coy Laboratory Products, Inc., Grass Lake, USA
hypoxia chamber	Whitley H35 Hypoxystation, Don Whitley Scientific, Shipley, United Kingdom
iBlot 2 Dry Blotting System	Thermo Fisher Scientific Inc., Waltham, USA
incubator	Varocell, Varolab GmbH, Giesen, Germany
incubator	Forma Reach-In CO_2 Incubator, Thermo Fisher Scientific Inc., Waltham, USA
infrared imager	LI-COR Odyssey, LI-COR Biosciences GmbH, Bad Homburg, Germany
inverted digital microscope	EVOS FL Imaging System, Thermo Fisher Scientific, Ulm,
laser scanning microscope	LSM 710, Carl Zeiss MicroImaging GmbH, Jena, Germany
microplate reader	SPARK, Tecan, Meannedorf, Switzerland
microplate reader	Infinite M200, Tecan, Meannedorf, Switzerland
Mini Gel Tank	Thermo Fisher Scientific Inc., Waltham, USA
nitrogen tank	K SERIES cryostorage system, tec-lab GmbH, Taunusstein, Germany
qPCR device	qPCR Cfx96 device, Biorad, Munich, Germany
rotary microtome	RM2255 Mikrotom, Leica Biosystems Nussloch GmbH, Nussloch, Germany
shaking platform	Sarstedt TPM-2, Nuembrecht, Germany
sonifier	SONOPLUS HD 200, BANDELIN electronic GmbH & Co. KG, Berlin, Germany

spectrophotometer	NanoDrop Spectrophotometer ND-1000, Thermo Fisher Scientific, Ulm, Germany
XCell4 SureLock Midi-Cell	Thermo Fisher Scientific Inc., Waltham, USA

2.5 Kits

DyNAmo ColorFlash SYBR Green qPCR Kit	Biozym Scientific GmbH, Hessisch Oldendorf, Germany
Proteome Profiler Human Apoptosis Array Kit	R&D Systems, RTechne GmbH, Wiesbaden-Nordenstadt, Germany
QuantiTect Reverse Transcriptase Kit	QIAGEN, Hilden, Germany
RNeasy Plus Mini Kit	QIAGEN, Hilden, Germany

2.6 Consumables and laboratory equipment

Bolt 4-12% Bis-Tris Plus Gel 1.0 mm x 10 well	Thermo Fisher Scientific Inc., Waltham, USA
Bolt 4-12% Bis-Tris Plus Gel 1.0 mm x 15 well	Thermo Fisher Scientific Inc., Waltham, USA
Bolt 4-12% Bis-Tris Plus Gel 1.0 mm x 17 well	Thermo Fisher Scientific Inc., Waltham, USA
cell culture flasks	Greiner bio-one, Frickenhausen, Germany
cell culture plates	Greiner bio-one, Frickenhausen, Germany
coverslips	Carl Roth GmbH & Co. KG, Karlsruhe, Germany
cryobox	Cryo 1°C Freezing Containers; NALGENE, Thermo Fisher Scientific, Ulm, Germany
cryovial	CELLSTAR; Greiner bio-one, Frickenhausen, Germany
eppendorf tubes	Eppendorf AG, Hamburg, Germany

falcons	Greiner bio-one, Frickenhausen, Germany
iBlot 2 NC Mini Stacks	Thermo Fisher Scientific Inc., Waltham, USA
iBlot 2 NC Regular Stacks	Thermo Fisher Scientific Inc., Waltham, USA
Neubauer counting chamber	Paul Marienfeld, GmbH & Co. KK, Lauda-Königshofen, Germany
NuPAGE 4-12% Bis-Tris Midi Gel 1.0 mm x 20 well	Thermo Fisher Scientific Inc., Waltham, USA
Page ruler Prestained Protein Ladder	Thermo Fisher Scientific Inc., Waltham, USA
PAP Pen for Immunostaining	Kisker Biotech GmbH & Co. KG, Steinfurt, Germany
pipettes	Eppendorf Research Family, Eppendorf AG, Hamburg, Germany; BRAND GmbH & CO. KG, Wertheim am Main, Germany
Polysine Microscope Adhesion Slides	Thermo Fisher Scientific Inc., Waltham, USA
Terasaki multiwell plate	Greiner bio-one, Frickenhausen, Germany
X-ray films	CEA, Stagnas, Sweden

2.7 Antibodies

2.7.1 Antibodies for flow cytometry

Antibody	species	dilution/ concentration	manufacturer
Alexa Fluor 488-conjugated goat ant-rabbit IgG (H+L)	goat	20 µg/ml	Thermo Fisher Scientific Inc., Waltham, USA
Alexa Fluor 488-conjugated goat ant-mouse IgG (H+L)	goat	10 µg/ml	Thermo Fisher Scientific Inc., Waltham, USA
Alexa Fluor 647-conjugated goat ant-mouse IgG (H+L)	goat	4 µg/ml	Thermo Fisher Scientific Inc., Waltham, USA
Alexa Fluor 654-conjugated goat ant-rabbit IgG (H+L)	goat	4 µg/ml	Thermo Fisher Scientific Inc., Waltham, USA
anti-caspase 8 [E6]	rabbit	4.72 µg/ml	Abcam, Cambridge, United Kingdom
anti-cFlip (7F10)	mouse IgG1	3 µg/ml	Enzo Life Sciences, Loerrach, Germany
anti-EGFR (528) fluorescein isothiocyanate (FITC)-conjugated	mouse IgG2a	2 µg/ml	Santa Cruz Biotechnology Inc., Santa Cruz, USA
anti-EGFR	mouse IgG2b	2 µg/ml	Santa Cruz Biotechnology Inc., Santa Cruz, USA
anti-FADD (1C11)	mouse IgG1	1:100	Abcam, Cambridge, United Kingdom
anti-Ki67	rabbit	1:400	Cell Signaling Technology, Danvers, MA, USA
anti-Ki67 (8D5)	mouse IgG1	0.55 µg/ml	Cell Signaling Technology, Danvers, MA, USA

anti-p27 Kip1 (D69C12) XP	rabbit	0.125 µg/ml	Cell Signaling Technology, Danvers, MA, USA
anti-TRAILR1 (MAB347)	mouse IgG1	4 µg/ml	R&D Systems, Wiesbaden-Nordenstadt, Germany
anti-TRAILR2 (MAB6311)	mouse IgG2b	4 µg/ml	R&D Systems, Wiesbaden-Nordenstadt, Germany
anti-TRAILR3 (MAB6302)	mouse IgG1	4 µg/ml	R&D Systems, Wiesbaden-Nordenstadt, Germany
anti-TRAILR4 (MAB633)	mouse IgG1	4 µg/ml	R&D Systems, Wiesbaden-Nordenstadt, Germany
isotype control	mouse IgG1		BD Pharmingen, Heidelberg, Germany
isotype control	mouse IgG2b		BD Pharmingen, Heidelberg, Germany
isotype control	mouse IgG2b		R&D Systems, Wiesbaden-Nordenstadt, Germany
isotype control	mouse IgG2a		BD Pharmingen, Heidelberg, Germany
isotype control	rabbit		Cell Signaling Technology, Danvers, MA, USA

2.7.2 Antibodies for western blotting

antibody	**species**	**dilution/ concentration**	**manufacturer**
anti-Bcl-xl (54H6)	rabbit	1:1000	Cell Signaling Technology, Danvers, USA
anti-BIP (76-E6)	rat IgG2a	1:1000	BioLegend, San Diego, USA
anti-CHOP (GADD 153 (B-3) sc-7351)	mouse IgG1	1:500	Santa Cruz Biotechnology Inc. Santa Cruz, USA

anti-COX II (D5H5)	rabbit	1:1000	Cell Signaling Technology, Danvers, USA
anti-Cox IV	rabbit	1:1000	Cell Signaling Technology, Danvers, USA
anti-Hif-1α (D5F3M)	mouse	1:1000	Cell Signaling Technology, Danvers, USA
anti-LC3-I/-II (LC3B (D11))	rabbit	1:1000	Cell Signaling Technology, Danvers, USA
anti-Mcl-1 (D2W9E)	rabbit	1:1000	Cell Signaling Technology, Danvers, USA
anti-procaspase 3 (8G10)	rabbit	1:1000	Cell Signaling Technology, Danvers, USA
anti-procaspase 3 (clone E83-103)	rabbit	1:1000	EMD Millipore Corporation, Temecula, USA
anti-procaspase 9	rabbit	1:1000	Cell Signaling Technology, Danvers, USA
anti-SMAC (79-1-83)	mouse IgG1	1:1000	Cell Signaling Technology, Danvers, USA
anti-TRAILR1 (DR4 (D9S1R))	rabbit	1:1000	Cell Signaling Technology, Danvers, USA
anti-TRAILR2 (DR5 (D4E9))	rabbit	1:1000	Cell Signaling Technology, Danvers, USA
anti-XBP-1s (Poly6195)	rabbit	1:500	BioLegend, San Diego, USA
anti-XIAP	mouse IgG1	1:1000	BD Biosciences, Heidelberg, Germany
anti-XIAP (3B6)	rabbit	1:1000	Cell Signaling Technology, Danvers, USA
anti-α-tubulin	mouse IgG1	1:1000	Cell Signaling Technology, Danvers, USA
horse radish peroxidase (HRP)-conjugated goat anti-mouse IgG+IgM	goat	1:10000	Dianova, Hamburg, Germany

horse radish peroxidase (HRP)-conjugated goat anti-rabbit IgG+IgM	goat	1:10000	Dianova, Hamburg, Germany
horse radish peroxidase (HRP)-conjugated goat anti-rat IgG (H+L)	goat	1:10000	Antikoerper-online, Aachen, Germany
IRDye 680 CW-conjugated goat anti-mouse IgG (H+L)	goat	1:10000	LI-COR Biosciences, Lincoln, USA
IRDye 680 CW-conjugated goat anti-rabbit IgG (H+L)	goat	1:10000	LI-COR Biosciences, Lincoln, USA
IRDye 800 CW-conjugated goat anti-mouse IgG (H+L)	goat	1:10000	LI-COR Biosciences, Lincoln, USA
IRDye 800 CW-conjugated goat anti-rabbit IgG (H+L)	goat	1:10000	LI-COR Biosciences, Lincoln, USA
IRDye 800 CW-conjugated goat anti-rat IgG (H+L)	goat	1:10000	Antikoerper-online, Aachen, Germany

2.7.3 Antibodies for immunohistochemistry (IHC)

antibody	**species**	**dilution/ concentration**	**manufacturer**
anti-Hif-1α (clone 54)	mouse IgG1	10 µg/ml	BD Biosciences, Heidelberg, Germany
anti-thymidine kinase 1	rabbit	10 µg/ml	Abcam, Cambridge, United Kingdom
anti-TRAILR1 (sc-6823)	goat	0.27 µg/ml	Santa Cruz Biotechnology Inc., Santa Cruz, USA
anti-TRAILR2 (TR2.21)	mouse IgG	20 µg/ml	AdipoGen Life Sciences, San Diego, USA

bridging antibody rabbit anti-goat	rabbit	1:500	Gentauer, Aachen, Germany

2.7.4 Antibodies for immunofluorescence staining

antibody	**species**	**dilution/ concentration**	**manufacturer**
Alexa Fluor 647-conjugated goat anti-mouse IgG (H+L)	goat	4 µg/ml	Thermo Fisher Scientific Inc., Waltham, USA
Alexa Fluor 647-conjugated goat anti-rabbit IgG (H+L)	goat	4 µg/ml	Thermo Fisher Scientific Inc., Waltham, USA
anti-cleaved caspase 3 (Asp 175)	rabbit	0.105 µg/ml	Cell Signaling Technology, Danvers, USA
anti-Ki67 (8D5)	mouse IgG1	0.55 µg/ml	Cell Signaling Technology, Danvers, USA
anti-p27 Kip1 (D69C12) XP	rabbit	0.5 µg/ml	Cell Signaling Technology, Danvers, USA

2.7.5 Blocking antibodies

Antibody	**species**	**dilution/ concentration**	**manufacturer**
anti-TRAILR1 (HS101)	mouse IgG1	20 µg/ml	AdipoGen Life Sciences, San Diego, USA
anti-TRAILR2 (HS201)	mouse IgG1	20 µg/ml	AdipoGen Life Sciences, San Diego, USA

2.8 Software

CFX Manager software	Biorad, Munich, Germany
Definiens Tissue Studio 64 software	Definiens AG, Munich, Germany
fiji	distribution of ImageJ (Schindelin et al., 2012)
flowing software 2.5.1	Cell Imaging Core, Turku Centre for Biotechnology, University of Turku and Åbo Akademi University, Finland
FlowJo 7.6.1	Tree Star Inc., Ashland, Oregon, USA
GraphPad Prism 5	GraphPad Software Inc., San Diego, CA, USA
MACSQuantify	MACS Miltenyi Biotec, Bergisch Gladbach, Germany
Photoshop Elements 10 software	Adobe Systems Inc., San Jose, USA
Zen 2010 (black edition)	Carl Zeiss MicroImaging GmbH, Jena, Germany
Zen Lite 2011 (black edition)	Carl Zeiss MicroImaging GmbH, Jena, Germany

3 Methods

3.1 2D Cell culture

Cell lines were cultivated in RPMI 1640 medium (+ 2 mM L-glutamine) which was supplemented with either 5% (v/v) heat-inactivated fetal calf serum (FCS) (NCI-H460) or 10% (v/v) FCS (HCT116, HCT116 T1 KO, HCT116 T2 sKO, HCT116 T2 KO, HCT116 T1 KO/T2 sKO, MEF-hTR1, MEF-hTR2, HT29). All stated cell lines grow adherently and were kept in cell culture flasks at 5% CO_2, 37°C and 96% relative humidity in an incubator (Varocell, Varbolab GmbH; Forma Reach-In CO_2 Incubator, Thermo Fisher Scientific Inc.). To maintain a proliferative cell culture, dilution was carried out every 2-3 days. For that purpose, as well as for harvesting, cells were washed with pH 7.4 phosphate buffered saline (PBS) and detached from the surface by treating them with 1 x trypsin (10 x trypsin/ethylenediaminetetraacetic acid (EDTA) solved in PBS) for 2 to 10 min in the incubator. Thereafter, the reaction was stopped with the appropriate amount of medium (10 times more medium than trypsin) and cells were either put back into the flask (diluted 1:10 or 1:20) or prepared for counting. Hereby, the cell suspension was mixed 1:2 with an eosin solution and the number of living cells was determined using a Neubauer counting chamber. For long-term storage, around 2 x 10^6 cells were pelleted by centrifugation (300 g for 5 min, Eppendorf centrifuge 5810R, Hettich lab technologies), supernatant was removed and cells were resuspended in freezing medium (10% (v/v) dimethyl sulfoxide (DMSO) in FCS) before finally transferring them to a sterile cryovial, placing them in a cryobox and freezing them at -80 °C (HT5786-A, Hettich lab technologies). After at least 24 h, frozen vials could then be transferred to a tank containing liquid nitrogen (K-series, tec-lab GmbH).

3.2 Generation of MCTSs

In order to generate equally sized MCTSs (3D cell culture), cells cultivated in cell culture flasks (2D cell culture) were washed with PBS, harvested with 1 x trypsin and finally diluted with the respective media. Thereafter, cells were counted using a Neubauer counting chamber and 25 µl of the prepared cell suspension, with a concentration of 4 x 10^3 cells/ml, were seeded into each well of a Terasaki multiwell plate (100 cells/well). Immediately after seeding, the lid of the Terasaki multiwell plate was closed and the plate was inverted to allow the cells to form small spheres at the bottom of the emerging hanging drop (Figure 8).

Inverted Terasaki multiwell plates were then placed in humid chambers, air permeable small boxes containing dishes with ddH_20 to prevent evaporation of the media, and finally put into the incubator (Varocell, Varbolab GmbH; Forma Reach-In CO_2 Incubator, Thermo Fisher Scientific Inc.). After 2 to 3 days of cultivation, the small spheres were transferred to F-bottom 96-well plates coated with agarose (1.5% (w/v) agarose in RPMI 1960 without FCS) in a volume of 200 µl medium using a pipette equipped with a cut tip. To guarantee sufficient nutrient supply, 50 µl old media was removed and 50 µl new media was added every 2 to 3 days.

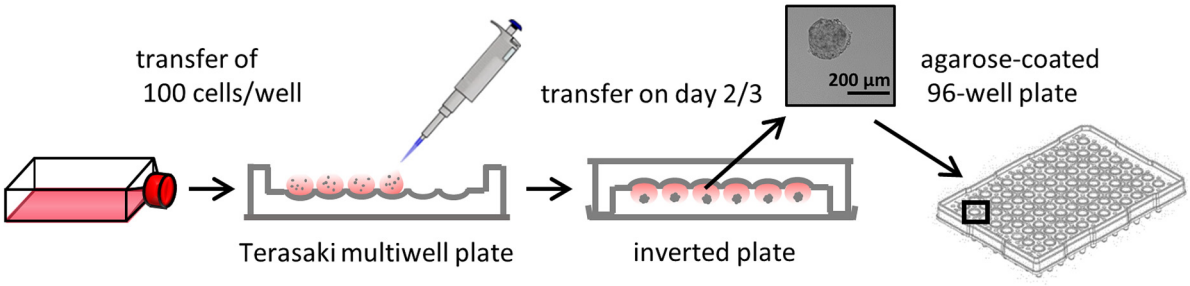

Figure 8: Procedure for MCTSs generation

3.3 Monitoring of MCTS growth

To investigate the growth behaviour of the generated MCTSs, transmitted light pictures were taken daily, every 2-3 days at the same time, with an inverted digital microscope (EVOS FL Imaging System, Thermo Fisher Scientific). Afterwards, images were analysed with the Fiji software (distribution of ImageJ (Schindelin et al., 2012)). It was assumed that generated MCTSs have the form of a sphere and therefore the following simple equation was used to calculate the diameter of the spheroids:

$$d = 2 * \sqrt{\frac{A}{\pi}} \qquad \text{(Eq. 1)}$$

where ***A*** is the measured area of the spheroid and ***d*** is the diameter.

3.4 Determination of cell number per MCTS

2D-cultivated cells were harvested as described above, counted using a Neubauer counting chamber and a cell suspension with 4 x 10^3 cells/ml was prepared. After additionally determining the cell concentration with a flow cytometer (MACSQuant Analyser 10, Miltenyi Biotec) cells were seeded into Terasaki multiwell plates to generate spheroids. At respective days, 7 to 15 spheroids were collected in a 1.5 ml eppendorf tube, washed with PBS and finally incubated with 300 µl 1 x trypsin for 10 min at 37°C on a shaking heat block (Thermomixer compact, Eppendorf). After dissociation of spheroids by pipetting up and down with a 200 µl pipette, cells were transferred into a 15 ml falcon containing 3 ml RPMI 1640 medium with FCS. Following centrifugation (5 min, 500 g, room temperature (RT)) and removal of the supernatant, cell pellet was then solved in exact 200 µl of PBS and cell number per ml was determined via flow cytometry. By knowing the exact volume of the cell suspension and the number of spheroids that were harvested, the number of cells per spheroid can be calculated.

3.5 Flow cytometry

3.5.1 Flow cytometric analysis of cell surface proteins

Cells cultivated in cell culture flasks or 6-well plates (2D cell culture) were washed with PBS and harvested by incubating them for ~10 min with 1 x trypsin at 37°C. After stopping the reaction with cell culture medium, cells were counted and 1 x 10^5 cells per sample were spun down with 500 g for 5 min at 4 °C. Subsequently, the formed pellet was resuspended in ice-cold PBA (0.05% (w/v) bovine serum albumin (BSA) + 0.02% (w/v) NaN_3 in PBS) containing the primary antibody (100 µl/sample) and transferred to a 96-well plate (V bottom) placed on ice. To prepare samples of 3D-cultivated cells, MCTSs (12 spheroids/sample) were collected in a reaction tube (1.5 ml), washed once with PBS and incubated with 1 x trypsin at 37°C on a shaking heat block (Thermomixer compact, Eppendorf) for 10 min to prepare a single cell suspension. After stopping the reaction with medium and dissolving the spheroids by pipetting up and down, the generated cell suspension was in the following treated the same way as the 2D cell culture. After 30 min of incubation with the primary antibody, the plate was spun down at 500 g, for 5 min at 4°C, pelleted cells were resuspended in PBS and after one more centrifugation step cells were incubated with the secondary antibody diluted

in ice-cold PBA (100 µl/sample) for 1 h on ice. Then cells were washed again once with PBA, transferred to a 96-well plate (U bottom) in 100 µl PBA and fluorescence was measured by flow cytometry (MACSQuant Analyser 10, Miltenyi Biotec; LSRFortessa, BD Biosciences).

3.5.2 Analysis of surface TRAILR expression of re-plated MCTS

At day 11 of spheroid cultivation, MCTSs were collected and analysed together with 2D-cultivated cells for their surface TRAILR expression by flow cytometry as described previously. At the same time 2D- and 3D-cultured cells were counted using a Neubauer counting chamber and exact the same number of 2D- and 3D-cultivated cells was seeded into 6-well plates (HCT116: 4 x 10^5 cells/well; NCI-H460: 2 x 10^5 cells/well). At day 1, 2 and 3 after seeding, surface TRAILR expression was again determined by flow cytometry. During selected experiments, cell number was additionally determined every day using the Neubauer counting chamber.

3.5.3 Flow cytometric analysis of intracellular proteins

2D- and 3D-cultivated cells were harvested as described previously (2 x 10^5 cells/sample), washed with PBS and fixed with 4% paraformaldehyde (4% PFA (v/v) in PBS) for 10 min at RT. After two times washing with PBS, the pellet was resuspended in ice-cold PBS (10 µl) and 90 µl methanol (100%, stored at -20°C) was given drop wise to the cells by simultaneously pipetting up and down to prevent clumping. Following 30 min of incubation on ice, 50 µl PBA containing 5% (w/v) BSA (washing solution) was added to the samples prior to spinning them down at 500 g for 5 min at RT. After two more washing steps, cell pellets were suspended in 100 µl washing solution containing the respective primary antibodies and cells were incubated for 1 h at RT. After another washing step, cells were subsequently incubated with 100 µl washing solution containing the respective secondary antibodies for 1 h at RT. Finally, after a last washing step, cells were resuspended in PBA and fluorescence was measured by flow cytometry (MACSQuant Analyser 10, Miltenyi Biotec).

3.5.4 Combined staining of cell surface and intracellular proteins

In order to analyse receptor expression with regard to the amount of the proliferation marker Ki67 and the quiescence marker p27, protocols described in section 3.5.1 and 3.5.3 were combined.

3.5.5 Correlation analysis

To investigate a possible correlation between the surface expression of receptors (TRAILR1/2/4; EGFR) and the expression of either the proliferation marker Ki67 or the quiescence marker p27 within cells forming HCT116 and NCI-H460 MCTSs, first a linear regression was conducted and the coefficient of determination (R^2) was calculated. The closer R^2 is to 1 the better is the quality of the fit meaning that in case of R^2 equals 1 the linear regression perfectly describes the data. As the data were non-normally distributed, determined by d'Agostino-Pearson Omnibus tests, the Spearman's rank correlation coefficient (ρ) was determined that assesses a monotonic relationship independent if it is linear or not. Thereby, each measured value is assigned a rank relative to all other measured values. Whilst this leads to loss of information, at the same time this makes it more robust against outliers and allows the analyses of data that is not normally distributed. Two data sets are considered as correlated if ρ is close to 1. To test the obtained ρ values for significance, the p value was also determined. All described calculations were performed with the software GraphPad Prism 5 (GraphPad Software Inc.).

3.5.6 Determination of cell cycle status by staining of DNA/RNA with Hoechst 33342/Pyronin Y

Double staining with Hoechst 33342 and Pyronin Y is used to determine DNA and RNA content of living or fixed cells. Pyronin Y is a fluorescent dye that can bind to both DNA and RNA, however in the presence of the fluorescent dye Hoechst 33342 intercalated in DNA, it exclusively stains RNA.

The following protocol was performed either separately or in combination with the staining for intracellular proteins (section 3.5.3).

2D-cultivated cells were detached and MCTSs were dissociated with 1 x trypsin as described above. After centrifugation (500 g, 5 min, RT), the pellet containing single cells was resuspended in 1 ml of Hoechst 33342 staining solution (RPMI 1640 medium with FCS containing 10 µg/ml Hoechst 33342) and cells were incubated for 45 min at 37°C. At the end of incubation time, 5 µl of a Pyronin Y stock solution (100 µg/ml Pyronin Y in ddH_20) were added followed by incubation for another 15 min at 37°C. Finally, cells were centrifuged (500 g, 5 min, RT), resuspended in PBS and analysed by flow cytometry (MACSQuant Analyser 10, Miltenyi Biotec).

For combined staining, samples were first treated as described in section 3.5.2. After incubation with the secondary antibodies and one additional washing step, cells were then stained for Hoechst 33342, followed by Pyronin Y as described previously.

3.5.7 Cell death measurement with Annexin V-EGFP

In viable cells, phosphatidylserine (PS) is embedded in the cell membrane facing the cytoplasm. However, after induction of apoptosis, PS translocates from the inside of the cell membrane to the surface and can there be bound by the protein Annexin V. In the protocol described below, flow cytometry using Annexin V coupled to the enhanced green fluorescent protein (Annexin V-EGFP) was used to determine the percentage of cells that underwent apoptotic cell death.

2D-cultivated cells were harvested as described before and seeded into 96-well plates (F-bottom). Since HCT116 cells need longer than one day to completely attach to the surface they were seeded two days prior to stimulation (single treatment with Fc-scTRAIL 1551/$Db_{\alpha EGFR}$-scTRAIL (both manufactured at the Institute of Cell Biology and Immunology, University of Stuttgart): 7.5 x 10^3 cells/well; combined treatment with COX II inhibitors: 2 x 10^3 cells/well). Unlike HCT116 cells, NCI-H460 cells attach very rapidly and were therefore seeded only one day before stimulation (single treatment with Fc-scTRAIL 1551: 1 x 10^4 cells/well). After treatment with the different compounds for the respective periods of time, the supernatant was transferred to a 96-well plate (U-bottom) and remaining attached cells were washed once with 30 µl PBS that was afterwards also added to the supernatant. Cells were in the following detached with 1 x trypsin and reaction was stopped with the previously collected and centrifuged (5 min, 500 g, 4°C) supernatant. After transfer of all cells to the 96-well plate (U-plate), centrifugation was carried out (5 min, 500 g, 4°C), supernatant was discarded and cell pellets were solved in 100 µl Annexin V binding buffer

(BD Pharmingen, BD Biosciences) containing 1:200 diluted Annexin V-EGFP (produced by Dr. Fabian Richter, University of Stuttgart). After 10 min incubation protected from light, samples were analysed by flow cytometry. To investigate 3D-cultured cells, MCTSs were transferred one day prior to stimulation to an agarose-coated 96-well plate (F-bottom) in an exact volume of 75 µl medium. On treatment day, the different compounds were added (6 spheroids per condition) and stimulation was carried out for the respective periods of time. Thereafter, 3 spheroids plus the associated medium were transferred to a 1.5 ml eppendorf tube and cells were spun down at 500 g for 5 min at RT. Next, the cell pellet was washed once with PBS and spheroids were dissociated with 200 µl 1 x trypsin as described before. In the following, separated cells were treated the same way as 2D-cultured cells.

For stimulation in suspension, 2D-cultured cells were harvested as described previously and 3 x 10^4 cells per sample were seeded into a 96-well plate (U-bottom) in 75 µl cell culture medium. At the same time, around 2 x 30 MCTSs (day 11) were collected in two 1.5 ml eppendorf tubes and dissociated with 300 µl trypsin each, as described before. Thereafter, separated cells in both eppendorf tubes were combined, counted and seeded into a 96-well plate (U-bottom; 3 x 10^4 cells per sample in 75 µl cell culture medium.) Next, Fc-scTRAIL 1551 was added to both, detached 2D-cultured and separated 3D-cultured cells, for 6 hours (2 x concentrated in 75 µl). At the end of stimulation, plate was treated the same way as described for the attached 2D-cultured cells.

3.5.8 Analysis of flow cytometric data

To analyse the data generated by flow cytometry the software FlowJo 7.6.1 (Tree Star Inc.), MACSQuantify (MACS Miltenyi Biotec) and flowing software 2.5.1 (Cell Imaging Core, Turku Centre for Biotechnology, University of Turku and Åbo Akademi University) were used.

3.6 Analysis of localisation-dependent protein expression within sections of MCTSs

3.6.1 Preparation of spheroid cryosections

MCTSs (around 60 per sample) were collected in a 1.5 ml reaction tube, washed with PBS and fixed with 4% PFA for 10 min at RT followed by incubation with a sucrose solution (30% (w/v) sucrose in PBS) for 48 h at 4°C. After removal of the sucrose, 1 ml of Tissue Freezing Medium (Tissue-Tek O.C.T Compound (TTEK); A. Hartenstein GmbH) was added and spheroids were carefully distributed within the solution using a pipette tip. For easier mounting of the frozen spheroids on sample holders, a pipette tip was put on top of the prepared solution in a drop of additional Tissue Freezing Medium (Figure 9). Embedded spheroids were stored at -20°C until usage.

To prepare cryosections, spheroid cores were removed from the reaction tubes by using the embedded pipette tips and mounted on pre-cooled sample holders using one drop of the Tissue Freezing Medium (Figure 9). Afterwards the samples were placed in the pre-cooled cryostat (CM30505, Leica Biosystems; chamber temperature: -20°C; rotating block: -15°C) and finally cut into 10 µm slices. Prepared sections were mounted on Polysine Microscope Adhesion Slides (Thermo Fisher Scientific Inc.) and stored at -20°C.

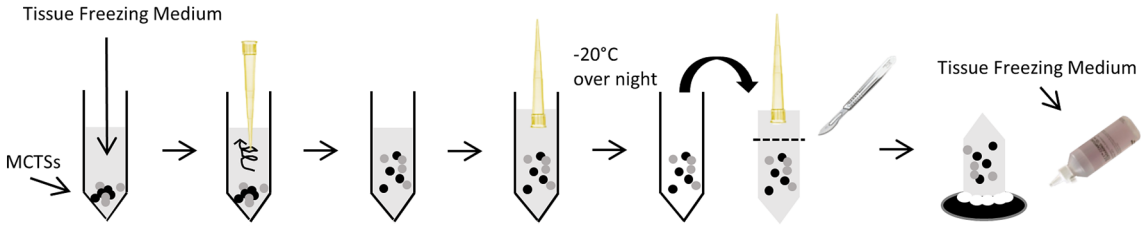

Figure 9: MCTS preparation for sectioning via a cryostat

3.6.2 Preparation of spheroid paraffin sections

MCTSs (around 60 per sample) were collected in a 1.5 ml reaction tube, washed once with PBS and transferred into an agarose bedding (4% (w/v) agarose in ddH_2O). After remaining PBS was removed, MCTSs were in the following stained with 10 µl of a haematoxylin solution

in order to facilitate the localisation of spheroids during the later process of cutting. After immediate removal of surplus haematoxylin, MCTSs were then incubated with 15 µl of a 4% PFA solution for 10 min at RT and finally, after removal of remaining supernatant, spheroids were covered with 1% agarose. Next, agarose cores containing the MCTSs were transferred to embedding cassettes and put into 4% PFA (Figure 10). At the same day, samples were transported to the Dr. Margarete Fischer-Bosch-Institute of Clinical Pharmacology in Stuttgart where the dehydration and subsequent embedding into paraffin took place. In the following, paraffin-embedded MCTSs were cut into 3 µm slices with a rotary microtome (RM 2255 Mikrotom, Leica Biosystems) and resulting sections were transferred to microscopy slides to ensure a tight connection between the spheroid tissue and the surface of the microscopy slides, afterwards samples were incubated at 56°C over night. Such prepared spheroid sections could be stored at RT or directly used for immunohistochemical staining of the respective proteins.

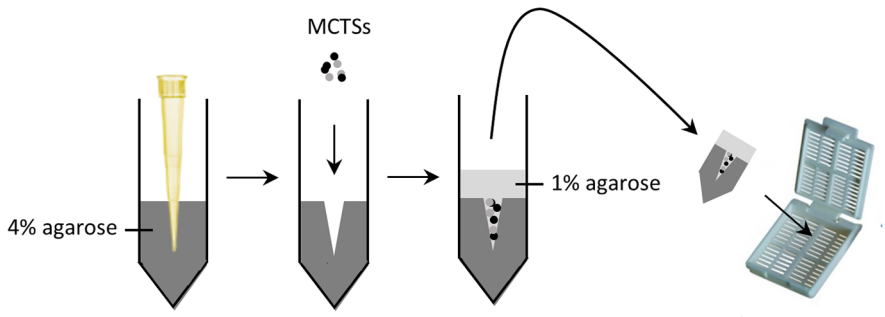

Figure 10: Preparation of MCTSs for embedding into paraffin

3.6.3 Immunostaining of prepared spheroid cryosections

To save antibodies, first MCTSs sections on the microscopy slides were framed using an appropriate pen (PAP Pen for Immunostaining, Kisker Biotech GmbH & Co. KG). Afterwards, sections were washed with PBS followed by fixation for 10 min at RT with 4% PFA and two washing steps with PBS for 5 min. After permeabilisation of the cells with 0.1% Triton X-100 (0.1% (v/v) Triton X-100 in PBS) at RT for 10 min, sections were treated with the blocking solution (5% (v/v) FCS and 0.1% (v/v) Triton X-100 in PBS) at RT for 30 min and then incubated with the respective primary antibodies, again diluted in blocking solution (100 µl), for 1 h at RT. Next, sections were washed two times and incubated with the respective Alexa 647-conjugated secondary antibodies (100 µl, diluted in blocking solution) for 1 h at RT.

After two more washing steps, the DNA was then stained using 4',6-diamidin-2-phenylindol (DAPI) (1 µg/ml in PBS, 10 min, RT). Finally, sections were washed two times with PBS and coverslips were mounted on top of the microscopy slides using Fluoromount-G (Southern Biotechnology Associates Inc.). After at least one night at RT (protected from light), samples were analysed using the laser scanning microscope LSM 710 (Carl Zeiss) and the associated software Zen 2010 black edition (Carl Zeiss).

3.6.4 Immunohistochemical staining of prepared spheroid cryosections

After thawing for 1 h at RT, cryosections were fixed with 100% methanol for 10 min at -20°C, washed with PBS (three times for 2 min) and blocked with a BSA solution (5% (w/v) BSA in PBS) for 10 min at RT. Then sections were washed again with PBS, incubated with 100 µl peroxidase blocking reagent (Dako, Agilent Technologies) for 5 min at RT and after washing with PBS the respective primary antibody (diluted in Antibody Diluent (Dako, Agilent Technologies)) was added for 1 h at RT (100 µl per sample). Next, sections were washed with PBS and then either incubated subsequently with 100 µl of a peroxidase labelled polymer, binding to rabbit or mouse derived primary antibodies (Dako, Agilent Technologies) for 30 min at RT, or in case of the TRAILR1 antibody which derived from goat, first samples were treated with 100 µl of a bridging antibody (rabbit anti-goat IgG, IgM, IgA, Gentauer) for 30 min at RT. Next, sections were washed again with PBS, incubated with 100 µl of a substrate-chromogen solution (chromogen 3, 3'-Diaminobenzidine 1:50 in substrate buffer, Dako, Agilent Technologies) for 10 min and washed under running tap water for 3 min. Staining of the cell nuclei was then performed with a haematoxylin solution (Merck) and stopped after 10 sec with tap water (3 min). Afterwards, cryosection were treated with alcohol solutions (70%, 90%, 100%, each 3 min) and finally incubated with the xylene substitute Neo-Clear (Merck) for 3 min. Lastly, coverslips were mounted on the stained cryosections using Neo-Mount (Merck) and dried samples (over night) were stored at RT until usage.

3.6.5 Immunohistochemical staining of prepared spheroid paraffin sections

Sections were at first deparaffinised with a Neo-Clear solution (Merck) for 30 min at RT and afterwards rehydrated with decreasing concentrations of alcohol (100%, 96%, 70%) and H_2O (3 min each). Next, samples were incubated with a Dako target retrieval solution pH 6 (Dako, Agilent Technologies) for 30 min inside a steam cooker and afterwards washed two times for

3 min with 1 x TBST (Tris-buffered saline with 0.1% (v/v) Tween-20). Treatment with the peroxidase blocking reagent (Dako, Agilent Technologies) as well as all other staining steps were then conducted as described above.

3.6.6 Analysis of stained spheroid cryosections and spheroid paraffin sections

For further investigations of the stained spheroids sections, pictures were taken using a bright field slide scanner (Leica SCN400, Leica Microsystems) and obtained images were analysed using the Definiens Tissue Studio 64 software (Definiens AG). Due to the staining with haematoxylin, the software is able to recognise single cells, which further allows it to show relative staining intensities for the investigated proteins per cell. By manually defining thresholds for different intensity groups, for example low or high expression of the respective protein, the software can visualise the differences in staining intensity by assigning different colours to the different groups (Figure 11B). To determine whether there exists a localisation-dependent expression pattern of the investigated protein, the diameter of the respective spheroid and if present, the diameter of the necrotic core was measured and the remaining area covered with cells was subdivided into three or six layers (Figure 11C/D). Finally, by using the Photoshop Elements 10 software (Adobe Systems Inc.), the percentage of cells in the different spheroid layers, belonging to the particular intensity group, could be determined by measuring the pixels in the respective spheroid layers (Figure 11E).

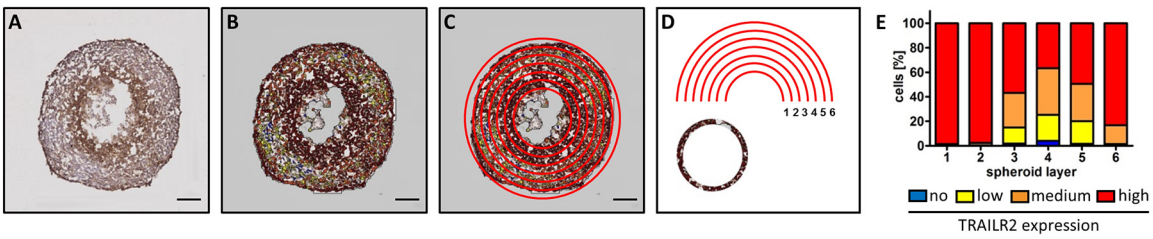

Figure 11: Analysis of immunohistochemically stained spheroid sections

Section of a HCT116 MCTS (d11) immunohistochemically stained for TRAILR2 was scanned with a bright field slide scanner **(A)**. The image was analysed with the Definiens Tissue Studio 64 software **(B)**. The obtained image was analysed for the percentage of cells with no, low, medium and high TRAILR2 expression in the indicated spheroid layers using the Photoshop Elements 10 software **(C/D)**. Scale bars = 100 µm

3.7 Real-time quantitative polymerase chain reaction (qPCR)

To compare mRNA amounts between 2D- and 3D-cultivated cells a qPCR was performed. First, RNA was extracted using the RNeasy Plus Mini Kit (QIAGEN), following the manufacturer's instruction (1 x 10^6 cells/sample; 350 µl RLT buffer; 30 µl RNase-free water). After preparation of RNA, concentration was measured by a spectrophotometer (NanoDrop Spectrophotometer ND-1000, Thermo Fisher Scientific) and samples were either frozen at -80°C or directly used for cDNA synthesis.

For the generation of cDNA, RNA extracts were diluted with RNase-free water (1:10) and RNA (100 ng) was mixed with 2 µl wipe out buffer (QuantiTect Reverse Transcriptase Kit, QIAGEN) to remove remaining DNA. After incubation at 42°C for 2 min, reverse transcriptase (RTase), RTase buffer as well as RTase primers were added and samples were incubated, first for 15 min at 42°C and then 3 min at 95°C, following the manufacturer's instructions (QuantiTect Reverse Transcriptase Kit, QIAGEN). Next, the concentration of generated cDNA was determined and samples were either frozen at -20°C or directly used for qPCR.

Primers used for the qPCR were designed with the webtool Primer-BLAST from NCBI and ordered from biomers. Prior to use, lyophilised primers were reconstructed with RNase-free water (100 pm/µl) and afterwards diluted (1:10) again with RNase-free water to finally use them in the qPCR (Table 2). Prepared reverse and forward primers were mixed with cDNA (100 ng) as well as DyNAmo ColorFlash SYBR Green qPCR Mix (2 x) following the manufacturer's instructions (DyNAmo ColorFlash SYBR Green qPCR Kit, Biozym) and reaction was measured with the qPCR Cfx96 device (Biorad), (Table 1). Control samples, containing RNA and water instead of DNA were run additionally to detect possible contaminations with DNA as well as to verify that the used primers did not bind to remaining RNA. Fold change expression of mRNA was calculated with the ΔΔCt method using the CFX Manager Software (Biorad).

Table 1: qPCR protocol

step	time	temperature	number of cycles
pre-denaturation	7 min	95°C	1
denaturation	10 s	95°C	40
annealing/extension	30 s	60°C	40
melting curve	incremental: 0.5°C for 5 s	65°C – 95°C	1

Table 2: qPCR primer

Primer	forward (5'-3')	reverse (5'-3')
GAPDH	CCCCTTCATTGACCTCAACTA	CGCTCCTGGAAGATGGTGAT
TRAILR1	GGTTGTTCCGTTGCTGTTGG	CCAGAAACACACCCTGTCCAT
TRAILR2-L	CCCTGTTCTCTCTCAGGCATC	CAGGTCGTTGTGAGCTTCTGT
TRAILR2-S	GTCCACAAAGAATCAGGCATC	CCAGGTCGTTGTGAGCTTCT
TRAILR4	GGAGACAGTGACCACCATCC	CGCCGGAAAAGGACTCTGT
COX II	GGCGCTCAGCCATACAG	CCGGGTACAATCGCACTTAT

3.8 Determination of protein amounts by western blot analysis

3.8.1 Preparation of whole cell extracts for western blotting

Cells cultivated in cell culture flasks or 6-well plates (2D cell culture) were washed with PBS and harvested using 1 x trypsin as described above. After the reaction was stopped with cell culture medium, cells were spun down at 500 g for 5 min at 4°C, washed with PBS, transferred to a reaction tube (1.5 ml) and spun down again. MCTSs were collected in a reaction tube (1.5 ml) and washed with PBS. In a next step, lysis buffer (RIPA buffer + protease inhibitor cocktail cOmplete, EDTA free, Roche Diagnostics AG) was added to both, harvested 2D-cultured cells and collected MCTSs, for 5 min on ice, followed by sonication (6 pulses, Bandelin Sonoplus HD 200, BANDELIN electronic GmbH & Co. KG), another incubation step on ice for 5 min and centrifugation for 1.6 x 10^4 g for 15 min at 4°C. Obtained cell lysates were transferred to a reaction tube (1.5 ml) and either frozen at -20°C or directly used for protein determination and sample preparation.

To determine the protein concentration of the generated cell lysates a Bradford assay was conducted. 10 µl of pre-diluted lysate (1:10; 1:20 with ddH_2O) as well as a BSA standard (Paesel + Lorei GmbH & Co; 0.0, 0.125, 0.25, 0.5, 0.75, 1.0, 1.5, 2.0 mg/ml BSA diluted in ddH_2O) and a blank (lysis buffer diluted 1:10 and 1:20 with ddH_2O) were transferred in duplicates to a 96-well plate (F-bottom, clear). After adding 200 µl of the Bradford reagent (Carl Roth GmbH & Co) and incubation for 5 min at RT, absorbance was measured at a wavelength of 595 nm with a microplate reader (Infinite M200 or SPARK, Tecan). Following calculation of the protein concentration, samples were prepared using ddH_2O and 5 x

loading buffer (final concentration: 1 µg/µl - 2 µg/µl protein), incubated for 5 min at 95°C on a heat block (HBT-1-131, Haep Labor Consult) and finally either frozen at -20°C or directly loaded onto the gel.

3.8.2 SDS-PAGE

Prepared samples were loaded together with a protein standard on the respective precast gel and run depending on the gel in the corresponding electrophoresis chamber using the indicated buffers, following the manufacturer's instructions (Table 3).

Table 3: SDS-PAGE supplies from Thermo Fisher Scientific Cooperation

gel	Buffer	Chamber
Bolt 4-12% Bis-Tris Plus Gel 1.0 mm x 10 well	Bolt MES SDS Running Buffer (20X)	Bolt Mini Gel Tank
Bolt 4-12% Bis-Tris Plus Gel 1.0 mm x 15 well	Bolt MES SDS Running Buffer (20X)	Bolt Mini Gel Tank
Bolt 4-12% Bis-Tris Plus Gel 1.0 mm x 17 well	Bolt MES SDS Running Buffer (20X)	Bolt Mini Gel Tank
NuPAGE 4-12% Bis-Tris Midi Gel 1.0 mm x 20 well	NuPAGE MES SDS Running Buffer + NuPAGE Antioxidant	XCell4 SureLock Midi-Cell

3.8.3 Western blot

After the SDS-PAGE, proteins were transferred to a nitrocellulose membrane using the iBlot 2 Dry Blotting System following the manufacturer's instructions (transfer settings: 20 V; 7 min, Thermo Fisher Scientific Inc.). Next, membranes were incubated for at least 1 h with blocking reagent (diluted 1:10 in TBST, Roche Diagnostics) washed three times with TBST for 10 min and incubated with the primary antibody (diluted in TBST with blocking reagent (1:20) and 0.02% (w/v) NaN_3)) over night at 4°C or for 1h at RT. After three more washing steps with TBST, membranes were either incubated with a horseradish peroxidase (HRP) coupled secondary antibody (diluted in TBST with blocking reagent (1:20)) or an IRDye-

conjugated secondary antibody (diluted in TBST with blocking reagent (1:20) and 0.02% (w/v) NaN_3)) for 1 h at RT.

Following three further washing steps, proteins were detected by either directly measuring fluorescence with an infrared imager (LI-COR Odyseey, LI-COR Biotechnolgy GmbH) or incubating the membrane with an HRP substrate (SuperSignal West Pico ECL Substrate/SuperSignal West Dura Extended, Pierce Protein Research Products; Luminata Forte Western HRP Substrate, Merck Millipore) and detecting the signals with an ECL imager (FUSION SOLO S, Vilber Lourmat; Amersham Imager 600, GE Healthcare Europe GmbH). In case of re-probing, membranes were washed three times with TBST before incubating them with additional antibodies.

3.9 Proteome Profiler Human Apoptosis Array Kit

2D-cultivated HCT116 and NCI-H460 as well as HCT116 and NCI-H460 MCTSs (Ø = 500 µm) were collected, washed with PBS and pellets were stored at -20°C. At the day of usage, cells were thawed on ice and resuspended in lysis buffer 17 (provided by the Proteome Profiler Human Apoptosis Array Kit (R&D Systems) and mixed with a protease inhibitor cocktail (cOmplete, Roche Diagnostics)) prior to usage to an approximate concentration of 1×10^7 cells/ml. After 10 min incubation on ice, cells were sonicated (6 pulses, Bandelin Sonoplus HD 200, BANDELIN electronic GmbH & Co. KG), kept on ice again for 10 min and finally centrifuged with 1.4×10^4 g for 5 min at 4°C. Protein concentrations of the lysates were determined using the Bradford assay as described previously and absorbance was measured with a microplate reader (Infinite 200, Tecan). Finally, 300 µg protein per membrane were used to proceed with the assay. All further steps of the array kit were done according to the manufacturer's protocol (Proteome Profiler Human Apoptosis Array Kit, R&D Systems (Bio-Techne GmbH)). At the end, proteins were detected with X-ray films and a film developing machine (Agfa Curix60, Agfa HealthCare GmbH).

3.10 Calculation of the coefficient of drug interaction

The coefficient of drug interaction (CDI) can be calculated to determine whether two drugs act synergistically, additive or antagonistically in inducing cell death (Cao and Zhen, 1989).

$$CDI = \frac{E(AB)}{E(A)*E(B)} \qquad \text{(Eq. 2)}$$

where ***E(A), E(B)*** and ***E(AB)*** are the ratios, in percentage surviving cells, of treating with compound A, B and A+B respectively compared to control groups. A CDI > 1 indicates antagonism while a CDI = 1 points to additivity and a CDI < 1 indicates synergism.

3.11 Clonogenic assay

To investigate long term survival and proliferative capacity of cells surviving treatment with TRAIL, a clonogenic assay was performed.

Thereby, 2D-cultivated HCT116 cells were seeded into 6-well plates 2 days prior to stimulation (4 x 10^5 cells/well) and HCT116 MCTSs (day 11) were transferred to agarose-coated 96-well plates in an exact volume of 75 µl 1 day prior to treatment. Before stimulation with 0.2 nM Fc-scTRAIL 1551 (24 h) was carried out, 2D- and 3D-cultivated cell were pre-treated with 20 µM of the pan caspase inhibitor QVD in DMSO (QVD-OPh, Sigma-Aldrich) for 1h. At the end of stimulation, the supernatant of the 2D-cultured cells was collected and remaining attached cells were harvested with 1 x trypsin. Afterwards, cells from the supernatant as well as detached cells were pooled, spun down (500 g, 5 min, RT) and resuspended in 1 ml of the appropriate cell culture medium. MCTSs (5 spheroids per sample) were collected together with the supernatant in 1.5 ml Eppendorf tubes and dissociated with 200 µl 1 x trypsin as described in section 3.5.1. Next, cells from control samples were counted and 200 cells were seeded into one well of a 6-well plate in a mixture of fresh cell culture medium (1 ml) and conditioned cell culture medium (1 ml). Conditioned cell culture medium is normal cell culture medium that was in contact with cells for 2 to 3 days and hence contains excreted growth factors (medium was centrifuged three times (500 g, 5 min, RT to remove cells)). For seeding an extremely low cell number such as 200 cells/well, these growth factors are needed to allow cell proliferation and prevent cells from undergoing anoikis. To compare long term survival of cells treated with QVD and/or TRAIL with that of cells in the unstimulated wells, exactly the same volume as calculated for the control was seeded from the stimulated samples. After 7 days of cultivation in the incubator,

cells were stained with crystal violet, pictures were taken with an infrared imager (LI-COR Odyseey, LI-COR Biotechnolgy GmbH) at 700 nm and images were analysed with the Fiji software for the number of colonies as well as for the area covered with cells per well of the 6-well plate.

3.12 Staining with crystal violet

Crystal violet is a triarylmethane dye that binds and stains proteins as well as DNA and facilitates the analysis of cell coverage within cell culture plates.

Cells cultivated in 96-well or 6-well plates were washed once with PBS and then incubated with 50 µl (96-well plate) or 300 µl (6-well plate) of a crystal violet solution (0.5% (w/v) crystal violet powder (Sigma-Aldrich), 20% (v/v) methanol in ddH_20) for 15 min at RT. Thereafter, the remaining crystal violet solution was transferred to a waste container, plates were carefully washed under running tab water and finally air-dried over night at RT. Now, either pictures of the plates could be taken with an infrared imager (LI-COR Odyseey, LI-COR Biotechnolgy GmbH) at 700 nm or the dye could be dissolved in methanol to allow cell confluence-dependent absorbance measurements with a microplate reader (Infinite 200, Tecan) at 550 nm. For the latter approach, 50 µl (96-well plate) or 300 µl (6-well plate) of 100% methanol was added into each well and plates were put on a shaking platform (Sarstedt TPM-2) until the dye was completely dissolved.

3.13 Investigation of apoptosis induction with antagonistic TRAILR antibodies

2D-cultured HCT116 and NCI-H460 cells were seeded in a 96-well plate (F-bottom; HCT116: 1 x 10^4 cells/well, NCI-H460: 7 x 10^3 cells/well) in a volume of 100 µl of their respective cell culture medium. The next day, medium was removed and cells were pre-incubated with the respective blocking antibodies for 30 min before they were finally stimulated with 0.1 nM Db_{EGFR}-scTRAIL for 6 h. At the end of treatment, cells were stained with crystal violet and absorbance was measured with a microplate reader at 550 nm (Infinite 200, Tecan), as described in the previous section.

3.14 Induction of hypoxia in 2D-cultivated cells

2D-cultivated HCT116 and NCI-H460 cells were harvested with PBS and 1 x trypsin as described above and seeded into three 6-well plates (1 x 10^5 cells/well). The next day (72 h time point) and the day after (48 h time point) one plate was placed in the hypoxia chamber (O_2 Control InVitro Glove Box, Coy Laboratory Products Inc.; 1% oxygen, 5% CO_2, 37 °C and 96% relative humidity), while the third plate continued to be cultivated in the incubator under standard cultivation conditions (20% oxygen, 5% CO_2, 37°C and 96% relative humidity). At the end of the experiment, cells were washed once with PBS then harvested with 1 x trypsin inside of the hypoxia chamber and immediately put on ice. Of note, to ensure that used solutions were saturated with 1% oxygen and that the air within the falcons used for harvesting was not falsifying the results, trypsin, PBS as well as all used plastic articles (falcons, pipettes, pipette tips) were put into the hypoxia chamber one day prior harvesting. Collected cells were then subsequently analysed for their surface TRAILR expression by flow cytometry or lysed and analysed for overall protein amounts by western blot analysis.

3.15 Glucose and serum starvation with 2D-cultivated cells

2D-cultivated HCT116 and NCI-H460 cells were harvested with PBS and 1 x trypsin as described previously and seeded into two 6-well plates (2 x 10^5 cells/well). The next day (72 h time point) and the day after (48 h time point), cells in the respective plate were washed three times with PBS and incubated with the different media stated in table 4. At the end of the experiment, cells were washed once with PBS and harvested with 1 x trypsin. Collected cells were then subsequently analysed for their surface TRAILR expression by flow cytometry or lysed and analysed for overall protein amounts by western blot analysis.

Table 4: Media used to induce serum starvation and glucose starvation

Media	condition	preparation
RPMI 1640 + 10% FCS + 2 mg/ml glucose (HCT116) + 5% FCS + 2 mg/ml glucose (NCI-H460)	control	
RPMI 1640 + 2 mg/ml glucose	serum starvation	
RPMI 1640 + 10% FCS + 1 mg/ml glucose(HCT116) + 5% FCS + 1 mg/ml glucose (NCI-H460)	glucose starvation 1 mg/ml	RPMI 1640 with glucose (2 mg/ml glucose; 5/10% FCS) mixed 1:2 with RPMI without glucose (5/10% FCS)
RPMI 1640 + 10% FCS + 0.5 mg/ml glucose (HCT116) + 5% FCS + 0.5 mg/ml glucose (NCI-H460)	glucose starvation 0.5 mg/ml	RPMI 1640 with glucose (2 mg/ml glucose; 5/10% FCS) mixed 1:4 with RPMI without glucose (5/10% FCS)
RPMI 1640 + 10% FCS + 0.25 mg/ml glucose (HCT116) + 5% FCS + 0.25 mg/ml glucose (NCI-H460)	glucose starvation 0.25 mg/ml	RPMI 1640 with glucose (2 mg/ml glucose; 5/10% FCS) mixed 1:8 with RPMI without glucose (5/10% FCS)

3.16 Statistical analysis

Statistical analysis was performed using the software GraphPad Prism 5 (GraphPad Software Inc.). Presented quantitative data are mean values plus and minus the standard deviation (SD) or standard error of the mean (SEM) as stated in the figure legends. Statistical significance of differences between groups was verified using the stated significance test. Significance level were denoted with asterisks: * = $p \leq 0.5$; ** = $p \leq 0.01$; *** = $p \leq 0.001$. Means were taken from independently performed experiments. Where applicable, results from each independent repeat were taken from the mean of non-independent technical replicates.

4 Results and discussion

Chapter 1 part 1: Characterisation of HCT116 and NCI-H460 MCTSs

In this chapter, MCTSs were generated from two human cancer cell lines, the colorectal cancer cell line HCT116 and the non-small-cell lung cancer cell line NCI-H460. These MCTSs were then characterised for their cell cycle status and expression of apoptosis-relevant proteins. Analysis of the generated HCT116 and NCI-H460 MCTSs revealed that, in spheroids with a diameter of around 500 µm, two to three layers of proliferative cells enclosed areas that contained high numbers of quiescent cells characterised by low amounts of RNA, low Ki67 and high expression of p27. Furthermore, MCTSs of that size started to undergo cell death from the inside out, which resulted in the formation of a necrotic core.

1.1. Cells within HCT116 and NCI-H460 MCTSs differ in their cell cycle length

In order to generate HCT116 and NCI-H460 MCTSs, 100 cells were seeded per well into Terasaki multiwell plates followed by inversion to allow the cells to form small spheres at the bottom of the emerging hanging drop. After two to three days, the small spheroids were then transferred to agarose coated 96-well plates in a volume of 200 µl and spheroid growth was monitored with an inverted digital microscope. MCTSs generated by HCT116 cells maintained their compact round form until approximately day 25, when they reached a diameter of about 1 mm. Thereafter, growth stagnated and spheroids started to lose their defined surface. For NCI-H460 MCTSs, growth was only monitored until around day 13-16, whereupon, after reaching a diameter of about 750 µm, these spheroids started to lose their round shape and grew unequally in different directions thus making further determination of the diameter impossible. Interestingly, NCI-H460 MCTSs grew faster than HCT116 MCTSs, reaching a diameter of 650 µm at day 11 of cultivation, which means that at this time they were already 30% larger than the HCT116 MCTSs of the same age (Figure 12A/B). To investigate how many cells the MCTSs contained at distinct days of cultivation, HCT116 spheroids were dissociated and the cell number was determined by flow cytometry. In a 2D cell culture, growth always follows a distinct pattern. First cells have to overcome a so-called lag phase in which frequency of division is reduced due to the cells needing to adjust to new environmental conditions. Thereafter, the cell population grows exponentially until finally cells enter a stationary phase where cells stop undergoing cell division due to contact

inhibition and/or nutrient starvation. By comparing the difference in the actual cell number per spheroid, between day 4 and day 7 of cultivation, with the theoretical cell number assuming exponential growth and a cell cycle length of 17.9 h (unpublished data, Daniela Stöhr, diploma thesis, 2013; Eq. 3), we observed a markedly lower cell number in 7-day-old MCTSs than expected (Figure 12C). This result indicates that the MCTSs might comprise of different populations of cells, which differ in their cell cycle length, including cells that need longer to divide than the determined cell cycle length of 17.9 h and cells that don't divide at all. Furthermore, the spheroids might also already contain a necrotic core due to limited access to nutrients, growth factors and oxygen, as well as poor clearance of waste products. This is not only caused by diffusion gradients but also due to the fact that cells at the outside of the spheroids consume the different molecules before they can reach the interior.

$$N_t = N_0 \times e^{\left(\frac{ln2}{17.9}\right)\times t} \qquad \text{(Eq. 3)}$$

Where $\boldsymbol{N_0}$ is the number of cells before and $\boldsymbol{N_t}$ the number of cells after a certain time interval $\boldsymbol{t}$.

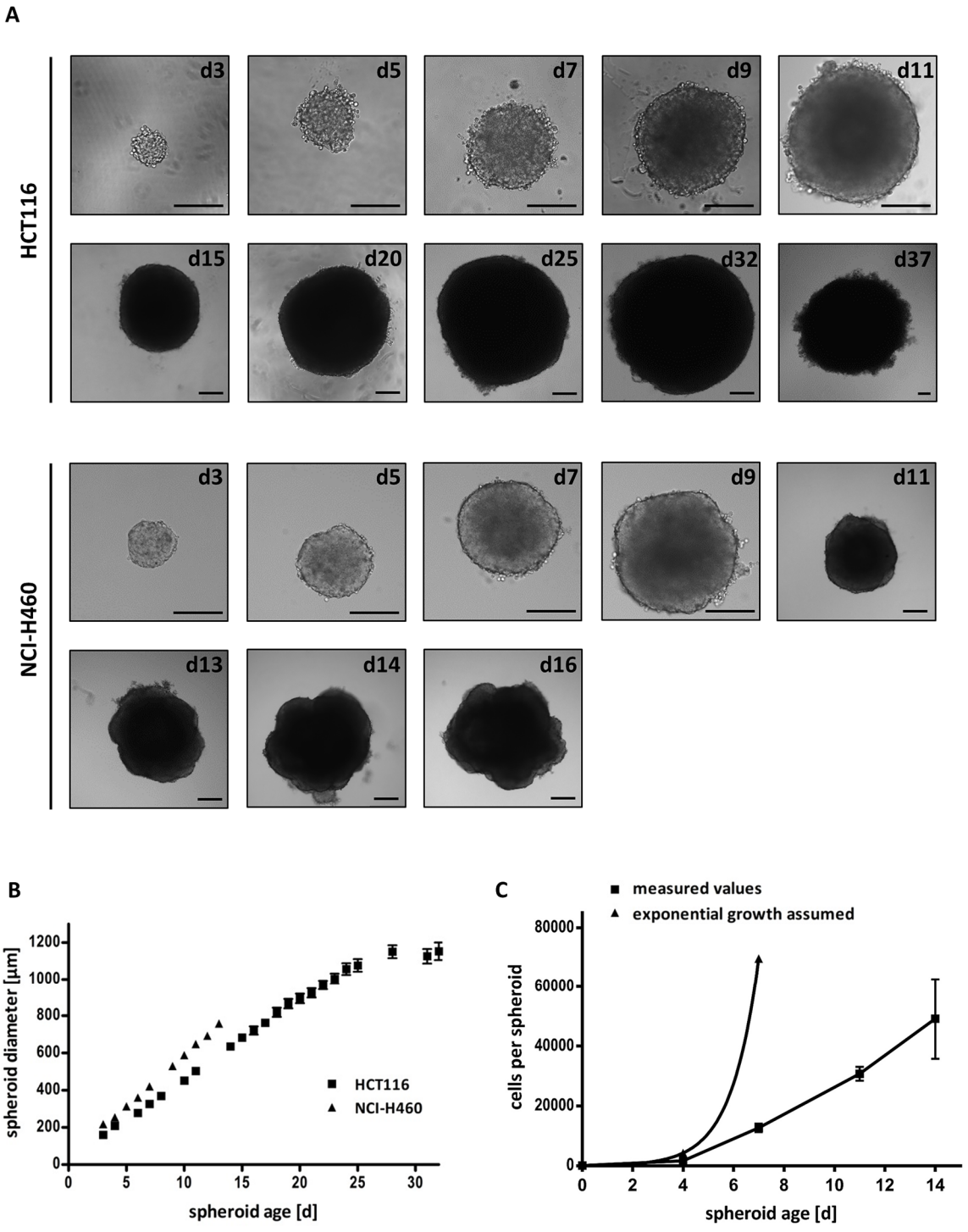
A
HCT116
d3
d5
d7
d9
d11
d15
d20
d25
d32
d37
NCI-H460
d3
d5
d7
d9
d11
d13
d14
d16
B
spheroid diameter [µm]
spheroid age [d]
HCT116
NCI-H460
C
measured values
exponential growth assumed
cells per spheroid
spheroid age [d]

Figure 12: Growth behaviour of HCT116 and NCI-H460 MCTSs

MCTSs were cultivated in agarose-coated 96-well plates with the media changed every third day. Pictures were taken with an EVOS inverted digital microscope and the diameter was determined using the Fiji software. Displayed is the result of one representative experiment of three independent replicates with mean values ± SEM of 3 to 8 spheroids. Scale bars = 200 µm **(A/B).** HCT116 MCTSs were dissociated with trypsin and the number of cells per spheroid was determined by flow cytometry. Shown are mean values ± SD of three to five independent experiments with 7 to 15 spheroids used per experiment and per time point. For comparison, the theoretical cell number of HCT116 MCTSs is shown assuming that all cells within the spheroid remain proliferative and divide, resulting in exponential growth with a cell cycle length of 17.9 h **(C)**.

1.2. MCTS growth gives rise to a cell population with low RNA amount

The growth behaviour of HCT116 and NCI-H460 MCTSs suggested that over time not all cells within the spheroids maintain the average cell cycle length of an exponentially growing 2D culture, with some probably stopping proliferation completely. In fact, it is known that cells which are undersupplied with nutrients, growth factors and oxygen, conditions that also occur in large MCTSs, can enter a so called quiescent state (Daignan-Fornier and Sagot, 2011; reviewed by Hubbi and Semenza, 2015). In this reversible phase, the cell pauses cell cycle progression and slows down its metabolism, which is reflected by a low RNA content. In the following section, HCT116 and NCI-H460 MCTSs were investigated for their percentage of proliferative and quiescent cells using different methods and markers. These experiments were performed together with the diploma student Daniela Maichl.

First, the cell cycle status of spheroid-forming cells was determined by measuring the content of DNA and RNA within single cells. For that purpose, MCTSs were dissociated and single cells were stained with Hoechst 33342/Pyronin Y followed by flow cytometric analysis. Pyronin Y is a fluorescent dye that can intercalate in double stranded DNA and RNA, however if Hoechst 33342 is present and bound to DNA, Pyronin Y selectively stains RNA. Applying this double staining, cells could be subdivided into 4 different populations: Cells in G_1 phase, indicated by diploid DNA content (2n) and high RNA content; quiescent (G_0) cells with the same amount of DNA (2n) but a reduced RNA content; cells in G_2, S, M phases with higher DNA (> 2n) and high RNA content; and cells undergoing cell death with a reduced DNA content (< 2n). An exponentially growing 2D cell culture of the respective cell line was used for gating of the cells (Figure 13A).

In an exponentially growing 2D culture of HCT116 cells, 44% of all cells were in G_1 phase of the cell cycle and around 55% in S/G_2/M phases whereas only a negligible quantity of cells (1%) showed a low RNA content and was therefore designated as quiescent. For the cell line

NCI-H460 the number of quiescent cells was comparable, however the relation between cells in G_1 phase to cells in the other phases was reversed with the majority of the cells being in G_1 phase (52%). After formation of MCTSs, the proportion of cells in the respective cell cycle phases was at first maintained (day 2). In HCT116 MCTSs the number of cells in G_1 phase then increased and the population of cells in $S/G_2/M$ simultaneously decreased until day 9 of cultivation (G_1 = 74%; $S/G_2/M$ = 22%). Two days later, 20% of all cells were quiescent with a consequent decrease in the population of G_1 cells while the quantity of $S/G_2/M$ cells was unchanged (20%). The number of quiescent cells reached approximately 30% by the end of observation (day 23) whereas only about 15% of cells remained in $S/G_2/M$ and 50% in G_1. Furthermore, the development of a cell population with sub G_1 DNA content, which indicates cell death, started at day 14 of cultivation and reached around 3% by day 23 (Figure 13B). For NCI-H460 MCTSs, a more gradual development of the quiescent cell population was observable. Here, the quantity of cells in G_1 phase remained relatively unchanged until the end of observation at day 14 while the number of quiescent cells increased from day 5 onwards with a simultaneous decrease in the $S/G_2/M$ population. In 14-day-old NCI-H460 MCTSs the quiescent cell population reached around 24% whereas only about 11% of all cells were in $S/G_2/M$ phases, 60% in G_1 phase and around 4% were dead (Figure 13C).

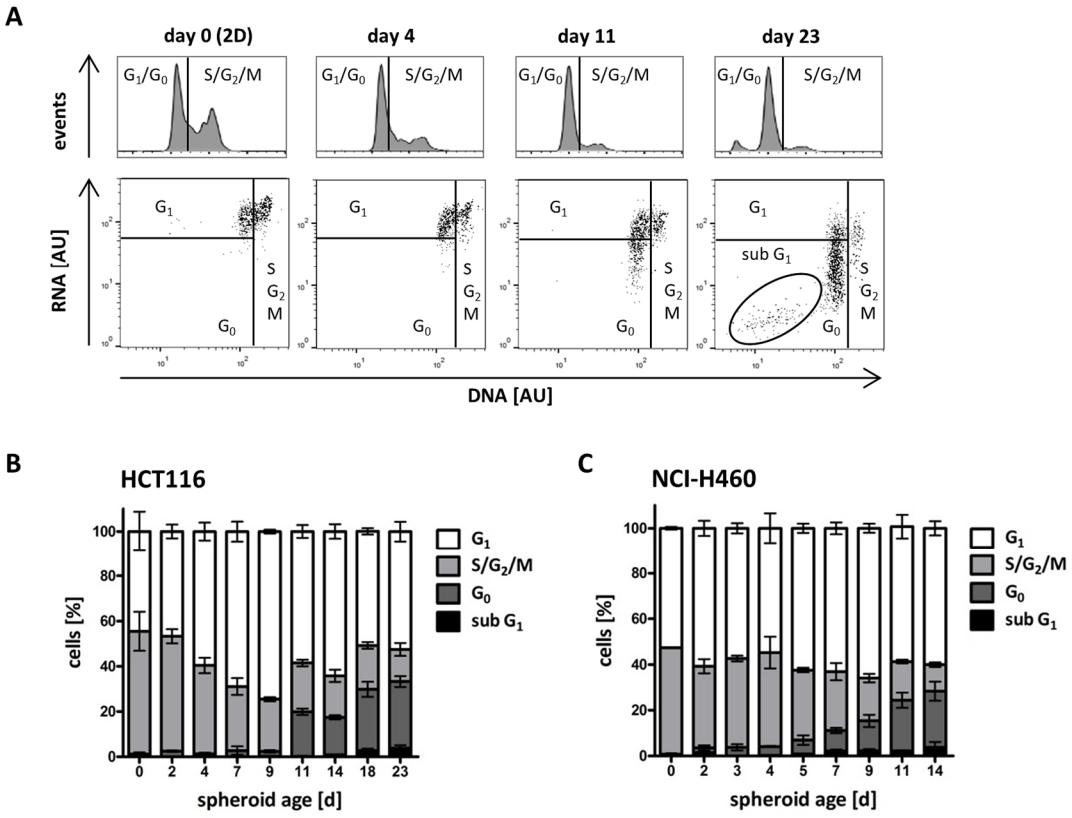

Figure 13: Age-dependent increase of a quiescent cell population within HCT116 and NCI-H460 MCTSs

At indicated days, HCT116 and NCI-H460 MCTSs were harvested, dissociated and the DNA/RNA content of single cells was determined by staining with Hoechst 33342/Pyronin Y following flow cytometry**.** Representative histograms and density blots of 2D-cultured HCT116 cells (day 0) and differently aged HCT116 MCTSs showing the gating strategy that was used to define sub G_1, G_1, $S/G_2/M$ and G_0 phase by the DNA/RNA profiles. AU stands for arbitrary units **(A)**. The percentage of cells in the distinct cell cycle phases, at the indicated time points of cultivation, are depicted. Values are mean ± SD of three independent experiments **(B/C)**. These experiments were conducted by Daniela Maichl.

1.3. With increasing age of MCTSs, the heterogeneity in cell cycle status increases in spheroid-forming cells

In addition to the determination of DNA and RNA content, spheroid-forming cells were also stained for the proliferation marker Ki67 as well as for p27, a protein that is known to be highly expressed in quiescent cells. Using the respective isotype controls to set the gates, spheroid-forming cells could be divided into four different populations: Cells which were positive for Ki67 and negative for p27 ($Ki67^+$ $p27^-$), cells which were positive for both markers ($Ki67^+$ $p27^+$), cells which were positive for the quiescence marker p27 but negative for Ki67 ($Ki67^-$ $p27^+$) and finally cells which were negative for both ($Ki67^-$ $p27^-$). Interestingly, even though the increase in the $p27^+$ cell population within HCT116 and NCI-H460 MCTSs was

comparable over time, the NCI-H460 cells expressed all together higher amounts of the protein. It could be furthermore shown that the population of proliferative $Ki27^+$ $p27^-$ cells within the spheroids, displayed all signs of an exponentially growing 2D cell culture, with cells evenly distributed between G_1, S, G_2 and M phase of the cycle and almost no cells with reduced metabolism, reflected in low amounts of RNA. In both $p27^+$ cell populations, a shift to G_1 phase of the cell cycle was evident together with an increase in the number of cells displaying low amounts of RNA (G_0). Finally, in the $Ki27^-$ $p27^-$ population of cells, the proportion of cells with low RNA content was highest and included cells that were dying or already dead as evident from their DNA content (Figure 14).

By quantifying the results of three independent experiments it could be shown that for both cell lines, with increasing age and diameter of the spheroids, the amount of $Ki67^+$ cells decreased, reaching around 60% in HCT116 MCTSs and 50% in NCI-H460 MCTSs at day 14 of cultivation. Interestingly, already the exponentially growing 2D cultures of both cell lines contained cells that were positive not only for Ki67 but also for p27. After 7 days of cultivation this population reached around 25% in HCT116 MCTSs and 12% in NCI-H460 MCTSs. At the same time, a $Ki67^-$ $p27^+$ as well as $Ki67^-$ $p27^-$ cell population started to develop. By day 14 of cultivation, the size of the latter population stayed approximately the same while the population of $Ki67^-$ $p27^+$ cells increased, reaching around 40% in NCI-H460 MCTS and 30% in HCT116 MCTS (Figure 15).

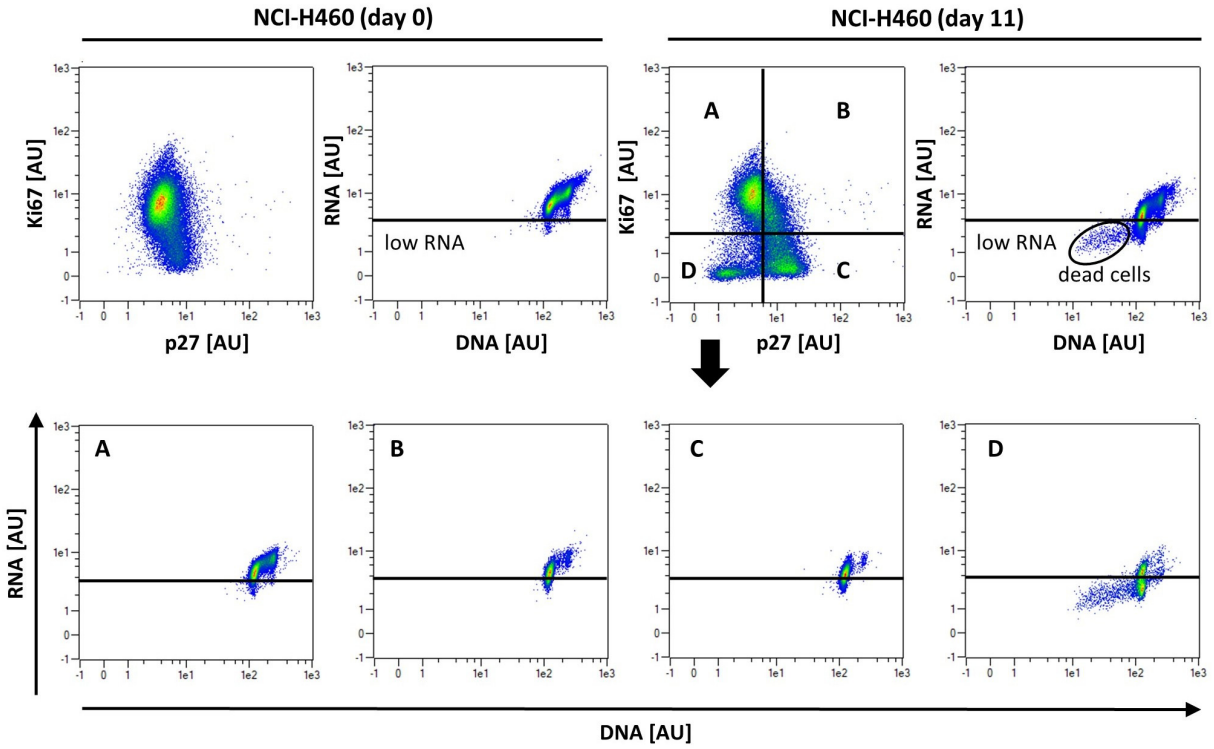

Figure 14: Simultaneous staining of DNA, RNA, Ki67 and p27 in MCTS-forming cells

After detachment of 2D-cultivated NCI-H460 cells and dissociation of NCI-H460 MCTSs, the DNA and RNA of single cells was stained by Hoechst 33342/Pyronin Y and the cells were simultaneously marked for p27, as well as Ki67, with specific antibodies. Thereafter, the fluorescence signals of all four dyes were measured by flow cytometry. Cells were gated for low RNA content according to 2D-cultivated cells. Gating for A: $Ki67^+$ $p27^-$; B: $Ki67^+$ $p27^+$; C: $Ki67^-$ $p27^-$ and D: $Ki67^-$ $p27^-$ was carried out using the respective isotype controls. These experiments were conducted by Daniela Maichl.

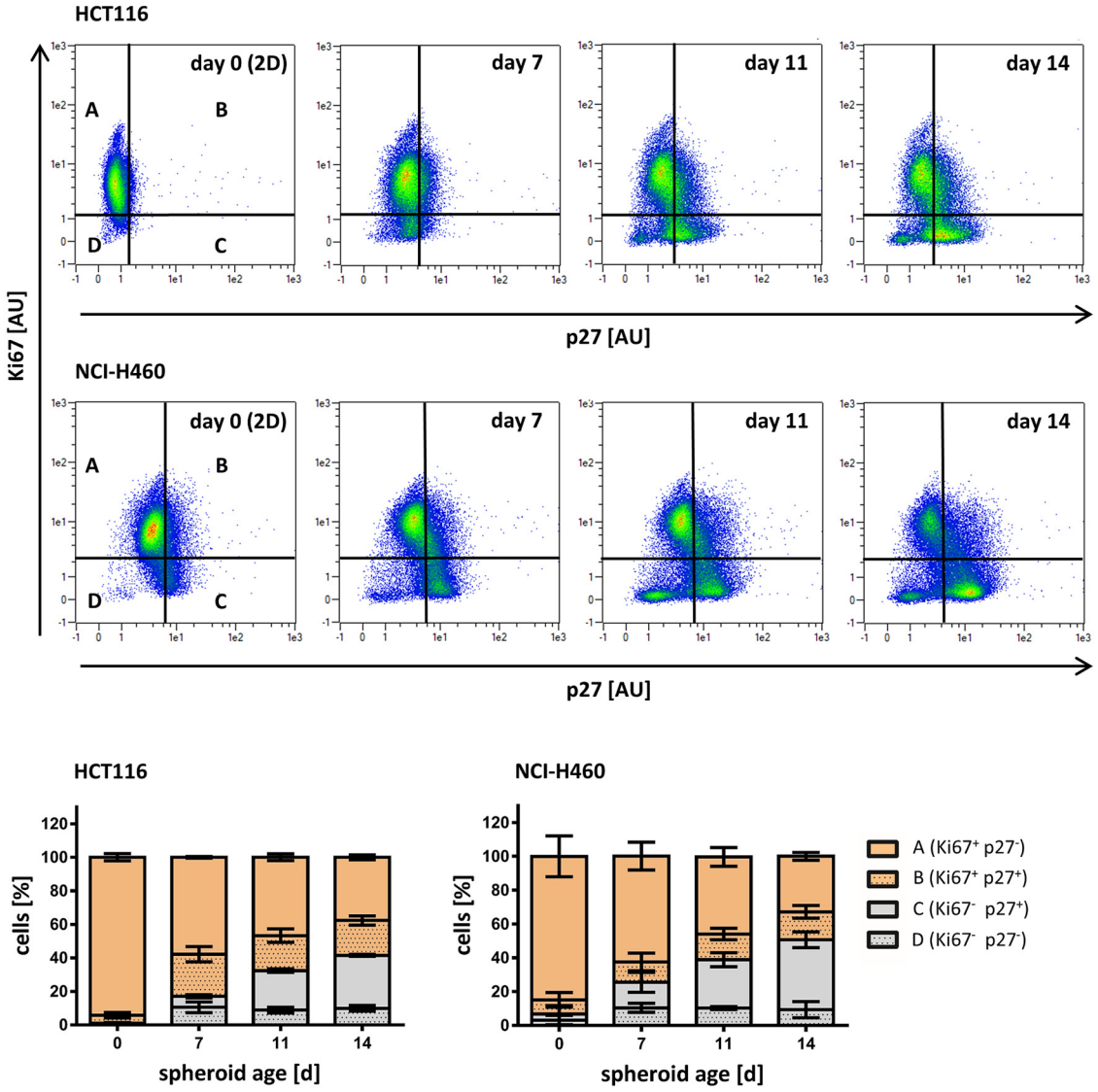

Figure 15: Decreased percentage of proliferative cells and increased percentage of quiescent cells within larger MCTSs

After detachment of 2D-cultivated HCT116 and NCI-H460 cells and dissociation of HCT116 and NCI-H460 MCTSs, the DNA and RNA of single cells was stained by Hoechst 33342/Pyronin Y and the cells were simultaneously marked for p27, as well as Ki67, with specific antibodies. Thereafter, the fluorescence signals of all four dyes were measured by flow cytometry. Gating was done according to the respective isotype controls. Both graphs show the result of three independent experiments with mean values ± SD. These experiments were conducted by Daniela Maichl.

1.4. In older MCTSs, proliferation is restricted to outer cell layers

To investigate the localisation of proliferative ($Ki67^+$) as well as quiescent ($p27^-$) cells, HCT116 and NCI-H460 MCTSs of different ages were cut into 10 µm slices and immunostained for Ki67 and p27. Fluorescence signals were analysed using a laser scanning microscope and the associated software Zen 2010 black edition.

Already during the process of cutting it was evident that, consistent with the finding of dead cells within 11-day-old NCI-H460 MCTSs and 14-day-old HCT116 MCTSs (Figure 13), a necrotic core had developed in spheroids of that age (Figure 16). However, recorded images also confirmed that cell death from the inside out started earlier in HCT116 spheroids, at day 11. The staining for Ki67 revealed that its expression was highest within cells in the outermost cells layers of the MCTSs, gradually decreasing towards the centre. Even though these differences in expression were most evident in 11 and 14-day-old HCT116 and NCI-H460 MCTSs they were also already visible at day 7 of cultivation. Conversely, p27 was only very weakly expressed in cells of 7 days old spheroids whereas in older MCTSs, cells close to the necrotic core displayed the highest amounts of the protein (Figure 16).

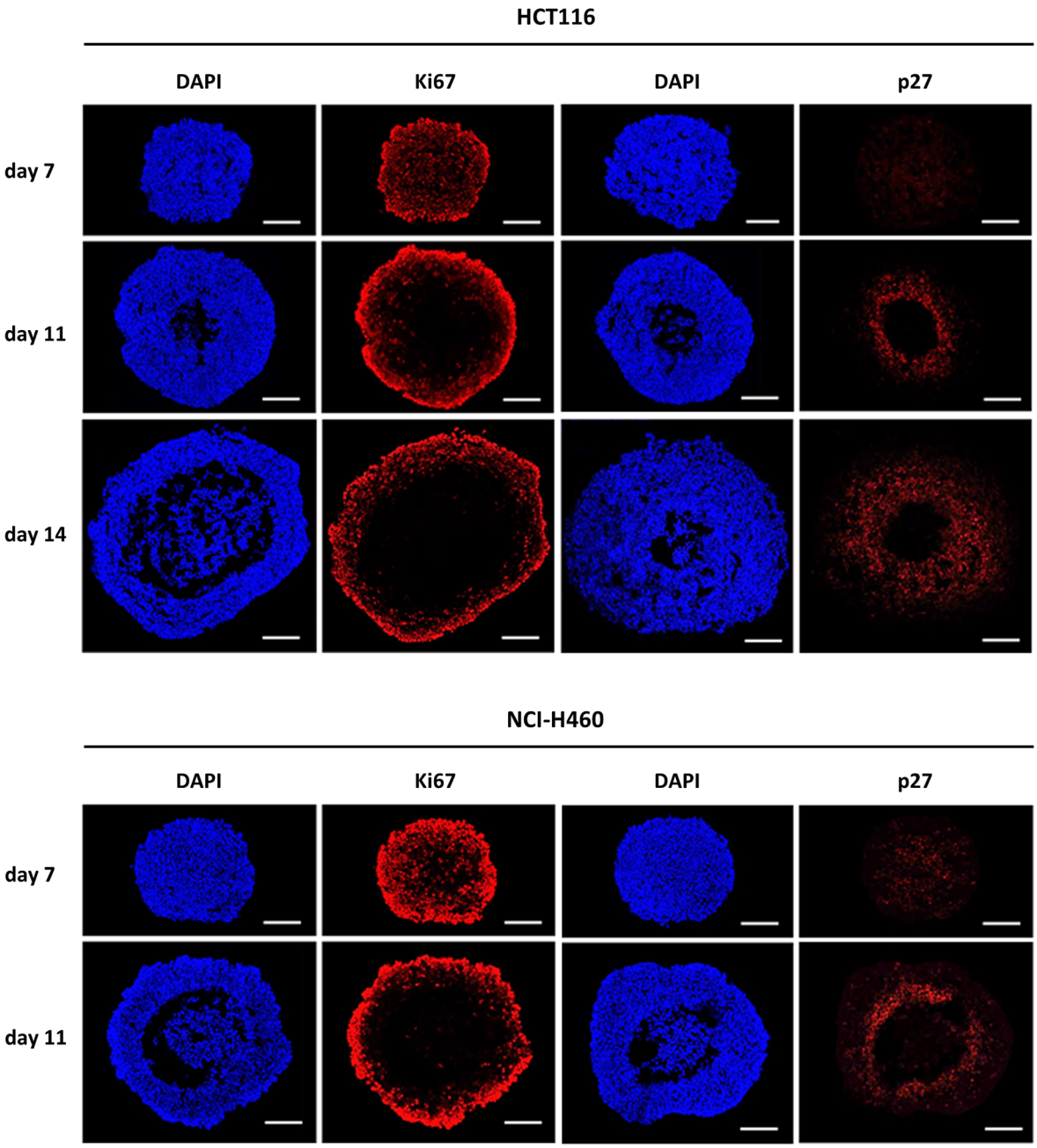

Figure 16: Staining of Ki67 and p27 in cryosections of HCT116 and NCI-H460 MCTSs

HCT116 and NCI-H460 MCTSs of the indicated age were fixed, embedded in Tissue Freezing Medium and cut into 10 µm slices using a cryostat. After permeabilisation, sections were incubated with specific antibodies against Ki67 or p27 and the cell nuclei were stained with DAPI. The shown images were obtained by laser scanning microscopy and are representative of three independent experiments. Respective isotype controls were used to adjust the exposure time of the laser. Scale bars = 100 µm. These experiments were conducted by Daniela Maichl.

Chapter 1 part 2: Only proliferative cells within MCTSs express high amounts of TRAILR1 while cells with high TRAILR2 expression can additionally be found close to the necrotic core

In this project it was further planned to subject the MCTSs to single treatment of 2nd generation TRAILR agonists. Therefore, the HCT116 and NCI-H460 MCTSs were next examined for their expression of apoptosis-relevant proteins. Close examination revealed that the expression of TRAILR1 and TRAILR2 differed strongly between individual spheroid-forming cells of both cell lines, meaning that only proliferative cells in the outer layers of the spheroids expressed high amounts of TRAILR1 while cells with high expression of TRAILR2 could additionally be found close to the necrotic core.

2.1. Initial screening for differences in the expression of apoptosis-relevant proteins between 2D- and 3D-cultivated cells

In order to perform a first broad-screen of the relative expression of apoptosis-relevant proteins in 2D-cultivated HCT116 and NCI-H460 cells and HCT116 and NCI-H460 MCTSs (Ø = 500 µm), a Proteome Profiler Human Apoptosis Array Kit was used which allowed the detection of 35 apoptosis-relevant proteins simultaneously, using the same lysates of cells. Following the manufacture's protocol, the different proteins could be detected at the end of the experiment using X-ray films and a film-developing machine. The determination of relative differences in protein amounts between 2D- and 3D-cultivated cells was later done by densitometric analysis of scanned films using the Fiji software (Figure 17). Unfortunately, results between independently performed experiments diverged widely and made it therefore difficult to give a reliable statement about differences in protein expression between 2D- and 3D-cultivated cells. Nevertheless, some trends were observable and served as a basis for further investigations.

After binding of death inducing ligands such as TRAIL to their respective receptors, a death inducing signalling complex (DISC) is formed which contains beside the receptors also adaptor proteins such as FADD that recruit initiator caspases. Since changes in the amounts of these proteins can strongly influence a cell's extrinsic apoptosis competency, the four death receptors, TNFR1, Fas, TRAILR1 and TRAILR2 as well as the adaptor protein FADD are

included in the assay and were in the following investigated for their expression in 2D- and 3D-cultivated cells.

Starting with TNFR1, it could be shown that its amount was below the detection level in NCI-H460 cells. However, in HCT116 cells, even though expression of TNFR1 also seemed low in this cell line, more of that receptor could be found in the cells cultivated as MCTSs. For Fas, a two-fold increase in the amount of protein was detected in 3D-cultivated HCT116 cells compared to the same cells cultivated in 2D in two out of three experiments. For NCI-H460 only one experiment could be evaluated and there, it seemed, that the amount of Fas was not changed between the two cultivation conditions. When the TRAILRs were evaluated, a strong downregulation of TRAILR1 was observed in two out of three experiments in HCT116 MCTSs and in both experiments for 3D-cultivated NCI-H460 cells. Conversely, the expression of TRAILR2 was upregulated in two out of three experiments in 3D-cultivated HCT116 MCTSs whereas the expression was not changed or even slightly reduced in NCI-H460 MCTSs. For the protein FADD, a downregulation could be observed in two out of three experiments when HCT116 cells were cultivated as MCTSs and the same held true for 3D-cultivated NCI-H460 cells (Figure 18).

The assay also included different downstream pro-apoptotic proteins, namely BAD, Bax, cytochrome c, SMAC, HTRA2 and caspase 3, as well as the anti-apoptotic proteins XIAP, cIAP-1/-2, survivin, livin, Bcl-2 and Bcl-xl. Expression of the Bcl-2/Bcl-xl inhibitor BAD was reduced in two out of three experiments in HCT116 MCTSs as well as in NCI-H460 MCTSs in comparison to the same cells cultivated in 2D. The results for the pore-forming protein Bax diverged widely in all experiments performed with both cell lines. However, taken together it seemed that its expression was not significantly changed in cells cultivated under 3D conditions. Furthermore, the amounts of SMAC, HTRA2 and cytochrome c, proteins that get released from mitochondria after membrane permeabilisation, were increased in at least two out of three experiments in HCT116 MCTSs and in at least one out of two experiments in 3D-cultivated NCI-H460 cells. The expression of caspase 3 was, compared to all other proteins, exceptionally high in both cell lines and made a densitometric analysis impossible. However, no observable differences, neither for the pro-form nor for cleaved caspase 3, were apparent between 2D- and 3D cultivation of both cell lines. Continuing with the anti-apoptotic proteins, the amount of the caspase inhibitor XIAP was strongly increased in two out of three experiments in HCT116 MCTSs including one experiment were XIAP was exclusively detected in 3D-cultivated cells (not shown). Conversely, for NCI-H460 cells the amount of XIAP was unchanged or even slightly reduced under 3D conditions. No strong differences in the expression of cIAP-1/-2 could be found between 2D-

and 3D-cultivated HCT116 cells while in NCI-H460 MCTSs the amount of cIAP-1 was increased. Expression of cIAP-2 was weak in this cell line but seemed unchanged under 3D conditions. Furthermore, less survivin was found in two out of three experiments in HCT116 MCTS and in both experiments in NCI-H460 MCTSs. Conversely, the expression of livin was increased in 3D-cultivated HCT116 cells in two out of three experiments including one experiment with exclusive protein detection in 3D (not shown). In NCI-H460 cells the expression of livin seemed to be generally low, however less protein was found when cells were cultivated as MCTSs. Finally, the investigation of the two inhibitors of apoptosis, Bcl-2 and Bcl-xl revealed that expression of Bcl-xl varied strongly between different experiments with HCT116 cells and was not detectable in NCI-H460 cells (Figure 18).

The assay also included four capture antibodies against targets involved in cell cycle control and DNA damage signalling, these were; claspin, a protein which plays a role in synthesis and repair of DNA; rad17, which is phosphorylated at serine 635 after DNA damage; and the two CDK inhibitors, p21 and p27. For claspin, all three experiments with HCT116 cells showed different results whereas in experiments with NCI-H460 cells, the protein amount was reduced when cells were cultivated as MCTSs. The phosphorylation level of rad17 was overall lower in MCTSs of both cell lines in comparison to cells cultivated in 2D. Furthermore, the protein amounts of both p21 and p27 seemed not significantly changed between 2D and 3D cultivation (Figure 18).

Included in the assay were also capture antibodies against different heat shock proteins that can function as inhibitors of apoptosis (Hsp27, Hsp60 and Hsp70) or have pro- and anti-apoptotic functions depending on their splice form and localisation within the cell (clusterin). The results for HCT116 varied strongly between the independent repeats however overall the expression of all four chaperones was not significantly changed between 2D and 3D conditions. In NCI-H460 cells, the expression of Hsp70 was found to be downregulated when cells were grown as MCTSs while clusterin showed a tendency to be upregulated in 3D. Furthermore, the amount of Hsp27 was unchanged between the two conditions whereas the results for Hsp60 were conflicting between different experiments, being strongly upregulated in one experiment and massively downregulated in the other (Figure 18).

Depending on the phosphorylation status of p53, the protein can either activate DNA repair mechanisms and stop cell cycle progression (phosphorylation at serine 15 and 392) or initiate apoptosis when DNA repair fails (phosphorylation at serine 46). The results of the assay showed that phosphorylation of p53 at the indicated serine residues was

downregulated under 3D conditions for NCI-H460 cells as well as in two out of three experiments in HCT116 MCTSs (Figure 18).

Finally, the assay also allowed the detection of five proteins related to hypoxia and oxidative stress: Catalase, an enzyme that catalyses the conversion of hydrogen peroxide to water and oxygen protecting thereby cells from oxidative stress; Serum paraoxonase (PON2) a protein that also acts as an antioxidant; Hif-1α, a transcription factor that is induced under hypoxic conditions; and finally haem oxygenase-1 and -2 (HO-1, HO-2), both mediate the first step of haem catabolism with HO-2 being constitutively expressed and the expression of HO-1 being induced by hypoxic conditions or oxidative stress via Hif-1α. Densitometric analysis of the blots revealed that less of the enzyme catalase was present in HCT116 cells grown as MCTSs in comparison to the same cells cultivated in 2D in two out of three experiments. In NCI-H460 cells, expression of catalase was comparably low and could only be detected in one experiment out of two, being hereby downregulated in 3D. Furthermore, the amounts of the hypoxia markers, Hif-1α and HO-1 were higher in HCT116 cells grown as MCTSs while the amount of the constitutively expressed enzyme HO-2 was unchanged between the two conditions. In contrast to that, the expression of Hif-1α and HO-2 was unchanged between 2D- and 3D-cultivated NCI-H460 cells whereas the amount of the inducible expressed form, HO-1 was even lower in 3D. Interestingly, both cell lines showed a very strong increase of PON2 expression when grown as spheroids (Figure 18).

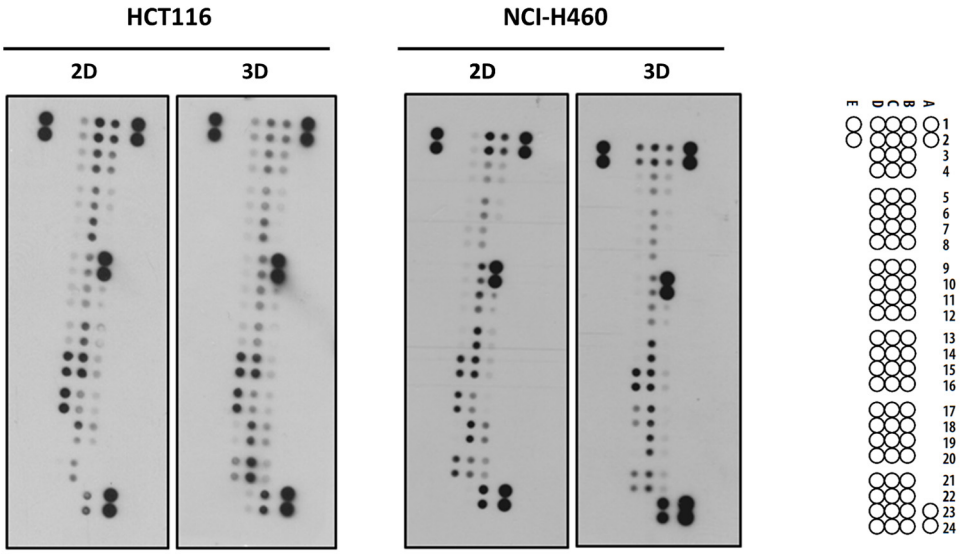

coordinate	target/control	coordinate	target/control	coordinate	target/control
A1, A2	**reference**	B23, B24	**cytochrome c**	D1, D2	**PON2**
A23, A24	**reference**	C1, C2	**TRAILR1**	D3, D4	**p21**
B1, B3	**BAD**	C3, C4	**TRAILR2**	D5, D6	**p27**
B3, B4	**Bax**	C5, C6	**FADD**	D7, D8	**phospho p53 (S15)**
B5, B6	**Bcl-2**	C7, C8	**Fas**	D9, D10	**phospho p53 (S46)**
B7, B8	**Bcl-xl**	C9, C10	**Hif-1α**	D11, D12	**phospho p53 (S392)**
B9, B10	**procaspase 3**	C11, C12	**HO-1**	D13, D14	**phospho rad17 (S635)**
B11, B12	**cleaved caspase 3**	C13, C14	**HO-2**	D15, D16	**SMAC**
B13, B14	**catalase**	C15, C16	**Hsp27**	D17,D18	**survivin**
B15, B16	**cIAP-1**	C17, C18	**Hsp60**	D19, D20	**TNFR1**
B17, B18	**cIAP-2**	C19, C20	**Hsp70**	D21, D22	**XIAP**
B19, B20	**claspin**	C21, C22	**HTRA2**	D23, D24	**PBS**
B21, B22	**clusterin**	C23, C24	**livin**	E1, E2	**reference**

Figure 17: Proteome Profiler Human Apoptosis Array Kit

2D-cultivated HCT116 and NCI-H460 cells, as well as HCT116 and NCI-H460 MCTSs (Ø = 500 µm), were used to perform the Proteome Profiler Human Apoptosis Array Kit (R&D Systems). Membranes coated with 35 different capture antibodies (spotted in duplicates) were incubated with the respective cell lysates overnight. After addition of the detection antibody cocktail as well as Streptavidin-HRP and luminol, the proteins could be visualised using X-ray films. Experiment was repeated two or three times for NCI-H460 and HCT116 respectively.

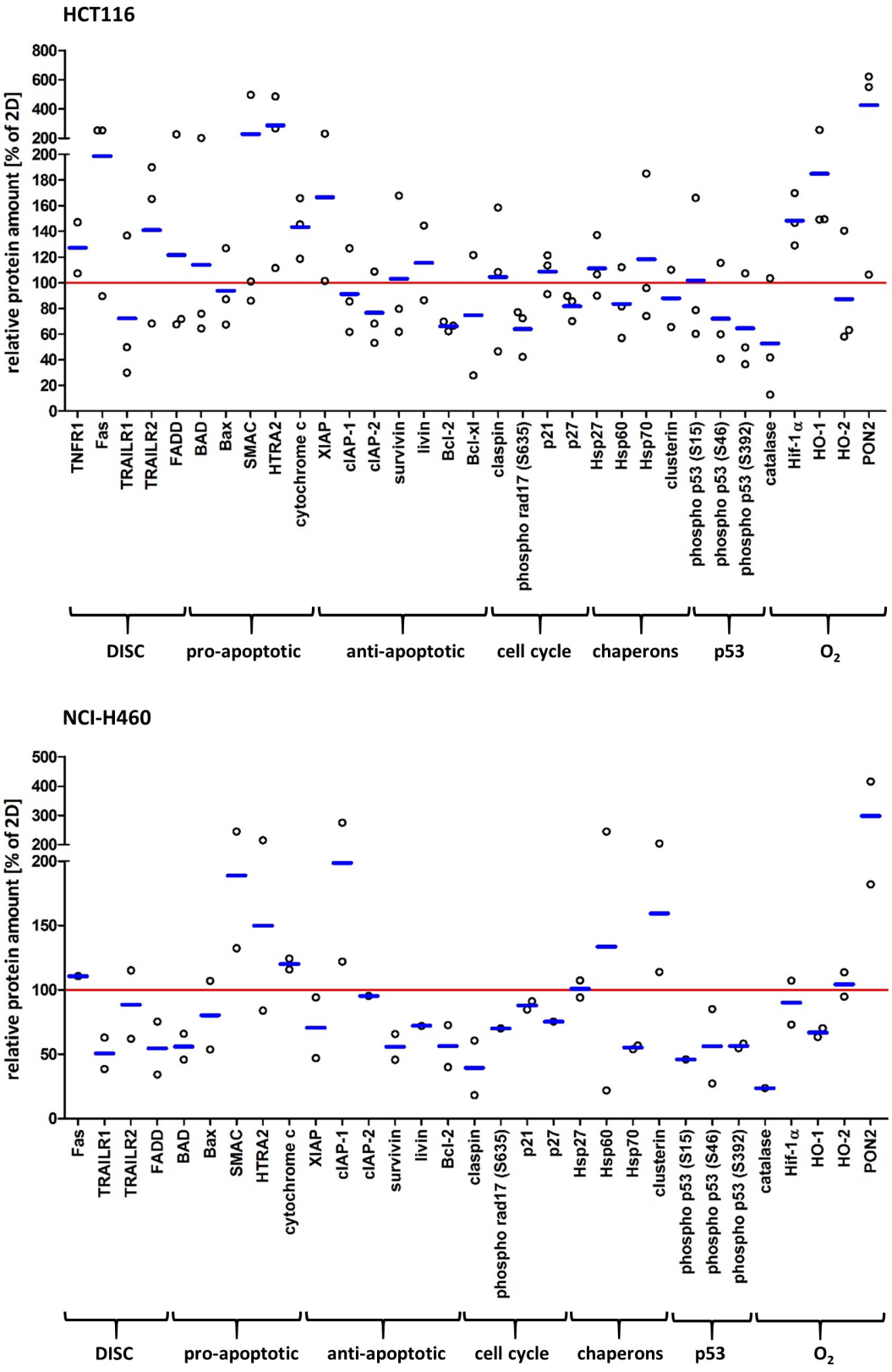
HCT116
relative protein amount [% of 2D]
800
600
400
200
200
180
160
140
120
100
80
60
40
20
0
TNFR1
Fas
TRAILR1
TRAILR2
FADD
BAD
Bax
SMAC
HTRA2
cytochrome c
XIAP
cIAP-1
cIAP-2
survivin
livin
Bcl-2
Bcl-xl
claspin
phospho rad17 (S635)
p21
p27
Hsp27
Hsp60
Hsp70
clusterin
phospho p53 (S15)
phospho p53 (S46)
phospho p53 (S392)
catalase
Hif-1 α
HO-1
HO-2
PON2
DISC
pro-apoptotic
anti-apoptotic
cell cycle
chaperons
p53
O2
NCI-H460
relative protein amount [% of 2D]
500
400
300
200
200
150
100
50
0
Fas
TRAILR1
TRAILR2
FADD
BAD
Bax
SMAC
HTRA2
cytochrome c
XIAP
cIAP-1
cIAP-2
survivin
livin
Bcl-2
claspin
phospho rad17 (S635)
p21
p27
Hsp27
Hsp60
Hsp70
clusterin
phospho p53 (S15)
phospho p53 (S46)
phospho p53 (S392)
catalase
Hif-1 α
HO-1
HO-2
PON2
DISC
pro-apoptotic
anti-apoptotic
cell cycle
chaperons
p53
O2

Figure 18: Expression of apoptosis-relevant proteins in 2D/3D-cultivated HCT116 and NCI-H460 cells

2D-cultivated HCT116 and NCI-H460 cells, as well as HCT116 and NCI-H460 MCTSs (Ø = 500 µm), were used to perform the Proteome Profiler Human Apoptosis Array Kit (R&D Systems). After detection of the indicated proteins with X-ray films, films were scanned and relative protein amounts were determined using Fiji. Data are shown as individual repeats (circles) and means (lines).

2.2. Independent validation of protein expression changes

Some proteins for which expression varied widely within the independent repeats of the proteome profiler human apoptosis array, as well as proteins that could not be detected or evaluated in the course of the assay, were investigated again for their expression in 2D- and 3D-cultivated HCT116 and NCI-H460 cells either by western blot analysis or flow cytometry. In addition, further important proteins of the apoptotic pathway, not included in the array, such as cFlip, Mcl-1, procaspase 8 and procaspase 9 were also examined (Figure 9A/B).

The amount of TRAILR1 and TRAILR2 varied strongly within the repeats of the human apoptosis array, especially in HCT116 cells. Therefore, a western blot analysis was performed and demonstrated decreased TRAILR1 expression under 3D conditions for both cell lines. Furthermore, TRAILR2 expression was increased in HCT116 MCTSs and decreased in NCI-H460 MCTSs compared to the equivalent cells cultivated in 2D (Figure 19A). Next, further proteins belonging to the DISC were analysed for their occurrence in 2D and 3D by flow cytometry. These proteins were cFlip, procaspase 8 and FADD, which were either absent from the original array or, in the case of FADD, the relative amounts were not comparable between different experiments. While the expression of FADD was similar in both 2D- and 3D-cultivated HCT116, as well as NCI-H460 cells, the population of 3D-cultivated procaspase 8 expressing cells was slightly shifted to the left in comparison to the 2D-cultivated cell population for both cell lines. Even though the expression of cFlip was relatively low in HCT116 cells, less protein was detected under 3D conditions. Conversely, for NCI-H460 cells, the expression pattern of cFlip was comparable between 2D and 3D cultivation (Figure 19B). For XIAP, as well as its inhibitor SMAC, it was shown by independently repeated western blot analyses that the amounts of both proteins were similar in 2D- and 3D-cultivated HCT116 cells. However, the expression of SMAC was slightly enhanced in NCI-H460 MCTSs and the amount of XIAP was unchanged between both 2D- and 3D-cultivated NCI-H460, in agreement with the previous data from the human apoptosis array for that cell line. Since Bcl-xl could not be detected with the human apoptosis array in NCI-H460 cells, it was separately investigated by western blot analysis, revealing that slightly less Bcl-xl protein was expressed under 3D conditions. Procaspase 3 was examined again for

both cell lines since its excessively high signal in the human apoptosis array made a densitometric analysis impossible. By performing independently repeated western blot analyses it could be shown that its expression was in fact similar in 2D- and 3D-cultivated HCT116 cells whereas its amount was decreased in NCI-H460 MCTSs in comparison to the same cells cultivated in 2D. Finally, Mcl-1 and procaspase 9, two further proteins which were not part of the array but are important components of the apoptotic pathway, were also investigated for their expression in 2D- and 3D-cultivated HCT116 and NCI-H460 cells by western blot analysis. Interestingly, while the amount of procaspase 9 was comparable between the two cultivation methods for both cell lines, the expression of Mcl-1, despite similar expression in 2D- and 3D-cultivated HCT116 cells, was strongly decreased in NCI-H460 MCTSs in comparison to the same cells cultivated in 2D (Figure 19).

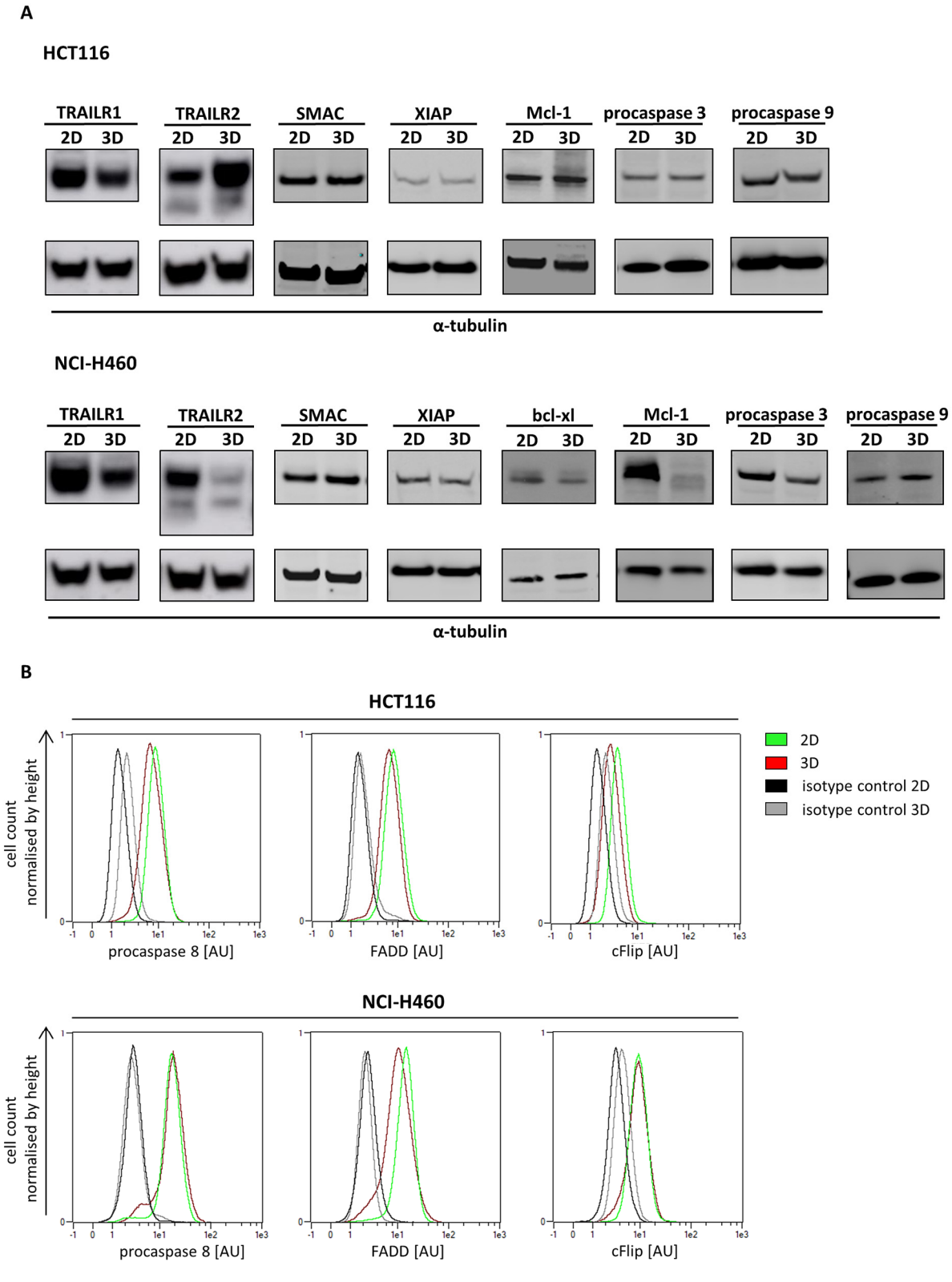
A
HCT116
TRAILR1
TRAILR2
SMAC
XIAP
Mcl-1
procaspase 3
procaspase 9
2D 3D
α-tubulin
NCI-H460
TRAILR1
TRAILR2
SMAC
XIAP
bcl-xl
Mcl-1
procaspase 3
procaspase 9
2D 3D
α-tubulin
B
HCT116
cell count
normalised by height
procaspase 8 [AU]
FADD [AU]
cFlip [AU]
2D
3D
isotype control 2D
isotype control 3D
NCI-H460
cell count
normalised by height
procaspase 8 [AU]
FADD [AU]
cFlip [AU]

Figure 19: Western blot and flow cytometric analyses reveal differences in the expression of apoptosis-relevant proteins in 2D/3D-cultivated HCT116 and NCI-H460 cells

Lysates of 2D-cultivated HCT116 and NCI-H460 cells, along with HCT116 and NCI-H460 MCTS lysates (day 11), were analysed by western blotting using the indicated antibodies. Blots shown are representative of three independently performed experiments **(A)**. 2D-cultivated HCT116 and NCI-H460 cells, along with HCT116 and NCI-H460 MCTS lysates (day 11), were analysed for the expression of indicated proteins by flow cytometry. Histograms shown are representative of two to three independently performed experiments **(B)**.

2.3. Cells within MCTSs differ in their surface expression of TRAILRs

Since TRAILR1 and TRAILR2 were differently expressed under 2D and 3D conditions for both cell lines and are at the same time the first proteins to be engaged during TRAIL-induced apoptosis, further investigations were conducted to elucidate their cultivation-dependent expression pattern.

First, 2D- and 3D-cultivated HCT116, as well as NCI-H460 cells, were investigated for their surface expression of both apoptosis-inducing TRAILRs, TRAILR1 and TRAILR2, but also for their expression of the two regulatory receptors, TRAILR3 and TRAILR4, by flow cytometry (Figure 20). Simultaneously, the expression of EGFR under both cultivation conditions was determined as one of the 2nd generation TRAILR agonists to be trialled later in this thesis contains a targeting moiety for that protein. Interestingly, 3D-cultivated cells of both cell lines showed a broad range of TRAILR1 expression. Some of the spheroid-forming cells still displayed TRAILR1 amounts comparable to 2D-cultivated cells, however many cells also showed decreased TRAILR1 expression or were completely devoid of this protein at the cell surface. Furthermore, surface expression of TRAILR2 was similar in 2D- and 3D-cultivated HCT116 cells while the TRAILR2 expression pattern of 3D-cultivated NCI-H460 was similar to that of TRAILR1 in NCI-H460 MCTSs. Surface expression of the two regulatory receptors could only be detected in HCT116 cells. Here, 2D- and 3D-cultivated cells did not differ in their expression of TRAILR3 whereas the expression pattern of TRAILR4 in spheroid-forming cells resembled those of TRAILR1 in HCT116 MCTSs. The surface expression of EGFR was shown to not differ in 2D- and 3D-cultivated HCT116 cells while the surface expression pattern of 3D-cultivated NCI-H460 cells was comparable to that of TRAILR1 and TRAILR2 in NCI-H460 MCTSs.

By calculating and comparing the relative protein expression of spheroid-forming cells to those of cells cultivated in 2D, using the median of the cell population, it could be shown

that on average HCT116 cells expressed lower amounts of TRAILR1 and TRAILR4 when grown as MCTSs. The expression of TRAILR2, TRAILR3 and EGFR, however, was comparable between the two cultivation methods. NCI-H460 cells forming MCTSs expressed on average less TRAILR1, TRAILR2 and EGFR as the same cells cultivated in 2D (Figure 20; Figure 21).

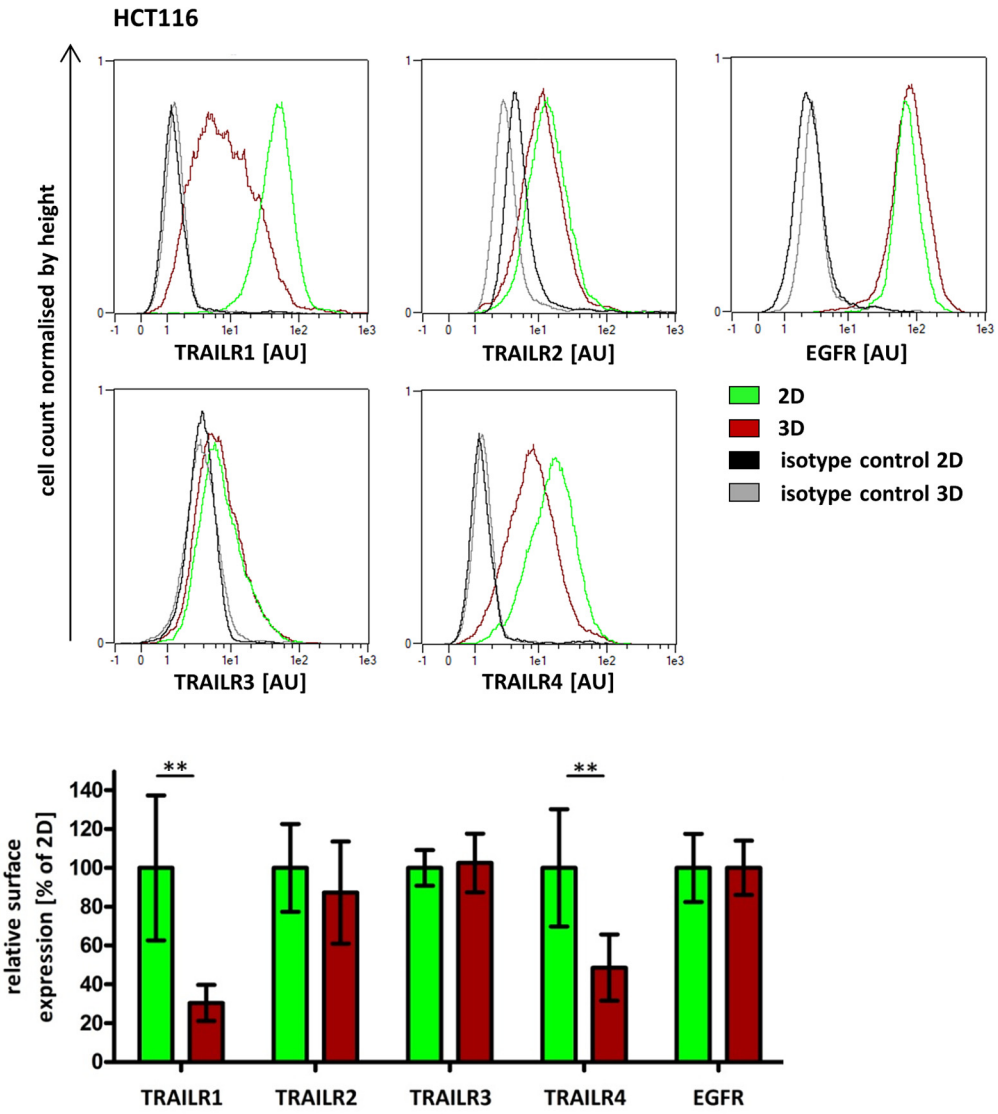

Figure 20: Differential expression of TRAILR1 and TRAILR4 on HCT116 cells from MCTSs and 2D cell cultures

2D-cultivated HCT116 cells and HCT116 MCTSs (day 11) were analysed for their surface expression of the indicated proteins by flow cytometry. Shown histograms are representative of at least three independent experiments. Population medians were used to calculate the differences in relative surface expression between 2D- and 3D-cultivated cells. Displayed data are mean values ± SD of at least three independent experiments. Asterisks indicate statistical significance (** = $p \leq 0.01$; unpaired t-test).

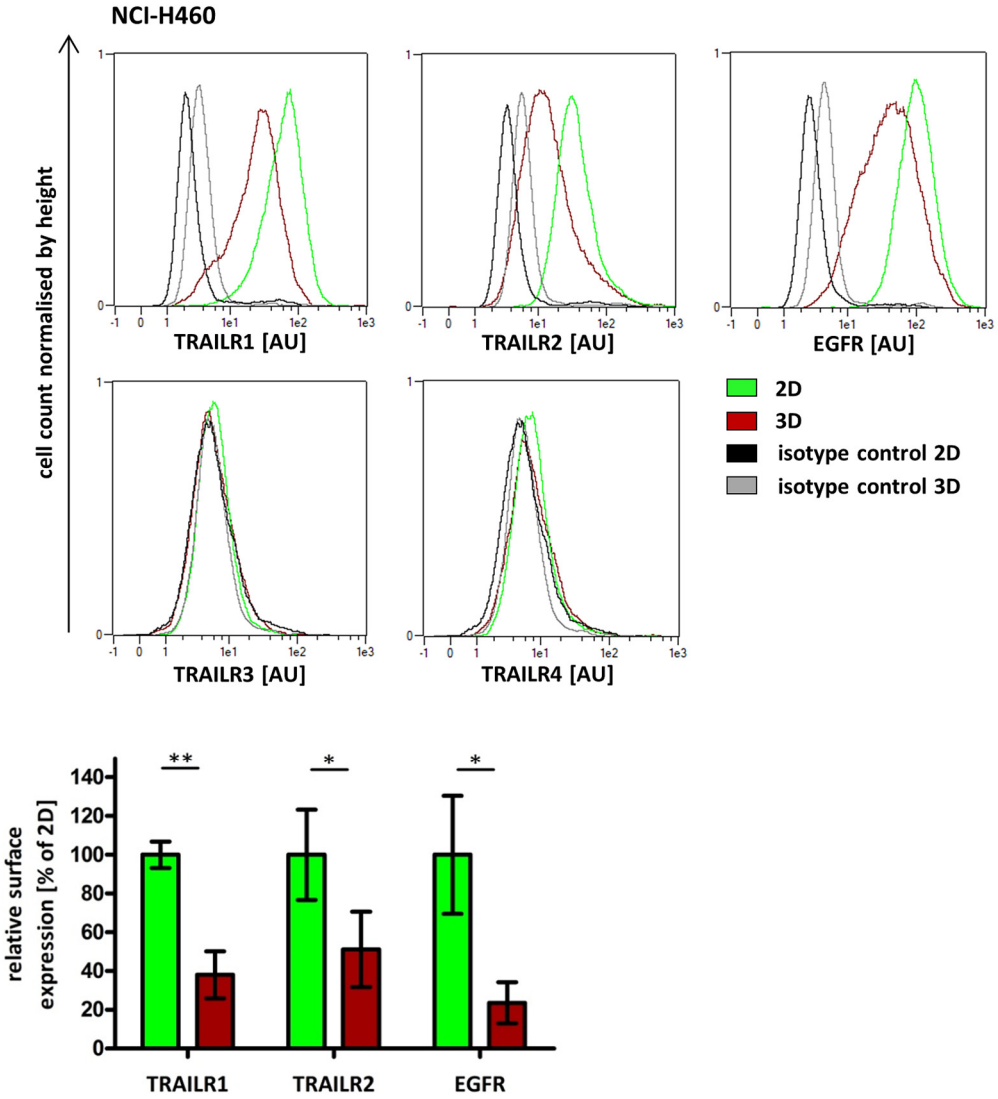

Figure 21: Differential expression of TRAILR1/R2 and EGFR on NCI-H460 cells from MCTSs and 2D cell cultures

2D-cultivated NCI-H460 cells and NCI-H460 MCTSs (day 11) were analysed for their surface expression of the indicated proteins by flow cytometry. Shown histograms are representative of at least three independent experiments. Population medians were used to calculate the differences in relative surface expression between 2D- and 3D-cultivated cells. Displayed data are mean values ± SD of at least three independent experiments. Asterisks indicate statistical significance (* = $p \leq 0.05$, ** = $p \leq 0.01$; unpaired t-test).

2.4. TRAILR expression profiles are restored after dissociation and re-plating of MCTSs

Next, it was investigated whether the decreased TRAILR expression of spheroid-forming cells is reversible when re-plating them and cultivating them under 2D conditions. One day after seeding, spheroid-forming cells displayed almost the same median surface TRAILR1/R2 expression as cells from a 2D cell culture. Re-plated HCT116 MCTSs reached around 80% of TRAILR1 expression in 2D. Furthermore, surface TRAILR2 expression was similar before and after re-plating in comparison to those of a 2D cell culture whereas expression of TRAILR4 remained low in spheroid-forming cells. Re-plated NCI-H460 MCTSs showed the same level of TRAILR1 expression as those from a 2D cell culture after 1 day of cultivation while expression of TRAILR2 reached 80%. At day two, an increase of expression to even higher level than those detected in 2D-cultivated cells, could be observed for TRAILR1 and TRAILR2 in re-plated HCT116 MCTSs and for TRAILR1 in re-plated NCI-H460 MCTSs. Finally, after three days of cultivation, re-plated spheroids were undistinguishable from 2D-cultivated cells in terms of TRAILR expression (Figure 22). Of note, the cell number of re-plated MCTSs was significantly lower than those of re-plated 2D-cultivated cells at day 1 (cell number 2D/cell number 3D = 1.62 for HCT116 (n=2); 1.88 for NCI-H460 (n=2)) indicating that either not all cells attached to the wells or that cell cycle length was increased or cell division impaired. After 3 days of cultivation under 2D conditions, the ratio between re-plated 2D- and 3D-cultivated HCT116 cells remained approximately the same (1.22 (n=1)) suggesting that from day 1 on, all remaining re-plated MCTSs cells divided the same way as the re-plated 2D-cultured cells. Interestingly, re-plated NCI-H460 MCTSs behaved in a different way, with the ratio reaching 7.31 (n=1), which indicates that either most cells didn’t undergo cell division and/or many cells underwent cell death.

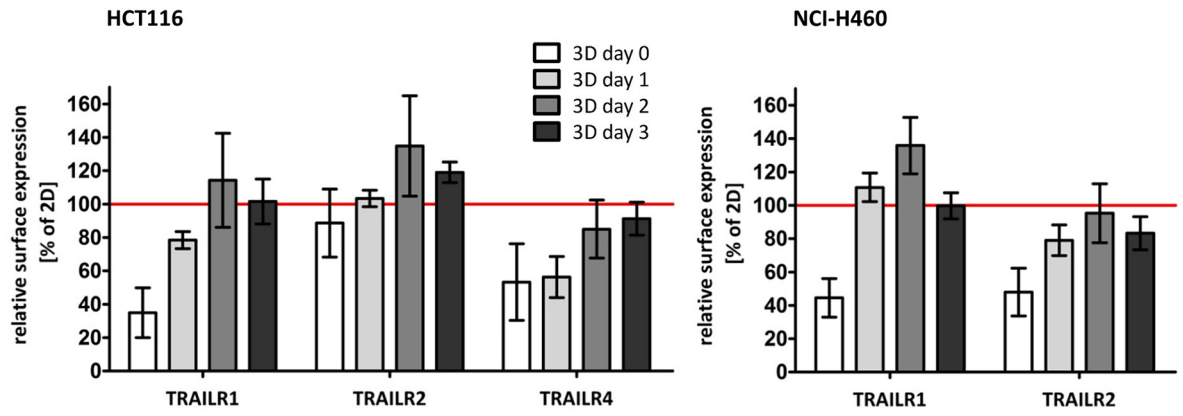

Figure 22: TRAILR expression of re-plated MCTS-forming HCT116 and NCI-H460 cells

2D-cultivated HCT116 and NCI-H460 cells as well as HCT116 and NCI-H460 MCTSs (day 11) were analysed for their expression of TRAILRs by flow cytometry (day 0). At the same time, 2D- and 3D-cultivated cells were re-plated and TRAILR expression was determined after 1, 2 and 3 days. Medians of the cell populations were used to calculate the surface TRAILR expression relative to 2D-cultivated cells. Data shown are mean values ± SD of three independent experiments.

2.5. Within HCT116 and NCI-H460 MCTSs only proliferative cells express high amounts of TRAILR1

To investigate whether there exists a correlation between cell cycle status and surface TRAILR (EGFR) expression of spheroid-forming cells, MCTSs (day 11) were dissociated and cells were analysed by flow cytometry for their simultaneous expression of either one of the indicated receptors together with the proliferation marker Ki67 or the quiescence marker p27. Thereafter, data were analysed for correlation by performing linear regressions and determine the Spearman's rank correlation coefficient (ρ) in Graphpad prism 5.

Investigations revealed that within HCT116 and NCI-H460 MCTSs, TRAILR1 amounts correlated positively with Ki67 (HCT116: linear regression R^2 = 0.2693, Spearman's rank ρ = 0.5683; NCI-H460: R^2 = 0.3704, ρ = 0.598) and negatively with p27 expression (HCT116: R^2 = 0.0558, ρ = -0.3018; NCI-H460: R^2 = 0.1814, ρ = -0.4154), meaning that only proliferative cells displayed surface TRAILR1 in high quantities. Conversely, no relation was found between cell cycle status and TRAILR2 surface expression in both HCT116 as well as NCI-H460 MCTSs. For TRAILR4 in HCT116 MCTSs analyses revealed no correlation between surface expression and cell cycle status, while interestingly EGFR amounts in NCI-H460 MCTS seemed to slightly correlate with the expression of Ki67 (R^2 = 0.0471; ρ = -0.2167) and p27 (R^2 = 0.0901; ρ = 0.3047), in a way that proliferative cells expressed less EGFR than quiescent cells (Figure 23).

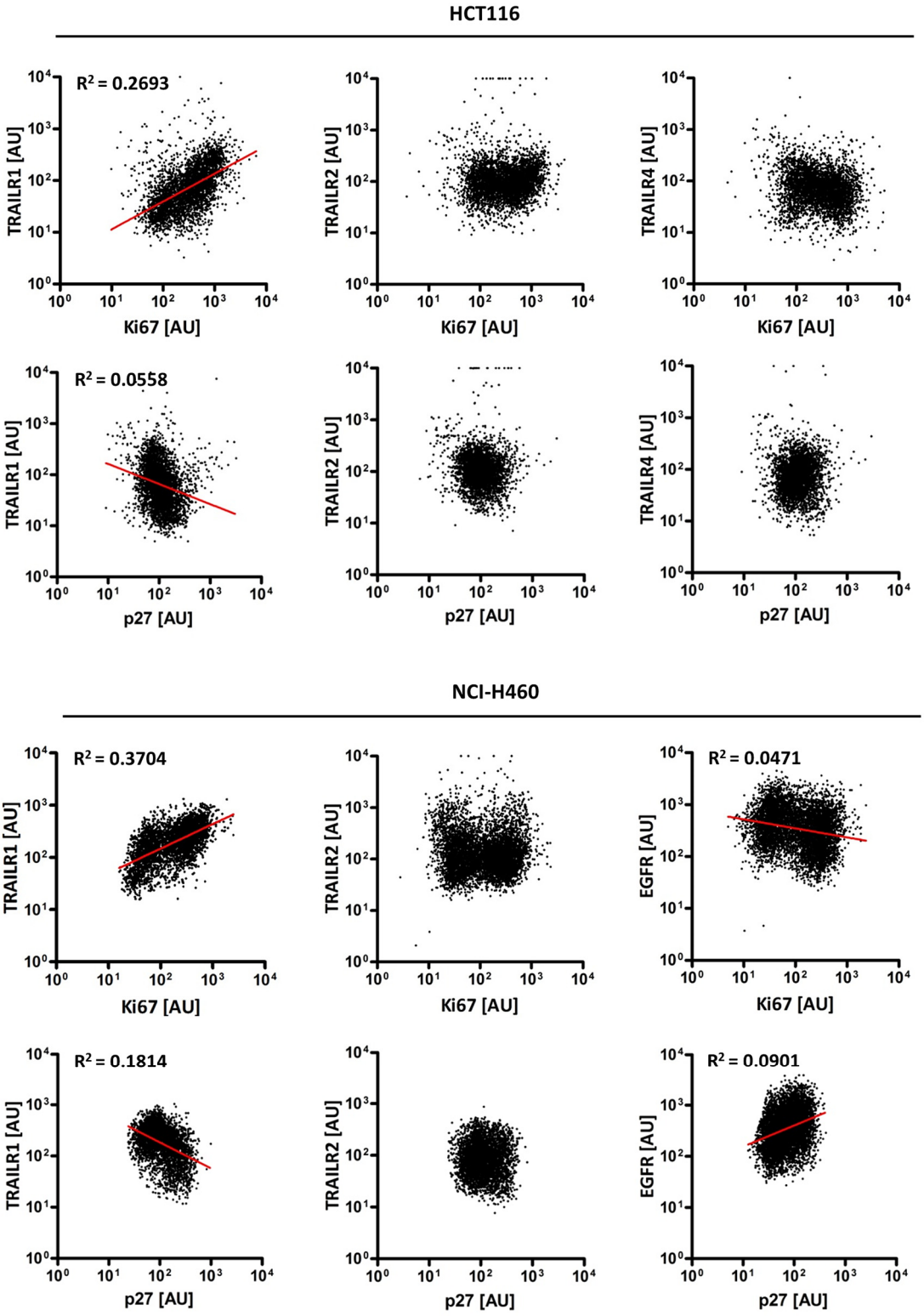

Figure 23: Correlation between cell cycle status and surface expression of TRAILR1/2/4 and EGFR in MCTS-forming cells

HCT116 and NCI-H460 MCTSs (day 11) were analysed for their simultaneous expression of the indicated proteins by flow cytometry. Shown scatter plots are representative of three independent experiments. Linear regressions were performed in GraphPad prism 5 and are shown as a red line when $R^2 \geq 0.04$.

Table 5: Correlation between surface receptor expression and Ki67 or p27

	Ki67		p27	
	P	**p value**	***ρ***	**p value**
HCT116 T1	0.5683	***	- 0.3018	***
HCT116 T2	0.1312	***	- 0.0917	***
HCT116 T4	- 0.0718	***	0.1157	***
NCI-H460 T1	0.598	***	- 0.4154	***
NCI-H460 T2	- 0.0145	ns	0.0009	ns
NCI-H460 EGFR	- 0.2167	***	0.3047	***

Spearman's rank correlation coefficient (ρ) was determined from data presented in figure 23. The calculated p significance value gives information about the robustness of the ρ value. *** = $p \leq 0.001$; ns = not significant.

2.6. TRAILR mRNA amounts are reduced in HCT116 and NCI-H460 MCTSs

To investigate whether the altered TRAILR expression in cells cultivated under 3D conditions, at the proteomic level, were due to changes at the mRNA level, qPCR was performed. Results showed that in contrast to 2D-cultivated HCT116 cells, the amount of TRAILR1, both isoforms of TRAILR2 and of TRAILR4 mRNA were decreased in HCT116 MCTSs. Similarly, 2D-cultivated NCI-H460 cells expressed higher amounts of TRAILR1 and TRAILR2 mRNA than the same cells grown as MCTSs (Figure 24).

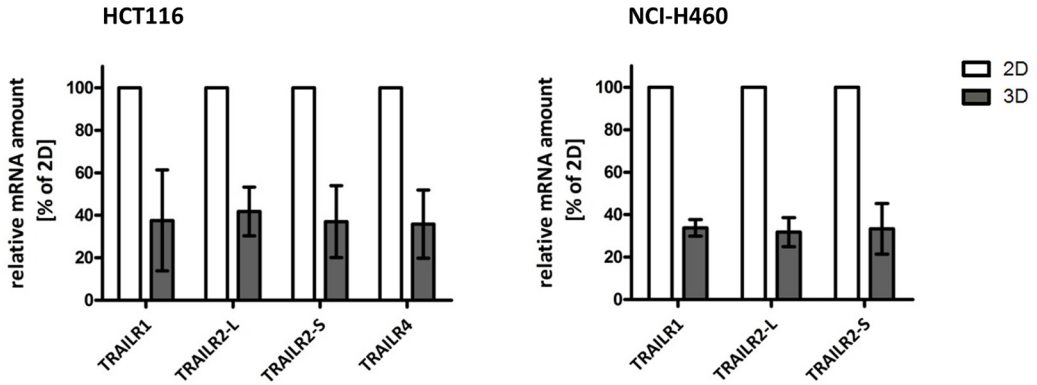

Figure 24: Comparison of TRAILR mRNA levels between 2D- and 3D-cultivated cells

2D-cultivated HCT116 and NCI-H460 cells as well as HCT116 and NCI-H460 MCTSs (day 11) were used to perform a qPCR. TRAILR2-L stands for the long isoform and TRAILR2-S for the short isoform of that receptor. Relative RNA amounts were calculated by the ΔΔCt method using GAPDH for normalisation. Data shown are mean values ± SD of three independent experiments.

2.7. TRAILR1 expression is restricted to the outer layers of MCTSs while cells with high TRAILR2 expression can be additionally found close to the centre

Finally, to investigate localisation-dependent TRAILR expression within MCTSs, spheroids of different ages were cut into 10 µm slices and immunohistochemically stained for TRAILR1 and TRAILR2. Receptor selectivity of both used antibodies was validated using MEFs transfected with either human TRAILR1 or human TRAILR2 (Figure 26A). In addition, sections were stained for the proliferation marker thymidine kinase 1 (TK1) to determine once more the proliferation status of the spheroid-forming cells. Of note, in contrast to the marker protein Ki67, which is present in all proliferating cells independent of the cell cycle phase, TK1 expression despite being only detectable in proliferating cells, is only highly expressed in S phase. Thus not all proliferating (Ki67 positive) cells are positive for TK1.

Similar to the staining for the proliferation marker Ki67 (Figure 16), cells with TK1 expression were exclusively found in the outer few cell layers of larger spheroids (HCT116 day 11 & day 14; NCI-H460 day 11) whereas in spheroids with a smaller diameter (day 7) cells marked as proliferative were distributed within the whole spheroid with slightly less positive cells to be found close to the centre (Figure 25).

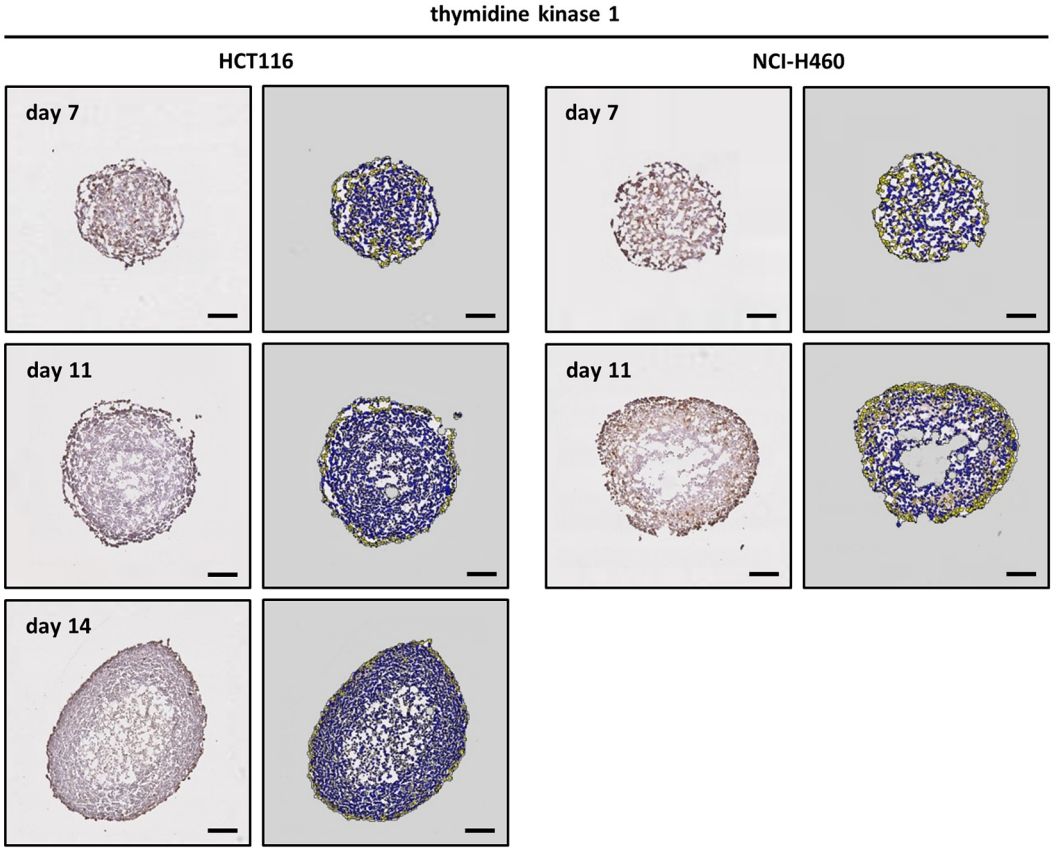

Figure 25: Thymidine kinase 1 expression of spheroid-forming cells

HCT116 and NCI-H460 MCTSs of different ages were embedded with Tissue Freezing Medium and cut into 10 µm slices using a cryotome. Spheroid sections were immunohistochemically stained for thymidine kinase 1 and counterstained with haematoxylin to visualise cell nuclei. Afterwards the software Definiens Tissue Studio 64 was used to identify positive (yellow) and negative (blue) cells. Pictures are representative of two to three independent experiments. Scale bars = 100 µm. Staining and analysis via the software was done by Dr. Jens Schmid, IKP, Stuttgart.

Analysis of TRAILR expression was performed by using the software Definiens Tissue Studio 64 to divide the cells in different colour-coded groups according to their TRAILR expression and then using Photoshop Elements 10 to determine the percentage of cells belonging to the distinct groups within the six spheroid layers.

Investigations revealed that in HCT116 MCTSs, TRAILR1 was mainly expressed in the outer cell layers, independent of spheroid size. Furthermore, in 7-day-old HCT116 spheroids, the number of cells with high TRAILR2 expression decreased from the outside to the centre. In older spheroids, however, the innermost layer, almost exclusively comprising of cells with high TRAILR2 expression, was seperated from the outermost highly TRAILR2 positive area by intermediate sections that contained distinct amounts of cells with only low and medium expression of TRAILR2 (Figure 26; Figure 27; Figure 28;). Similarly, in 7-day-old and 11-day-old NCI-H460 MCTSs, the number of cells with high TRAILR1 expression also decreased from

the outside to the inside. However, in contrast to HCT116 MCTSs, the amount of cells with low TRAILR1 expression did not decrease to the same extent and was even slightly higher in the innermost spheroid layer compared to the intermediate located areas. For TRAILR2 it was found that in 7 days old NCI-H460 MCTSs the number of cells with high expression of the receptor decreased while at the same time the amount of cells with low expression of TRAILR2 increased. In larger NCI-H460 spheroids, a similar pattern was observed to that seen in 11-day-old HCT116 MCTSs. Here, the innermost spheroid layer also comprised of less cells completely devoid of TRAILR2 than the surrounding areas. Comparable to TRAILR1 expression, the highest number of cells with large amounts of TRAILR2 could be found in the outermost spheroid layer (Figure 26; Figure 27; Figure 28).

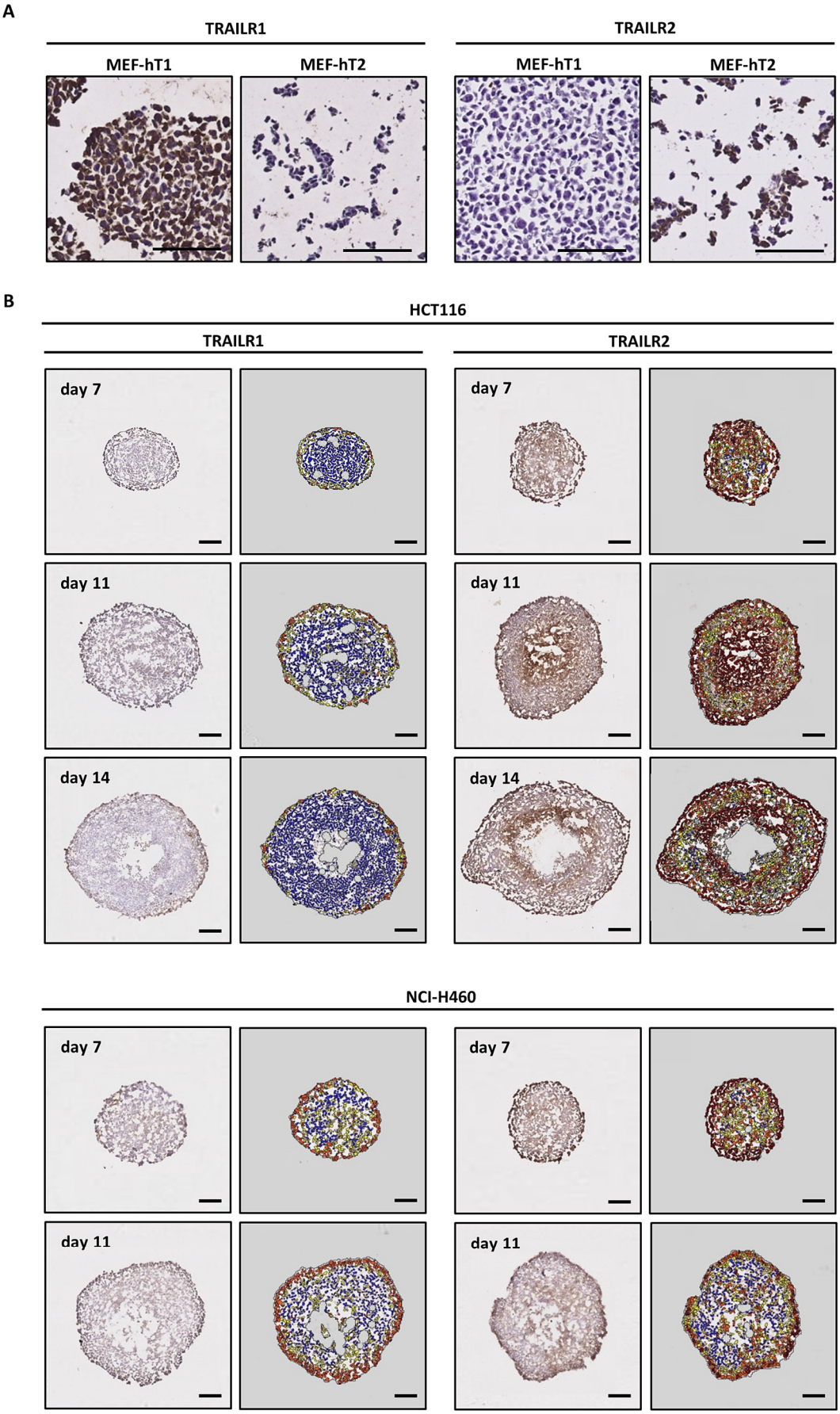
A
TRAILR1
TRAILR2
MEF-hT1
MEF-hT2
MEF-hT1
MEF-hT2
B
HCT116
TRAILR1
TRAILR2
day 7
day 11
day 14
NCI-H460
day 7
day 11

Figure 26

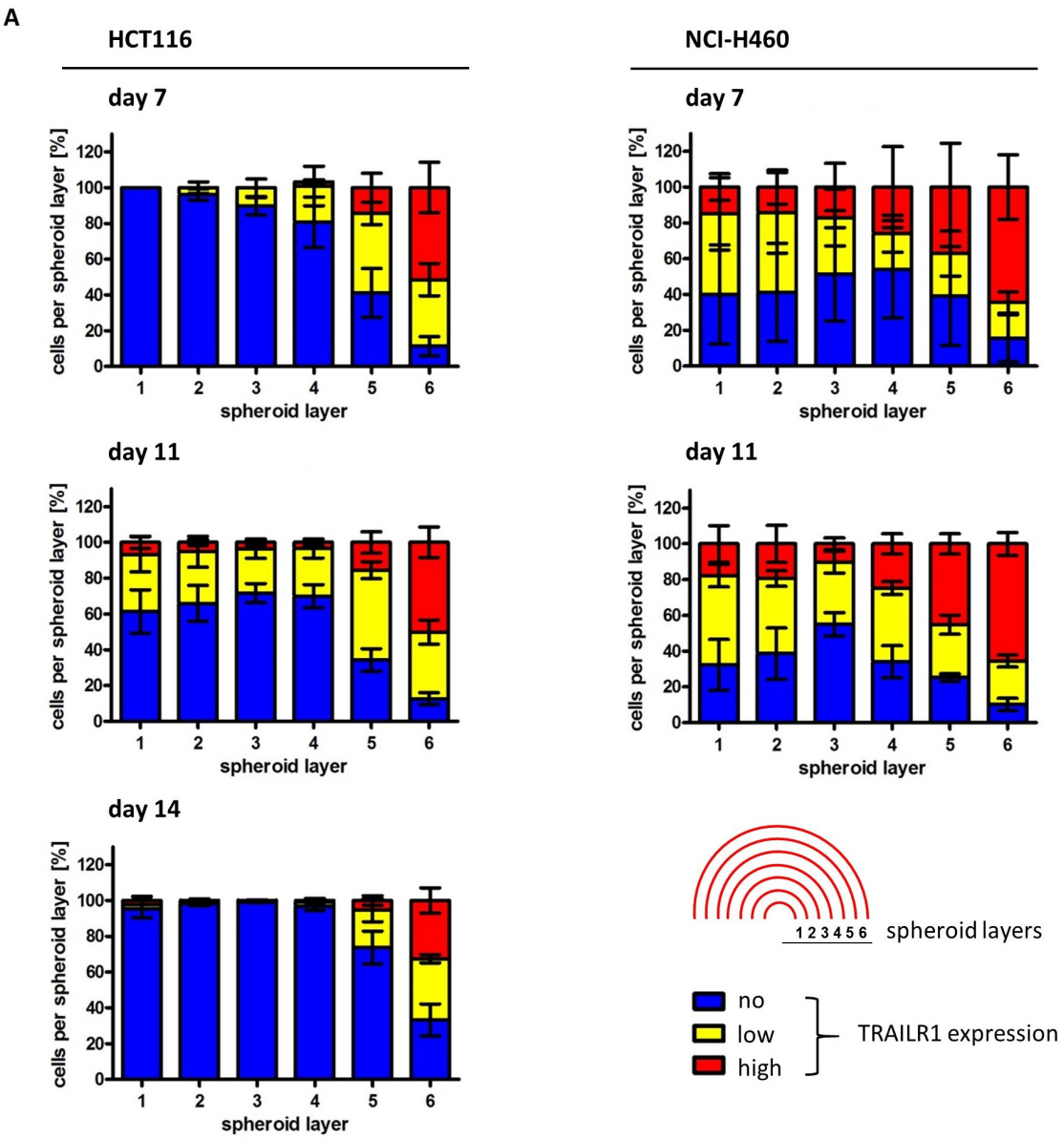
A
HCT116
NCI-H460
day 7
day 11
day 14
cells per spheroid layer [%]
spheroid layer
1 2 3 4 5 6
spheroid layers
no
low
high
TRAILR1 expression
B
HCT116 (day 11)
NCI-H460 (day 11)
hemispherical section
middle section (10 µm)

Figure 27

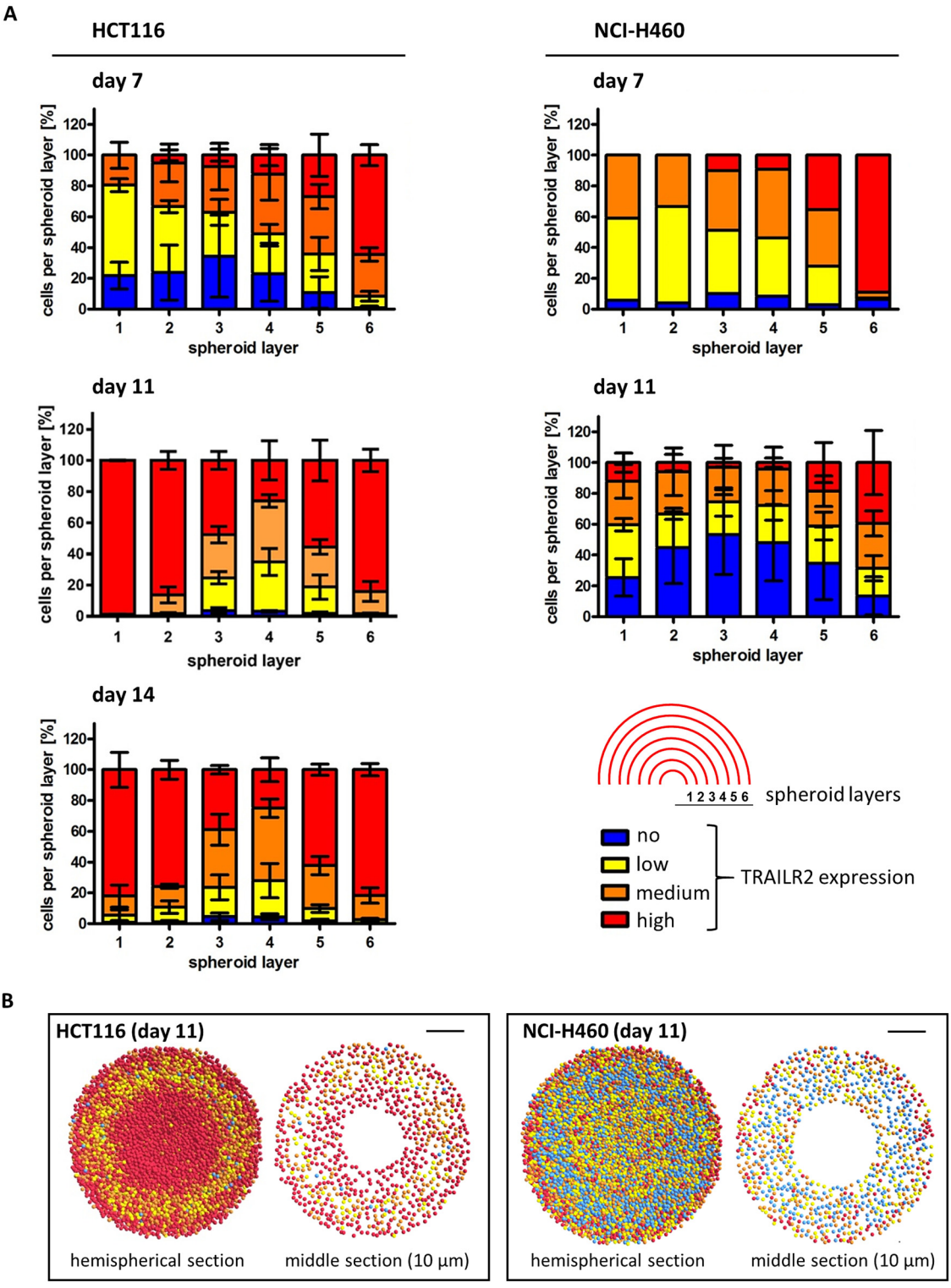
A
HCT116
NCI-H460
day 7
day 11
day 14
cells per spheroid layer [%]
spheroid layer
1 2 3 4 5 6 spheroid layers
no
low
medium
high
TRAILR2 expression
B
HCT116 (day 11)
NCI-H460 (day 11)
hemispherical section
middle section (10 µm)

Figure 28

Figure 26: Immunohistochemical staining of TRAILR1 and TRAILR2 in spheroid-forming cells

Mouse embryonic fibroblasts transfected with human TRAILR1 (MEF-hT1) or human TRAILR2 (MEF-hT2) were embedded with Tissue Freezing Medium, cut into 10 µm slices and immunohistochemically stained for TRAILR1 and TRAILR2 **(A)**. HCT116 and NCI-H460 MCTSs of different ages were embedded with Tissue Freezing Medium and cut into 10 µm slices. Spheroid sections were immunohistochemically stained for either TRAILR1 or TRAILR2 and counterstained with haematoxylin to visualise cell nuclei. Thereafter, the software Definiens Tissue Studio 64 was used to identify cells with no (blue), low (yellow), medium (orange) and high (red) TRAILR expression. Pictures are representative of two to three independent experiments except for NCI-H460 day 7 where only one experiment was performed for TRAILR2 **(B)**. Scale bars in all images = 100 µm. Staining and analysis via the software was done by Dr. Jens Schmid, IKP, Stuttgart.

Figure 27: Analysis of TRAILR expression in different spheroid layers

After image analysis with the Definiens Tissue Studio 64 software, spheroid sections were subdivided into six different layers and the percentage of cells with no, low and high TRAILR1 expression was determined using Photoshop Elements 10. Shown are mean values ± SEM of in total three spheroids out of two to three independent experiments **(A)**. HCT116 and NCI-H460 MCTSs (day 11) were simulated using mean spheroid metrics (spheroid diameter, diameter of the necrotic core and TRAILR1 expression levels by localisation). Simulation and subsequent visualisation, using the FLAME visualiser software, was done by Dr. Gavin Fullstone, IZI, University of Stuttgart, Stuttgart.

Figure 28: Analysis of TRAILR expression in different spheroid layers

After image analysis with the Definiens Tissue Studio 64 software, spheroid sections were subdivided into six different layers and the percentage of cells with no, low, medium and high TRAILR2 expression was determined using Photoshop Elements 10. In the case of NCI-H460 day 7 only the result of one analysed spheroid is displayed. In all other graphs values ± SEM of in total three spheroids out of two to three independent experiments are shown **(A)**. HCT116 and NCI-H460 MCTSs (day 11) were simulated using mean spheroid metrics (spheroid diameter, diameter of the necrotic core and TRAILR2 expression levels by localisation). Simulation and subsequent visualisation, using the FLAME visualiser software, was done by Dr. Gavin Fullstone, IZI, University of Stuttgart, Stuttgart.

2.8. Discussion

In the first part of this chapter it was shown that MCTSs can be generated from HCT116 and NCI-H460 cells by the hanging drop method. Furthermore, it was demonstrated that 11-day-old HCT116 and NCI-H460 MCTSs, having an approximate diameter of 500 µm, displayed a necrotic core and comprised of proliferative and quiescent cells. As a consequence, MCTSs did not grow exponentially as solely the outer proliferative cell layers contributed to the volume increase of the spheroids.

MCTSs generated by HCT116 and NCI-H460 cells were first investigated for their growth characteristics. Thereby it was apparent that even though NCI-H460 MCTSs grew faster on average than HCT116 MCTSs, they could only maintain their round shape until day 11 to 13 of cultivation, while HCT116 MCTSs stayed compact up to day 30. Interestingly, densely packed round-shaped MCTSs generated from human cancer cell lines, including HCT116, were shown by Park and colleagues to display enhanced activity of the Janus kinase-signal transducer and activator of transcription (JAK-STAT) pathway when compared to less compact MCTSs generated from, beside other cell lines, also NCI-H460 cells (Park et al., 2016). In these cases cytokines, like IL-6 or INF-γ, bind to their cognate receptors, JAKs are activated and in turn phosphorylate different STAT proteins. One of these transcription factors, STAT3, is known to upregulate the expression of cluster of differentiation 44 (CD44), a protein involved in cell-to-cell adhesion (Chung et al., 2013). Therefore, the enhanced activity of the JAK-STAT pathway in spheroid-forming HCT116 cells might account for the observed sustained compactness of HCT116 MCTSs. Alongside their differences in shape, HCT116 and NCI-H460 MCTSs were also shown in this work to differ in their rate of volume increase. Starting with the same number of cells, NCI-H460 MCTSs reached a diameter of approximately 650 µm after 11 days, while HCT116 at the same day of cultivation only displayed a diameter of around 500 µm. Since NCI-H460 cells were demonstrated to have an approximately 1 µm larger diameter than HCT116 cells when cultivated in 2D, these differences in the volume increase of MCTSs over time might simply be a result of the varying cell size (Nexcelom, 2003). Furthermore, differences in cell cycle length might also contribute to the larger volume of NCI-H460 MCTSs as 2D-cultured NCI-H460 cells had a mean division time of 15.6 h while HCT116 cells needed additional 2.3 h longer to undergo cell division (unpublished data Daniela Stöhr; Daniela Stöhr, diploma thesis, 2013). Finally, discrepancies in the relative number of proliferative cells within MCTSs of both cell lines can be excluded as the reason for the varying size of the spheroids since the proportions of proliferative and quiescent cells were comparable between 7-day-old HCT116 and NCI-H460 MCTSs.

HCT116 cells, when grown as MCTSs, demonstrated a reduced cell proliferation rate than expected from the 2D cell cycle length, suggesting a small proportion of cells remained proliferative only within larger spheroids or that cells within the spheroid slowed down their cell cycle progression remarkably. Simulations performed by Karsten Kuritz revealed that the growth behaviour of HCT116 MCTSs was best reproduced by assuming that in older spheroids only the outer 2 to 3 cell layers were comprised of proliferative cells. In accordance with this finding, only the outermost cell layers within sections of 11-day-old HCT116 and NCI-H460 MCTSs were stained strongly positive for the proliferation marker Ki67. These observations concur with literature where spheroid growth is often depicted as a three-step process (Wallace and Guo, 2013). First, the formed small spheres mainly comprise of proliferative cells. At a later time point, only cells in the outer rim of the MCTSs remain proliferative while cells in inner layers stop cell cycle progression and enter the quiescent stage due to a reduced supply with nutrients, oxygen and growth factors as well as decreased clearance of waste products such as lactate (Groebe and Mueller-Klieser, 2004; Preisler et al., 1977; Sherar et al., 1987; Sutherland et al., 1986). After the MCTSs reach a diameter of about 400 to 500 µm, cells in the middle begin to undergo cell death and a necrotic core starts to develop as shown for HCT116 and NCI-H460 MCTSs (Kunz-Schughart et al., 2004). Resulting out of the restricted proliferation, growth of MCTSs slows down in this stage until it stagnates completely as demonstrated here for HCT116 MCTSs. Interestingly, it was observed that spheroid growth on average comes to a halt when the necrotic core occupies 50%-70% of the spheroid volume. Thus, it was suggested that the necrotic cells release factors that inhibit proliferation of cells in the outer layers (Freyer, 1988). Furthermore, it was described that in a hypoxic environment EMT can be induced (Wu et al., 2011; Yang et al., 2008). Consequently, spheroid-forming cells might downregulate E-cadherin and subsequently lose connection to the other cells which results in cell shedding from the outside of the MCTSs thus contributing to the observed stagnation of spheroid growth.

In accordance with the literature, in this work it was demonstrated that large HCT116 and NCI-H460 MCTSs comprised of cells that were found to be in a quiescent state, as demonstrated by their low RNA content and the lack of expression of the proliferation marker Ki67 as well as their high expression of p27. In contrast, 2D-cultivated HCT116 and NCI-H460 cells were all proliferative and thereby evenly distributed between G_1 phase and the rest of the cell cycle, which concurred with values for human cell lines stated in the literature (Cooper, 2000). Interestingly, experiments revealed that the emergence of the quiescent cell population within MCTSs was dependent on the spheroid diameter since the same percentage of cells with low RNA content was found in equal-sized HCT116 (day 18)

and NCI-H460 (day 14) MCTSs. Furthermore, it was shown in this work that the development of a cell population characterised by a low RNA content differed substantially between growing HCT116 and NCI-H460 MCTSs. In HCT116 MCTSs initially the percentage of cells with a DNA content corresponding to the G_1 phase of the cell cycle increased while the amounts of cells in $S/G_2/M$ phases decreased. Finally, at day 11, cells in G_1 started to enter the quiescent state, characterised by a low RNA content. At the same time, the size of the proliferative pool of cells remained unchanged until the end of the experiment. This observation is in accordance with literature where it has been described that quiescence is not a unique condition but rather a term for a multitude of different states and stages (Rodgers et al., 2014; Yao, 2014). Spheroid-forming HCT116 cells seemed first to adopt a stage of light quiescence in which they discontinued cell cycle progression but did not yet display a decreased RNA content. At a certain point, probably when nutrient and oxygen deprivation exceeded a certain limit, these cells finally entered a deeper state of quiescence. In contrast to the sequence of events for HCT116 cells entering the quiescent state, the cell population with a low RNA content developed more gradually in NCI-H460 MCTSs. During spheroid growth, proliferative cells constantly entered first the lighter stage and subsequently the deeper stage of quiescence. Naturally, this led to a gradual reduction in the proliferative cell fraction in growing NCI-H460 MCTSs.

As mentioned previously, quiescence is not a unique condition but a collection of different stages. Therefore, additionally to the determination of the RNA content, the amounts of Ki67 and p27 were also analysed in growing HCT116 and NCI-H460 MCTSs. It was found that in larger spheroids, cells in the outermost spheroid layers expressed the highest amounts of Ki67 while cells close to the centre were completely devoid of the proliferation marker but expressed high amounts of p27. However, since it was shown by Bullwinkel and colleagues that low basal levels of Ki67 can also be found in quiescent cells at sites related to ribosomal RNA synthesis, it has yet to be investigated whether cells within the MCTSs are actually completely devoid of Ki67 or the used techniques were just not sensitive enough to detect remaining expression of the protein (Bullwinkel et al., 2006). As presumed from data about the RNA content, staining for Ki67 and p27 suggested again that the entrance into the quiescent state occurred gradually. It seemed that cells first started to enhance the expression of p27, before they lost the expression of Ki67. Reduction of the RNA content is probably the last step within the development of the quiescent state and can therefore be considered a sign for a deep stage of this condition. Interestingly, the flow cytometric experiments revealed that growing spheroids also contained cells that were devoid of Ki67 and p27. Furthermore, this cell population was comprised mostly of cells with low RNA content but additionally cells that, according to their DNA content, underwent cell death. It

might therefore be speculated that cells without expression of either Ki67 and p27 were in a condition just prior to necrosis.

In the second part of this chapter, spheroid-forming cells were investigated for their amounts of apoptosis-relevant proteins. Thereby, it was shown that overall spheroid-forming cells expressed less TRAILR1 than cells cultivated in 2D. Furthermore, it was revealed that, in addition to cells with surface TRAILR1 amounts comparable to 2D-cultivated cells, HCT116, NCI-H460 and HT29 MCTSs also comprised of a large number of cells with decreased or no expression of the protein (appendix: Figure 61). Interestingly this finding concurs with literature were the same TRAILR1 surface pattern was demonstrated for MCTSs generated from a breast cancer cell line (Chandrasekaran et al., 2014). Since in the present work spheroid sections and flow cytometric experiments showed that within MCTSs only proliferative cells expressed high amounts of TRAILR1, it can be hypothesised that the undersupply of nutrients and oxygen, that is very likely responsible for the induction of the quiescent state, might also account for the decrease in receptor expression. Furthermore, the fact that not only TRAILR1 protein but also TRAILR1 mRNA amounts were reduced, points to a regulation at the transcriptional level. TRAILR1 expression is known to be regulated by various transcription factors. For example, it has been shown that silencing of the transcriptional repressor GLI3 increased the expression of TRAILR1 in cholangiocarcinoma cells (Kurita et al., 2010). GLI3 is known to be activated by the hedgehog pathway, however it was also shown that the PI3K/Akt pathway influenced its signalling capacity (Gonnissen et al., 2015; Riobó et al., 2006). Since the PI3K/Akt signalling cascade can be activated in response to hypoxia, it might be speculated that quiescent cells within MCTSs showed decreased TRAIL1 expression due to enhanced activity of GLI3 (Lee et al., 2006). Another transcription factor that was recently shown to be involved in TRAILR1 expression is Sp1. Kwon and co-workers demonstrated in 2016 that expression of SP1 was promoted by the monooxygenase cytochrome P450 1B1 (CYP1B1) (Kwon et al., 2016). Furthermore, it has been shown that enhanced expression of SP1 correlated with enhanced expression of DNA methyltransferase-1 (DNMT-1) (Lin et al., 2010). The fact that overexpression of CYP1B1 was shown to increase the methylation on the TRAILR1-promoter region and blocking of SP1 as well as DNMT-1 could enhance TRAILR1 expression, points to an interconnected mechanism (Kwon et al., 2018). Furthermore, since it was demonstrated that hypoxia increased the binding of SP1 to DNA and enhanced the expression of CYP1B1, it can be speculated that in quiescent cells within HCT116 and NCI-H460 MCTSs, the TRAILR1 promoter is silenced by methylation (Chua et al., 2016; Elvidge et al., 2006). Interestingly it was also demonstrated that the transcription factor NF-κB can influence TRAILR1 expression depending on the subunits it is comprised of. In the presence of RelA, TRAIL1 expression was

decreased while the occurrence of c-Rel increased TRAILR1 amounts (Chen et al., 2003). Since it is known that cellular stresses such as nutrient starvation or hypoxia can induce NF-κB signalling, this transcription factor might also contribute to the downregulation of TRAILR1 in quiescent cells (Koong et al., 1994; reviewed by Moretti et al., 2012).

To further analyse a potential transcriptional regulation, inhibitors of GLI3, SP1, CYP1B1, DNMT- 1 and NF-κB could be applied on 11-day-old MCTSs followed by an investigation of the spheroid-forming cells for their expression of TRAILR1. Furthermore, these results could then be verified by an inducible knockdown of the proteins. In order to find out whether methylation of the TRAILR1 promotor is induced in quiescent, spheroid-forming cells, cells within the MCTSs might be sorted by TRAILR1 expression and thereafter analysed for methylation of the promotor region by pyrosequencing (Busato et al., 2018). Furthermore, the drug 5-Aza-2'-deoxycitidine could be used to investigate whether inhibiting the activity of DNA methyltransferases and demethylating of DNA restores TRAILR1 expression. Of note, not only the reduced transcription of the TRAILR1 gene but also decreased stability of the TRAILR1 mRNA might be responsible for the observed reduction in TRAILR1 mRNA level in quiescent, spheroid-forming cells. For example, it was shown that enhanced hedgehog signalling could promote the expression of miR25, a miRNA which was shown to inhibit TRAILR1 protein expression (Razumilava et al., 2012). MiRNAs can influence protein expression by either inducing degradation of the mRNA or inhibiting protein translation. Even though the latter was the case in the mentioned study, it cannot be excluded that in quiescent, spheroid-forming cells, the reduced amount of TRAILR1 mRNA was the result of increased mRNA degradation, potentially resulting from miRNA targeting. Alongside miRNAs, RNA binding proteins such as HuR can regulate mRNA stability and translation (Kullmann et al., 2002; Levy et al., 1998). In response to stresses such as hypoxia and nutrient starvation HuR was shown to be translocated from the nucleus to the cytoplasm subsequently binding to many different mRNAs (Blanco et al., 2016; Burkhart et al., 2013). Recently it was demonstrated that HuR can also bind to the 3'-untranslated region (UTR) of TRAILR1 mRNA which correlated with a decrease in TRAILR protein amounts. However, whether this is the result of reduced translation or HuR even additionally inhibits mRNA transcription has yet to be elucidated (Romeo et al., 2016). A way to determine whether mRNA stability is changed in quiescent cells when compared to proliferative cells, would be to treat the MCTSs with the transcriptional inhibitor actinomycin D for different time points. Thereafter, spheroid-forming cells might be sorted again by TRAILR1 surface expression and the TRAILR1 mRNA level at the distinct time points could be determined by qPCR to analyse a potential difference in mRNA stability in proliferative and quiescent cells.

Compared to cultivation in 2D, HCT116 and NCI-H460 MCTSs differed slightly in their global TRAILR2 expression. While spheroid-forming NCI-H460 cells showed on average lower TRAILR2 protein and RNA amounts than 2D-cultivated NCI-H460 cells, the expression of TRAILR2 was increased in HCT116 MCTSs in comparison to 2D cultivation, while the RNA amounts were decreased. However, interestingly in MCTSs generated from both cell lines the same localisation-dependent TRAILR2 expression was observed. While cells with high TRAILR2 amounts were localised mainly to the outermost cell layers and close to the necrotic core, cells within intermediate spheroid layers showed a reduced expression of the receptor.

The fact that 3D-cultivated HCT116 cells expressed overall more TRAILR2, in comparison to 2D-cultivated cells, while the surface expression of the 2D and 3D cell population was indistinguishable, points to spheroid-forming HCT116 cells containing intracellular TRAILR2. Indeed, it was already shown that many cell lines, including HCT116 cells, can express TRAILR2 that is localised to the cytoplasm or the nucleus (Chen et al., 2012; Haselmann et al., 2014; Kojima et al., 2011). Furthermore, nuclear TRAILR2 was also found in tissue samples of patients with advanced or recurrent non-small-cell lung cancer or pancreatic ductal adenocarcinoma (Haselmann et al., 2014; Leithner et al., 2009). Of note, in non-malignant pancreatic tissue, TRAILR2 was much less localised to the nucleus (Haselmann et al., 2014). In functional studies of nuclear TRAILR2 it was shown that interaction of the receptor with the core microprocessor components Drosha and DGCR8 resulted in the decrease of the mature miRNA let-7. Subsequently, this led to an increased expression of the let-7 targets LIN28B and HMGA2 and enhanced proliferation. Based on the findings of the present work and information from the literature, it can be hypothesised that in HCT116 and to a lesser extent also in NCI-H460 MCTSs, cells close to the necrotic core contained distinct amounts of intracellular, most likely nuclear TRAILR2. Since so far nothing is known about the signals that induce the translocalisation of TRAILR2, it can be speculated that persistent starvation of nutrients, growth factors and oxygen are the triggering factors. The increased nuclear TRAILR2 amounts might then help the cells to abandon the hostile environment. In order to investigate this in further detail, spheroid-forming cells could be sorted by TRAILR1 surface expression to separate proliferative and quiescent cells. Thereafter, the sorted cell populations could be investigated for their intracellular TRAILR2 localisation by cell fractionation and western blot analysis. If the hypothesis of nuclear TRAILR2 turns out to be correct, 2D-cultivated cells might be starved of nutrients and oxygen to investigate a possible participation of these factors in the translocalisation signalling.

In MCTSs generated out of both cell lines it was apparent that cells within intermediate spheroid layers showed overall a reduced TRAILR2 expression. Furthermore, spheroid-

forming cells of both investigate cell lines displayed on average reduced TRAILR2 mRNA levels in comparison to the corresponding 2D cell cultures. As previously described in this work for TRAILR1, TRAILR2 can also be downregulated by different mechanisms that decrease transcription and/or translation of TRAILR2 mRNA. To date, two transcription factors, NF-κB and Yin yang 1 were reported to be involved in the direct transcriptional downregulation of TRAILR2. In spheroid sections generated in this work it was observed that already in intermediated layers, cells begun to enter the quiescent state probably due to nutrient and oxygen starvation. As described earlier, such conditions can induce the expression of NF-κB which in turn is able to act as a direct transcriptional suppressor of TRAILR2 (Chen et al., 2003; Koong et al., 1994; reviewed by Moretti et al., 2012). Furthermore, NF-κB was shown to cooperate with the transcription factor Yin yang 1 which can in its active form bind to the TRAILR2 promotor and inhibit its activity (Baritaki et al., 2007; Lee et al., 2007; Sepulveda et al., 2004). Another protein that has been demonstrated to regulate TRAILR2 expression is the transcription factor Foxo3a which in its phosphorylated state is able to activate the transcription of TRAILR2. However, nutrient starvation or growth factor withdrawal were shown to downregulate PI3K/Akt signalling which in turn led to the inactivation of Foxo3a and subsequent inhibition of TRAILR2 transcription (Chen et al., 2010; Fu and Tindall, 2008; Shoeb et al., 2013). Interestingly, alongside transcription factors, also the mRNA-binding protein HuR has been described to decrease TRAILR2 amounts in response to stresses such as hypoxia and starvation (Blanco et al., 2016; Burkhart et al., 2013; Pineda et al., 2012).

The fact that overall protein expression was again increased in cells close to the necrotic core suggests that either, the previously described mechanisms of downregulation were terminated, or that induction of TRAILR2 expression through persistent and more severe hypoxia and nutrient starvation overran the processes of downregulation. For example, it was shown that hypoxia can activate the PI3K/Akt pathway, which could restore the phosphorylation of Foxo3a and subsequently led to an upregulation of TRAILR2 expression (Lee et al., 2006). Thus, it can be hypothesised that cells in growing MCTSs were first starved of nutrients which led to an inactivation of Foxo3a before they became depleted of oxygen which resulted in an activation of the transcription factor. In accordance, investigations discussed later in this work regarding the hypoxia marker Hif-1α revealed that solely cells close to the necrotic core expressed high amounts of the protein. In addition to Foxo3a, also the transcription factors, SP1, AP1 and p53 are known to increase TRAILR2 expression (Kang et al., 2011; Moon et al., 2010; Portanova et al., 2013; Takimoto and El-Deiry, 2000). Interestingly, all three are transferred into an active form in response to hypoxia and nutrient starvation (Aubrey et al., 2017; Chua et al., 2016; Takimoto and El-Deiry, 2000; Zhou

et al., 2015; Zou, 2004). Another transcription factor that might be involved in the upregulation of TRAILR2, in cells close to the necrotic core, is the protein CHOP which is part of the ER stress-induced UPR (reviewed by Hetz et al., 2015). It is known that in the absence of glucose and/or oxygen, unfolded and misfolded proteins accumulate in the cell, causing ER stress (reviewed by Kaufman et al., 2002; reviewed by Schönenberger, 2015; Sies and Bruene, 2007). In response to such stresses, the UPR is activated which in the beginning helps to protect cells from damage but in case of unsolved ER stress results in the induction of apoptosis. As part of this machinery the expression of the transcription factor CHOP was shown to be induced and bind to the 5'-flanking region of the TRAILR2 gene enhancing transcription (Yamaguchi and Wang, 2004). Furthermore, it was demonstrated that in response to ER stress, two further transcription factors, ELK-1 and ATF3, can cooperate with CHOP to induce the expression of TRAILR2 (Edagawa et al., 2014; Oh et al., 2010). However, it was also suggested that the UPR can increase TRAILR2 amounts in a CHOP-independent manner. After glucose starvation, ATF4 as well as the ATF6/IRE1α/XBP-1 axis were shown to enhance the expression of TRAILR2 (Iurlaro et al., 2017; Liu et al., 2009). The observation made in this work that spheroid-forming cells expressed on average more TRAILR2 than 2D-cultivated cells while displaying lower total RNA amounts of the receptor, indicates that TRAILR2 might be more stable in 3D-cultured cells or that protein translation is reduced under 2D cultivation. TRAILR degradation was shown to be regulated by the E3 ubiquitin ligase c-Cbl as well as the protein MCPIP1 (Oh et al., 2010; Song et al., 2010). However, at this time, nothing has been reported regarding a decreased function of those two proteins under stress conditions. Since recently it has been predicted that 32 mRNA-binding proteins, including HuR, can bind to TRAILR2 transcripts, it might be hypothesised that stability of TRAILR mRNA was increased while protein translation was strongly reduced in 2D in comparison to 3D-cultivated HCT116 cells (Mert and Sanlioglu, 2016).

As suggested for TRAILR1, regulation of TRAILR2 expression within spheroid-forming cells might also be investigated by inhibition or inducible knockdown of the previously described transcription factors and underlying signalling cascades. Furthermore, differences in TRAILR2 mRNA stability between 2D- and 3D-cultivated cells could be analysed by blocking of transcription with actinomycin D for different time points and subsequent qPCR. Furthermore, to investigate localisation-dependent TRAILR2 mRNA expression levels in spheroid sections, fluorescence *in situ* hybridisation (FISH) could be used (Querido et al., 2017).

In accordance with literature it has been shown in this work that NCI-H460 cells were completely devoid of surface regulatory receptor expression while HCT116 cells only expressed surface TRAILR4 in appreciable quantities (Kischkel et al., 2000). Flow cytometric studies furthermore revealed that HCT116 MCTSs varied widely in their surface TRAILR4

expression. While some cells displayed amounts comparable to those found in 2D-cultivated HCT116 cells, surface expression of TRAILR4 was strongly reduced in most spheroid-forming cells. However, since no correlation between the amounts of proliferation markers and the surface expression of the regulatory receptor was found in spheroid-forming cells and immunohistochemical staining of TRAILR4 could not be carried out due to the lack of a specific antibody, a localisation-dependent expression of TRAILR4 remains highly speculative. Nevertheless, a correlation between a cell's localisation in the MCTS and its overall TRAILR4 expression is still conceivable since recently TRAILR4 was also found in the cell nucleus (Zhang, Franco, et al., 2000). Similar to the other TRAILRs, TRAILR4 expression is also known to be regulated by different mechanisms. On the one hand, TRAILR4 amounts can be reduced due to promotor methylation or destabilisation of mRNA (Todorova et al., 2015; Wu, Chen, et al., 2016). On the other hand, hypoxia was shown to upregulate TRAILR4 expression probably through Hif-1α acting as a transcription factor (Pei et al., 2010). Furthermore, the fact that the TRAILR4 gene contains a binding site for p53 suggests an additional mechanism of transcriptional regulation (Liu et al., 2005). Thus, it can be hypothesised that, comparable to the amounts of TRAILR1 and TRAILR2 in MCTSs, also TRAILR4 expression was influenced by the shortage of oxygen and nutrients.

Interestingly, investigations of further surface receptors and apoptosis-relevant proteins conducted in this thesis revealed that the expression of the epidermal growth factor receptor EGFR and the anti-apoptotic protein Mcl-1 was considerably downregulated under 3D cultivation in NCI-H460 but not HCT116 cells. Flow cytometric analyses showed that, similar to TRAILR1 and TRAILR2, also the surface expression of the EGFR varied widely in spheroid-forming NCI-H460 cells. However, unlike TRAILR1, quiescent cells displayed the highest amounts of EGFR, which is in accordance with various studies that showed enhanced EGFR expression in response to oxygen deprivation (Bos et al., 2005; Misra et al., 2012; Wang et al., 2013). For Mcl-1 only the overall protein amounts in 2D- and 3D-cultivated cells were investigated but the localisation-dependent expression within MCTSs has yet to be determined. However, since it was shown in the literature that hypoxia and nutrient starvation both can lead to a downregulation of Mcl-1, it can be speculated that quiescent cells within NCI-H460 MCTSs expressed less amounts of the protein (Fang and Yeh, 2017; Harrison et al., 2011; Leclerc et al., 2015; Senichkin et al., 2018). Further analysed apoptosis-relevant proteins such as FADD, procaspase 8, cFlip and XIAP were not expressed differently in 2D- and 3D-cultivated cells, as apparent from western blot analysis and flow cytometric experiments. However, a localisation-dependent expression of these proteins in MCTSs could not be excluded by these analysis methods and has yet to be investigated.

Taken together, TRAILR expression was found to be localisation-dependent in HCT116 and NCI-H460 MCTSs. While large TRAILR1 amounts were exclusively found in proliferative cells, the highest expression of TRAILR2 was detected in proliferative cells forming the outermost spheroid layer and additionally in quiescent cells close to the necrotic core. Interestingly, the reduced TRAILR expression of cells in intermediate spheroid layers was also already observed in patient samples. For example, it has been shown that in colon carcinoma, the highest expression of TRAILR2 could be found in cells forming the invasive front (Sträter et al., 2002). However, in NSCLCs with squamous cell differentiation, both the expression of TRAILR1 and TRAILR2 was highest in the basal layer of tumours while cells located in supra basal areas showed decreased expression or were completely devoid of the two receptors (Spierings et al., 2003).

Chapter 2 part 1: Investigation of TRAIL-induced apoptosis in 2D- and 3D-cultivated HCT116 and NCI-H460 cells

In the previous chapter it was shown that culturing cells as MCTSs increased their heterogeneity, not only concerning cell cycle status, but also concerning the expression of apoptosis-relevant proteins. As in a nascent tumour, quiescent and finally necrotic cell populations developed in larger MCTSs, most likely as a consequence of the undersupply of the inner cell layers with nutrients, growth factors and oxygen. Hence, localisation-dependent changes in the expression of apoptosis-relevant proteins, such as TRAILR1 and TRAILR2, might not only occur in MCTSs but probably also *in vivo.* MCTSs seem therefore to represent a better *in vitro* model system than 2D-cultured cells for the investigation of drug responsiveness. In the framework of this project, HCT116 and NCI-H460 MCTSs were next examined for their susceptibility to two 2nd generation TRAILR agonists, Db$_{\alpha EGFR}$-scTRAIL and Fc-scTRAIL 1551. In this chapter, it was shown that MCTSs of both cell lines are less susceptible to TRAIL than the corresponding 2D cell cultures and that within MCTSs less susceptible cells shield TRAIL-hypersensitive cells from TRAIL-induced apoptosis.

3.1. HCT116 MCTSs are less susceptible to TRAIL-induced cell death than corresponding 2D cell cultures

It is known that changes in the expression of death receptors, such as TRAILR1 and TRAILR2, can influence a cell's susceptibility to the corresponding death ligands, such as TRAIL (reviewed by Pennarun et al., 2010). Hence, the results of the previous chapter gave rise to the hypothesis that within larger MCTSs (day 11), intermediate layers, comprised of cells less susceptible to TRAIL due to reduced expression of both TRAILR1 and TRAILR2, might protect highly TRAILR2-positive and therefore TRAIL-sensitive cells close to the centre from TRAIL-induced apoptosis (Figure 29).

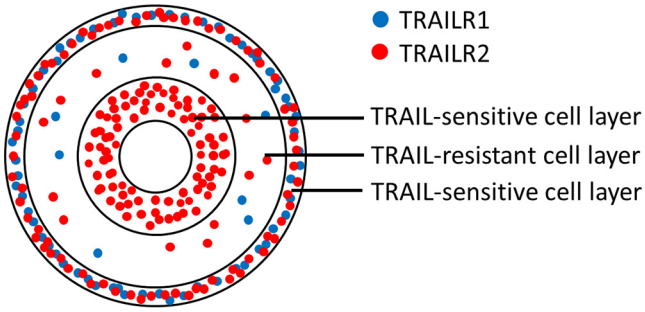

Figure 29: Schematic of localisation-dependent expression of TRAILR1 and TRAILR2

To examine this hypothesis, 11-day-old HCT116 MCTSs and 2D-cultured HCT116 cells were stimulated with two different 2nd generation TRAILR agonists, $Db_{\alpha EGFR}$-scTRAIL and Fc-scTRAIL 1551, and induction of cell death was determined by Annexin V-EGFP staining and flow cytometry. $Db_{\alpha EGFR}$-scTRAIL and Fc-scTRAIL 1551 are both fusion proteins, however while in the case of Fc-scTRAIL 1551, single chains of TRAIL (scTRAIL) are fused to the Fc part of an IgG antibody, in $Db_{\alpha EGFR}$-scTRAIL the scTRAILs are bound to EGFR-specific scFV antibody fragments. Hence, in contrast to Fc-scTRAIL 1551, $Db_{\alpha EGFR}$-scTRAIL can not only bind to TRAILR1 and TRAILR2 but also to the EGFR, which was shown to enhance its activity of inducing cell death in 2D-cultured HCT116 and Colo 205 cells (Hutt, 2017). However, since no beneficial effect of targeting could be found when applied in a Colo 205 xenograft tumour model it was investigated within this project whether $Db_{\alpha EGFR}$-scTRAIL was superior in inducing cell death in MCTSs (Hutt, 2017). In a first step both fusion proteins were solely applied to 2D- and 3D-cultured HCT116 cells, since in HCT116 MCTSs localisation-dependent differences in TRAILR expression were more pronounced than in NCI-H460 spheroids. Furthermore, in contrast to cells within NCI-H460 MCTSs, spheroid-forming HCT116 cells seemed not to differ in their expression of the EGFR, which simplified the comparison of $Db_{\alpha EGFR}$-scTRAIL and Fc-scTRAIL 1551 concerning their efficacy in inducing cell death (Figure 20; Figure 21).

Thereby, investigations revealed that, independent of the fusion protein and the treatment length, HCT116 MCTSs (day 11) were more resistant to TRAIL than the corresponding 2D cell cultures. Stimulation with $Db_{\alpha EGFR}$-scTRAIL for 24 h resulted in an half maximal effective concentration (EC_{50}) value that was approximately 20 times higher for the stimulation of 3D-cultivated cells than of 2D-cultivated cells. After 6 h treatment the differences in the responsiveness of 2D- and 3D-cultured HCT116 cells were comparable to that observed after 24 h, an EC_{50} value for the stimulation of HCT116 MCTSs was not calculable at the trialled concentrations. Treatment with the non-targeting construct Fc-scTRAIL 1551 resulted in an

EC_{50} value that was about 10 times (24 h) and 4.4 times (6 h) higher in case of stimulation of the HCT116 MCTSs compared to treatment of the corresponding 2D cell cultures. Comparing $Db_{\alpha EGFR}$-scTRAIL with Fc-scTRAIL 1551, it could be shown that after 24 h stimulation, the targeting construct $Db_{\alpha EGFR}$-scTRAIL was slightly more effective in inducing cell death in 2D as well as 3D-cultivated HCT116 cells than the non-targeting construct Fc-scTRAIL 1551. However, a treatment time of 6 h was not enough to reveal the differences between the both fusion proteins in their capacity to induce apoptosis (Figure 30; Table 6).

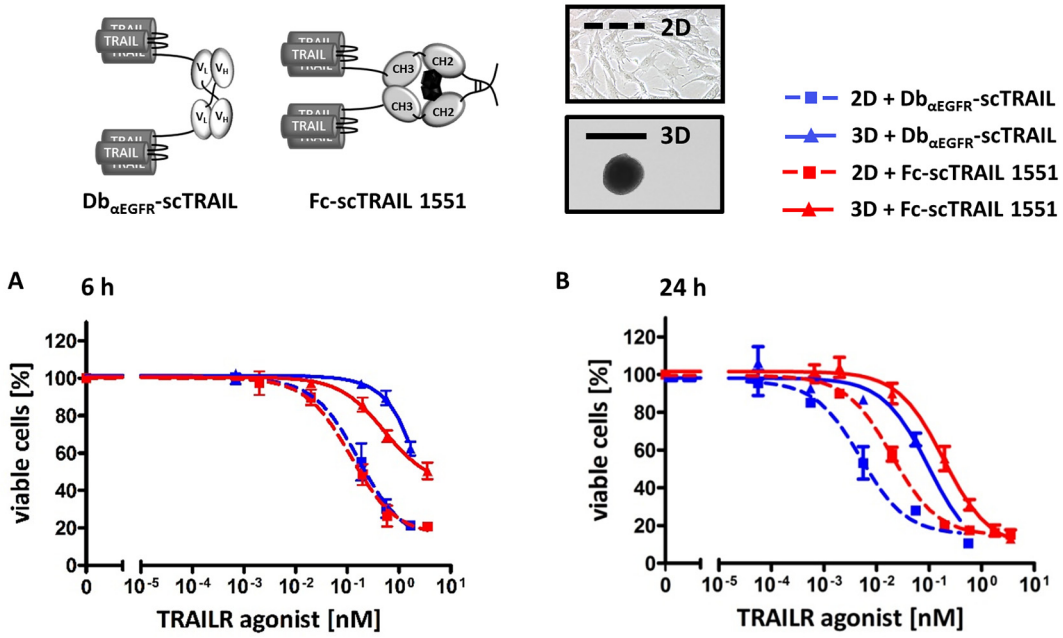

Figure 30: HCT116 MCTSs are less susceptible to TRAIL than 2D-cultivated HCT116 cells

2D-cultivated HCT116 cells and HCT116 MCTSs (day 11) were stimulated for 6 h or 24 h with increasing concentrations of either $Db_{\alpha EGFR}$-scTRAIL or Fc-scTRAIL 1551 and cell death was measured afterwards by staining with Annexin V-EGFP followed by flow cytometry. Data shown are mean values ± SEM of three independent experiments each performed in duplicates. Nonlinear regressions (sigmoidal dose-response) were performed in GraphPad prism 5 **(A/B)**.

Table 6: Bioactivity of $Db_{\alpha EGFR}$-scTRAIL and Fc-scTRAIL 1551 on 2D- and 3D-cultivated HCT116 cells

	6 h		24 h	
	$Db_{\alpha EGFR}$-scTRAIL EC_{50} [nM]	**Fc-scTRAIL 1551 EC_{50} [nM]**	**$Db_{\alpha EGFR}$-scTRAIL EC_{50} [nM]**	**Fc-scTRAIL 1551 EC_{50} [nM]**
2D	0.169	0.118	0.005	0.020
3D	> 2	0.520	0.097	0.190

Shown EC_{50} values derive from nonlinear regression curves displayed in figure 30.

3.2. Cells less susceptible to TRAIL shield TRAIL-hypersensitive cells in HCT116 MCTSs from TRAIL-induced cell death

The finding that HCT116 MCTSs are more resistant to TRAILR agonists than HCT116 cells cultivated in 2D was in agreement with the hypothesis, that a subpopulation comprised of cells less susceptible to TRAIL exist within larger MCTSs. However, the performed experiments did not reveal whether there are protected TRAIL-sensitive cells close to the necrotic core. In order to test this assumption, as well as to exclude effects caused by diffusion barriers, HCT116 MCTSs (day 11) were dissociated and together with detached 2D-cultured HCT116 cells stimulated in suspension. Since it had been shown before that cells deriving from dissociated MCTSs regained, within one day, almost the same level of TRAILR expression as cells growing exponentially in 2D (Figure 22), treatment was only conducted for 6 h. Thereby, it could be demonstrated that detachment of 2D-cultivated HCT116 cells did not change their susceptibility to Fc-scTRAIL1551 (adherent: EC_{50} = 0.12 nM; detached: EC_{50} = 0.10 nM) whereas cells were much more sensitive to $Db_{\alpha EGFR}$-scTRAIL than before (adherent EC_{50} = 0.118 nM; detached EC_{50} = 0.007 nM). The determined curve progression for the dissociated MCTSs looked similar for both fusion proteins. At lower concentrations, cells derived from dissociated MCTSs were more susceptible to the TRAILR agonists than the detached 2D-cultured cells. However, at higher concentrations a comparable percentage of cells under 2D and 3D cultivation conditions, or in case of treatment with $Db_{\alpha EGFR}$-scTRAIL slightly more of the 3D-cultivated than the 2D-cultivated cells, survived the treatment. This result confirmed the hypothesis that spheroid-forming cells exist that are more susceptible to TRAIL than corresponding 2D-cultured cells (TRAIL-hypersensitive cells) which, however, become only visible when dissociation was conducted, as they are in non-dissociated MCTSs shielded by a TRAIL-resistant subpopulation of cells. The bioactivites of $Db_{\alpha EGFR}$-scTRAIL and

Fc-scTRAIL 1551 were again compared and it could be shown that, in contrast to before when cells were adherent and MCTSs were not dissociated, 6 h is sufficient to reveal the higher efficacy of $Db_{\alpha EGFR}$-scTRAIL to induce apoptosis in 2D- and 3D-cultivated cells (Figure 31).

A

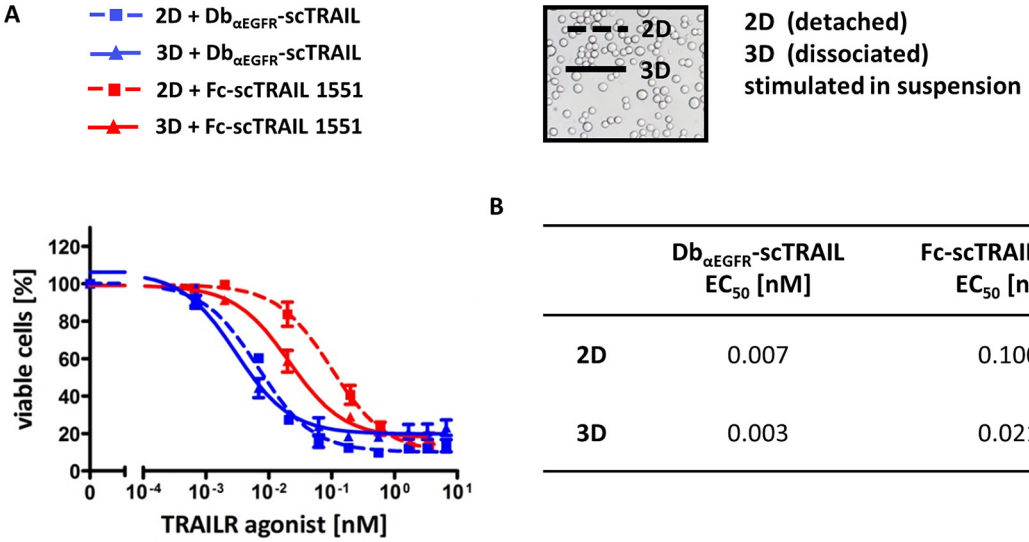

B

	$Db_{\alpha EGFR}$-scTRAIL EC_{50} [nM]	Fc-scTRAIL 1551 EC_{50} [nM]
2D	0.007	0.100
3D	0.003	0.021

Figure 31: Within HCT116 MCTSs, cells less susceptible to TRAIL shield TRAIL-hypersensitive cells from TRAIL-induced cell death

2D-cultivated HCT116 cells were detached and HCT116 MCTSs (day 11) were dissociated before stimulating single cells in suspension with increasing concentrations of either Db_{EGR}-scTRAIL or Fc-scTRAIL 1551 for 6 h. Cell death was afterwards measured by staining with Annexin V-EGFP followed by flow cytometry. Data shown are mean values ± SEM of three independent experiments each performed in duplicates. Nonlinear regressions (sigmoidal dose-response) were performed in GraphPad prism 5 **(A)**. Table shows the EC_{50} values corresponding to the performed nonlinear regressions **(B)**.

3.3. Cells less susceptible to TRAIL shield TRAIL-hypersensitive cells in NCI-H460 MCTSs from TRAIL-induced cell death

To verify whether the assumption of a TRAIL-resistant subpopulation that shields TRAIL-hypersensitive cells from TRAIL-induced cell death also applied to NCI-H460 MCTSs, adherent and detached 2D-cultivated NCI-H460 cells, along with non-dissociated and dissociated NCI-H460 MCTSs, were treated with Fc-scTRAIL 1551 for 6 h and cell death was analysed again by staining with Annexin V-EGFP and flow cytometry. As stated previously spheroid-forming NCI-H460 cells varied widely in their expression of the EGFR, therefore

stimulation with $Db_{\alpha EGFR}$-scTRAIL was not conducted, as it would have complicated any interpretation of generated data (Figure 21).

Comparable with the results for the HCT116 cell line, stimulation of adherent 2D-cultured NCI-H460 cells and non-dissociated NCI-H460 MCTSs with Fc-scTRAIL 1551 revealed that spheroids were less susceptible to treatment than the corresponding 2D cell cultures (2D EC_{50} = 0.105 nM; 3D EC_{50} = 0.205 nM). Detachment of 2D-cultured NCI-H460 cells did not change their susceptibility to Fc-scTRAIL 1551 whereas cells derived from the dissociation of MCTSs showed a similar pattern as cells from dissociated HCT116 spheroids. At low concentrations of Fc-scTRAIL 1551, 3D-cultured cells were more susceptible than 2D-cultured cells whereas at higher concentrations the percentage of surviving 2D- and 3D-cultivated cells was comparable. It can therefore be concluded that, similarly to HCT116 MCTSs, cells less susceptible to Fc-scTRAIL 1551 protect TRAIL-hypersensitive cells within non-dissociated NCI-H460 MCTSs (Figure 32).

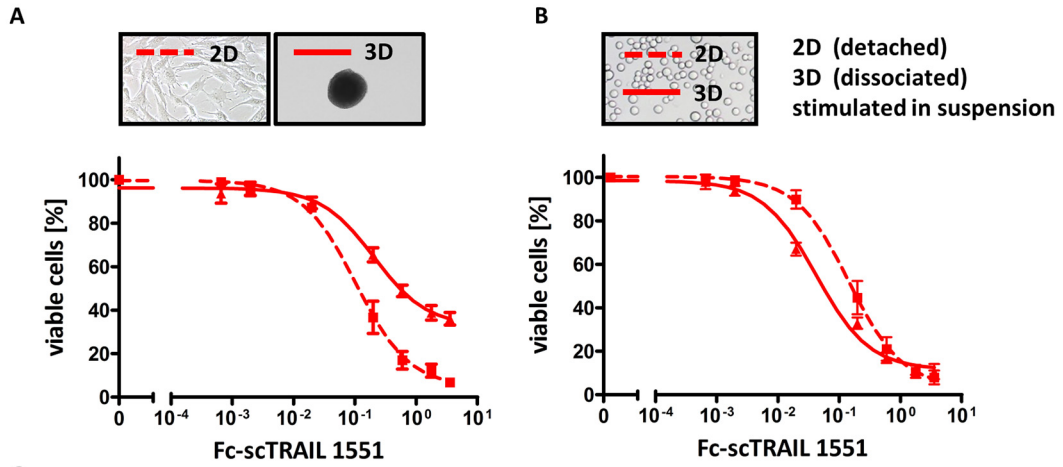

C

	not dissociated Fc-scTRAIL 1551 EC_{50} [nM]	in suspension Fc-scTRAIL 1551 EC_{50} [nM]
2D	0.105	0.145
3D	0.205	0.042

Figure 32: Within NCI-H460 MCTSs, cells less susceptible to TRAIL shield TRAIL-hypersensitive cells from TRAIL-induced cell death

2D-cultivated NCI-H460 cells and NCI-H460 MCTSs (day 11) were stimulated for 6 h with increasing concentrations of Fc-scTRAIL 1551 **(A)** or 2D-cultivated NCI-H460 cells were detached and NCI-H460 MCTSs (day 11) were dissociated before stimulating single cells in suspension with increasing concentrations of Fc-scTRAIL 1551 for 6 h **(B)**. Cell death was afterwards measured by staining with Annexin V-EGFP followed by flow cytometry. Data shown are mean values ± SEM of three independent experiments each performed in duplicates (A/B). The table shows the EC_{50} values resulting out of performed nonlinear regressions (sigmoidal dose-response) **(C)**.

3.4. After stimulation with TRAIL, 2D- and 3D-cultivated cells die by apoptosis

As described previously, phosphatidylserine flips from the inside to the outside of the cell membrane during the process of apoptosis and can then be bound by Annexin V-EGFP. However, necrotic cells can also appear positive for Annexin V-EGFP since due to permeabilisation of the cell membrane, the fluorescently-labelled protein is able to enter the cell and bind to phosphatidylserine located on the inside of the membrane. To determine whether cells in the previous experiments exclusively died by apoptosis, 2D-cultured HCT116 cells and HCT116 MCTSs (11 days) were stimulated for 24 h with the highest concentration of Fc-scTRAIL 1551 used before, in the presence and absence of the pan caspase inhibitor QVD. Thereby, it could be shown that 2D-cultured HCT116 cells exclusively died by apoptosis

as cell death could be completely prevented by blocking caspase activity with QVD. In the case of HCT116 MCTSs, treatment with the pan caspase inhibitor alone led to cell death in around 10% of all cells. Stimulation of the spheroids with Fc-scTRAIL 1551 and QVD together could therefore not restore the level of viable cells to that found in the control. However, no significant difference ($p > 0.05$; unpaired t-test) between the percentage of dead cells in the samples solely treated with QVD and that treated with both of the drugs together could be detected, indicating that also in the 3D scenario all cells died by apoptosis after stimulation with Fc-scTRAIL 1551. Furthermore, staining of cleaved caspase 3 in sections of 11-day-old HCT116 MCTSs, previously stimulated with 0.1 nM $Db_{\alpha EGFR}$-scTRAIL for 24 h, revealed that apoptosis was induced in the outer cell layers of the spheroids (Figure 33).

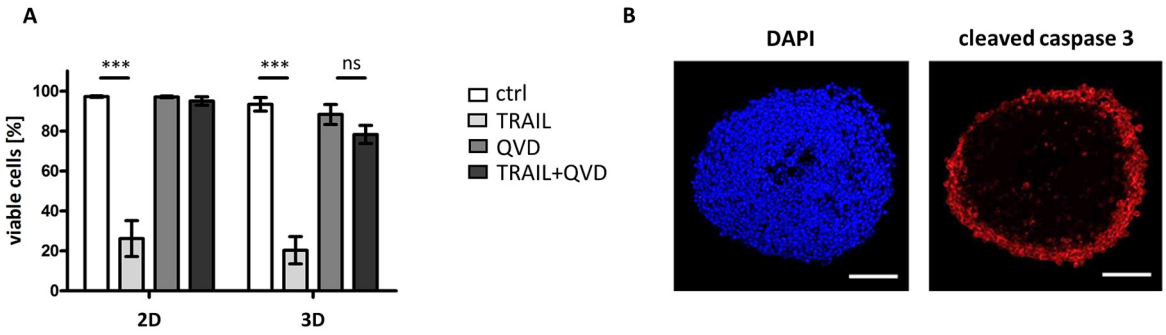

Figure 33: 2D- and 3D-cultivated HCT116 cells die by apoptosis after stimulation with TRAIL

2D- and 3D- (day 11) cultivated HCT116 cells were pre-incubated with 20 µM QVD or DMSO as a control (ctrl) for 1 h and afterwards stimulated with 3.55 nM Fc-scTRAIL 1551 for 24 h. At the end of treatment, cell death was measured by staining with Annexin V-EGFP followed by flow cytometry. Data shown are mean values ± SD of three independent experiments each performed in duplicates. Statistical significance was verified with an One-way ANOVA in combination with the Tukey's Multiple Comparison test (*** = $p \leq 0.001$, ns = not significant) **(A)**. HCT116 MCTSs (day 11) were treated for 24 h with 0.1 nM $Db_{\alpha EGR}$-scTRAIL. Afterwards spheroids were cut into 10 µm slices using a cryostat and sections were stained with DAPI along with a specific antibody against cleaved caspase 3. Pictures were taken using a confocal laser scanning microscope. Scale bars = 100 µm. Experiment was conducted by Daniela Maichl **(B)**.

3.5. 3D-cultivated cells that survive treatment with TRAIL can proliferate and form colonies

To investigate whether 2D- and 3D-cultivated HCT116 cells that survived treatment with Fc-scTRAIL 1551 were in the following able to proliferate and form colonies, cells within unstimulated wells were counted post treatment and 200 cells for the control as well as the same volume for the other conditions were seeded into 6-well plates. After 7 days of cultivation, the number of colonies and the area covered by cells was then determined by staining with crystal violet and subsequent analysis with the Fiji software.

Investigations revealed that 2D- and 3D-cultivated cells that survived the treatment with Fc-scTRAIL 1551 were able to proliferate and form colonies. Thereby, the number of colonies was slightly higher and the area covered by cells was slightly larger in wells with stimulated and re-seeded MCTS-forming cells than in the wells harbouring the stimulated and re-seeded 2D-cultivated cells. However, the differences between 2D-cultured cells and MCTSs were not as pronounced as they were for the determination of survivors directly after treatment by staining with Annexin V-EGFP and flow cytometry (Figure 30). This might be due to the fact that some of the Annexin V-EGFP negative cells within the stimulated 3D cell culture were already damaged and would just undergo cell death at a later time point. The fact that ~20% more colonies could be found and ~20% more area was covered with cells, in wells harbouring the survivors of stimulated MCTSs than in wells containing the resistant 2D-cultured cells, indicated that the colony size of 2D- and 3D-cultivated survivors was comparable, which was simultaneously also evident from the displayed images. This meant that surviving 3D-cultivated cells had the same capacity to proliferate as the survivors of a 2D cell culture. As in the previous experiment, QVD alone did not affect the colony forming capacity of re-seeded 2D-cultivated cells, however, it seemed that it had again a minor effect on 3D-cultivated cells in terms of slightly reducing colony number and area covered by cells in comparison to the control. Nevertheless, the number of colonies as well as the area covered by cells could be restored to the level of untreated 2D- and 3D-cultivated cells by incubating them with TRAIL and QVD together, confirming that cells died by apoptosis after treatment with Fc-scTRAIL 1551 (Figure 34).

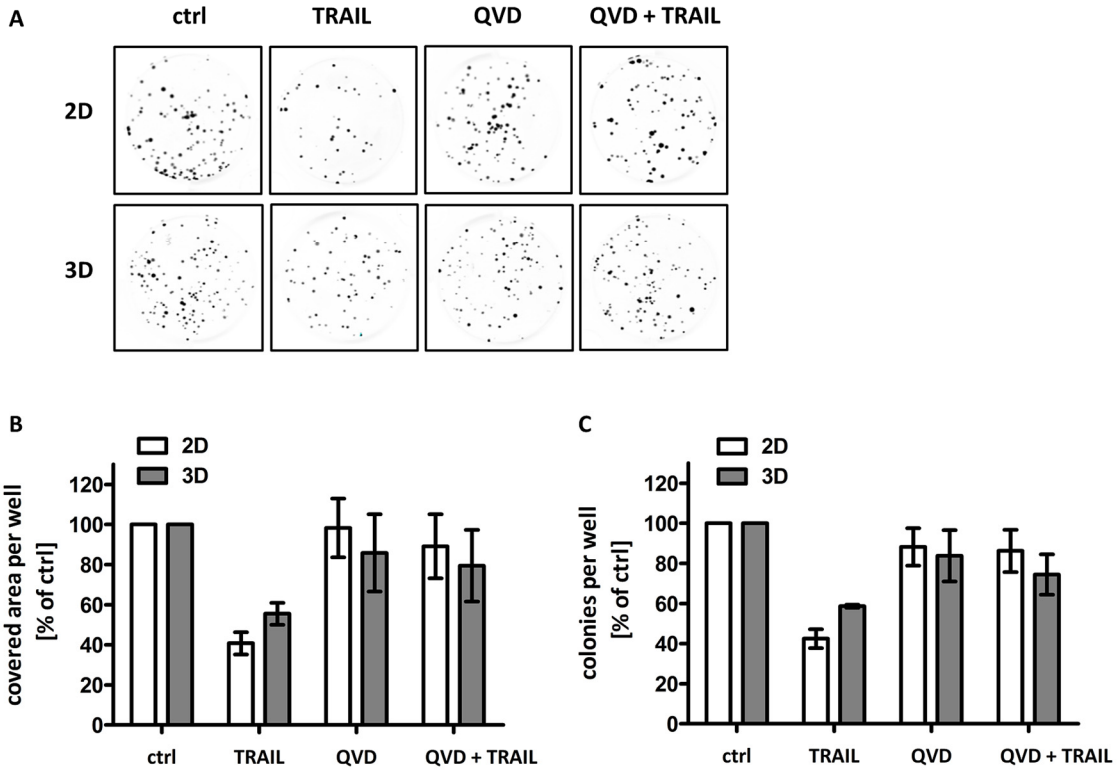

Figure 34: 2D- and 3D-cultivated TRAIL-resistant cells can proliferate and form colonies

2D- and 3D- (day 11) cultivated HCT116 cells were pre-incubated with 20 µM QVD or DMSO as a control (ctrl) for 1 h and afterwards stimulated with 0.2 nM Fc-scTRAIL 1551 with or without QVD for 24 h. Thereafter, 2D- and 3D-cultivated cells were harvested (spheroids were dissociated) and cells were seeded into 6-well plates to determine clonogenic survival. Cells in the control wells were counted (200 cells/well) and the same volume was seeded for the other conditions. After 7 days, the assay was stopped with crystal violet and pictures were taken using a microplate reader **(A)**. Images were analysed with the Fiji software. Data shown are mean values ± SD of three independent experiments each performed in triplicates. An One-way ANOVA in combination with the Dunn's Multiple Comparison test showed no significant difference between 2D- and 3D cells stimulated with TRAIL **(B/C)**.

3.6. TRAILR1 and TRAILR2 equally contribute to apoptosis induction in 2D-cultured HCT116 and NCI-H460 cells

Interestingly, in some cell lines TRAIL-induced apoptosis is preferentially activated via one of the two death-inducing TRAILRs (Kelley et al., 2005; MacFarlane et al., 2005). To determine which TRAILR is more important in transmitting apoptotic signals in HCT116 and NCI-H460 cells, antagonistic blocking antibodies against either TRAILR1 or TRAILR2 were applied on these cells before stimulating them with 0.1 nM $Db_{\alpha EGFR}$-scTRAIL together with blocking antibodies for 6 h. At the end of the experiment, remaining adherent cells were stained with crystal violet and absorbance was measured with a microplate reader. These experiments

revealed that apoptosis could be completely prevented by pre-incubating HCT116 and NCI-H460 cells with both of the blocking antibodies together. Furthermore, pre-treatment with either one or the other of the two antagonistic antibodies could reduce cell death to the same extent but not completely in both cell lines, indicating that TRAILR1 and TRAILR2 contribute equally to the induction of apoptosis in HCT116 and NCI-H460 cells (Figure 35).

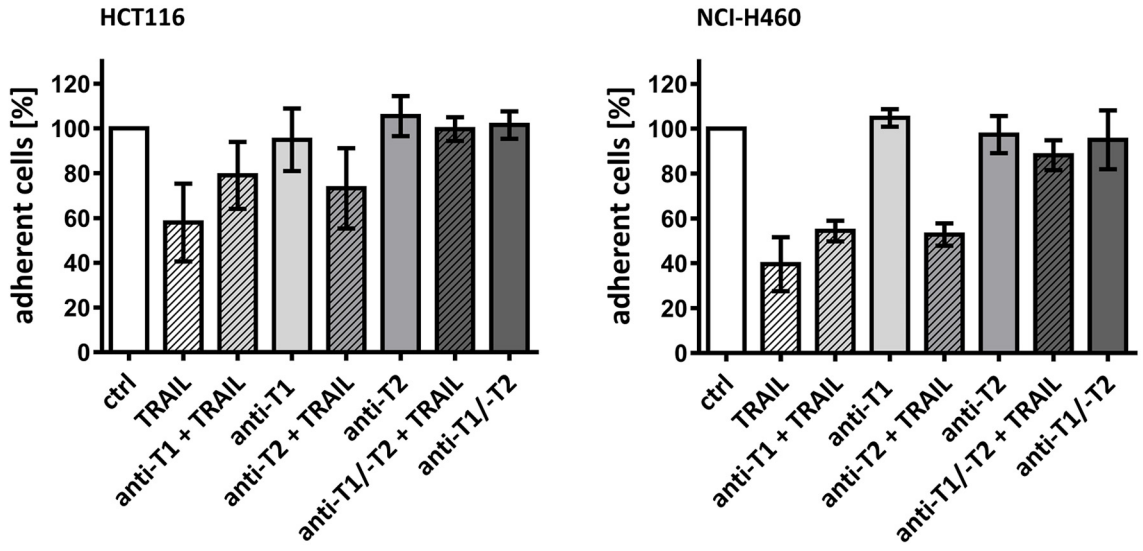

Figure 35: TRAIL induces apoptosis via TRAILR1 and TRAILR2 in 2D-cultivated HCT116 and NCI-H460 cells

2D-cultured HCT116 and NCI-H460 cells were incubated with the blocking antibodies anti-TRAILR1 (anti-T1) and anti-TRAILR2 (anti-T2) for 30 min, followed by stimulation with 0.1 nM $Db_{\alpha EGFR}$-scTRAIL together with blocking antibodies for 6 h. At the end of treatment, cells were stained with crystal violet and absorbance was measured with a microplate reader at 550 nm. Data shown are mean values ± SD of three independent experiments, each conducted in triplicates.

Chapter 2 part 2: TRAILR KO influences proliferation and TRAIL-susceptibility of HCT116 cells

Since it is known that TRAILRs are not only major players of the apoptosis pathway but can be also be involved in proliferation and migration, it was investigated whether knockout (KO) of TRAILR1 and TRAILR2 influences the spheroid-forming capacity and MCTS growth of HCT116 as a model cell line. Thereby, it could be shown that TRAILR1 as well as TRAILR2 KO did not affect spheroid formation but slowed down growth of HCT116 MCTSs. Furthermore, investigations into TRAIL susceptibly of HCT116 TRAILR KO cell lines showed that KO of TRAILR2 rendered HCT116 cells less susceptible to TRAIL-induced cell death and prevented the formation of a TRAIL-hypersensitive subpopulation within MCTSs.

4.1. Analysis of TRAILR expression within HCT116 TRAILR KO cell lines generated by the TALEN and CRISPR/Cas9 approach

To investigate the role of TRAILR1 and TRAILR2 in spheroid formation as well as their respective contribution to the observed heterogeneity of MCTS-forming cells concerning TRAIL susceptibility, clonal HCT116 TRAILR KO cell lines generated by the TALEN approach were generously provided by Olivier Micheau (INSERM, France).

Before starting with the 3D cultivation, obtained cell lines were first analysed for their surface expression of TRAILRs by flow cytometry and for their total (surface + intracellular) TRAILR expression by western blot analysis. Thereby, it was found that the HCT116 TRAILR1 KO cell line (HCT116 T1 KO) was indeed completely devoid of surface as well as intracellular TRAILR1, whereas their surface expression of TRAILR2 was comparable to that detected in HCT116 wildtype (WT) cells. Interestingly, the total TRAILR2 amount, determined by western blot analysis, was slightly higher in the TRAILR1 KO cell line then in the WT cells, indicating that this clonal cell line contained slightly higher amounts of intracellular TRAILR2. As expected, the HCT116 TRAILR2 surface KO cell line (HCT116 T2 sKO) was completely devoid of surface TRAILR2 expression however surprisingly western blotting revealed that it contained large amounts of intracellular TRAILR2. In accordance with that, the cell line HCT116 T1 KO/T2 sKO showed no expression of both TRAILRs at the cell surface but high intracellular expression of TRAILR2.

Of note, in this clonal cell line solely the long isoform of TRAILR2 was found which additionally seemed to be post-translationally modified since a second band with a higher molecular weight ran above the band for TRAILR2-L (Figure 36; Figure 37).

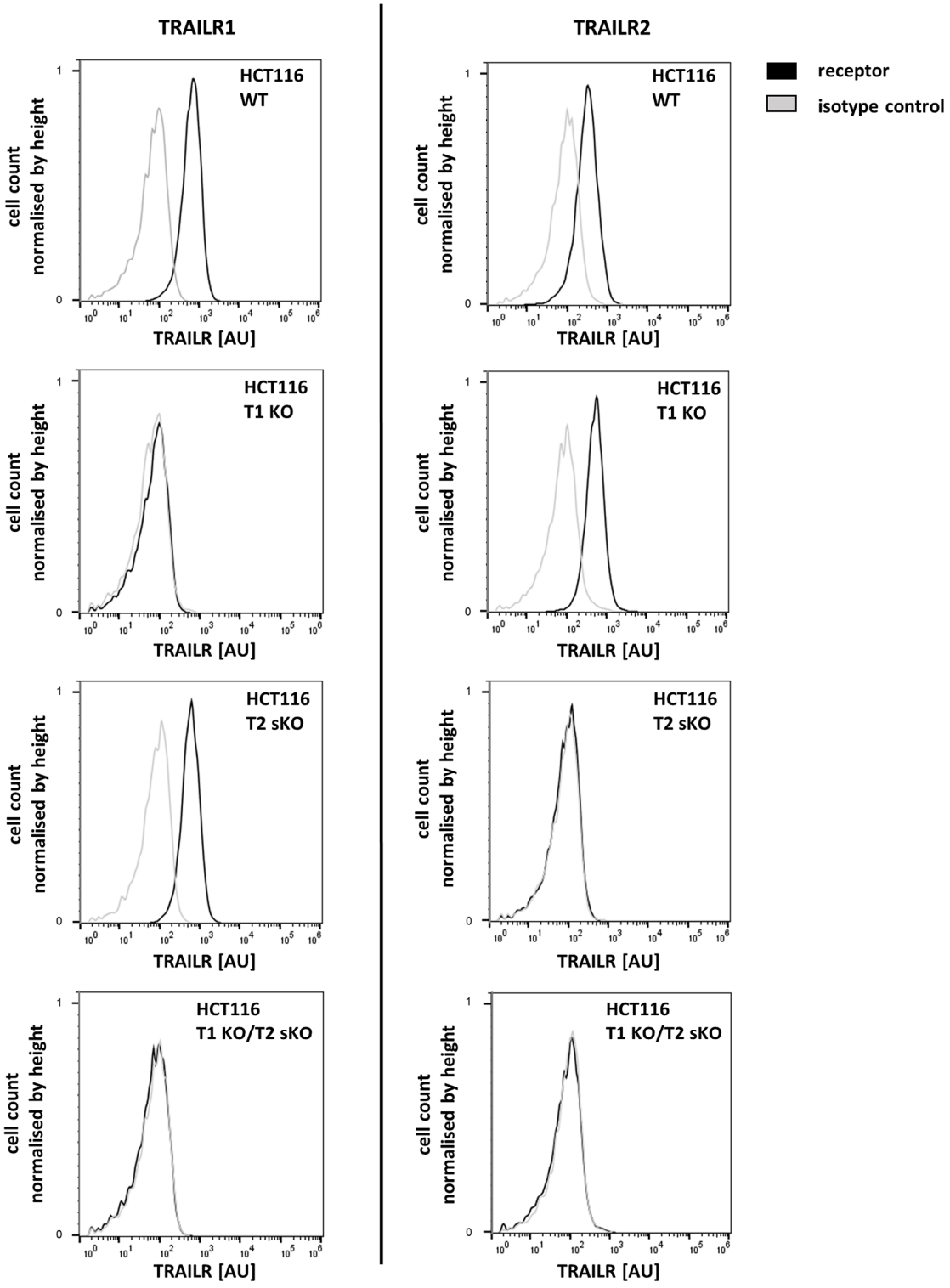

Figure 36: Surface TRAILR1 and TRAILR2 expression in HCT116 TRAILR KO cell lines

Indicated 2D-cultivated HCT116 WT cells and TRAILR KO cell lines (sKO = surface KO) were stained for TRAILR1 and TRAILR2 with specific antibodies and surface expression was analysed by flow cytometry. The shown histograms are representative of two independently performed experiments.

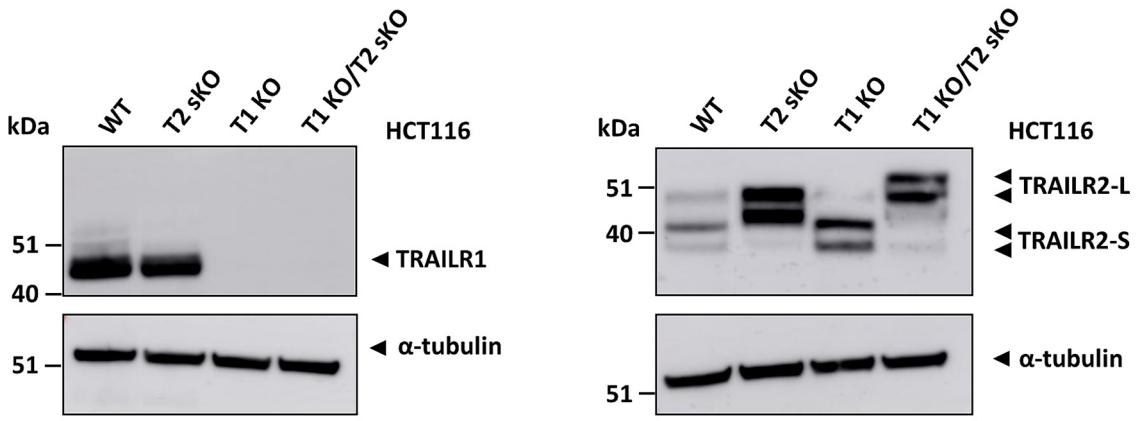

Figure 37: Total expression of TRAILR1 and TRAILR2 in HCT116 TRAILR KO cell lines

Total cell lysates of 2D-cultivated HCT116 WT cells and TRAILR KO cell lines (sKO = surface KO) were analysed by western blotting using the indicated antibodies (TRAILR2-L = long isoform of TRAILR2; TRAILR2-S = short isoform of TRAILR2). Blots shown are representative of three independently performed experiments.

Since the provided HCT116 TRAILR2 sKO cell line was only devoid of surface TRAILR2 but expressed large quantities of the protein intracellulary, a clonal HCT116 cell line with a complete knockout of TRAILR2 was generated in our lab by Alexandra Mack using the CRISPR/Cas9 approach. Investigations revealed that surface expression of TRAILR2 was completely abrogated in this generated cell line whereas surface expression of TRAILR1 was comparable to that detected in HCT116 WT cells. In contrast to the HCT116 T2 sKO cell line generated by the TALEN approach the HCT116 T2 KO cell line was also completely devoid of intracellular TRAILR2 (Figure 38).

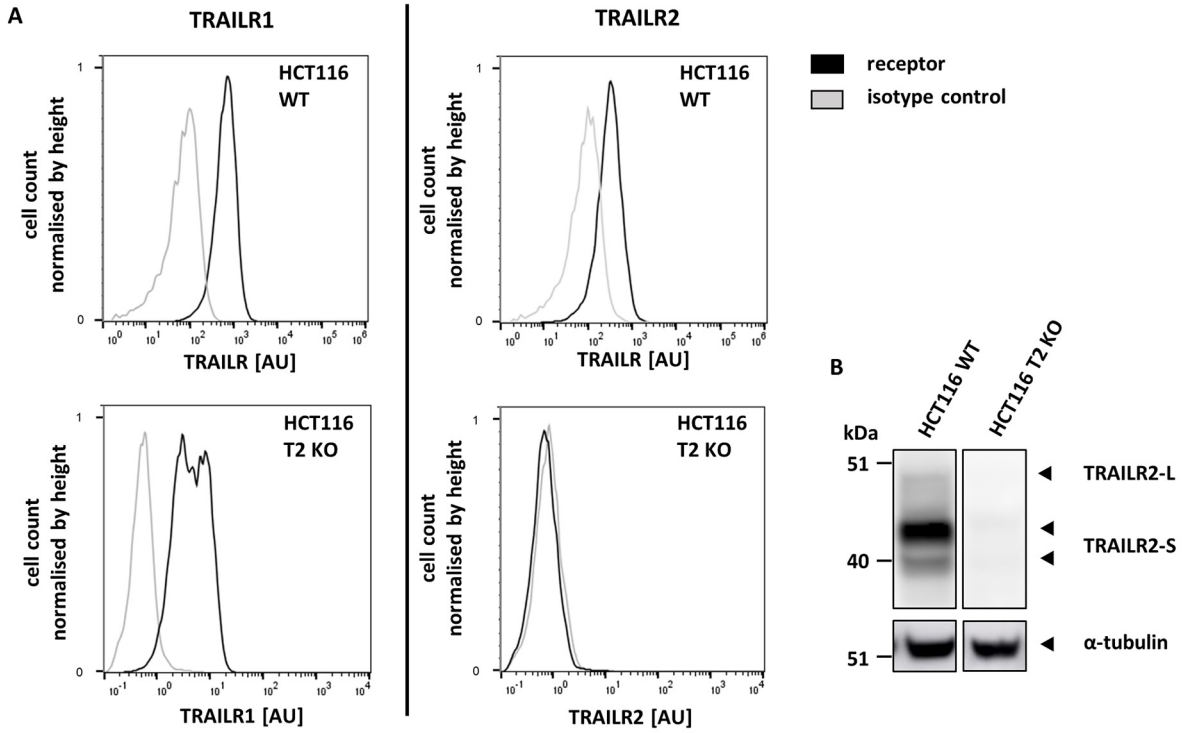

Figure 38: TRAILR expression of the HCT116 T2 KO cell line generated by the CRISPR/Cas9 approach
HCT116 WT and HCT116 T2 KO cells were stained for TRAILR1 and TRAILR2 with specific antibodies and surface expression was analysed by flow cytometry. The shown histograms are representative of two independent experiments **(A)**. Lysates of 2D-cultivated HCT116 WT and HCT116 T2 KO cells were analysed by western blotting using the indicated antibodies (TRAILR2-L = long isoform of TRAILR2; TRAILR2-S = short isoform of TRAILR2). Blots shown are representative of three independently performed experiments.

4.2. TRAILR2 KO renders 2D-cultured HCT116 cells less susceptible to TRAIL

All four HCT116 TRAILR KO cell lines were in a next step compared to HCT116 WT cells concerning their susceptibility to Fc-scTRAIL 1551 when cultivated in 2D. Of note, even though $Db_{\alpha EGFR}$-scTRAIL was more potent in induction of apoptosis than the non-targeting construct it was in the following not further investigated since binding and eventually activation of the EGFR might interfere with the apoptotic machinery and makes therefore an investigation of pure TRAIL-induced effects impossible.

Cells were seeded into 96-well plates, stimulated two days later for 6 h with 2 nM Fc-scTRAIL 1551 and the percentage of viable cells was determined by Annexin V-EGFP staining and flow cytometry. Thereby, experiments revealed that the HCT116 T1 KO cell line showed a susceptibility to Fc-scTRAIL 1551 that was comparable to that of HCT116 WT cells. Furthermore, both TRAILR2 KO cell lines, the one with complete KO of the receptor and the

one with remaining intracellular TRAILR2, were more resistant to Fc-scTRAIL 1551 than HCT116 WT cells. However, the effect was only very pronounced for the cell line with surface TRAILR2 KO whereas sensitivity to Fc-scTRAIL 1551 of the cell line with complete KO of the receptor was only very slightly different to that of HCT116 WT cells. As expected, the cell line with no surface expression of either TRAILR1 or TRAILR2 (HCT116 T1 KO/T2 sKO) was completely resistant to stimulation with Fc-scTRAIL 1551 (Figure 39).

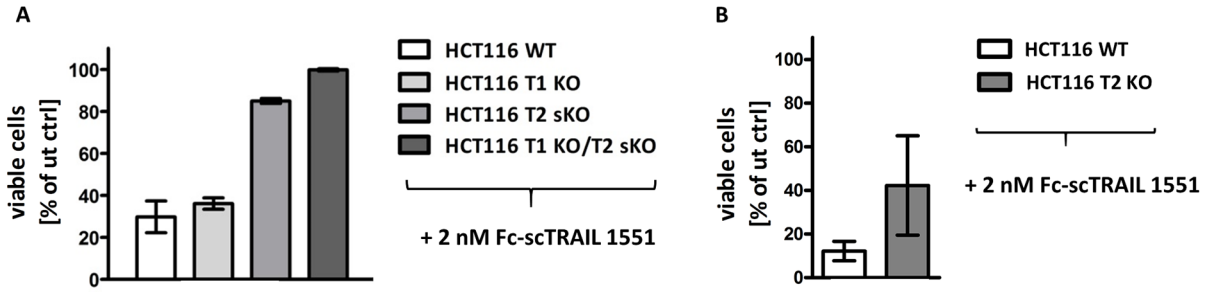

Figure 39: Analysis of 2D-cultivated HCT116 TRAILR KO cell lines for their susceptibility to TRAIL

The indicated cell lines were cultivated in 2D and stimulated for 6 h with 2 nM Fc-scTRAIL 1551. Afterwards, the percentage of viable cells was determined by Annexin V-EGFP staining and flow cytometry. Displayed are the percentages of viable cells normalised to the respective untreated sample (ut ctrl). Data shown are mean values ± range of two independent experiments each performed in duplicates **(A/B)**. Experiment shown in **(B)** was conducted by Alexandra Mack.

4.3. Complete KO of TRAILR1 or TRAILR2 slows down MCTS growth of HCT116 cells

Next, HCT116 TRAILR KO cell lines were investigated for their capacity to form MCTSs. It could be shown that neither KO of TRAILR2 (surface or complete) nor complete KO of TRAILR1 or double KO (complete KO of TRAILR1 and surface KO of TRAILR2) could prevent spheroid formation. During further cultivation it became apparent that growth of HCT116 T1 KO MCTSs were strongly reduced in comparison to HCT116 WT MCTSs and the same but less pronounced effect could be observed for the HCT116 cell line with complete KO of TRAILR2. In contrast, MCTSs generated out of HCT116 cells that lack only surface TRAILR2, as well as MCTSs out of HCT116 T1 KO/T2 sKO, cells did not differ in their size compared to HCT116 WT MCTSs after 11 days of cultivation. Since it was already observed under 2D conditions that HCT116 T1 KO cells and HCT116 T2 KO cells needed longer to undergo cell division than HCT116 WT cells, the differences in spheroids size may be caused by a reduction in proliferation (Figure 40).

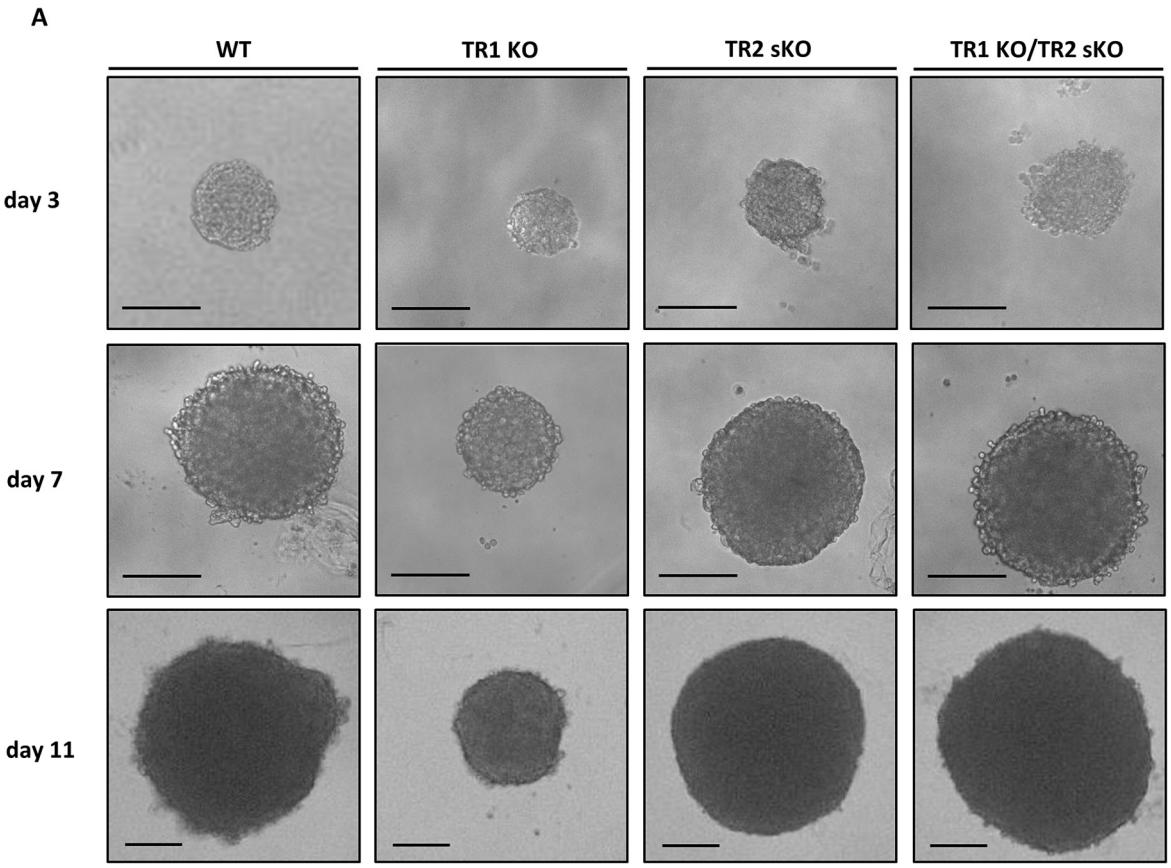
A
WT
TR1 KO
TR2 sKO
TR1 KO/TR2 sKO
day 3
day 7
day 11

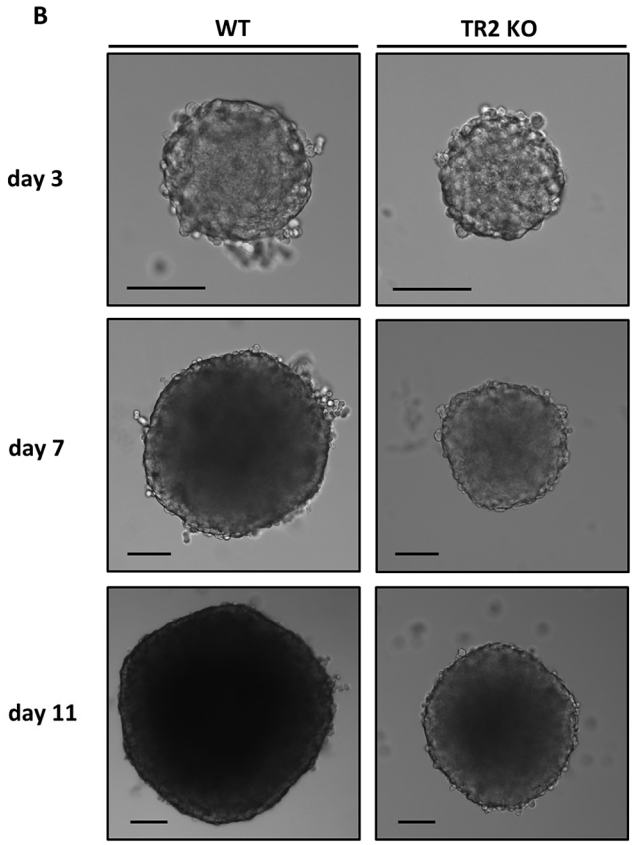
B
WT
TR2 KO
day 3
day 7
day 11

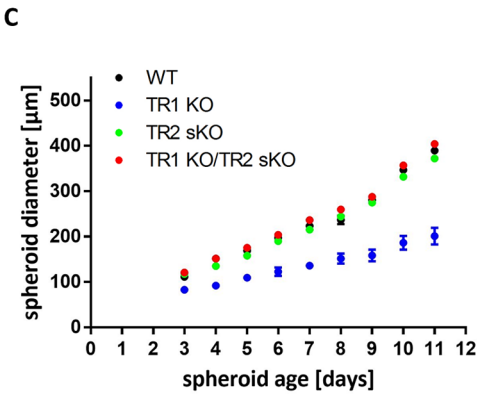
C
WT
TR1 KO
TR2 sKO
TR1 KO/TR2 sKO
spheroid diameter [µm]
spheroid age [days]

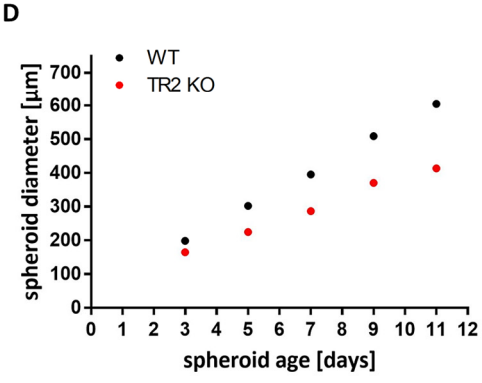
D
WT
TR2 KO
spheroid diameter [µm]
spheroid age [days]

Figure 40: Growth behaviour of MCTSs generated out of HCT116 TRAILR KO cell lines

Indicated MCTSs were cultivated in agarose-coated 96-well plates with the media changed every third day. Pictures were taken with an EVOS inverted digital microscope and the diameter was determined using the Fiji software **(A/B)**. Displayed are the results of one representative experiment of two independent replicates with mean values ± SEM of 4 **(C)** and 5 **(D)** spheroids. Error bars in **(D)** are too small to be seen. Scale bars = 100 µm **(A/B).** Experiment was conducted by Alexandra Mack **(D)**.

To investigate whether cells within MCTSs generated from the TRAILR KO cell lines show the same pattern of surface expression of the remaining TRAILR as cells within HCT116 WT spheroids, 11-day-old MCTSs were dissociated and single cells were analysed for their surface TRAILR expression by flow cytometry. Investigations revealed that 3D-cultured HCT116 T1 KO cells expressed the same amounts of TRAILR2 at their surfaces as cells within HCT116 WT MCTSs. Furthermore, even though 11-day-old HCT116 T2 KO MCTSs were slightly smaller than HCT116 WT MCTSs of similar age, cells within these spheroids showed the same heterogeneity of TRAILR1 surface expression as 3D-cultivated HCT116 WT cells. A small part of the cell population expressed a similar amount of surface TRAILR1 as 2D-cultivated HCT116 WT cells while in the other spheroid-forming cells TRAILR1 expression was reduced or completely absent. As expected the same held true for the cells within HCT116 T2 sKO MCTSs (Figure 41).

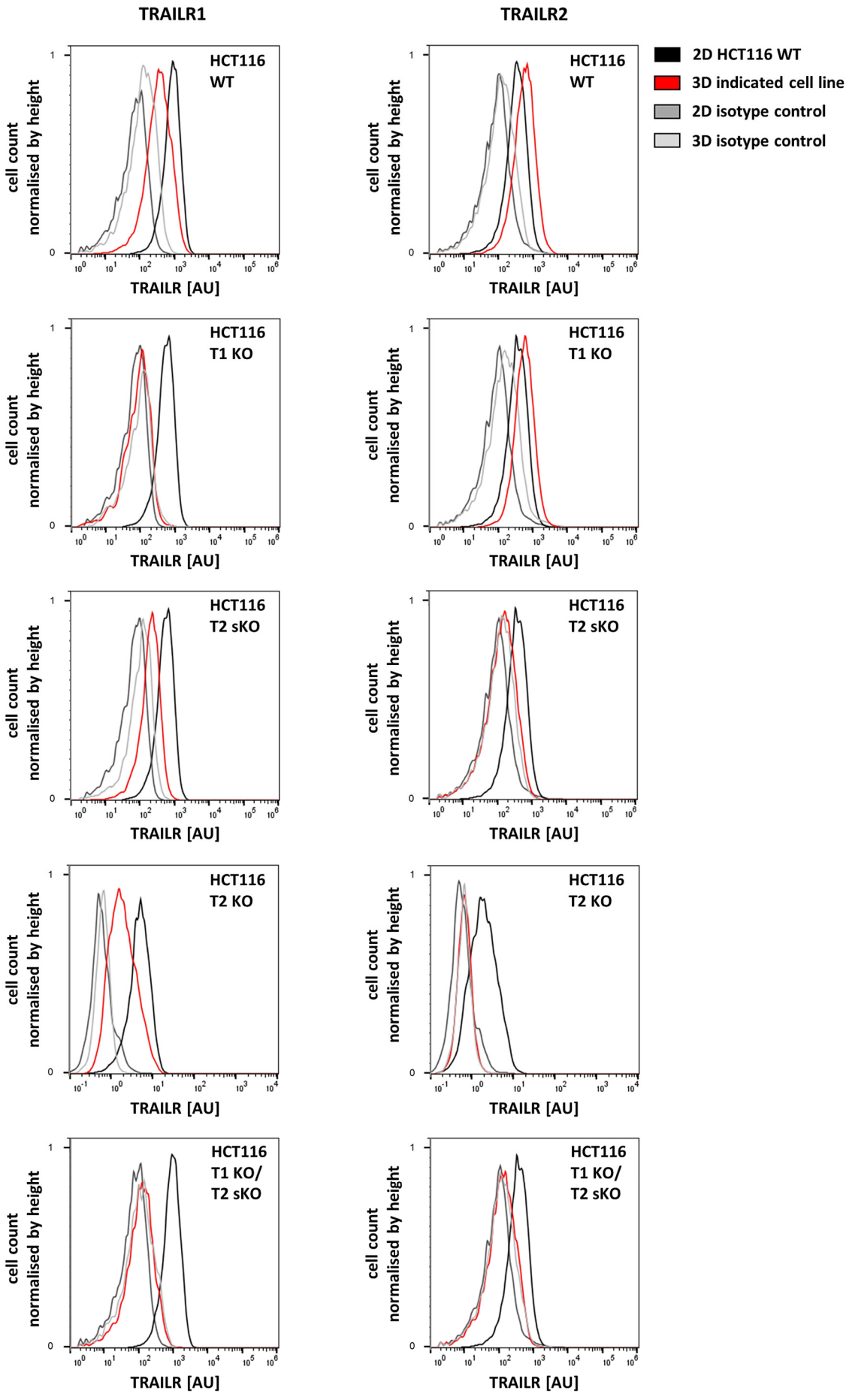
TRAILR1
TRAILR2
2D HCT116 WT
3D indicated cell line
2D isotype control
3D isotype control
HCT116 WT
HCT116 T1 KO
HCT116 T2 sKO
HCT116 T2 KO
HCT116 T1 KO/ T2 sKO
cell count normalised by height
TRAILR [AU]

Figure 41: Surface TRAILR1 and TRAILR2 expression in 3D-cultivated HCT116 TRAILR KO cell lines
Indicated 3D-cultivated HCT116 WT cells and TRAILR KO cell lines (day 11) were stained for TRAILR1 and TRAILR2 with specific antibodies and surface expression was analysed by flow cytometry. The shown histograms are representative of two independent experiments.

4.4. No TRAIL-hypersensitive cell population within HCT116 T2 KO MCTSs

Since HCT116 T1 KO MCTSs cells did not grow very large, only 3D-cultured HCT116 T2 KO cells were investigated for their susceptibility to Fc-scTRAIL 1551. Therefore, 2D-cultured HCT116 T2 KO cells and HCT116 T2 KO MCTSs (day 11) were stimulated for 6 h with Fc-scTRAIL 1551 and their susceptibility was afterwards compared to that of 2D-cultured HCT116 WT cells. As before, the same experiment was repeated with detached cells and dissociated MCTSs. This revealed, once again, that adherent 2D-cultured HCT116 WT cells were more susceptible to Fc-scTRAIL 1551 than 2D-cultured HCT116 T2 KO cells (WT EC_{50} = 0.06 nM; T2 KO EC_{50} = 0.2 nM). Furthermore, HCT116 KO T2 MCTSs turned out to be even more resistant to treatment with Fc-scTRAIL 1551 than HCT116 WT MCTSs (Figure 30; Figure 42). To investigate whether KO of TRAILR2 could prevent the formation of a TRAIL-hypersensitive cell population, HCT116 T2 KO MCTSs were dissociated and single cells were stimulated together with detached 2D-cultured HCT116 T2 KO cells and HCT116 WT cells with Fc-scTRAIL 1551. As shown before, detachment of 2D-cultured HCT116 WT cells did not change their sensitivity to Fc-scTRAIL 1551 (adherent EC_{50} = 0.06 nM; detached EC50 = 0.08 nM). However, 2D-cultivated HCT116 T2 KO cells seemed to become slightly less susceptible to Fc-scTRAIL 1551 when stimulated in suspension. In contrast to what was observed for HCT116 WT cells, dissociation of HCT116 T2 KO MCTSs did not reveal the existence of a TRAIL-hypersensitive subpopulation. Even though they were slightly more sensitive to Fc-scTRAIL 1551 than before dissociation, probably due to better access of Fc-scTRAIL 1551 to the cells, 3D-cultivated HCT116 T2 KO cells remained over all more resistant than the corresponding 2D cell culture (Figure 42).

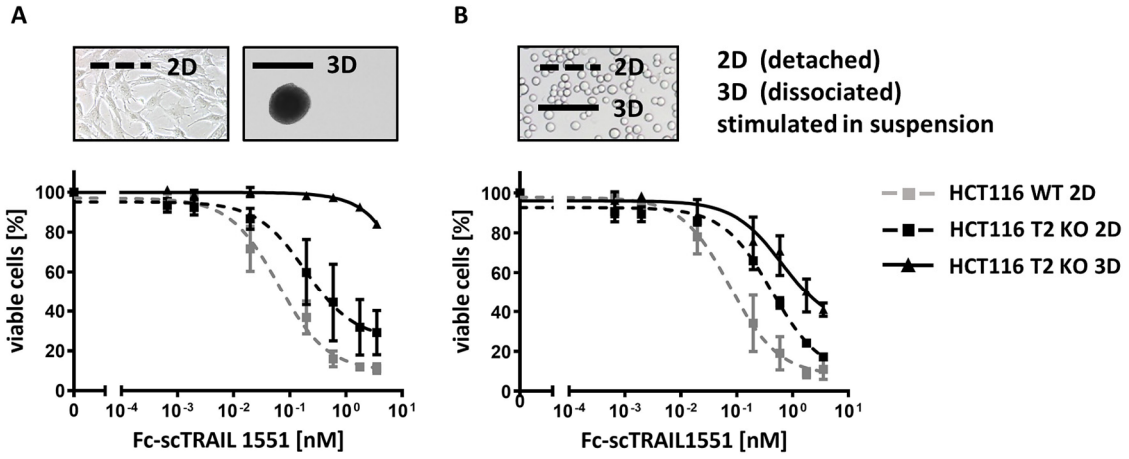

C

	not dissociated Fc-scTRAIL 1551 EC_{50} [nM]	in suspension Fc-scTRAIL 1551 EC_{50} [nM]
2D HCT116 WT	0.063	0.076
2D HCT116 T2 KO	0.191	0.425
3D HCT116 T2 KO	> 3.6	0.647

Figure 42: TRAIL susceptibility of 2D- and 3D-cultivated HCT116 T2 KO cells

2D-cultivated HCT116 WT and HCT116 T2 KO cells, along with HCT116 T2 KO MCTSs (day 11), were stimulated for 6 h with increasing concentrations of Fc-scTRAIL 1551 **(A)** or 2D-cultivated cells were detached and MCTSs (day 11) were dissociated before stimulating single cells in suspension with increasing concentrations of Fc-scTRAIL 1551 for 6 h **(B)**. Cell death was measured by staining with Annexin V-EGFP followed by flow cytometry. Data shown are mean values ± SEM of three independent experiments each performed in duplicates except for 3D-cultivated HCT T2 KO cells in **(B)** where data are mean values ± range of two independent experiments each performed in duplicates **(A/B)**. Table shows the EC_{50} values resulting out of performed nonlinear regressions (sigmoidal dose-response) **(C)**.

4.5. Discussion

In chapter 2 it was shown that within HCT116 and NCI-H460 MCTSs, TRAILR-resistant cells shield TRAIL-hypersensitive cells from TRAIL-induced apoptosis. Furthermore, it was demonstrated that the hypersensitive cell population most likely was comprised of cells with enhanced TRAILR2 expression close to the necrotic core as after knockout of TRAILR2, MCTSs were completely devoid of TRAIL-hypersensitive cells.

It is known that low expression of the two apoptosis-inducing TRAILRs can render cells resistant to TRAIL-induced apoptosis (reviewed by Pennarun et al., 2010). This fact alongside the observation that TRAILR1 and TRAILR2 contributed comparably to the induction of apoptosis in 2D-cultured HCT116 and NCI-H460 cells gave rise to the hypothesis that cells with reduced TRAILR expression in intermediate spheroid layers might be TRAIL-resistant and protect sensitive cells further inside from TRAIL-induced apoptosis. Indeed, experiments revealed that MCTSs of both investigated cell lines were less susceptible to TRAIL than 2D-cultured cells. Furthermore, staining for cleaved caspase 3 in sections of stimulated MCTSs demonstrated that apoptosis was mainly induced in cells localised to the outer spheroid layers. However, since no penetration studies were conducted, to date, with the two investigated 2nd generation TRAILR agonists, it cannot be excluded that the observed resistance of 3D-cultured cells is only or mainly due to hindered diffusion of the two fusion proteins. Unfortunately, comparison with other studies is difficult in this special case, since the capability of molecules and proteins to penetrate tissue or MCTSs is not only dependent on the molecule size and charge of the substance but also on their consumption by the cells (Minchinton and Tannock, 2006). Furthermore, also the grade of connection between cells by tight junctions, gap junctions and desmosomes can, to a great extent, influence the spreading of substances within MCTSs (Grantab et al., 2006; Liang et al., 2015; Qiu et al., 2012). For example, it was shown that doxorubicin, a drug that is even smaller than the two fusion proteins, was not able to penetrate far into tissue because it was taken up by cells close to blood vessels and got stored into acidic endosomes (Lee and Tannock, 2006). On the other hand, Barbone and colleagues demonstrated that soluble TRAIL was distributed equally within large mesothelioma MCTSs (Ø ~500 µm) after 6 h of stimulation (Barbone et al., 2008). Nevertheless, the observation made in this thesis that a resistant cell population was still to be found after treatment for 24 h as well as after stimulation of dissociated MCTSs, points to the existence of innately TRAIL-resistant cells within MCTSs. This finding concurs with literature where it was shown that MCTSs generated from breast cancer cell lines were less susceptible to TRAIL than 2D-cultured cells due to downregulation of TRAILR1 and TRAILR2 (Chandrasekaran et al., 2014). Interestingly, stimulation of dissociated MCTSs

also revealed the occurrence of a population of cells that was more susceptible to TRAIL than 2D-cultured cells. Since these TRAIL-hypersensitive cells were only visible after dissociation, they are very likely to be localised close to the necrotic core and therefore were protected in undissociated spheroids from TRAIL-induced apoptosis by enclosing layers of resistant cells. Furthermore, the observation that after knockout of TRAILR2 in HCT116 cells no TRAIL-hypersensitive cell population was detectable anymore within HCT116 MCTSs, points to enhanced TRAILR2 expression as the reason for enhanced susceptibility. However, the fact that flow cytometric experiments revealed the absence of a cell population with, in comparison to 2D-cultured cells, increased surface TRAILR2 expression within MCTSs, suggest that cells were sensitised due to enhanced intracellular amounts of the receptor. Of note it is also conceivable that changed expression of another apoptosis-relevant protein is responsible for the increased TRAIL susceptibility of cells close to the necrotic core. After knockout of TRAILR2, cells near the spheroid centre were completely devoid of apoptosis-inducing TRAILRs which inhibits the activation of the apoptotic cascade and might mask the influence of another protein. To investigate this in further detail, most likely only an indirect approach will be expedient, in which the localisation-dependent expression of further apoptosis-relevant proteins is investigated. In case of observed differences, it could then be examined by inhibition or inducible knockout whether the particular protein participated in the enhanced TRAIL-susceptibility of cells close to the necrotic core. In general, to verify the localisation-dependent differences in TRAIL-susceptibility of spheroid-forming cells, different methods might be applied. For example, after stimulation, MCTSs could be dissociated and single cells might be stained for Ki67 and/or p27 together with Annexin V-EGFP to investigate apoptosis induction depending on the cell cycle status of the spheroid-forming cell. Furthermore, stimulated MCTSs could also be treated with the dye Hoechst 33342 just shortly before dissociation and staining with Annexin V-EGFP, which in the following would allow the determination of a cell's localisation within the spheroid due to its differential staining with the dye (Beaumont et al., 2015).

As part of this thesis it was also investigated whether targeting of TRAILR agonists to the EGFR enhances their capability to induce apoptosis within MCTSs. Since the EGFR is overexpressed in many malignant tissues, an additional binding site for the receptor in a TRAILR agonist should efficiently target the drug to the tumour site (reviewed by Ciardiello and Tortora, 2003; reviewed by Seshacharyulu et al., 2013). Furthermore, by binding to the EGFR, the TRAIL-antibody fusion proteins are also mimicking membrane-bound TRAIL which results in enhanced TRAILR oligomerisation and subsequent activation (reviewed by de Miguel et al., 2016). Interestingly, in cells with a non-mutated EGFR signalling pathway,

blocking of the EGFR by an EGFR-targeting TRAIL-antibody fusion protein was also shown to reduce ligand-induced and basal proliferation (Möller et al., 2014).

In the present study the non-targeted TRAIL-antibody fusion protein Fc-scTRAIL 1551 was compared to $Db_{\alpha EGFR}$-scTRAIL, a construct that contains a binding site for the EGFR in its antibody moiety. While in Fc-scTRAIL 1551 the two TRAIL chains are connected via the attached covalently linked antibody fragments, forming an hexameric construct, two $Db_{\alpha EGFR}$-scTRAIL molecules bind two each other non-covalently resulting also in a molecule with six TRAIL-binding sites (Hutt, 2017; Siegemund et al., 2016). Of note, solely HCT116 cells were utilised for investigations as due to flow cytometric analysis NCI-H460 cells were presumed to display localisation-dependent EGFR expression within MCTSs. Experiments of the present work demonstrated that the targeted construct was superior in inducing apoptosis within 2D-cultivated HCT116 cells only after 24 h but not after 6 h. This finding is in accordance with another study in which the comparison between targeted and non-targeted TRAIL-antibody fusion proteins demonstrated enhanced apoptosis induction in 2D-cultured HCT116 cells after treatment for 16 h with the targeted construct (Hutt, 2017). In the same work it has also been shown that the observed increased bioactivity of the targeted protein was indeed due to its binding to the EGFR, as pre-treatment with EGFR-blocking antibodies in high excess reduced the apoptosis inducing capacity of the targeted construct to that of the non-targeted protein (Hutt, 2017). However, whether the observed higher bioactivity of $Db_{\alpha EGFR}$-scTRAIL is exclusively due to the enhanced crosslinking of TRAILRs caused by the molecules binding to the EGFR, or binding to the receptor sensitises the cells to TRAIL through influencing signalling via the EGFR has yet to be investigated. As HCT116 cells possess activating mutations in KRAS and phosphatidylinositol-4,5-bisphosphate 3-kinase, catalytic subunit α (PIK3CA), resulting in constitutive EGFR signalling, the latter described mechanism of sensitisation is not very likely but cannot be completely excluded (Ahmed et al., 2013). The observation made in this study that 6 h was not sufficient to reveal differences in apoptosis induction between the two TRAIL-antibody fusion proteins might be due to the fact that the targeted molecule attaches stepwise to the cell surface. First binding to the EGFR before subsequent binding to the TRAILRs or *vice versa*. However, the beneficial effect of targeting only comes into effect when both binding sites of the fusion protein attach to their respective receptors, which may take some time causing a delay in cell death but results in greater potency at longer stimulation times. Interestingly, when 2D-cultured cells were treated in suspension, a stimulation period of only 6 h was enough to reveal the enhanced bioactivity of the targeted construct. It can therefore be hypothesised that the detachment made a larger area of the cell surface accessible to the TRAIL-antibody fusion protein. Furthermore, the fact that cells were not strongly adhered together makes it

more likely that a TRAIL-antibody fusion protein binds with one part to the EGFR localised on one cell's surface while it activated TRAILRs on a different cell.

Alongside 2D-cultured HCT116 cells also HCT116 MCTSs were treated with the targeted and the non-targeted construct. Thereby it was revealed that during a short stimulation period of 6 h the non-targeted protein was more efficient in inducing apoptosis within HCT116 MCTSs, while after 24 h treatment the targeted construct was slightly more bioactive. This observation, alongside the fact that after dissociation spheroid-forming cells were more susceptible to the targeted construct, points to hindered penetration as reason for the reduced bioactivity of the targeted protein during short stimulation times. Even though both TRAIL-antibody fusion proteins are of comparable size, an impeded diffusion of the targeted protein due to its slightly different structure cannot be excluded. To investigate this in more detail a non-targeted Db construct could be compared to the Fc-scTRAIL format. However, it is also conceivable that the EGFR-binding of the targeted protein slowed down its penetration. Indeed, the fact that *in vivo* studies revealed that non-targeting Fc-scTRAIL was slightly more effective in reducing tumour size than a EGFR-targeting Fc-scTRAIL construct, points to EGFR binding as reason for impaired delivery to, and/or impeded penetration of the tumour (Hutt, 2017). It can therefore be hypothesised that reducing the binding affinity to the EGFR within the TRAIL-antibody fusion protein may diminish the off-target binding to non-malignant tissue with low EGFR expression and increase the amount of drug that would actually reach the tumour side characterised by enhanced EGFR expression. Indeed, such a mechanism was already described in the literature under the term super selectivity. It was shown that particles that have more than one binding site for a particular target, such as a receptor, could attach strongly to surfaces with high expression of the respective target even though the individual bindings are weak. As a result, such molecules act switch like, binding only to surfaces with receptor amounts above a certain limit but not at all to surfaces with lower expression (Curk et al., 2016). In further studies, spheroids might be pre-treated with EGFR-blocking antibodies prior to stimulation with $Db_{\alpha EGFR}$-scTRAIL to investigate whether strong binding to the EGFR decreased the penetration and thus the bioactivity of $Db_{\alpha EGFR}$-scTRAIL in, respectively on, MCTSs.

In the second part of the chapter, different HCT116 TRAILR knockout cell lines were investigated for their susceptibility to TRAIL and their ability to grow as MCTSs. Of note only the non-targeted TRAIL construct was utilised for investigations since, as mentioned previously in this thesis, it cannot be completely excluded that binding of $Db_{\alpha EGFR}$-scTRAIL to the EGFR influences the cells' susceptibility to TRAIL, independently of its capacity to enhance oligomerisation of TRAILRs. As expected, HCT116 cells devoid of total TRAILR1 and

surface TRAILR2 expression were completely resistant against TRAIL. Furthermore, HCT116 TRAILR1 KO cells showed a comparable susceptibility to TRAIL as WT cells, which would suggest that in HCT116 cells, apoptosis is exclusively induced via TRAILR2. The finding that KO of TRAILR2 surface expression rendered HCT116 cells almost completely resistant against TRAIL further supported this interpretation. Nevertheless, in literature it was shown that in HCT116 cells, TRAIL-induced apoptosis was mainly triggered via TRAILR1 (Florent et al., 2016). Furthermore, experiments with selectively blocking TRAILR antibodies conducted in this thesis suggested comparable contribution of both TRAILRs to apoptosis. In accordance with this result, it was found that after complete KO of TRAILR2 only ~50% of the cells survived treatment with TRAIL. The observed discrepancies between the different experiments might simply be caused by the clonal origin of the HCT116 KO cell lines. For example, it cannot be excluded that decreased susceptibility of the surface TRAILR2 KO cell line was not only due the absence of TRAILR2 but also the result of changed expression of another apoptosis-relevant protein. To verify the previously described findings, further clones for each KO condition should be investigated for their susceptibility to TRAIL.

Interestingly, cells with total KO of TRAILR2 but not cells with remaining intracellular expression of the receptor showed decelerated growth as MCTSs. Thus, it can be hypothesised that intracellular TRAILR2 is involved in proliferation of HCT116 cells, as it was suggested in the literature (Haselmann et al. 2014). Furthermore, it has been observed that KO of TRAILR1 reduced the volume increase of generated spheroids even to a larger extent than KO of total TRAILR2. However, as MCTSs generated from cells with complete TRAILR1 and surface TRAILR2 KO did not grow slower than MCTSs generated from HCT116 WT cells, the reduced volume increase of TRAILR1 KO MCTSs was most likely caused by decelerated cell cycle progression of that particular HCT116 TRAILR1 KO clone. As suggested previously, experiments have to be repeated with further clones for each KO condition in order to make a reliable statement concerning a participation of both TRAILRs in cell proliferation and spheroid growth.

Chapter 3: Hypoxia, glucose starvation and serum deprivation are all factors that influence TRAILR expression

It was previously shown that expression of TRAILR1 and TRAILR2 varied within cells depending on their localisation within the MCTSs and furthermore experiments strongly indicated that this influences the cells' susceptibility to TRAIL. Therefore, it was investigated which environmental factors inside the MCTSs cause the localisation-dependent expression of TRAILRs. It is known that due to diffusion limitations and consumption, gradients of oxygen, nutrients and growth factors develop within larger micrometastases (reviewed by Millard et al., 2017). The experiments performed in this section revealed that this holds also true for larger HCT116 and NCI-H460 MCTSs. Individual cells within the spheroids displayed not only classic markers for hypoxia and enhanced autophagy but also displayed signs of ER stress. Furthermore, it could be shown that depriving 2D-cultured HCT116 and NCI-H460 cells of nutrients, growth factors and oxygen led to changes in TRAILR expression that reflected the expression pattern of a quiescent cell. More precisely, hypoxia led to downregulation of TRAILR1 in the investigated cell lines, while hypoxia and glucose deprivation both enhanced TRAILR2 expression in HCT116 and NCI-H460 cells.

5.1. Cells within larger MCTSs are deprived of oxygen

Cells that are deprived of oxygen can be determined by measuring the level of Hif-1α. Under normoxic conditions, Hif-1α is hydroxylated and binds to the Hippel-Lindau tumour suppressor (pVHL) E3 ligase complex, which leads to rapid ubiquitination and subsequent degradation of the protein via the proteasome (Koh et al., 2008). However, under hypoxia, Hif-1α can no longer bind to the E3 ligase complex due to its lack of hydroxylation. In this case, Hif-1α forms a transcriptionally active heterodimer with Hif-1β that can induce the expression of many genes, for example those involved in angiogenesis or glucose metabolism. Western blot analysis with total cell lysates of 2D-cultured HCT116 and NCI-H460 cells along with lysates of HCT116 and NCI-H460 MCTSs (day 11) revealed that only 3D-cultured cells had detectable levels of Hif-1α, confirming the hypothesis that an oxygen gradient is established within MCTSs leading to hypoxia (Figure 43).

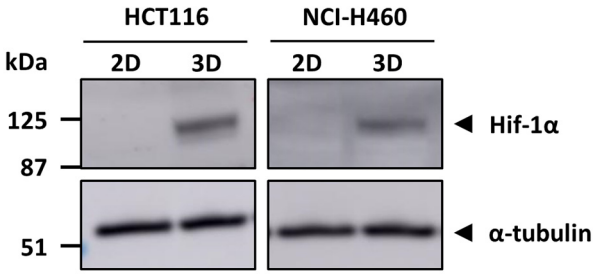

Figure 43: MCTSs are comprised of cells that are deprived of oxygen

Lysates of 2D-cultivated HCT116 and NCI-H460 cells along with lysates of HCT116 and NCI-H460 MCTSs (day 11) were analysed by western blotting using the indicated antibodies. Blots shown are representative of three independently performed experiments.

5.2. Oxygen-deprived cells are located mainly close to the necrotic core

To investigate the localisation of oxygen-deprived cells within MCTSs, day 7 and day 11 spheroids were embedded into paraffin, cut into 3 µm slices and immunohistochemically stained for Hif-1α. Thereafter, the software Definiens Tissue Studio 64 and Photoshop Elements 10 were used to determine the total percentage of Hif-1α positive cells within 7- and 11-day-old HCT116 and NCI-H460 MCTSs, as well as the percentage of Hif-1α positive cells in the different spheroid layers of 11-day-old HCT116 and NCI-H460 MCTSs. Performed experiments revealed that in comparison to 7-day-old MCTSs, 11-day-old MCTSs are comprised of significantly more cells that are positive for Hif-1α (HCT116 day 7: ~1%, HCT116 day 11: ~7%; NCI-H460 day 11: ~2%, NCI-H450 day 11 ~7%) (Figure 45A/B). Furthermore, analysis of the spheroid sections demonstrated that in 11-day-old HCT116 and NCI-H460 MCTSs the outer two cell layers were almost completely devoid of Hif-1α positive cells, which means that oxygen-deprived cells were mainly found close to the necrotic core (Figure 44; Figure 45C/D).

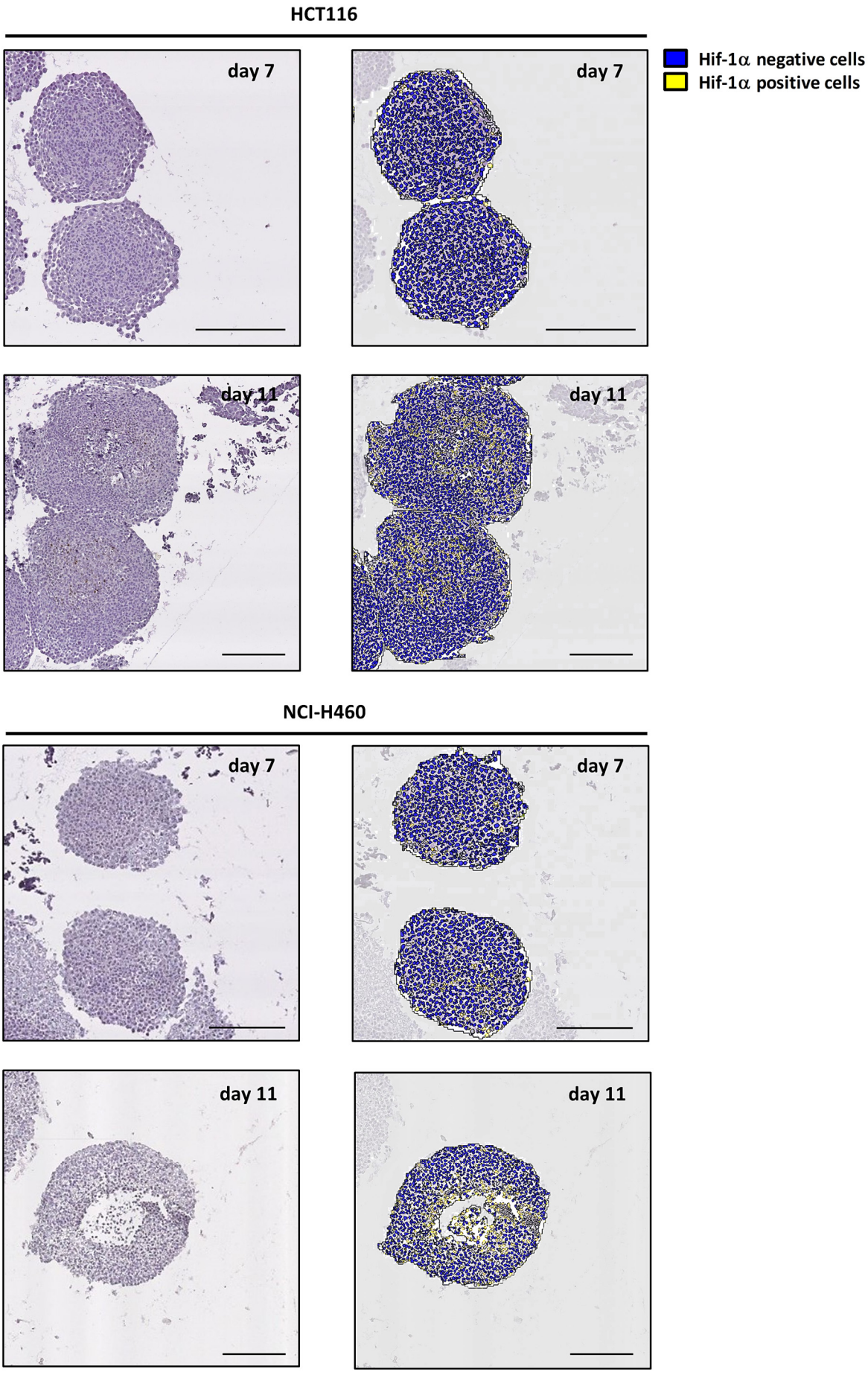
HCT116
day 7
day 7
Hif-1α negative cells
Hif-1α positive cells
day 11
day 11
NCI-H460
day 7
day 7
day 11
day 11

Figure 44: Staining of Hif-1α in 7-day-old and 11-day-old MCTSs

HCT116 and NCI-H460 MCTSs (day 7 and day 11) were embedded in paraffin and cut into 3 µm slices. Middle sections of MCTSs were immunohistochemically stained for Hif-1α and counterstained with haematoxylin to visualise cell nuclei. Thereafter, the software Definiens Tissue Studio 64 was used to identify cells with (yellow) and without (blue) Hif-1α expression. Pictures are representative of three independent experiments. Scale bars in all images = 200 µm. Staining was performed by Dr. Jens Schmid, IKP, Stuttgart.

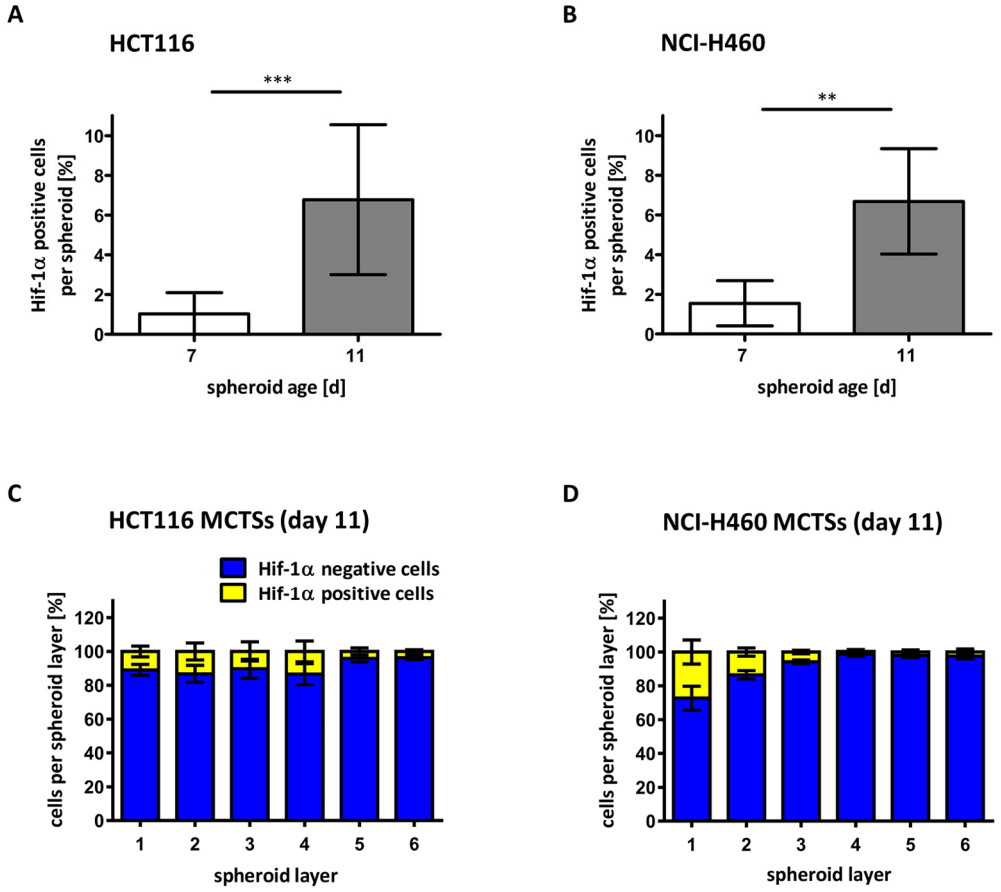

Figure 45: Investigation of the occurrence and distribution of Hif-1α positive cells within HCT116 and NCI-H460 MCTSs

After image analysis with the Definiens Tissue Studio 64 software the percentage of cells with or without Hif-1α expression was determined using Photoshop Elements 10. Shown are mean values ± SD of, in total, four to sixteen MCTSs out of three independent experiments. Asterisks indicate statistical significance (** = $p \leq 0.01$, *** = $p \leq 0.001$; unpaired t-test) **(A/B)**. After image analysis with the Definiens Tissue Studio 64 software, spheroid sections (day 11) were subdivided into six different layers and the percentage of Hif-1α negative and positive cells was determined using Photoshop Elements 10. Shown are mean values ± SEM of from four (NCI-H460) or five (HCT116) MCTSs out of three independent experiments **(C/D)**.

5.3. Depriving 2D-cultured cells of oxygen decreases TRAILR1 and increases TRAILR2 expression

Next, it was examined whether the gradient of oxygen within MCTSs accounts for the localisation-dependent TRAILR expression of spheroid-forming cells. Therefore, 2D-cultured HCT116 and NCI-H460 cells were cultivated under 1% oxygen conditions for 48 h and 72 h followed by determination of TRAILR surface expression by flow cytometry and total expression of TRAILRs by western blot analysis. By investigating the prepared whole cell lysates of 2D-cultured HCT116 and NCI-H460 for the expression of Hif-1α it was shown that cultivation for 48 h and 72 h under 1% oxygen conditions could induce hypoxia in the examined cells (Figure 46A). Furthermore, the expression of the quiescence marker p27 was enhanced after oxygen deprivation in both investigated cell lines (Figure 46A). Under hypoxic conditions, TRAILR1 surface and overall expression was downregulated in HCT116 and NCI-H460. Conversely, oxygen deprivation led to the upregulation of TRAILR2 on the cell surface and overall in both examined cell lines (Figure 46A/B/C). These findings correlate well with the finding that quiescent cells close to the necrotic core, under hypoxia, showed high expression of TRAILR2 and almost no expression of TRAILR1.

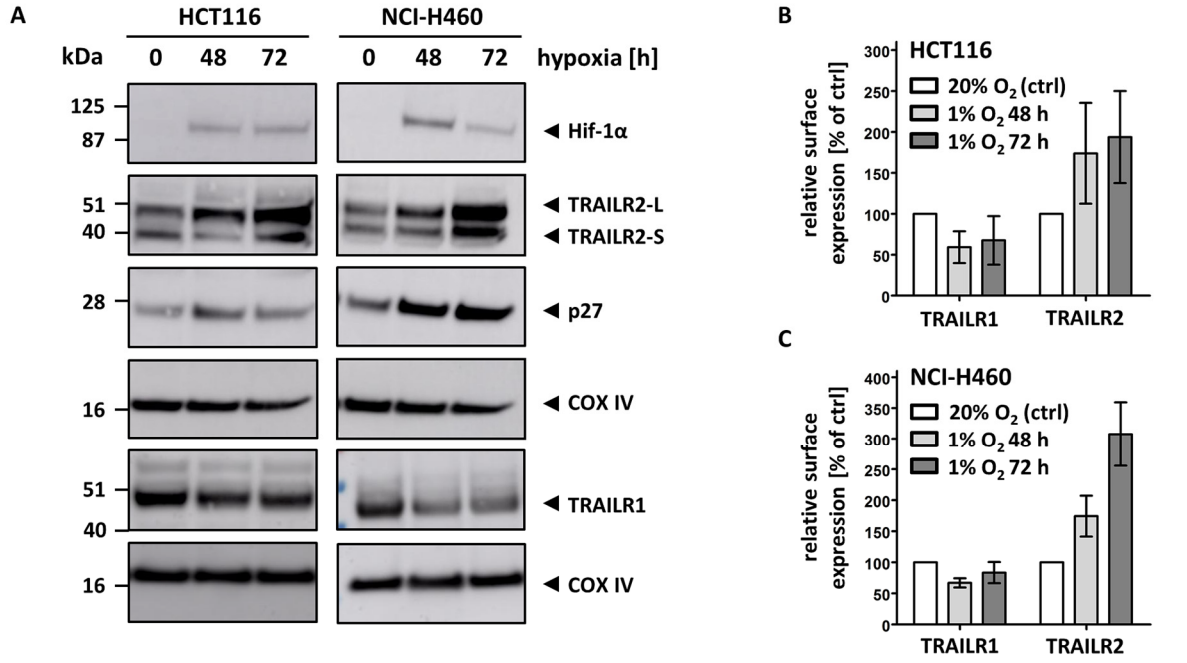

Figure 46: Hypoxia causes enhanced TRAIL2 expression and decreased TRAILR1 expression

HCT116 and NCI-H460 cells (2D) were cultivated under 1% oxygen conditions for 48 h and 72 h and cell lysates were analysed by western blotting using the indicated antibodies. Blots shown are representative of three independently performed experiments **(A)**. HCT116 and NCI-H460 cells (2D) were cultivated for 48 h and 72 h under 1% oxygen. Thereafter, TRAILR expression was determined by flow cytometry. Medians of the cell populations were used to calculate the surface TRAILR expression relative to cells cultivated with 20% oxygen (ctrl). Displayed data are mean values ± SD of at least three independent experiments **(B/C)**.

5.4. Cells within large MCTSs show signs of nutrient starvation

As described previously, cells within tumours and MCTSs might not only be deprived of oxygen but are also starved of nutrients and growth factors due to impeded diffusion of substrates such as glucose, amino acids, vitamins or EGF (reviewed by Milliard et al., 2017). It is known that such starvation can induce autophagy, a mechanism that supplies the cell with amino acids or fatty acids. This is mediated by the degradation of dispensable cytoplasmic material, such as mitochondria or proteins, which is initiated when autophagosomes fuse with lysosomes. During the process of autophagy, the protein microtubule-associated 1A/1B light chain 3B-I (LC3-I) is converted by lipidation to microtubule-associated 1A/1B light chain 3B-II (LC3-II) and can then associate with the autophagosomal membrane, which contributes to the enclosure of the autophagosome (reviewed by Bento et al., 2016). By investigating total cell lysates of 2D- and 3D- (day 11) cultivated HCT116 and NCI-H460 it was shown that

in both cell lines LC3-II could only be detected in MCTS-forming cells strongly pointing to enhanced autophagy and nutrient deprivation within those cells.

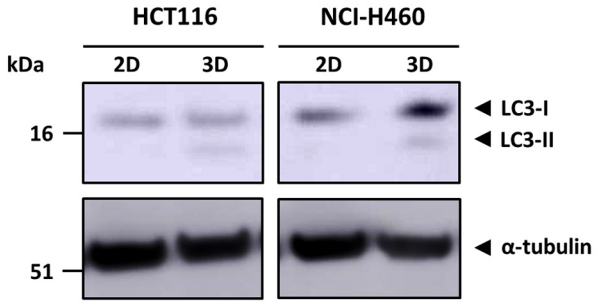

Figure 47: MCTSs are comprised of cells that are metabolically stressed

Lysates of 2D-cultivated HCT116 and NCI-H460 cells along with lysates of HCT116 and NCI-H460 MCTSs (day 11) were analysed by western blotting using the indicated antibodies. Blots shown are representative of three independently performed experiments.

5.5. Depriving 2D-cultured cells of glucose or serum increases TRAILR2 expression

Glucose deprivation as well as the absence of vital nutrients and growth factors may, similarly to hypoxia, have an influence on TRAILR expression when cells are cultured as MCTSs. Therefore, it was next investigated whether glucose or serum deprivation can also influence TRAILR expression in 2D-cultured HCT116 and NCI-H460 cells. To achieve glucose deficiency, cells were cultivated in medium containing 1 mg/ml, 0.5 mg/ml or 0.25 mg/ml glucose. In another approach HCT116 and NCI-H460 cells were completely deprived of FCS (serum starvation), which contains a variety of vitamins, hormones, growth factors and amino acids that are necessary for cell growth. Thereafter, the expression of TRAILRs was investigated by flow cytometry and western blot analysis. In HCT116 cells, glucose starvation but not serum deprivation led to enhanced amounts of LC3-II within total cell lysates (Figure 48A). Furthermore, in accordance with this finding, only the lack of glucose influenced TRAILR expression. Already after a starvation period of 48 h, the amount of TRAILR2 on the cell surface and overall expression was notably increased in a concentration-dependent manner and remained at that level for another 24 h (Figure 48B/C). In contrast, surface expression of TRAILR1 remained unchanged. However, accompanying western blots showed that TRAILR1 amounts were decreased overall when HCT116 cells were deprived of glucose. Furthermore, the occurrence of bands running lower than 40 kilo Dalton (kDa) point to a degradation of TRAILR1 after glucose starvation (Figure 48A). In NCI-H460 cells, glucose

deprivation and withdrawal of serum for 48 h both increased the amount of LC3-II while simultaneously decreasing the level of LC3-I in total cell lysates. After 72 h starvation, the amount of LC3-II no longer changed while LC3-I was still decreased (Figure 48A). Comparable to HCT116 cells, glucose starvation for 48 h led to a concentration-dependent increase of surface expression and overall protein amounts of TRAILR2 in 2D-cultured NCI-H460 cells with the effect being even more pronounced after 72 h. Interestingly, in this cell line, the withdrawal of serum also enhanced TRAILR2 expression to the same level as the lowest concentration of glucose (0.25 mg/ml) (Figure 48D/E). Regarding the expression of TRAILR1, it was shown that serum starvation decreased the amount of the protein both at the cell surface and in total cell lysates. Of note, no degradation products were visible under these conditions in the western blot. In contrast, withdrawal of glucose led to a concentration-dependent upregulation of surface TRAILR1 expression. However, in the western blot the increase of TRAILR1 expression was not as apparent but, similarly to HCT116 cells, was accompanied by the occurrence of degradation products (Figure 48A/D/E).

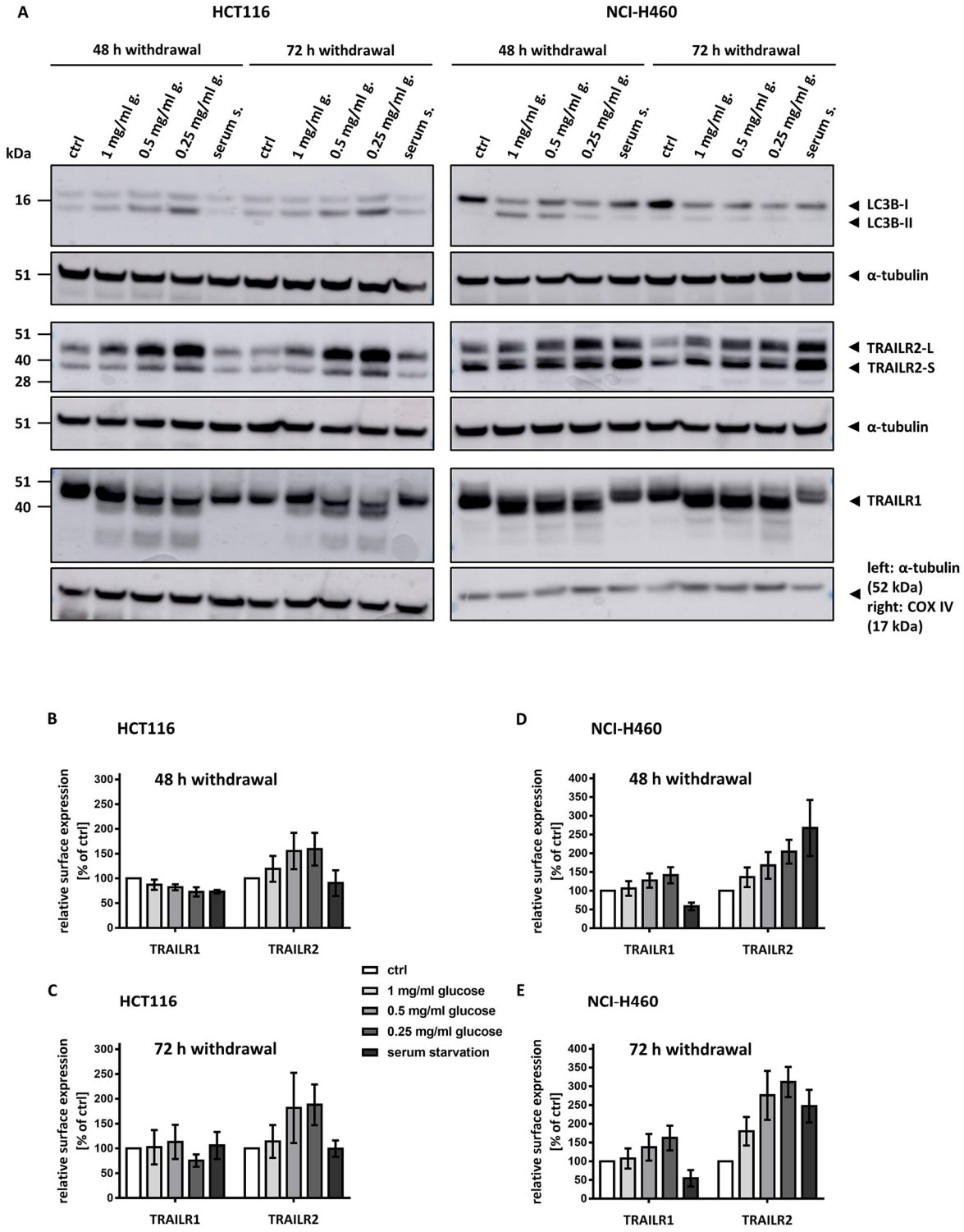
A
HCT116
NCI-H460
48 h withdrawal
72 h withdrawal
ctrl
1 mg/ml g.
0.5 mg/ml g.
0.25 mg/ml g.
serum s.
kDa
16
51
40
28
LC3B-I
LC3B-II
α-tubulin
TRAILR2-L
TRAILR2-S
TRAILR1
left: α-tubulin (52 kDa)
right: COX IV (17 kDa)
B
HCT116
48 h withdrawal
C
HCT116
72 h withdrawal
D
NCI-H460
48 h withdrawal
E
NCI-H460
72 h withdrawal
relative surface expression [% of ctrl]
TRAILR1
TRAILR2
ctrl
1 mg/ml glucose
0.5 mg/ml glucose
0.25 mg/ml glucose
serum starvation

Figure 48: Glucose and serum starvation influence TRAILR expression in 2D-cultured HCT116 and NCI-H460 cells

HCT116 and NCI-H460 cells (2D) were cultivated for 48 h and 72 h under serum starvation (serum s.) or glucose starvation (g.) and cell lysates were analysed by western blotting using the indicated antibodies. Blots shown are representative of three independently performed experiments **(A)**. HCT116 and NCI-H460 cells (2D) were cultivated for 48 h and 72 h under serum starvation (serum s.) or glucose starvation (g.). Thereafter, TRAILR expression was determined by flow cytometry. Medians of the cell populations were used to calculate the surface TRAILR expression relative to cells cultivated under normal conditions (ctrl). Displayed data are mean values ± SD of three independent experiments **(B/C/D/E)**.

5.6. Cells within MCTSs show signs of an activated UPR

Adverse conditions such as hypoxia and nutrient starvation are known to induce ER stress within cells due to the accumulation of unfolded or misfolded proteins. As a consequence, the UPR is activated which includes different signalling pathways that lead to the induction of many different genes involved in protein folding, protein quality control, autophagy, apoptosis, amino acid metabolism, antioxidant response and phospholipid synthesis (reviewed by Lindholm et al. 2017; reviewed by Schröder et al., 2005]. An important protein of the UPR is the chaperon BIP. Under normal conditions BIP is bound to all three ER stress sensors and inhibits their activity. However, in ER stress, BIP translocates from these sensors to bind to unfolded or misfolded proteins and allows the activation of the three branches of the UPR. Since the expression of BIP is enhanced during ER stress, increased amounts of BIP can be used as a marker for an activated UPR. Activation of the ER stress sensor IRE1α leads to the processing of mRNA resulting in the active transcription factor XBP-1, therefore XBP-1 can also be used as an indicator of ER stress. Furthermore, ER stress also activates the sensor PERK, which subsequently leads to the expression of the protein CHOP. CHOP in turn regulates the activity of many apoptosis-relevant proteins and is also used as a marker for ongoing ER stress and activated UPR. To investigate whether cells within HCT116 and NCI-H460 MCTSs (day 11) underwent increased ER stress, potentially due to nutrient starvation and hypoxia, total cell lysates of 3D and 2D-cultivated HCT116 and NCI-H460 cells were analysed for the expression of BIP, XBP-1 and CHOP by western blot analysis. It was shown that while no XBP-1 and CHOP were expressed in 2D-cultured NCI-H460 cells, in NCI-H460 MCTSs (day 11) considerable amounts of these proteins were detected, indicating an ongoing UPR. Additionally, an increased expression of the chaperon BIP was observed when cells were grown as MCTSs. In 2D-cultured HCT116 cells, already a basal expression of CHOP and XBP-1 was detected, which was elevated in HCT116 MCTSs (day 11). As further sign of an activated UPR the enhanced expression of BIP was apparent in 3D-cultured HCT116 cells.

Taken together, these results demonstrate that culturing both cell lines as MCTSs increased the expression of markers that are indicators for ER stress (Figure 49).

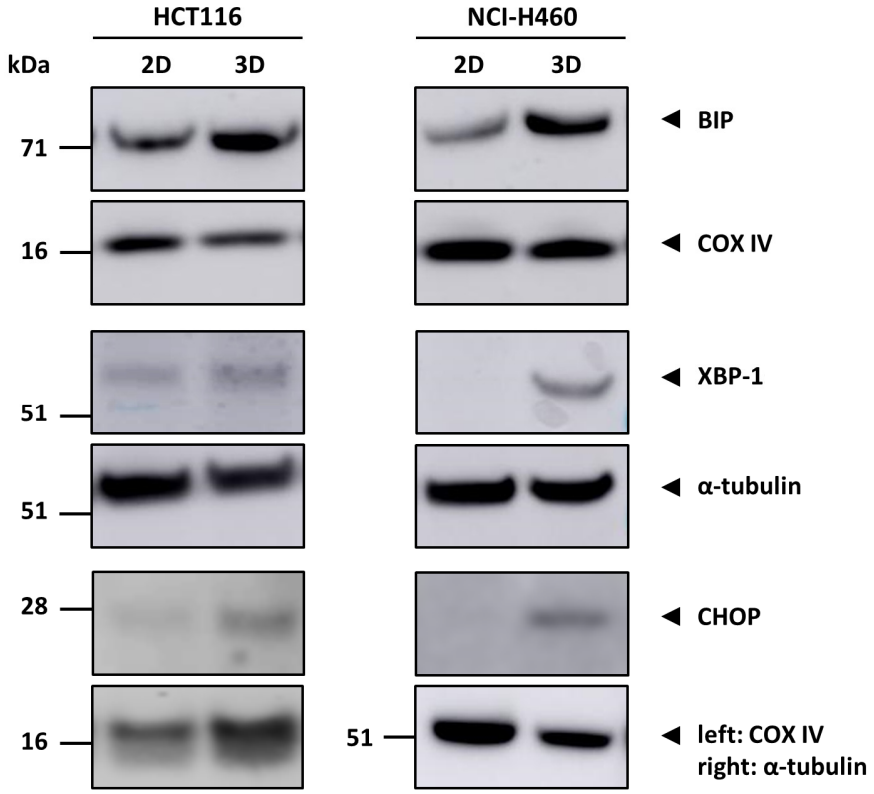

Figure 49: Cells within MCTSs show signs of ER stress

Lysates of 2D-cultivated HCT116 and NCI-H460 cells, along with HCT116 and NCI-H460 MCTSs (day 11), were analysed by western blotting using the indicated antibodies. Blots shown are representative of two to three independently performed experiments.

5.7. Discussion

In chapter 3 it was shown that a population of cells within MCTSs was deprived of oxygen and displayed signs of nutrient starvation as well as activation of the UPR. In order to investigate whether adverse conditions such as hypoxia and nutrient deprival could be accountable for the observed localisation-dependent TRAILR expression of spheroid-forming cells, 2D-cultured cells were starved of oxygen, glucose and serum and analysed for surface and total TRAILR1 and TRAILR2 amounts. Thereby it was demonstrated that depriving cells of oxygen enhanced TRAILR2 and decreased TRAILR1 expression, while starving cells of glucose increased the expression of TRAILR2. Interestingly, serum deprivation only led to an upregulation of TRAILR2 in NCI-H460 cells but not in HCT116 cells.

In solid, rapidly growing tumours vascularisation often cannot occur fast enough to supply all malignant cells with sufficient oxygen. Depending on the tumour type, already in 50 to 200 µm distance from the nearest blood vessel, cells start to display signs of hypoxia (reviewed by Forster et al., 2017). Interestingly, it was described in the literature that, as a consequence of reduced oxygen supply, tumours without vascularisation cannot reach a diameter larger than 2 to 3 mm which is in accordance with the size limit for HCT116 MCTSs observed in this work (Gimbrone et al., 1972). In cells starved of oxygen the protein Hif-1α, which is under normoxic conditions rapidly degraded, gets stabilised and forms together with Hif-1β an active transcription factor that can induce the expression of numerous genes involved in the adaption to hypoxia (Koyasu et al., 2018). In this study it was shown that solely 3D but not 2D-cultured HCT116 and NCI-H460 cells expressed Hif-1α. Furthermore, cells stained positively for the protein were mostly localised close to the centre in larger HCT116 and NCI-H460 MCTSs, which concurs with a study where it was shown that in HCT116 MCTSs (Ø~1 mm) Hif-1α positive cells were found solely close to the necrotic core (Harrison et al., 2011). In general, in literature it is described that the development of an oxygen-deprived cell population starts when MCTSs reach a diameter larger than 200 µm which correlates well with the observation made in this thesis that 11-day-old HCT116 and NCI-H460 MCTSs comprised of cells that express Hif-1α but not 7-day-old MCTSs, (Curcio et al., 2007; Sutherland et al., 1986). Since, depending on their origin, cells can endure different concentrations of low oxygen before they show signs of hypoxia, it would be interesting to investigate what oxygen amount can be found inside of HCT116 and NCI-H460 MCTSs (Semenza, 2017; Spencer et al., 2014). Notably, very recently Murphy and colleagues successfully measured the oxygen tension in different depths of large MCTSs with an oxygen microsensor (Murphy et al., 2017).

In order to investigate whether oxygen withdrawal is able to change TRAILR expression in HCT116 and NCI-H460 cells and thus be involved in the localisation-dependent TRAILR expression within the MCTSs, HCT116 and NCI-H460 cells were cultured in 2D under 1% oxygen for 48 and 72 h. In accordance with literature it was shown that already 48 h of hypoxia were sufficient to lead to a robust expression of Hif-1α in both investigated cell lines. Of note, the amount of the quiescent marker p27 was simultaneously enhanced in concurrence with studies demonstrating that oxygen deprivation stopped cell cycle progression of many different cell types (Eliasson et al., 2010; Shrieve and Begg, 1985). Interestingly, consistent with the observation that quiescent cells close to the spheroid centre displayed very low amounts of TRAILR1 but high amounts of TRAILR2, cultivation under hypoxia increased surface and total expression of TRAILR2 and decreased surface and total expression of TRAILR1 in 2D-cultured HCT116 and NCI-H460 cells. However, it has also to be mentioned that, while hypoxia increased the surface expression of TRAILR2 in the HCT116 cell line, cells close to the spheroid centre did, most likely, not display high surface but high intracellular amounts of the receptor. Thus, it might be speculated that in oxygen-deprived cells close to the necrotic core, the expression of TRAILR2 was induced but the receptor was not shuttled to the surface. Interestingly, in accordance with the previously described results, it was shown by Park and colleagues that depriving lung cancer cells of oxygen led to increased total amounts of TRAILR2 and decreased TRAILR1 expression (Park et al., 2002). However, another study suggests that the observed regulation of TRAILR expression is cell line-dependent, as only 1 out of 7 investigated cell lines displayed increased amounts of surface TRAILR2 after oxygen deprivation (Gobbi et al., 2010). As already discussed in chapter 1, underlying mechanisms for the observed changes in TRAILR expression after oxygen deprivation could be various and might involve transcription factors, miRNAs and RNA-binding proteins. Since cells close to the necrotic core were most likely highly susceptible to TRAIL, it should be investigated whether the cultivation under 1% oxygen altered the TRAIL-sensitivity of HCT116 and NCI-H460 cells. It was already shown in literature that hypoxia can render cells susceptible to TRAIL. However, this was not attributed to changes in TRAILR expression but to the regulation of the amounts of other proteins such as protein kinase C (Gobbi et al., 2010; Weinmann et al., 2004). Thus, in cases where hypoxia is found to change TRAIL-susceptibility of HCT116 and NCI-H460 cells, the changed expression of further proteins also may contribute to the sensitisation and must be taken into account.

Due to insufficient vascularisation of rapidly growing tumours, cells that are a large distance from the nearest blood vessel are, besides being deprived of oxygen, also less supplied with nutrients. In literature it was not only demonstrated that various human tumour xenografts

showed uneven distribution of glucose but also that the glucose concentration was lowered in the centre of large MCTSs (Ø ~1mm) (Kallinowski et al., 1988; Tamulevicius and Streffer, 1995; Teutsch et al., 1995; Walenta et al., 2000). In nutrient-starved cells, organelles and proteins are digested in a process called autophagy to maintain metabolism. To break down the substrates into their individual components (amino acids, lipids), they are engulfed by autophagosomes that later fuse with lysosomes. A common method to investigate cells for ongoing autophagy is to determine the quantities of LC3-I and LC3-II. During the process of autophagosome formation LC3-I gets lipidated to LC3-II, allowing it to associate with the autophagosomal membrane (reviewed by Bento et al., 2016; reviewed by White, 2015). Consequently, to investigate whether some cells within large HCT116 and NCI-H460 are deprived of nutrients, total cell lysates were analysed for signs of ongoing autophagy by western blotting for LC3-I and LC3-II. Thereby it was shown that, compared to 2D-cultured HCT116 and NCI-H460 cells, more LC3-II was to be found in total lysates of HCT116 and NCI-H460 MCTSs, pointing to enhanced autophagy in the 3D scenario. However, it has to be mentioned that the increase of LC3-II alone is not a sufficient marker for amplified autophagic flux. Large amounts of this protein can also be the result of inhibited autophagosomal degradation (Mizushima and Yoshimori, 2007). To investigate that in more detail, 2D- and 3D-cultured cells might be treated with chloroquine, a drug that inhibits the degradation of autophagosomes (reviewed by Kimura et al., 2013). In the event that comparable amounts of LC3-II will be found in 2D- and 3D-cultured cells after treatment with chloroquine, it can be assumed that not the autophagic flux is increased but rather autophagosomal degradation is inhibited in HCT116 and NCI-H460 MCTSs. As autophagy is most likely enhanced in cells localised in some distance from the MCTS surface, spheroid-forming cells might be sorted by TRAILR1 expression to compare LC3-II quantities or autophagy related 5 (Atg5) amounts, a further marker for increased autophagy, between proliferative and quiescent cell populations. Furthermore, spheroid sections could also be stained for LC3 to reveal a potential accumulation of autophagosomes in cells close to the necrotic core. Finally, to prove that cells within HCT116 and NCI-H460 MCTSs are actually deprived of glucose, spheroid sections could be investigated by bioluminescence imaging (Kallinowski et al., 1988; Walenta et al., 2000).

To investigate if and to what extent nutrient deprivation plays a role in the observed localisation-dependent TRAILR expression within HCT116 and NCI-H460 MCTSs, 2D-cultured HCT116 and NCI-H460 cells were starved of either serum or glucose. Induction of autophagy as result of the applied nutrient withdrawal was again verified by determining the cells' quantities of LC3-I and LC3-II. Experiments revealed that in HCT116 cells, the deprivation of glucose led to enhanced amounts of LC3-II and increased expression of TRAILR2. Conversely

serum starvation did not induce autophagy and consistently did not influence TRAILR2 expression. In NCI-H460 cells starved for 48 h of serum and glucose, increased amounts of LC3-II and decreased quantities of LC3-I were detected. After 72 h nutrient withdrawal, the amounts of LC3-I were still lowered while additionally also the amounts of LC3-II were noticeably decreased. Since it is known that prolonged autophagy can lower the amounts LC3-II due to degradation of autophagosomes, it can be assumed that already after 48 h and still after 72 h of nutrient starvation, autophagy was induced in 2D-cultured NCI-H460 cells. In accordance with this finding, both serum and glucose starvation increased TRAILR2 expression in this cell line. These results concur with literature where it was shown that glucose starvation enhanced TRAILR2 expression on the transcriptional level in various cell lines (Carr et al., 2016; Iurlaro et al., 2017; Liu et al., 2009). Interestingly Iurlaro and colleagues could also demonstrate that not only surface expression of TRAILR2 was enhanced after glucose deprivation but that the receptor also accumulated intracellularly (Iurlaro et al., 2017). Furthermore, it was shown that upregulation of TRAILR2 induced by glucose deprivation, contributed to the simultaneously occurring sensitisation of the cells to TRAIL-induced apoptosis (Carr et al., 2016). However, whether investigated 2D-cultured HCT116 and NCI-H460 cells are indeed more susceptible to TRAIL after upregulation of TRAILR2 has yet to be investigated.

Nevertheless, the observations fit the hypothesis that within MCTSs, cells close to the necrotic core display increased, most likely intracellularly-localised, TRAILR2 amounts as a result of nutrient deprivation. It might further be hypothesized that large amounts of intracellular TRAILR2 can ligand-independently pre-assemble and function as a platform to activate procaspase 8 after endocytosis of TRAIL-TRAILR complexes from the surface, sensitising the cell to TRAIL-induced apoptosis. Furthermore, it is also conceivable that pre-assembled TRAILR2 results in low ligand-independent procaspase 8 activation that lowers the threshold for ligand-induced apoptosis.

In contrast to TRAILR2, the amount of TRAILR1 was not altered by glucose or nutrient starvation in 2D-cultured HCT116 cells. Conversely, glucose deprivation led to a slight increase, and serum starvation to a decrease, of TRAILR1 expression in 2D-cultured NCI-H460 cells. It seems that glucose withdrawal indeed influences TRAILR1 expression dependent on the cell line since studies with human colorectal cancer and melanoma cell lines reported no change in TRAILR1 expression after glucose starvation, while experiments done in Hela cells showed non-transcriptional upregulation of the receptor (Carr et al., 2016; Iurlaro et al., 2017; Liu et al., 2009). Interestingly in the present work, TRAILR1 was also found to display a slightly decreased molecular weight after glucose but not after serum

starvation in both cell lines which is most likely the result of insufficient glycosylation of the protein. Since in literature it was shown that N-glycosylation of TRAILR1 was necessary for its apoptosis-inducing capacity, it might be hypothesised that in intermediate, nutrient-starved spheroid layers, cells are not only resistant as a result of reduced TRAILR expression but also due to insufficient glycosylation of the proteins (Florent et al., 2016; Yoshida et al., 2007). Alongside insufficiently glycosylated TRAILR1, also additional anti-TRAILR1 antibody binding protein fragments with much smaller molecular weight were found in total protein extracts of glucose-starved HCT116 and NCI-H460 cells. However, whether these fragments are for example degradation products of TRAILR1 due to ongoing cell death in response to glucose withdrawal has yet to be investigated.

Taken together, hypoxia and nutrient starvation were both shown to influence TRAILR expression. While each condition led to increased TRAILR2 amounts, fitting the observation that cells close to the necrotic were enriched in the protein, only hypoxia reduced the amounts of TRAILR1 and might therefore contribute to the downregulation of this receptor in quiescent cells. In the future, it might be interesting to apply both conditions together on 2D-cultured cells, to investigate whether observed changes in TRAILR expression get even more pronounced. Nevertheless, the fact that neither hypoxia nor nutrient starvation were able to mimic the downregulation of TRAILR2 in intermediate spheroid cell layers suggest that in addition to these conditions, other factors must contribute to the localisation-dependent TRAILR expression within MCTSs. Beside the waste product lactate, these might also comprise factors released by dying cells in the spheroid centre.

As mentioned previously in this thesis, the underlying mechanism for the observed altered TRAILR expression during hypoxia and nutrient starvation might be influenced by various pathways and could include different transcription factors, miRNAs or RNA-binding proteins. However, it is known that both, oxygen and nutrient deprivation, can lead to ER stress followed by the induction of the UPR which was already shown by many studies to upregulate TRAILR2 expression (Iurlaro et al., 2017; Li et al., 2015; Liu et al., 2009; Sies and Bruene, 2007; Yamaguchi and Wang, 2004). To investigate whether this might also hold true for spheroid-forming HCT116 and NCI-H460 cells, MCTSs were analysed for the expression of different marker proteins for an ongoing UPR. Thereby, it was demonstrated that, in comparison to 2D-cultivated HCT116 and NCI-H460 cells, the ER chaperon BIP, whose enhanced expression is indicative for the induction of ER stress, was upregulated in HCT116 and NCI-H460 MCTSs. Furthermore, the analysis of the two UPR-related transcription factors XBP-1 and CHOP also suggested enhanced ER stress in 3D-cultured HCT116 and NCI-H460 cells. To investigate whether ER stress is actually induced in spheroid-forming cells close to

the necrotic core, as was suggested in the literature, sections of HCT116 and NCI-H460 MCTSs could be stained for ER stress markers such as BIP, XBP-1 and CHOP (Zhang et al., 2014). Furthermore, since TRAILR2 upregulation via the UPR was shown to be mediated either by AFT4, CHOP or the ATF6/IRE1α/XBP-1 axis, inducible knockout of the involved proteins in HCT116 and NCI-H460 MCTSs might reveal their contribution in the observed TRAILR2 upregulation in spheroid-forming cells close to the centre (Iurlaro et al., 2017; Liu et al., 2009; Yamaguchi and Wang, 2004).

Chapter 4: COX II inhibitors upregulate TRAILR2 within MCTS-forming cells and sensitise them to TRAIL

As shown previously in this thesis HCT116 and NCI-H460 MCTSs (day 11) are comprised of TRAIL-resistant cells that protect TRAILR-hypersensitive cells close to the centre from TRAIL-induced apoptosis. The fact that cells within these MCTSs also differ in their expression of TRAILR1 and TRAILR2, dependent on their localisation within the spheroids, led to the hypothesis that the differences in TRAILR expression account for the varying TRAIL susceptibility of spheroid-forming cells. Since experiments with HCT116 T2 KO cells revealed that TRAIL-hypersensitivity of spheroid-forming cells is most likely caused by increased expression of TRAILR2, it was next investigated whether MCTSs can sensitise to TRAIL by upregulating TRAILR2 in cells localised in intermediate layers of the spheroids. Cyclooxygenase II inhibitors (COX II inhibitors), such as NS-398 and celecoxib, are known to enhance TRAILR2 expression by different suggested mechanisms (Chandrasekaran et al., 2014; Edagawa et al., 2014; He et al., 2008; Oh et al., 2010). In this work treatment of HCT116 and NCI-H460 MCTSs with both COX II inhibitors increased the expression of TRAILR2 in spheroid-forming cells and led to a sensitisation of MCTSs to TRAIL. Of note, both inhibitors enhanced the activation of the UPR indicating that an induction of ER stress might be accountable for the increased expression of TRAILR2.

6.1. Only MCTS-forming NCI-H460 cells express COX II

Cyclooxygenase is an enzyme in the human body that catalyses the conversion of arachidonic acid to prostaglandins. One of the two existing isoforms, COX I, is constitutively active and ensures the supply of the body with prostaglandins that are necessary for the protection of gastric mucosa, regulation of the blood flow in the kidneys and the aggregation of platelets. In contrast, the other isoform, COX II is mainly expressed during inflammation (reviewed by Greenhough et al., 2009). Interestingly, it was shown that high amounts of COX II are to be found in many tumours such as prostate cancer, colorectal cancer and non-small lung cancer (Brown and DuBois, 2005; Gupta et al., 2000; Kelley et al., 2005; Williams et al., 1999). Large quantities of COX II enzyme seem to protect the malignant cells from apoptosis, attenuate the immune response of the host against the tumour and increase angiogenesis and proliferation (reviewed by Choy, 2003). As a consequence, inhibition of COX II should be beneficial in cancer treatment, which was already shown both *in vitro* and *in vivo* with COX II inhibitors such as NS-398 and celecoxib (reviewed by Grösch et al., 2001; reviewed by

Jendrossek, 2013). Of note, some of the inhibitors showed anti-cancer activity independent of COX II expression which points to additional COX II-independent methods of action (Chen et al., 2007; Smith et al., 2000; Sobolewski et al., 2015). To investigate whether COX II is expressed in HCT116 and NCI-H460 cells, as well as to examine if culturing cells as MCTSs increases the expression of the enzyme, 2D- and 3D-cultivated HCT116 and NCI-H460 cells were analysed for their total COX II expression at the protein and mRNA level. Thereby, it could be shown that neither of those two cell lines expressed COX II when cultivated in 2D, while in MCTS-forming NCI-H460 cells both protein and mRNA was detected (Figure 50).

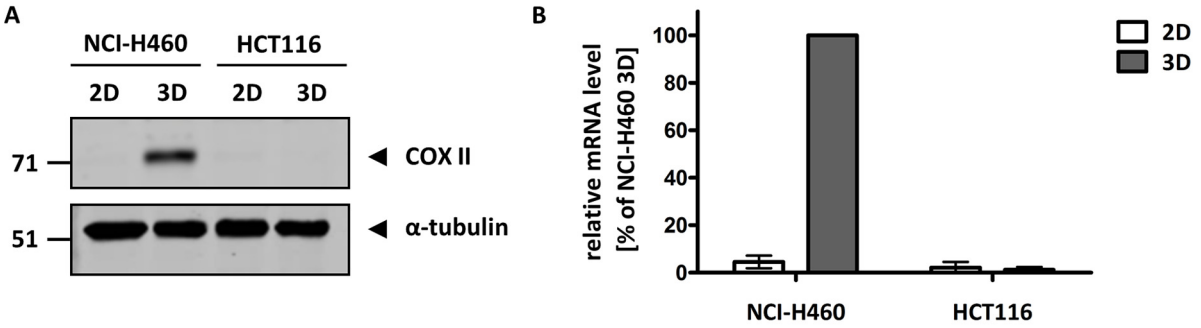

Figure 50: Only MCTS-forming NCI-H460 cells show expression of COX II on the protein and mRNA level

Lysates of 2D-cultivated HCT116 and NCI-H460 cells, along with lysates of HCT116 and NCI-H460 MCTSs (day 11), were analysed by western blotting using the indicated antibodies. Blots shown are representative of three independently performed experiments **(A)**. 2D-cultivated HCT116 and NCI-H460 cells as well as HCT116 and NCI-H460 MCTSs (day 11) were used to perform a qPCR. Relative RNA amounts were calculated by the ΔΔCt method using GAPDH for normalisation. COX II mRNA expression of 3D-cultivated NCI-H460 cells was set to 100%. Data shown are mean values ± SD of three independent experiments **(B)**.

6.2. COX II inhibitors increase the unfolded protein response in MCTSs

As mentioned previously COX II inhibitors were shown to exert their effects also in cell lines that are completely devoid of the enzyme. One suggested mechanism is hereby the ER stress-induced activation of the UPR which can subsequently lead to upregulation of TRAILR2 and induction of apoptosis (Cano-González et al., 2018; Edagawa et al., 2014; Jendrossek, 2013; Lu et al., 2014; Yamaguchi and Wang, 2004). To investigate whether celecoxib and NS-398 induce ER stress in HCT116 and NCI-H460 MCTSs, whole cell lysates of stimulated spheroids were investigated for the expression of markers for an ongoing UPR. Thereby it was demonstrated that celecoxib and NS-398 enhanced slightly the expression of the

chaperon BIP and the transcription factor XBP-1 in HCT116 MCTSs. Furthermore, NS-398 did to some extent increase the expression of the UPR-induced transcription factor CHOP in HCT116 MCTSs while the compound celecoxib only marginally, if at all, enhanced CHOP amounts in HCT116 and NCI-H460 MCTSs.

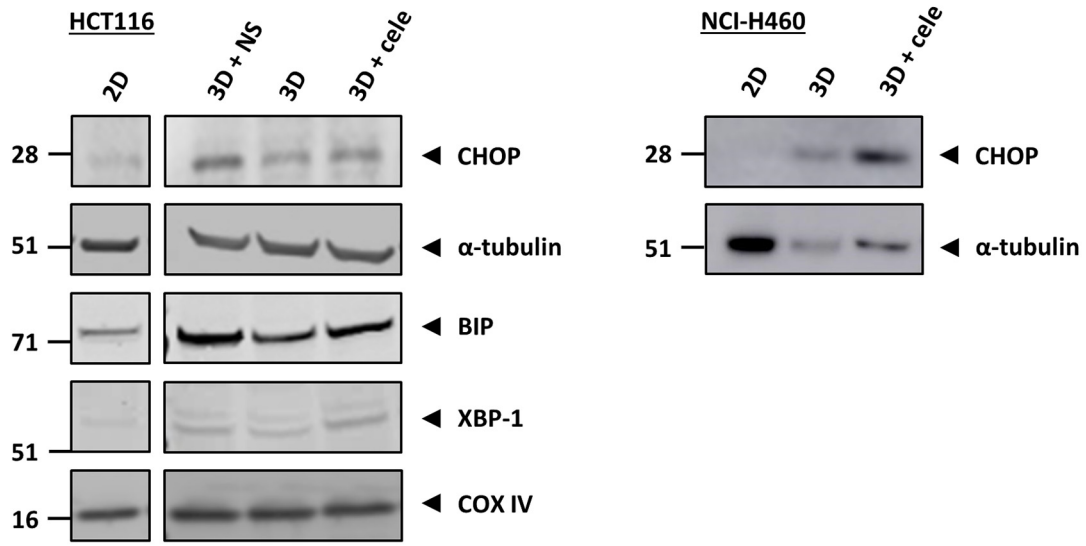

Figure 51: Increased expression of markers for an ongoing UPR after stimulation of MCTSs with COX II inhibitors

HCT116 and NCI-H460 MCTSs (day 11) were stimulated with 100 µM NS-398 (NS) or 50 µM celecoxib (cele) for 72 h. Thereafter, lysates of 2D-cultured cells (as a control) and MCTSs were analysed for their expression of the indicated proteins. Blots shown are representative of two to three independently performed experiments

6.3. COX II inhibitors increase TRAILR2 expression in MCTS-forming HCT116 cells and sensitise them to TRAIL

As mentioned previously, it has been described that overexpression of COX II in human colon carcinoma cell lines can decrease TRAILR2 expression and render these cells resistant to TRAIL (Tang et al., 2002). Conversely, it was shown that treatment with COX II inhibitors can increase TRAILR expression thereby enhancing the susceptibility of the cells to TRAIL-induced apoptosis even in the absence of any detectable COX II expression (Chandrasekaran et al., 2014; He et al., 2008). In order to investigate if the same holds true for 2D- and 3D-cultivated HCT116 and NCI-H460 cells, treatment with two different COX II inhibitors, NS-398 and celecoxib, was carried out. The results revealed that treatment with both drugs only influenced TRAILR2 and not TRAILR1 expression within HCT116 cells. Interestingly,

stimulation with NS-398 enhanced surface TRAILR2 expression only under 2D but not under 3D cultivation conditions (Figure 52A/B). In accordance with this finding, sensitisation to TRAIL by NS-398 was much more pronounced in 3D than in 2D-cultivated cells. (Figure 52E/F). Treatment with the second COX II inhibitor, celecoxib, enhanced the TRAILR2 surface expression in spheroid-forming HCT116 cells even to a larger extent than NS-398 (NS-398: ~1.5 fold higher expression; celecoxib: ~2.5 fold higher expression) (Figure 50; Figure 52D). Furthermore, in contrast to NS-398, celecoxib also enhanced the surface expression of TRAILR2 in 2D-cultured cells (Figure 52C). Regarding a sensitisation of MCTS-forming cells to TRAIL, results obtained after treatment with celecoxib were comparable to that after incubation with NS-398. Both drugs could decrease the percentage of viable cells at the highest concentration of TRAIL from around 15% to 8% (celecoxib) and 5% (NS-398), respectively (Figure 52H). Stimulation of 2D-cultivated cells was only carried out once, however the result indicated that the cells could be sensitised to TRAIL-induced apoptosis by celecoxib which is in accordance with the finding that celecoxib was able to enhance TRAILR2 expression even under 2D cultivation (Figure 52C/G). To analyse whether both drugs worked synergistically in inducing cell death, the coefficient of drug interaction (CDI) was calculated for each concentration of TRAIL and celecoxib, respectively NS-398. If the CDI equals 1, the action of two drugs is referred to as additive while at a CDI below 1 two drugs are presumed to act synergistically. Of note, at a CDI below 0.7 two drugs are supposed to act highly synergistic in inducing cell death (Cao et al., 1989). As mentioned previously in this thesis, treatment with NS-398 could only sensitise 2D-cultivated HCT116 cells to TRAIL-induced cell death at the highest concentration of TRAIL and the calculation of the CDI (0.71) revealed that in this case the two drugs acted synergistically. In contrast, incubation of HCT116 MCTSs with NS-398 could sensitise the cells at all investigated TRAIL concentrations to cell death, with the two drugs acting synergistically in all cases. (0.02 nM TRAIL: CDI = 0.84; 0.2 nM TRAIL: CDI = 0.54; 3.5 nM TRAIL: CDI = 0.38). Calculation of the CDI for treatment with celecoxib and TRAIL revealed that the action of the two drugs was highly synergistic at 0.2 nM and 3.5 nM TRAIL in 2D (0.2 nM TRAIL: CDI = 0.71; 3.5 nM TRAIL: CDI = 0.3) and 3D (0.2 nM TRAIL: CDI = 0.55; 3.5 nM TRAIL: CDI = 0.53) cultivated HCT116 cells (Table 7).

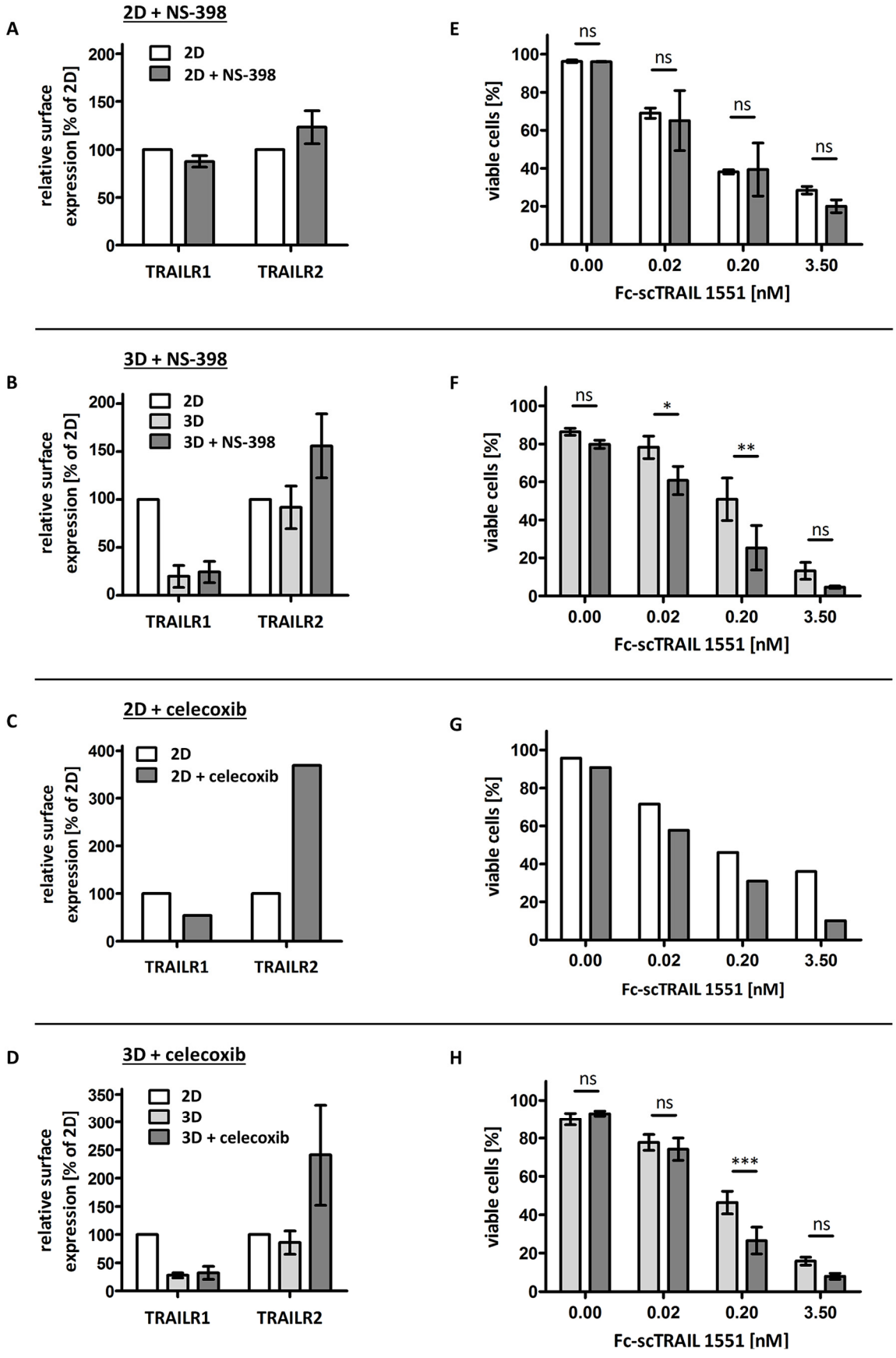
A
2D + NS-398
2D
2D + NS-398
relative surface expression [% of 2D]
TRAILR1
TRAILR2
E
viable cells [%]
ns
0.00
0.02
0.20
3.50
Fc-scTRAIL 1551 [nM]
B
3D + NS-398
3D
3D + NS-398
*
**
F
C
2D + celecoxib
2D + celecoxib
G
D
3D + celecoxib
3D + celecoxib
***
H

Figure 52: Treatment with COX II inhibitors enhances TRAILR2 expression within MCTS-forming HCT116 cells and sensitises them to TRAIL

2D-cultivated HCT116 cells along with HCT116 MCTSs (day 11) were treated for 72 h with 100 µM NS-398 or 50 µM celecoxib. Thereafter, TRAILR expression was determined by flow cytometry. Medians of the cell populations were used to calculate the surface TRAILR expression relative to 2D-cultivated cells. Displayed data are mean values ± SD of at least three independent experiments except for the stimulation of 2D-cultured cells with celecoxib where only one experiment was performed **(A/B/C/D)**. 2D-cultivated HCT116 cells along with HCT116 MCTSs (day 11) were stimulated for 48 h with 100 µM NS-398 or 50 µM celecoxib and for an additional 24 h with the respective drug together with or without the indicated concentrations of Fc-scTRAIL 1551. The percentage of viable cells was determined afterwards by Annexin V-EGFP staining and flow cytometry. Data shown are mean values ± SD of three independent experiments, each performed in duplicates except for the stimulation of 2D-cultured cells with celecoxib and Fc-scTRAIL 1551 where only one experiment was performed **(E/F/G/H)**. Asterisks indicate statistical significance (* = $p \leq 0.05$, ** = $p \leq 0.01$, *** = $p \leq 0.001$, ns = not significant; Two-way ANOVA with Bonferroni correction).

Table 7: Calculation of the coefficient of drug interaction to investigate drug synergy

	CDI		
	NS-398 [100 µM] + TRAIL [0.02 nM]	**NS-398 [100 µM] + TRAIL [0.2 nM]**	**NS-398 [100 µM] + TRAIL [3.5 nM]**
HCT 116 2D	0.94	1.03	0.71
HCT116 3D	0.84	0.54	0.38
	celecoxib [50 µM] + TRAIL [0.02 nM]	**celecoxib [50 µM] + TRAIL [0.2 nM]**	**celecoxib [50 µM] + TRAIL [3.5 nM]**
HCT116 2D	0.85	0.71	0.3
HCT116 3D	0.92	0.55	0.53

The coefficient of drug interaction (CDI) was calculated from data shown in Figure 52. CDI > 1 indicates antagonism; CDI = 1 indicates additivity; CDI < 1 indicates synergism.

In addition to HCT116 cells, NCI-H460 cells cultivated in 2D or as MCTSs were treated with the two COX II inhibitors with similar results. As for HCT116, treatment with NS-398 and celecoxib increased the surface expression of TRAILR2 but not TRAILR1 in MCTS-forming NCI-H460 cells. Interestingly, NS-398 only restored TRAILR2 expression to the level observed in 2D-cultivated cells while TRAILR2 expression in MCTS-forming cells was around 6-fold higher than under 2D cultivation after treatment with celecoxib (Figure 53B/C). Furthermore, similar to HCT116 cells, NS-398 could only slightly enhance TRAILR2 expression in 2D-cultivated NCI-H460 cells (Figure 53A). Simultaneous stimulation with TRAIL and NS-398 or TRAIL and celecoxib revealed that both drugs can sensitise MCTS-forming NCI-H460 cells to TRAIL-induced cell death (Figure 53D/E). Furthermore, calculation of the CDI revealed that at

all TRAILR concentrations, NS-398 and celecoxib acted highly synergistic with TRAIL in inducing cell death (Table 8).

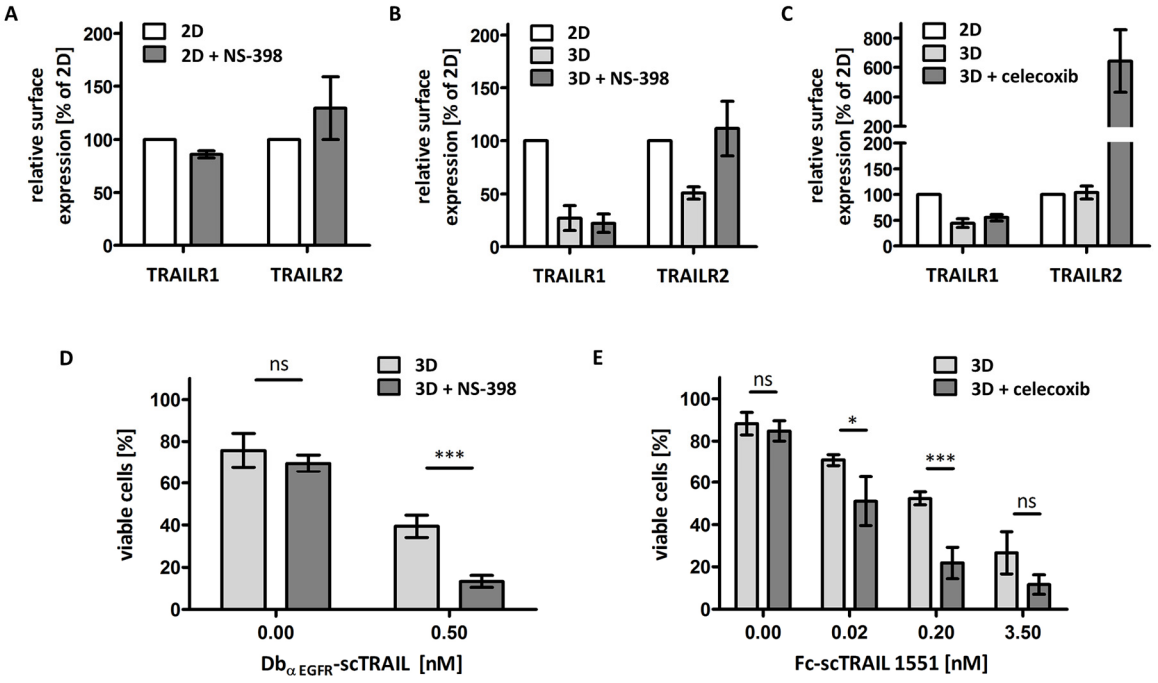

Figure 53: Treatment with COX II inhibitors enhances TRAILR2 expression within MCTS-forming NCI-H460 cells and sensitises them to TRAIL

2D-cultivated NCI-H460 cells along with NCI-H460 MCTSs (day 11) were treated for 72 h with 100 µM NS-398 or 50 µM celecoxib. Thereafter, TRAILR expression was determined by flow cytometry. Medians of the cell populations were used to calculate the surface TRAILR expression relative to 2D-cultivated cells. Displayed data are mean values ± SD of at least three independent experiments **(A/B/C)**. 2D-cultivated NCI-H460 cells along with NCI-H460 MCTSs (day 11) were stimulated for 48 h with 100 µM NS-398 or 50 µM celecoxib and for additional 24 h with the respective drug together with or without the indicated concentrations of Fc-scTRAIL 1551. The percentage of viable cells was determined afterwards by Annexin V-EGFP staining and flow cytometry. Data shown are mean values ± SD of three independent experiments each performed in duplicates **(D/E)**. Asterisks indicate statistical significance (* = $p \leq 0.05$, *** = $p \leq 0.001$, ns = not significant; Two-way ANOVA with Bonferroni correction).

Table 8: Calculation of the coefficient of drug interaction to investigate drug synergy

	CDI			
	NS-398 [100 µM] + TRAIL [0.5 nM]	**celecoxib [50 µM] + TRAIL [0.02 nM]**	**celecoxib [100 µM] + TRAIL [0.2 nM]**	**celecoxib [100 µM] + TRAIL [3.5 nM]**
NCI-H460 3D	0.48	0.75	0.44	0.37

The coefficient of drug interaction (CDI) was calculated from data shown in Figure 53. CDI > 1 indicates antagonism; CDI = 1 indicates additivity; CDI < 1 indicates synergism.

6.4. COX II inhibitors reduce proliferation within MCTSs

It is known that COX II inhibitors can reduce cell proliferation (Sobolewski et al., 2015; Beak et al., 2007). To investigate whether this was reflected by a smaller spheroid diameter as well as a reduced number of proliferative cells per spheroid, HCT116 and NCI-H460 MCTSs (day 11) were stimulated for 72 h with NS-398, respectively HCT116 MCTSs (day 11) were stimulated for 72 h with celecoxib. Thereafter, spheroids were embedded in paraffin, cut into 3 µm slices and sections were immunohistochemically stained for the proliferation marker TK1. Alongside the determination of the percentage of TK1 positive cells within stimulated MCTSs, compared to unstimulated spheroids of the same age, the spheroids' diameters were measured. Thereby, it could be shown that treatment with NS-398 significantly reduced the percentage of TK1 positive cells in both HCT116 and NCI-H460 MCTSs when compared to their respective controls. After treatment of HCT116 MCTSs with the COX II inhibitor only around 3% of all cells were positive for TK1, compared to ~12% in unstimulated spheroids. Furthermore, in two out of three NCI-H460 MCTSs, no cells with TK1 expression could be detected after treatment with NS-398 in comparison to around 5% in the unstimulated control spheroids (Figure 54A/B). This deficiency in proliferative cells was also reflected in the diameter of the respective MCTSs. HCT116 MCTSs treated with NS-398 displayed smaller diameter of around 50 µm than unstimulated spheroids and the diameter of treated NCI-H460 MCTSs was around 100 µm smaller than that of control spheroids (Figure 56A/C). Since treated NCI-H460 spheroids were completely devoid of TK1 positive cells, it can be speculated that they didn't grow at all after addition of the COX II inhibitor. As mentioned above, HCT116 MCTSs were also treated with celecoxib and the percentage of TK1 positive cells as well as the diameter of the MCTSs were determined in the same way as for the experiments with NS-398. Interestingly, treatment with celecoxib only decreased the percentage of TK1 positive cells within HCT116 MCTSs to around 8% but this difference between the percentage of positive cells in the treated and the control spheroids was not significant (unpaired t-test, p value > 0.05) (Figure 55A/B). Nevertheless, stimulated HCT116 MCTSs (Ø ~ 400 µm) displayed a significant smaller diameter than control spheroids (Ø ~460 µm) (Figure 56B).

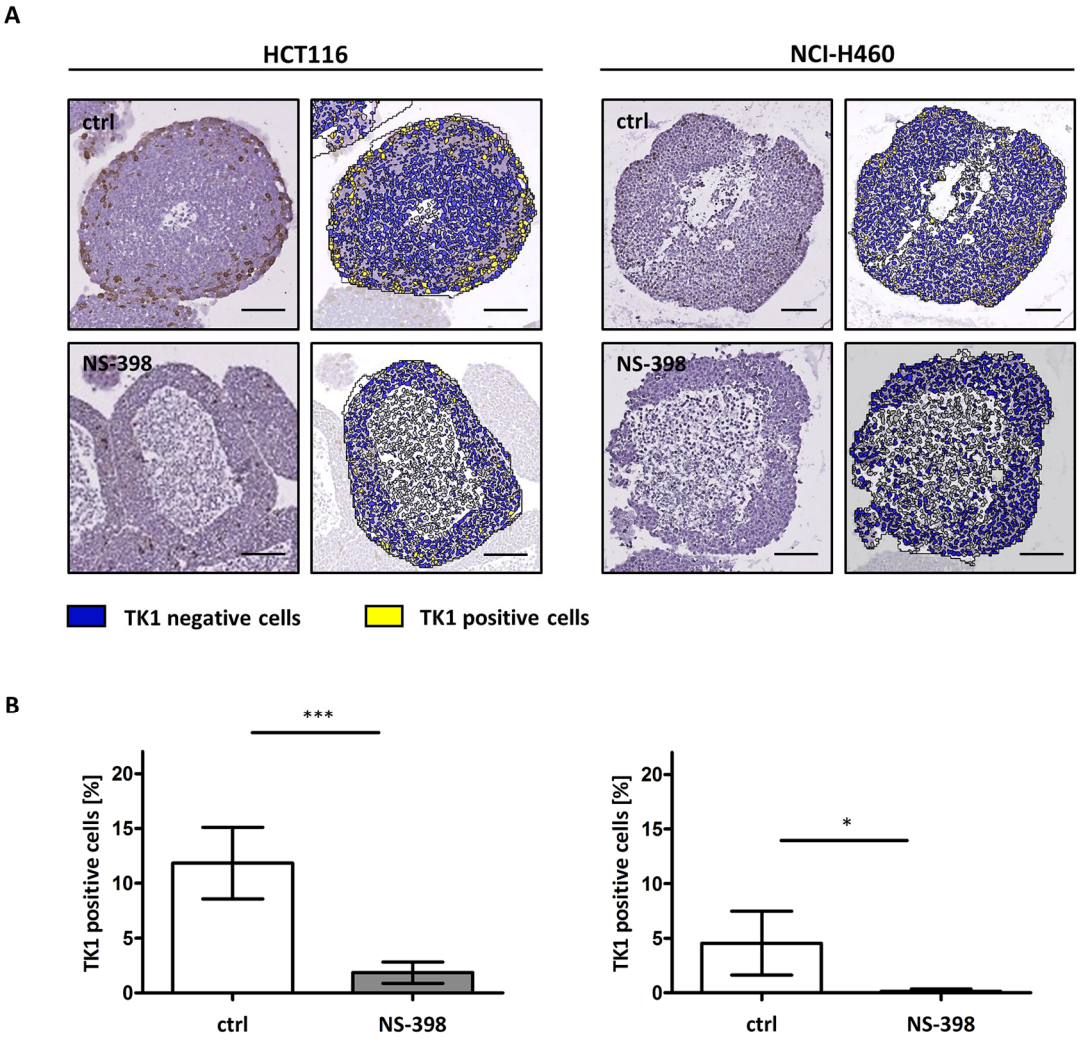

Figure 54: Reduced proliferation in MCTSs after treatment with NS-398

HCT116 and NCI-H460 MCTSs (day 11) were stimulated for 72 h with 200 µM NS-398. Thereafter, MCTSs were embedded in paraffin and cut into 3 µm slices. Middle sections of MCTSs were immunohistochemically stained for thymidine kinase 1 (TK1) and counterstained with haematoxylin to visualise cell nuclei. Then, the software Definiens Tissue Studio 64 was used to identify cells with (yellow) and without (blue) TK1 expression. Pictures are representative of two to three independent experiments. Scale bars in all images = 100 µm **(A)**. After image analysis with the Definiens Tissue Studio 64 software the percentage of cells with or without TK1 expression was determined using Photoshop Elements 10. Shown are mean values ± SD of in total three to seven MCTSs out of two to three independent experiments. Asterisks indicate statistical significance (* = $p \leq 0.05$, ** = $p \leq 0.01$, ns = not significant; unpaired t-test **(B)**. Staining and analysis via the software was done together with Tobias Beigl.

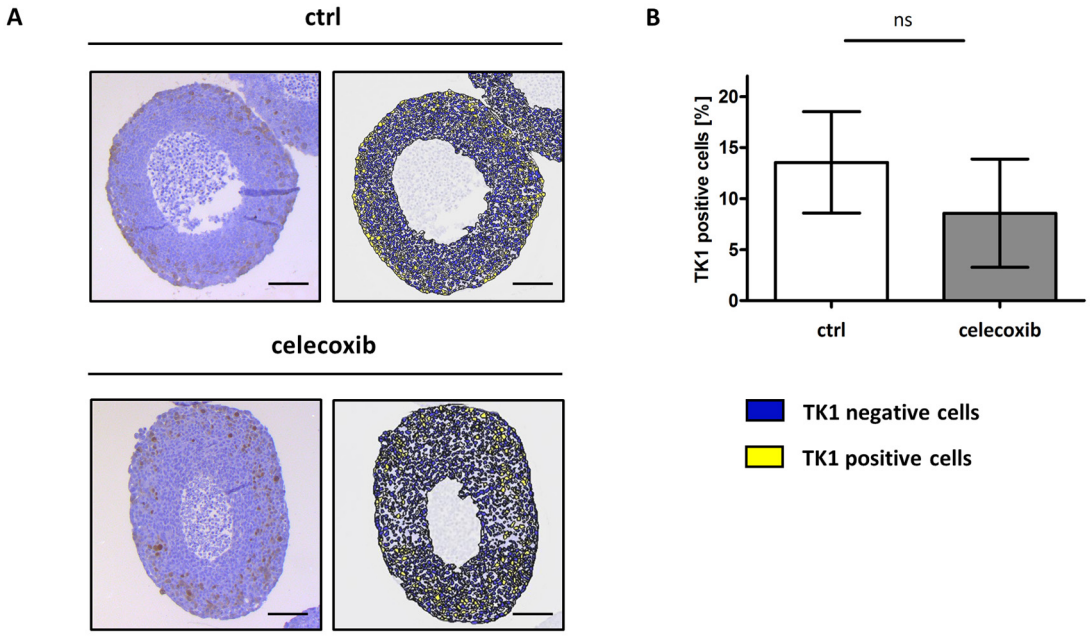

Figure 55: Treatment with celcecoxib does not significantly reduce proliferation in HCT116 MCTSs
HCT116 (day 11) were stimulated for 72 h with 50 µM celecoxib. Thereafter, MCTSs were embedded in paraffin and cut into 3 µm slices. Middle sections of MCTSs were immunohistochemically stained for thymidine kinase 1 (TK1) and counterstained with haematoxylin to visualise cell nuclei. Then, the software Definiens Tissue Studio 64 was used to identify cells with (yellow) and without (blue) TK1 expression. Pictures are representative of three independent experiments. Scale bars in all images = 100 µm **(A)**. After image analysis with the Definiens Tissue Studio 64 software the percentage of cells with or without TK1 expression was determined using Photoshop Elements 10. Shown are mean values ± SD of in total 7 (ctrl) or 11 (celecoxib) MCTSs out three independent experiments. Statistical significance was verified with an unpaired t-test; ns = not significant **(B)**.

6.5. NS-398 increases the necrotic core in MCTSs

By observing the spheroid sections, it was apparent that after treatment with NS-398 the necrotic core was enlarged in HCT116 and NCI-H460 MCTSs (Figure 54A). To verify this observation, the diameter of the necrotic core was measured and displayed as percentage of the whole spheroid diameter. Thereby it could be shown that the necrotic core diameter was significantly increased in both HCT116 and NCI-H460 MCTSs, after treatment with NS-398. In stimulated NCI-H460 MCTSs it was around one third larger than in control spheroids while in treated HCT116 MCTSs it had even twice the size than in the unstimulated spheroids (Figure 56A/C). In comparison, celecoxib seemed not to influence the size of the necrotic core which was confirmed by measuring the necrotic core diameter (Figure 56B).

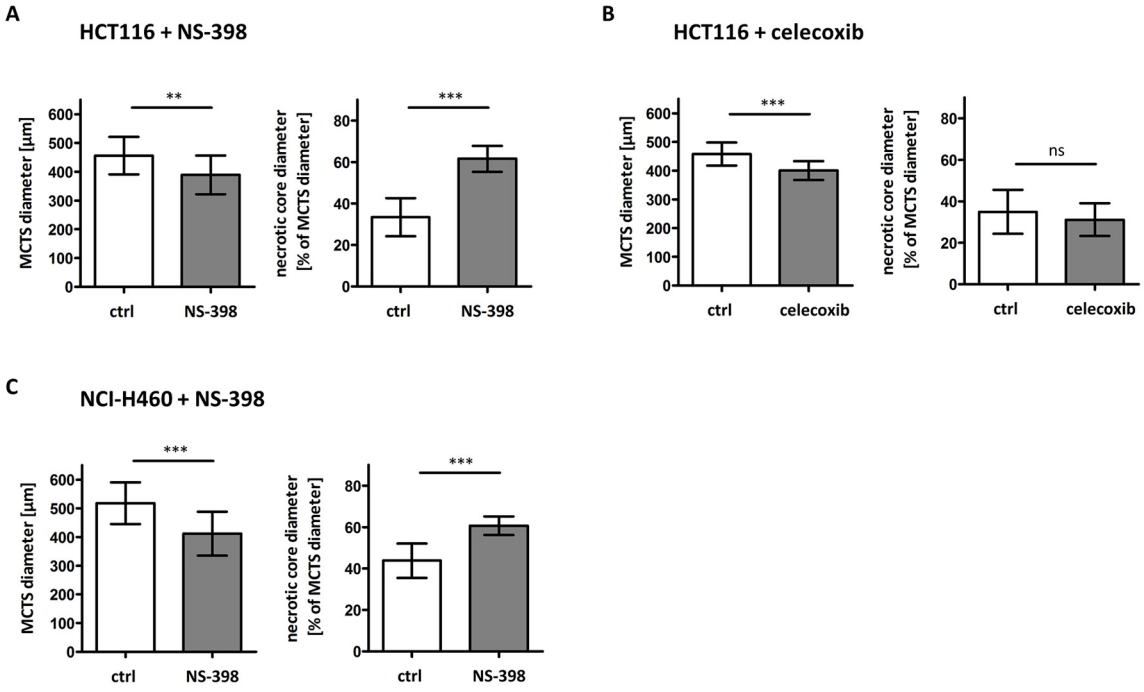

Figure 56: Treatment with NS-398 increases the necrotic core within MCTSs

HCT116 and NCI-H460 MCTSs (day 11) were stimulated for 72 h with 200 µM NS-398 or 50 µM celecoxib. Thereafter, MCTSs were embedded in paraffin and cut into 3 µm slices. Middle sections of MCTSs were analysed for their total diameter and diameter of the necrotic core. Shown are mean values ± SD of in total ten to thirty MCTSs out of three independent experiments. Asterisks indicate statistical significance (** = $p \leq 0.01$, *** = $p \leq 0.001$, ns = not significant; unpaired t-test). Analysis was done together with Tobias Beigl **(A/B/C)**.

6.6. Treatment with COX II inhibitors increases TRAILR1 amounts in innermost spheroid-forming cells and conversely decreases expression in the outermost cells layer of MCTSs

Beside TK1, spheroid sections were also stained for TRAILR1 and TRAILR2. To evaluate the respective TRAILR expression within distinct spheroids sections, the area covered with cells was divided into six different layers and the percentage of cells with no, low, medium and high TRAILR expression was determined with the software Definiens Tissue Studio 64 software and Photoshop Elements 10. Of note, in case of treatment with NS-398, the innermost three spheroid layers were lost due to enhanced death of central cells. Experiments revealed that celecoxib and NS-398 slightly decreased TRAILR1 expression in the outermost cell layers of HCT116 and NCI-H460 MCTSs (Figure 57; Figure 58). Conversely treatment with both COX II inhibitors increased to a certain extent TRAILR1 expression in spheroid-forming HCT116 cells close to the necrotic core (Figure 57; Figure 58B/C).

Interestingly, this effect was not observable in NS-398 incubated NCI-H460 MCTSs (Figure 57; Figure 58E). In summary, treatment with NS-398 and celecoxib did not change the overall proportion of cells with no, low, medium and high TRAILR1 expression within HCT116 and NCI-H460 MCTSs but altered in the case of 3D-cultured HCT116 cells the distribution of those cells in the different spheroid layers (Figure 57; Figure 58).

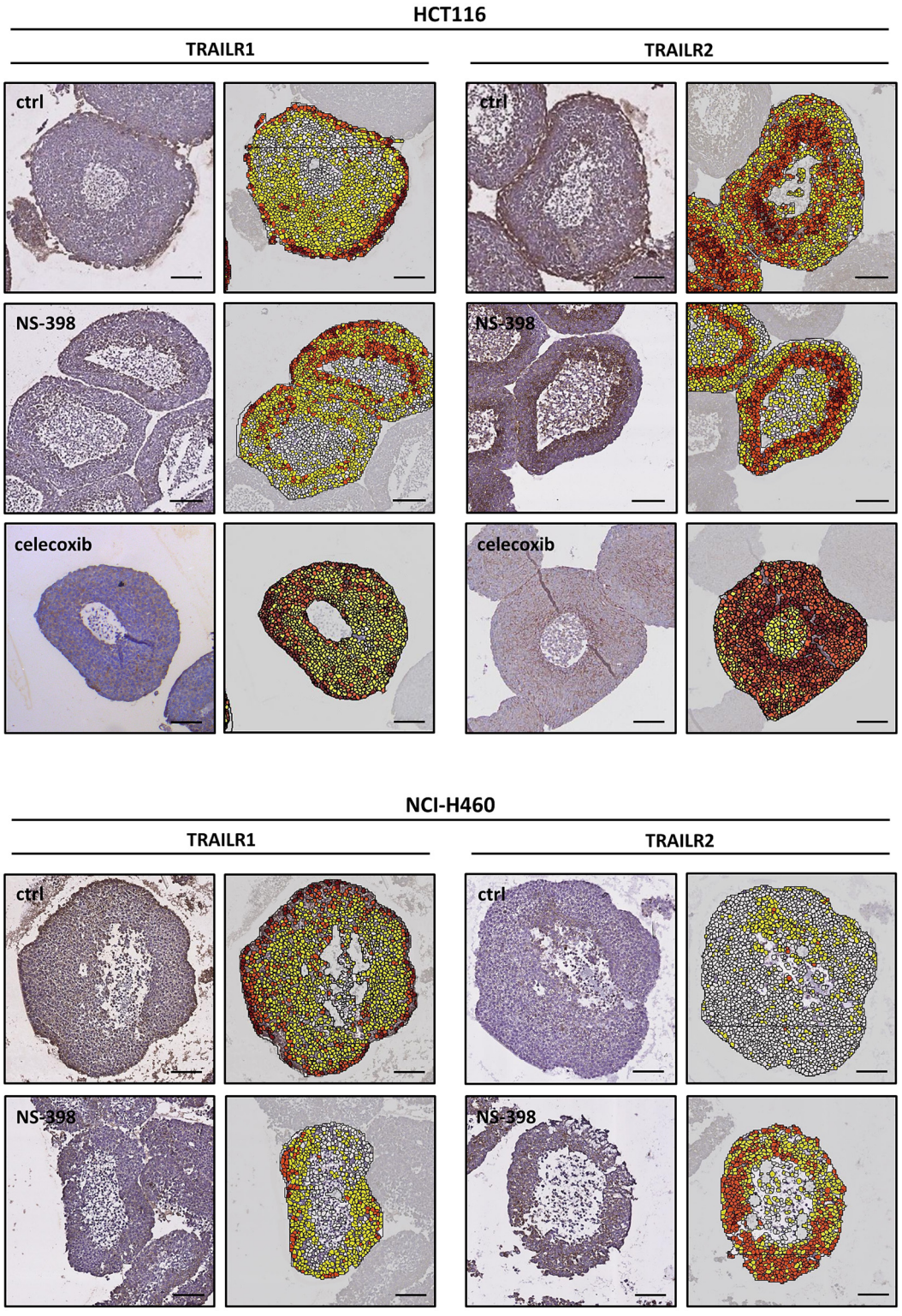
HCT116
TRAILR1
TRAILR2
ctrl
ctrl
NS-398
NS-398
celecoxib
celecoxib
NCI-H460
TRAILR1
TRAILR2
ctrl
ctrl
NS-398
NS-398

Figure 57: Localisation-dependent TRAILR expression pattern in MCTSs after stimulation with COX II inhibitors.

HCT116 and NCI-H460 MCTSs (day 11) were stimulated for 72 h with 200 µM NS-398 or 50 µM celecoxib. Thereafter, MCTSs were embedded in paraffin and cut into 3 µm slices. Spheroid sections were immunohistochemically stained for either TRAILR1 or TRAILR2 and counterstained with haematoxylin to visualise cell nuclei. Then, the software Definiens Tissue Studio 64 was used to identify cells with no (white), low (yellow), medium (orange) and high (red) TRAILR expression. Pictures are representative of three independent experiments. Scale bars in all images = 100 µm. Staining and analysis via the software was done together with Tobias Beigl.

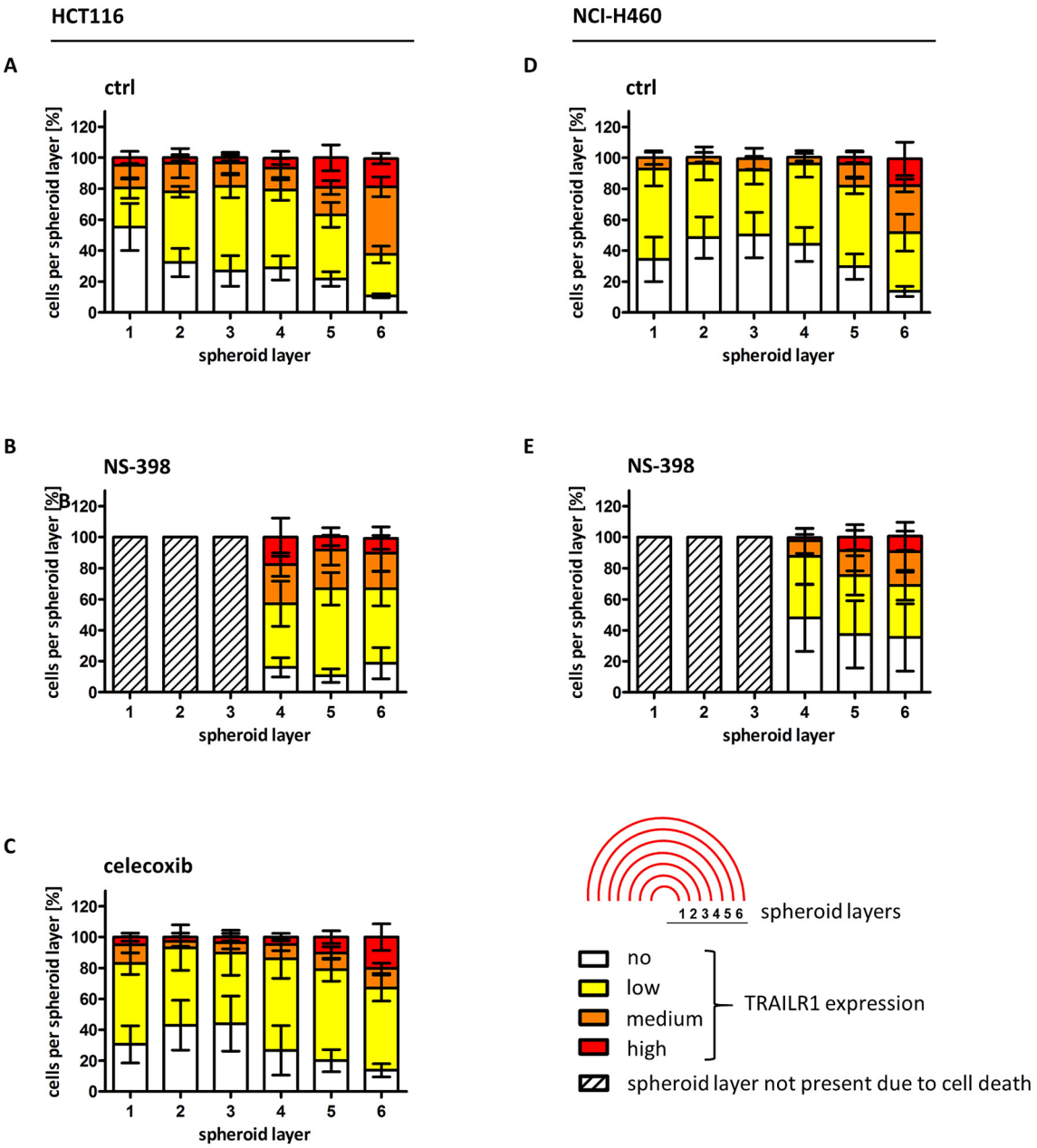

Figure 58: Treatment with COX II inhibitors changes the proportion of cells with different TRAILR1 expression in distinct spheroid layers

After image analysis with the Definiens Tissue Studio 64 software, spheroid sections were subdivided into six, respectively three different layers and the percentage of cells with no, low, medium and high TRAILR1 expression was determined using Photoshop Elements 10. Shown are mean values ± SEM of in total three to six MCTSs out of two to three independent experiments.

6.7. COX II inhibitors increase TRAILR2 expression in all spheroid layers

In comparison to TRAILR1, treatment with the two COX II inhibitors not only changed the proportion of cells with different TRAILR2 expression in distinct spheroid layers, but also altered the overall expression of TRAILR2 in HCT116 and NCI-H460 MCTSs (Figure 57; Figure 59). Treatment with NS-398 drastically increased the expression of the receptor in every layer of NCI-H460 MCTSs. Around 70% of all cells within each of the three cell layers expressed either medium or high amounts of TRAILR2. In comparison to that, in untreated NCI-H460 MCTSs only the innermost cell layer contained around 8% cells with medium TRAILR2 expression and about 90% cells with no or low expression of the receptor. Further to the outside of the spheroids, the percentage of cells completely devoid of TRAILR2 even increased (Figure 57; Figure 59D/E). In HCT116 MCTSs treatment with NS-398 also increased TRAILR2 expression in the 4^{th} and 5^{th} layer but interestingly not in the outermost cell layer (Figure 57; Figure 59B). Furthermore, incubation with celecoxib strongly increased the percentage of cells with high and medium TRAILR expression in each of the different spheroid layers in HCT116 MCTSs. More precisely, in treated HCT116 MCTSs only the outermost spheroid layer contained around 10% of cells completely devoid of TRAILR2 while in untreated spheroids every spheroid layer was comprised of up to 40% cells without expression of the receptor (Figure 57; Figure 59C).

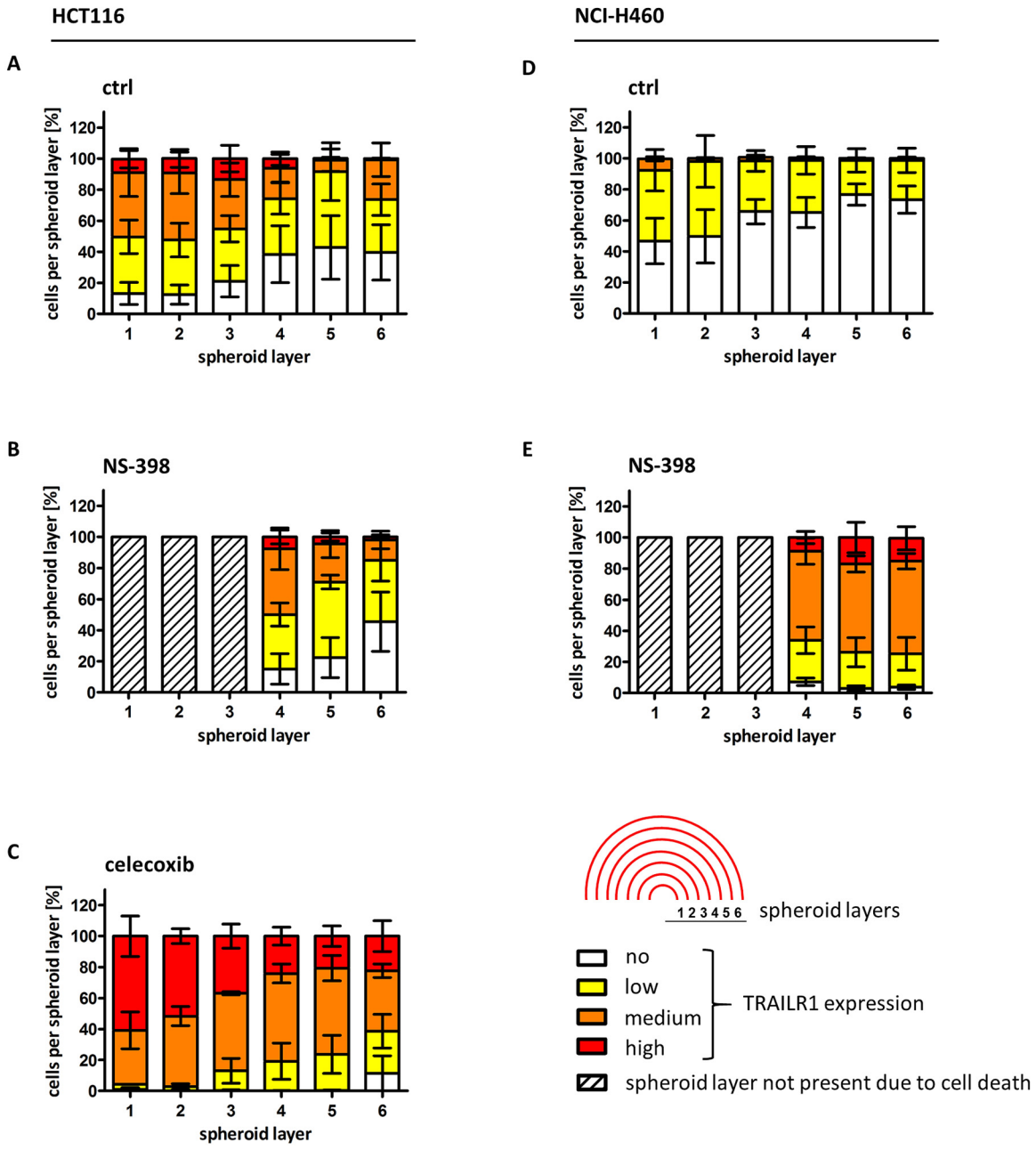

Figure 59: **Enhanced TRAILR2 expression in MCTSs after treatment with COX II inhibitors**

After image analysis with the Definiens Tissue Studio 64 software, spheroid sections were subdivided into six or three different layers and the percentage of cells with no, low, medium and high TRAILR2 expression was determined using Photoshop Elements 10. Shown are mean values ± SEM of in total three to five MCTSs out of two to three independent experiments. Analysis via the software was done together with Tobias Beigl.

6.8. Celecoxib does not change the expression of further apoptosis-relevant proteins within MCTS-forming HCT116 cells

Finally, it was investigated whether the treatment with COX II inhibitors not only changes the expression of TRAILR2 within MCTS-forming cells, but also the amounts of other apoptosis-relevant proteins further downstream of the receptors. For that, total cell lysates of HCT116 MCTSs treated with celecoxib were compared to lysates of untreated spheroids for the expression of FADD, cFlip, procaspase 8, XIAP, Mcl-1, Bcl-xl and survivin by western blotting. Thereby it could be shown that after stimulation with the COX II inhibitor celecoxib the amounts of all these proteins remained the same within MCTS-forming HCT116 cells (Figure 60).

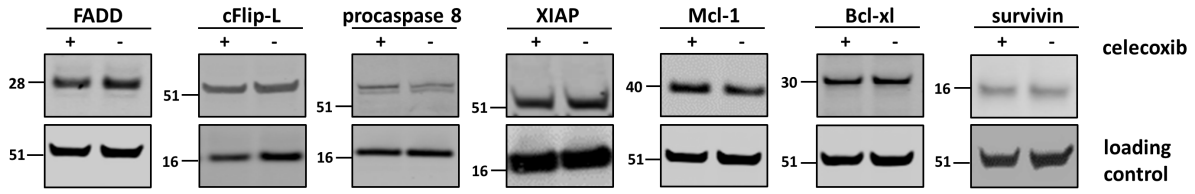

Figure 60: Expression of different apoptosis-relevant proteins in HCT116 MCTSs after treatment with celecoxib

HCT116 MCTSs (day 11) were stimulated for 72 h with 50 µM celecoxib. Thereafter, lysates of stimulated or unstimulated MCTSs were analysed by western blotting using the indicated antibodies. Blots shown are representative of two to three independently performed experiments. Loading control: FADD, Mcl-1, Bcl-xl, survivin = α-tubulin; cFlip-L, procaspase 8, XIAP = COX IV.

6.9. Discussion

In chapter 4 it was shown that treatment of 3D-cultured HCT116 and NCI-H460 cells with two different COX II inhibitors led to a reduction of MCTSs growth and upregulation of TRAILR2 in spheroid-forming cells. Furthermore, both inhibitors were shown to sensitise HCT116 and NCI-H460 MCTSs to TRAIL. This was most likely due to their capability to enhance TRAILR2 expression within all spheroid layers.

As mentioned previously, the enzyme COX catalyses the conversion of arachidonic acid to prostaglandin H_2 which in turn can be converted to various other prostaglandins by specific prostaglandin synthases. The first isoform, COX I, is constitutively active in most tissues and ensures the maintenance of cellular processes such as the cytoprotection of gastric mucosa and platelet aggregation in response to injury. In contrast to that, the expression of the second isoform, COX II, is induced by various growth factors and cytokines during inflammation (reviewed by Sobolewski et al., 2010; reviewed by Patrignani and Patrono, 2015). Interestingly, COX II amounts were also found to be increased in many tumours of epithelial origin such as colon, lung, breast and prostate correlating with a poor prognosis due to enhanced proliferation, vascularisation, invasion and metastasis (Brown and DuBois, 2005; Gupta et al., 2000; Soslow et al., 2000). Alongside the global change during the development of cancer, COX II expression was also shown to be regulated by the tumour microenvironment. More precisely, during hypoxia the expression of the enzyme was enhanced, mediated by binding of Hif-1α to the promoter region of the COX II gene (Kaidi et al., 2006). Since in this work and also in literature it was shown, that culturing cells in 3D increased COX II amounts, it might be speculated that expression of the enzyme is induced in oxygen-deprived cells close to the spheroid centre (Chandrasekaran et al., 2014; Salmenperä et al., 2008). Of note, it was also shown by Sha and colleagues that central necrotic cells stimulated the expression of COX II in prostate cancer spheroids (Sha et al., 2013). To investigate a potential localisation-dependent COX II expression within MCTSs, spheroid sections could be immunohistochemically stained for the protein and/or oxygen-deprived 2D-cultured cells might be investigated for increased expression of the enzyme. Alongside its positive effects on tumour progression, high amounts of COX II were also observed to correlate with TRAIL resistance due to a downregulation of TRAILR1 and TRAILR2 which could be reversed by knockdown of the enzyme or treatment with COX II inhibitors (Chandrasekaran et al., 2014; Tang et al., 2002). However, the underlying mechanism for this observation has yet to be investigated. Indeed in this study, incubation of HCT116 and NCI-H460 MCTSs with two different COX II inhibitors, celecoxib and NS-398, also increased TRAILR2 expression in all spheroid-layers suggesting that low TRAILR2 expression in

intermediate cell layers might be attributed to an upregulation of the enzyme. However, the observation that treatment with both inhibitors also enhanced TRAILR2 expression in the completely COX II devoid cell line HCT116, points to an additional, COX II-independent mechanism of receptor upregulation as described in literature. It was shown that agents, such as celecoxib, can block the sarco/endoplasmic reticulum Ca^{2+} APTase (SERCA) which in turn leads to a rapid increase of intracellular Ca^{2+} and subsequent induction of ER-stress as well as activation of the UPR (Johnson et al., 2002; Pyrko et al., 2007). As mentioned previously UPR-related transcription factors CHOP and ATFR3 were shown to bind to the promotor of TRAILR2 and induce its expression (Edagawa et al., 2014). Furthermore, Oh and colleagues also demonstrated celecoxib-induced activation of ERK/ribosomal protein S6 kinase (RSK) signalling in colorectal cancer cell lines, leading to activation of ELK-1 which was shown to, in combination with CHOP, enhance TRAILR2 expression (Oh et al., 2010). Since increased expression of UPR-related proteins was detected in 3D-cultivated HCT116 and NCI-H460 after treatment with COX II inhibitors, the previously described mechanism of TRAILR2 upregulation is conceivable in these cell lines. In comparison to TRAILR2, both COX II inhibitors did not enhance the overall surface expression of TRAILR1 in 3D-cultivated HCT116 and NCI-H460. However, spheroid sections revealed that celecoxib and NS-398 decreased TRAILR1 expression in the outermost spheroid layer in HCT116 and NCI-H460 MCTSs while at least in HCT116 spheroids, both inhibitors conversely increased the expression of the receptor in cells close to the necrotic centre. Indeed, it was already shown in the literature that celecoxib and NS-398 are not only able to upregulate the expression of TRAILR2 but also of TRAILR1 in different human cancer cell lines (Chandrasekaran et al., 2014; Kern et al., 2006; Liu et al., 2004; Yamanaka et al., 2006). As it was furthermore demonstrated that TRAILR1 can be upregulated in response to ER stress, it might be speculated that celecoxib and NS-398 enhance the receptors' expression via an induction of ER-stress induced UPR (Iurlaro et al., 2017; Iurlaro and Muñoz-Pinedo, 2016; Li et al., 2015). The observation made in this thesis that TRAILR1 is downregulated in the outermost spheroid layer might be due to the inhibitors' capacity to impede cell cycle progression. As it was already shown that the expression of TRAILR1 is solely high in proliferative cells, the inhibitors' capacity to upregulate the receptor via the induction of ER stress might be overrun by the mechanism that downregulates TRAILR1 amounts in non-cycling cells. To investigate the underlying regulation of TRAILR expression in more detail, MCTSs might be pre-treated with inhibitors of the UPR before stimulating them with celecoxib or NS-398 (reviewed by Schönthal, 2012; Tomasio et al., 2013).

Further experiments indeed demonstrated that treatment of HCT116 and NCI-H460 MCTSs with both COX II inhibitors decelerated spheroid growth and reduced the number of cells

positive for the proliferation marker TK1 which is in accordance with many studies that showed reduced proliferation of various human cancer cell lines after treatment with celecoxib or NS-398. As an underlying mechanism it was suggested that inhibition of COX II can reduce the amount of enzymatically generated prostaglandin E_2, a molecule that is known to increase the proliferation in different tumour cell lines (Castellone and Teramoto, 2005; Yu et al., 2009). However, the fact that derivatives of COX II inhibitors, lacking the binding site for the enzyme, retained their anti-proliferative capacity, led to the discovery of COX II-independent mechanisms in which treatment with the inhibitors leads to an inhibition of proliferation due to changes in the expression of proteins relevant for cell cycle progression. Many studies for example showed that COX II-independent arrest in G_0/G_1 after treatment with celecoxib was mediated by a downregulation of the transcription factor c-myc that was accompanied in a lot of cases with simultaneous downregulation of many cell cycle related proteins such as cyclin A/B1/D1 and upregulation of the cell cycle inhibitors p27 and p21 (Grösch et al., 2001; Sobolewski et al., 2010, 2015). NS-398 was also demonstrated to induce cell cycle arrest in G_0/G_1, partly independent of COX II, however exact underlying mechanisms have yet to be investigated (Nakanishi et al., 2001; Smith et al., 2000). Furthermore, during other studies with celecoxib, arrest in G_2 or G_2/M was also observed which was suggested to be regulated either by changes in the expression of cell cycle-related proteins or by downregulation of key players in the kinetochore/centromere complex as well as inhibition of prostaglandin E_1 receptor (EP1) signalling (Bieniek et al., 2014; Gallouet et al., 2014; Zhang et al., 2007). Interestingly, Young-Mee and colleagues showed that in HCT116 cells, the type of cell cycle arrest was dependent on the applied celecoxib concentration. A high concentration, as was used in the present thesis, arrested the cells In G_2/M phase of the cell cycle while lower concentrations led to a halt in G_1/G_0 (Young-Mee et al., 2013). To investigate the cell cycle status of MCTS-forming cells after treatment with celecoxib and NS-398, spheroids could be dissociated and cells could be analysed for their RNA and DNA content.

Of note, experiments with MCTSs also revealed an enlargement of the necrotic core after incubation with NS-398 but not with celecoxib. The discrepancy between this observation and the result that no increased cell death could be detected after stimulation of MCTSs with NS-398 by flow cytometric analysis might be most likely attributed to the higher concentration of NS-398 used for the preparation of the spheroid cryosections. Furthermore, it is also conceivable that after 72 h treatment, cells which died from the stimulation with NS-398, were no longer detectable by flow cytometry due to their advanced disintegration. It is well described in literature that both celecoxib and NS-398 can, concentration-dependently, induce apoptosis in colorectal and lung cancer cell lines (Grösch et al., 2001;

Liu et al., 2004; Smartt et al., 2003). However, even though it has been shown that apoptosis after incubation with NS-398 was often accompanied with a downregulation of survivin and upregulation of caspase 3, the underlying signalling cascade has yet to be elucidated (Li et al., 2011; Qiu et al., 2012). The observation of a larger necrotic core after treatment with NS-398 suggests that cells with initial high TRAILR2 expression were highly susceptible to NS-398 induced cell death. Furthermore, the fact that the increase of the necrotic core was also detectable in COX II devoid HCT116 MCTSs points to an COX II-independent mechanism of sensitisation. Indeed, it was already shown by different groups that persistent ER stress and activation of the UPR, as may be induced by COX II inhibitors, resulted in an upregulation of TRAILR2 and subsequent ligand-independent apoptosis. (Cano-González et al., 2018; Liu et al., 2004; Martín-Pérez et al., 2012; Yamaguchi and Wang, 2004). More precisely, in HCT116 cells it was shown that intracellular TRAILR2 can form together with FADD a platform in which caspase-8 gets activated, resulting in apoptotic cell death (Lu et al., 2014). To investigate whether ligand-independent cell death was actually initiated in MCTSs after treatment with NS-398, spheroids could be pre-treated with inhibitors of the UPR and thereafter analysed for the size of the necrotic core. Furthermore, MCTSs stimulated with NS-398 might also be investigated at slightly earlier time points for cleaved caspase 3 and pre-treated with QVD to investigate whether observed cell death is apoptotic. However, the fact that incubation with celecoxib did not result in an increased necrotic core, even though it also strongly enhanced TRAILR2 expression, indicates that high TRAILR2 alone is not sufficient to explain cell death in cells close to the necrotic core after stimulation with NS-398.

Since it was shown in this work that celecoxib and NS-398 enhanced TRAILR2 expression in all spheroid layers it was lastly investigated whether HCT116 and NCI-H460 MCTSs could be sensitised to TRAIL-induced apoptosis by treatment with the two COX II inhibitors. Thereby, it was shown that both drugs acted synergistically with TRAIL in inducing cell death in spheroids generated from both cell lines. The result that 3D-cultured HCT116 T2 KO cells could not be sensitised to TRAIL by treatment with celecoxib points to TRAILR2 upregulation as reason for the observed sensitisation to TRAIL (appendix: Figure 62). However, due to the localisation-dependent expression of TRAILR1, most cells in MCTSs lacked any form of the apoptosis-inducing receptors when TRAILR2 was knocked out, thus the contribution of a protein downstream of the TRAILRs in the sensitisation process, even if existing, would not have been detectable. To verify the importance of TRAILR2 upregulation in this scenario, the participation of other apoptosis-relevant proteins has first to be ruled out. At least for HCT116 cells treated with celecoxib a contribution of survivin, cFlip, Mcl-1, XIAP and Bcl-xl,

all proteins that were shown to be regulated by COX II inhibitors, can most likely be excluded (Gallouet et al., 2014; Liu et al., 2006; Yamanaka et al., 2006). Interestingly it was already

demonstrated by Chen and colleagues that NCI-H460 cells could be sensitised to TRAIL treatment by 2,5-dimethyl-celecoxib (celecoxib analogue without the capability to inhibit COX II) due to an upregulation of TRAILR2 together with a downregulation of cFlip, suggesting a COX II-independent mechanism (Chen et al., 2007). In other NSCLC cell lines, it was shown that upregulation of TRAILR2 by celecoxib was sufficient to enhance the cells' sensitivity to TRAIL (Liu et al., 2004). Furthermore, experiments with HCT116 p53 $^{-/-}$ cells demonstrated that celecoxib sensitised the colorectal cancer cells to TRAIL by upregulating TRAILR2 (Edagawa et al., 2014). Since results obtained in this work with the COX II devoid cell line HCT116 as well as observations made in the literature suggest that celecoxib and NS-398 sensitise cells to TRAIL mostly without a participation of COX II, slightly different working mechanisms of both drugs are to be expected.

Taken together, results of this work as well as other studies suggest that COX II inhibitors are able to induce apoptosis in cancer cells by itself and sensitise TRAIL-resistant cells to TRAIL-induced apoptosis. The fact that in most *in vitro* studies, similarly to in this thesis, applied concentrations of celecoxib were much higher than the maximal reached concentration in human plasma, might raise the concern that results obtained from *in vitro* experiments are irrelevant *in vivo*. However, it was already shown that celecoxib exerted the same effects in mouse tumour models and human tumour xenograft models as *in vitro*, when it was applied in lower concentrations but for a longer time period (Basu et al., 2004; Narayanan et al., 2004; Patel et al., 2007; Pyrko et al., 2006). This could be attributed to the capability of celecoxib to accumulate in plasma membranes resulting in high local concentrations that are sufficient to induce apoptosis even though the plasma concentration of the drug is relatively low (Maier et al., 2009). Alongside its ability to reduce tumour burden by inducing cell death, COX II inhibitors are also known to inhibit neovascularisation and the phoenix rising pathway, where cells dying by apoptosis induce bystander cells to proliferate (Li et al., 2010). Thus, celecoxib has been investigated and is currently undergoing further testing as a single or combination treatment against different cancer types in various clinical trials (DrugLib.com, 2006; National Cancer Institute).

5 Summary and conclusion

In this work, in agreement with data from literature it was demonstrated that culturing cancer cells as MCTSs can significantly alter their cell cycle status. Similar to solid tumours within the human body, gradients of oxygen, nutrients as well as waste products established in larger spheroids and resulted in the development of a zonation. Close to the spheroid surface, supply with nutrients and oxygen was sufficient to allow cell proliferation while further inside, cells first entered a quiescent state and finally underwent cell death. Thus, this study verifies the superiority of 3D cell culture over 2D cell culture regarding the recapitulation of a solid tumour *in vitro*. Already for quite a long time, TRAIL has been investigated for its potential as an anti-cancer agent, however only with limited success. Alongside issues with the generated TRAILR agonist, this failure can also be attributed to many tumour types being initially TRAIL-resistant. In this study, MCTSs were stimulated with 2nd generation TRAILR agonists to investigate emerging resistance mechanisms. Interestingly, it was thereby found that MCTS-forming cells were highly heterogenous in their susceptibility to TRAIL. While several cells appeared to be resistant against the investigated TRAILR agonists, some cells showed even enhanced susceptibility compared to stimulated 2D cell cultures. For the first time, it was demonstrated that the observed heterogenous TRAIL susceptibility is most likely a result of heterogenous TRAILR expression of MCTS-forming cells. It was found that solely proliferative cells displayed high amounts of TRAILR1 while in quiescent cells TRAILR1 expression was largely reduced or completely absent. Furthermore, TRAILR2 expression was highest in cells at the spheroid surface but additionally also in cells close to the necrotic core. Interestingly, in these quiescent cells, most TRAILR2 was localised intracellularly. The observation that the TRAIL-hypersensitive subpopulation was only visible when MCTSs were dissociated prior to stimulation suggested that within undissociated spheroids, TRAIL-hypersensitive cells close to the centre were protected by a ring of TRAIL-resistant cells with low TRAILR1/2 expression. Furthermore, the fact that the TRAIL-hypersensitive cell population was not to be found anymore after knockout of TRAILR2 points strongly to large amounts of intracellular TRAILR2 sensitising cells to TRAIL-induced apoptosis. It might be hypothesised that ligand-independent aggregation of TRAILR2 already results in weak procaspase 8 processing that adds to the activation of the procaspase after binding of TRAIL to surface TRAILRs. Furthermore, it is also conceivable that pre-aggregated TRAILR2 forms a platform in which TRAIL, derived from endocytosed TRAIL-TRAILR complexes, can activate procaspase 8. Regarding causative factors for the observed heterogenous TRAILR expression, experiments with 2D-cultured cells suggested a contribution of hypoxia and/or nutrient starvation as both conditions were

shown to alter TRAILR amounts. As MCTSs resemble in their zonation of proliferative and quiescent cells closely the structure of solid tumours, it will be of major interest to investigate whether the same localisation-dependent TRAILR expression is present *in vivo* and represents one of the mechanisms of TRAIL resistance observed in clinical studies. If this is the case it will be of great importance in the future to combine TRAILR agonists with other compounds that can reverse TRAILR expression. In this study it was already shown *in vitro* that application of COX II inhibitors sensitised MCTSs to TRAIL-induced apoptosis most likely by upregulation of TRAILR2. Taken together, the conducted study emphasises once again the importance of 3D cell culture as an *in vitro* model system. Furthermore, obtained results may explain to some extent the failure of TRAILR agonists in clinical trials.

6 Bibliography

Aggarwal, B.B., Gupta, S.C. and Kim, J.H. (2012), "Historical perspectives on tumor necrosis factor and its superfamily: 25 years later, a golden journey", *Blood*, Vol. 119 No. 3, pp. 651–665.

Aggarwal, B.B., Kohr, W.J., Hass, P.E., Moffat, B., Spencer, S.A., Henzel, W.J., Bringman, T.S., et al. (1985), "Human tumor necrosis factor. Production, purification, and characterization.", *The Journal of Biological Chemistry*, Vol. 260 No. 4, pp. 2345–54.

Ahmed, D., Eide, P.W., Eilertsen, I.A., Danielsen, S.A., Eknæs, M., Hektoen, M., Lind, G.E., et al. (2013), "Epigenetic and genetic features of 24 colon cancer cell lines", *Oncogenesis*, Vol. 2 No. 424, available at:https://doi.org/10.1038/oncsis.2013.35.

Alberts, B., Johnson, A., Lewis, J., Raff, M., Roberts, K. and Walter, P. (2002), *Molecular Biology of the Cell*, 4th ed., Garland Science.

Altieri, D.C. (2015), "Survivin - The inconvenient IAP", *Seminars in Cell and Developmental Biology*, Elsevier Ltd, Vol. 39, pp. 91–96.

Arandjelovic, S. and Ravichandran, K.S. (2015), "Phagocytosis of apoptotic cells in homeostasis", *Nat Immunol*, Vol. 16 No. 9, pp. 907–917.

Asghar, U., Witkiewicz, A.K., Turner, N.C. and Knudsen, E.S. (2015), "The history and future of targeting cyclin-dependent kinases in cancer therapy", *Nature Reviews Drug Discovery*, Nature Publishing Group, Vol. 14 No. 2, pp. 130–146.

Aubrey, B.J., Kelly, G.L., Janic, A., Herold, M.J. and Strasser, A. (2017), "How does p53 induce apoptosis and how does this relate to p53-mediated tumour suppression?", *Cell Death and Differentiation*, Nature Publishing Group, pp. 1–10.

Bae, S.I., Cheriyath, V., Jacobs, B.S., Reu, F.J. and Borden, E.C. (2008), "Reversal of methylation silencing of Apo2L/TRAIL receptor 1 (DR4) expression overcomes resistance of SK-MEL-3 and SK-MEL-28 melanoma cells to interferons (IFNs) or Apo2L/TRAIL", *Oncogene*, Vol. 27 No. 4, pp. 490–498.

Baek, J.Y., Hur, W., Wang, J.S., Bae, S.H. and Yoon, S.K. (2007), "Selective COX-2 inhibitor, NS-398, suppresses cellular proliferation in human hepatocellular carcinoma cell lines via cell cycle arrest", *World Journal of Gastroenterology*, Vol. 13 No. 8, pp. 1175–1181.

Baisch, H. (1988), "Different quiescence states of three culture cell lines detected by acridine orange staining of cellular RNA", *Cytometry*, Vol. 9 No. 4, pp. 325–331.

Barbone, D., Yang, T.M., Morgan, J.R., Gaudino, G. and Broaddus, V.C. (2008), "Mammalian target of rapamycin contributes to the acquired apoptotic resistance of human mesothelioma multicellular spheroids", *Journal of Biological Chemistry*, Vol. 283 No. 19, pp. 13021–13030.

Baritaki, S., Huerta-Yepez, S., Sakai, T., Spandidos, D.A. and Bonavida, B. (2007), "Chemotherapeutic drugs sensitize cancer cells to TRAIL-mediated apoptosis: up-regulation of DR5 and inhibition of Yin Yang 1", *Molecular Cancer Therapeutics*, Vol. 6 No. 4, pp. 1387–1399.

Basu, G.D., Pathangey, L.B., Tinder, T.L., Lagioia, M. and Gendler, S.J. (2004), "Cyclooxygenase-2 Inhibitor Induces Apoptosis in Breast Cancer Cells in an In vivo Model of Spontaneous Metastatic Breast Cancer", *Molecular Cancer Research*, Vol. 2 No. November, pp. 632–643.

Baumeister, P., Luo, S., Skarnes, W.C., Sui, G., Seto, E., Shi, Y. and Lee, A.S. (2005), "Endoplasmic Reticulum Stress Induction of the Grp78 / BiP Promoter : Activating Mechanisms Mediated by YY1 and Its Interactive Chromatin Modifiers", *Molecular and Cellular Biology*, Vol. 25 No. 11, pp. 4529–4540.

Beaumont, K.A., Anfosso, A., Ahmed, F., Weninger, W. and Haass, N.K. (2015), "Imaging- and Flow Cytometry-based Analysis of Cell Position and the Cell Cycle in 3D Melanoma Spheroids", *Journal of Visualized Experiments*, No. 106, available at:https://doi.org/10.3791/53486.

Bento, C.F., Renna, M., Ghislat, G., Puri, C., Ashkenazi, A., Vicinanza, M., Menzies, F.M., et al. (2016), "Mammalian Autophagy: How Does It Work?", *Annual Review of Biochemistry*, Vol. 85 No. 1, pp. 685–713.

Berg, D., Lehne, M., Müller, N., Siegmund, D., Münkel, S., Sebald, W., Pfizenmaier, K., et al. (2007), "Enforced covalent trimerization increases the activity of the TNF ligand family members TRAIL and CD95L", *Cell Death and Differentiation*, Vol. 14 No. 12, pp. 2021–2034.

Bernard, D., Quatannens, B., Vandenbunder, B. and Abbadie, C. (2001), "Rel/NF-κB Transcription Factors Protect against Tumor Necrosis Factor (TNF)-related Apoptosis-inducing Ligand (TRAIL)-induced Apoptosis by Up-regulating the TRAIL Decoy Receptor DcR1", *Journal of Biological Chemistry*, Vol. 276 No. 29, pp. 27322–27328.

Bhise, N.S., Ribas, J., Manoharan, V., Zhang, Y.S., Polini, A., Massa, S., Dokmeci, M.R., et al. (2014), "Organ-on-a-chip platforms for studying drug delivery systems", *Journal of Controlled Release*, Elsevier B.V., Vol. 190, pp. 82–93.

Bieniek, J., Childress, C., Swatski, M.D. and Yang, W. (2014), "COX-2 inhibitors arrest prostate cancer cell cycle progression by down-regulation of kinetochore/centromere proteins", *Prostate*, Vol. 74 No. 10, pp. 999–1011.

Blanco, F.F., Jimbo, M., Wulfkuhle, J., Gallagher, I., Deng, J., Enyenihi, L., Meisner-Kober, N., et al. (2016), "The mRNA-binding protein HuR promotes hypoxia-induced chemoresistance through posttranscriptional regulation of the proto-oncogene PIM1 in pancreatic cancer cells", *Oncogene*, Nature Publishing Group, Vol. 35 No. 19, pp. 2529–2541.

Bodmer, J.L., Meier, P., Tschopp, J. and Schneider, P. (2000), "Cysteine 230 is essential for the structure and activity of the cytotoxic ligand TRAIL", *Journal of Biological Chemistry*, Vol. 275 No. 27, pp. 20632–20637.

Bodmer, J.L., Schneider, P. and Tschopp, J. (2002), "The molecular architecture of the TNF superfamily", *Trends in Biochemical Sciences*, Vol. 27 No. 1, pp. 19–26.

Bos, R., Van Diest, P.J., De Jong, J.S., Van Der Groep, P., Van Der Valk, P. and Van Der Wall, E. (2005), "Hypoxia-inducible factor-1α is associated with angiogenesis, and expression of bFGF, PDGF-BB, and EGFR in invasive breast cancer", *Histopathology*, Vol. 46 No. 1, pp. 31–36.

Bouralexis, S., Findlay, D.M., Atkins, G.J., Labrinidis, A., Hay, S. and Evdokiou, A. (2003), "Progressive resistance of BTK-143 osteosarcoma cells to Apo2L/TRAIL-induced apoptosis is mediated by acquisition of DcR2/TRAIL-R4 expression: Resensitisation with chemotherapy", *British Journal of Cancer*, Vol. 89 No. 1, pp. 206–214.

Boyle, W.J., Simonet, W.S. and Lacey, D.L. (2003), "Osteoclast differentiation and activation", *Nature*, Vol. 423 No. May, pp. 337–342.

Brown, J.R. and DuBois, R.N. (2005), "COX-2: A molecular target for colorectal cancer prevention", *Journal of Clinical Oncology*, Vol. 23 No. 12, pp. 2840–2855.

Brücher, B.L.D.M. and Jamall, I.S. (2014), "Cell-cell communication in the tumor microenvironment, carcinogenesis, and anticancer treatment", *Cellular Physiology and Biochemistry*, Vol. 34 No. 2, pp. 213–243.

Bullwinkel, J., Baron-Lühr, B., Lüdemann, A., Wohlenberg, C., Gerdes, J. and Scholzen, T. (2006), "Ki-67 protein is associated with ribosomal RNA transcription in quiescent and proliferating cells", *Journal of Cellular Physiology*, Vol. 206 No. 3, pp. 624–635.

Burkhart, R.A., Pineda, D.M., Chand, S.N., Romeo, C., Londin, E.R., Karoly, E.D., Cozzitorto, J.A., et al. (2013), "HuR is a post-transcriptional regulator of core metabolic enzymes in pancreatic cancer", *RNA Biology*, Vol. 10 No. 8, pp. 1312–1323.

Busato, F., Dejeux, E., El abdalaoui, H., Gut, I.G. and Tosr, J. (2018), *DNA Methylation Protocols (3rd Edition)*, *Methods in Molecular Biology*, Vol. 3rd editio, available at:https://doi.org/10.1385/1-59259-182-5:001.

von dem Bussche, A., MacHida, R., Li, K., Loevinsohn, G., Khander, A., Wang, J., Wakita, T., et al. (2010), "Hepatitis C virus NS2 protein triggers endoplasmic reticulum stress and suppresses its own viral replication", *Journal of Hepatology*, Vol. 53 No. 5, pp. 797–804.

Camidge, D.R., Herbst, R.S., Gordon, M.S., Eckhardt, S.G., Kurzrock, R., Durbin, B., Ing, J., et al. (2010), "A phase I safety and pharmacokinetic study of the death receptor 5 agonistic antibody PRO95780 in patients with advanced malignancies", *Clinical Cancer Research*, Vol. 16 No. 4, pp. 1256–1263.

Cano-González, A., Mauro-Lizcano, M., Iglesias-Serret, D., Gil, J. and López-Rivas, A. (2018), "Involvement of both caspase-8 and Noxa-activated pathways in endoplasmic reticulum stress-induced apoptosis in triple-negative breast tumor cells", *Cell Death & Disease*, Springer US, Vol. 9 No. 2, p. 134.

Cao, S. song and Zhen, Y. su. (1989), "Potentiation of antimetabolite antitumor activity in vivo by dipyridamole and amphotericin B", *Cancer Chemotherapy and Pharmacology*, Vol. 24 No. 3, pp. 181–186.

Carr, R.M., Qiao, G., Qin, J., Jayaraman, S., Prabhakar, B.S. and Maker, A. V. (2016), "Targeting the metabolic pathway of human colon cancer overcomes resistance to TRAIL-induced apoptosis", *Cell Death Discovery*, Nature Publishing Group, Vol. 2 No. June, p. 16067.

Carswell, E.A., Old, L.J., Kassel, R.L., Green, S., Fiore, N. and Williamson, B. (1975), "An endotoxin-induced serum factor that causes necrosis of tumors.", *Proceedings of the National Academy of Sciences*, Vol. 72 No. 9, pp. 3666–3670.

Castellone, M.D. and Teramoto, H. (2005), "Prostaglandin E 2 Promotes Colon Cancer Cell Growth Through a G s -Axin- b -Catenin Signaling Axis", No. December, pp. 1504–1511.

Chan, F.K.M. (2007), "Three is better than one: Pre-ligand receptor assembly in the regulation of TNF receptor signaling", *Cytokine*, Vol. 37 No. 2, pp. 101–107.

Chandrasekaran, S., Marshall, J.R., Messing, J.A., Hsu, J.-W. and King, M.R. (2014), "TRAIL-Mediated Apoptosis in Breast Cancer Cells Cultured as 3D Spheroids", *PLoS ONE*, Vol. 9 No. 10, p. e111487.

Chandrasekharan, N. and Simmons, D.L. (2004), "The cyclooxygenases", *Genome Biology*, Vol. 5 No. 9, p. 241.

Chen, D., Yu, J. and Zhang, L. (2016), "Necroptosis: An alternative cell death program defending against cancer", *Biochimica et Biophysica Acta - Reviews on Cancer*, Elsevier B.V., Vol. 1865 No. 2, pp. 228–236.

Chen, J.-J., Shen, H.-C.J., Rivera Rosado, L.A., Zhang, Y., Di, X. and Zhang, B. (2012), "Mislocalization of death receptors correlates with cellular resistance to their cognate ligands in human breast cancer cells.", *Oncotarget*, Vol. 3 No. 8, pp. 833–42.

Chen, Q., Ganapathy, S., Singh, K.P., Shankar, S. and Srivastava, R.K. (2010), "Resveratrol induces growth arrest and apoptosis through activation of FOXO transcription factors in prostate cancer cells", *PLoS ONE*, Vol. 5 No. 12, available at:https://doi.org/10.1371/journal.pone.0015288.

Chen, S., Liu, X., Yue, P. and Schönthal, A. (2007), "CCAAT/Enhancer Binding Protein Homologous Protein-Dependent Death Receptor 5 Induction and Ubiquitin/Proteasome-Mediated Cellular FLICE-Inhibitory Protein", *Mol Pharmacol*, Vol. 6, pp. 1269–1279.

Chen, W., Dong, J., Haiech, J., Kilhoffer, M.C. and Zeniou, M. (2016), "Cancer stem cell quiescence and plasticity as major challenges in cancer therapy", *Stem Cells International*, Hindawi Publishing Corporation, Vol. 2016, available at:https://doi.org/10.1155/2016/1740936.

Chen, X., Kandasamy, K., Srivastava, R.K. and Signaling, N.F.A.L. (2003), "Differential Roles of RelA (p65) and c-Rel Subunits of Nuclear Factor κ B in Tumor Necrosis Factor-related Apoptosis-inducing Ligand Signaling", pp. 1059–1066.

Choy, H. (2003), "Enhancing Radiotherapy With Cyclooxygenase-2 Enzyme Inhibitors: A Rational Advance?", *CancerSpectrum Knowledge Environment*, Vol. 95 No. 19, pp. 1440–1452.

Chua, S.-K., Shyu, K.-G., Lin, Y.-F., Lo, H.-M., Wang, B.-W., Chang, H. and Lien, L.-M. (2016), "Tumor Necrosis Factor-Alpha and the ERK Pathway Drive Chemerin Expression in Response to Hypoxia in Cultured Human Coronary Artery Endothelial Cells.", *PloS One*, Vol. 11 No. 10, p. e0165613.

Chung, S.S., Aroh, C. and Vadgama, J. V. (2013), "Constitutive activation of STAT3 signaling regulates hTERT and promotes stem cell-like traits in human breast cancer cells", *PLoS ONE*, Vol. 8 No. 12, available at:https://doi.org/10.1371/journal.pone.0083971.

Ciardiello, F. and Tortora, G. (2003), "Epidermal growth factor receptor (EGFR) as a target in cancer therapy: Understanding the role of receptor expression and other molecular determinants that could influence the response to anti-EGFR drugs", *European Journal of Cancer*, Vol. 39 No. 10, pp. 1348–1354.

Clancy, L., Mruk, K., Archer, K., Woelfel, M., Mongkolsapaya, J., Screaton, G., Lenardo, M.J., et al. (2005), "Preligand assembly domain-mediated ligand-independent association between TRAIL receptor 4 (TR4) and TR2 regulates TRAIL-induced apoptosis", *Proceedings of the National Academy of Sciences*, Vol. 102 No. 50, pp. 18099–18104.

Coe, H. and Michalak, M. (2009), "Calcium binding chaperones of the endoplasmic reticulum", *General Physiology and Biophysics*, Vol. 28, pp. 96–103.

Coley, W.B. (1891), "Contribution to the knowledge of sarcoma", *Annals of Surgery*, Vol. 14 No. 199, pp. 199–200.

Coller, H.A., Sang, L. and Roberts, J.M. (2006), "A new description of cellular quiescence", *PLoS Biology*, Vol. 4 No. 3, pp. 0329–0349.

Collison, A., Foster, P.S. and Mattes, J. (2009), "Emerging role of tumour necrosis factor-related apoptosis-inducing ligand (TRAIL) as a key regulator of inflammatory responses", *Clinical and Experimental Pharmacology and Physiology*, Vol. 36 No. 11, pp. 1049–1053.

Cooper, G.M. (2000), "The Cell: A Molecular Approach", 2nd ed., Sinauer Associates, available at: https://www.ncbi.nlm.nih.gov/books/NBK9876/.

Cowling, V., Downward, J. (2002), "Caspase-6 is the direct activator of caspase-8 in the cytochrome c-induced apoptosis pathway: absolute requirement for removal of caspase-6 prodomain", *Cell Death and Differentiation*, pp. 1946-1056

Creagh, E.M. (2014), "Caspase crosstalk: Integration of apoptotic and innate immune signalling pathways", *Trends in Immunology*, Elsevier Ltd, Vol. 35 No. 12, pp. 631–640.

Curcio, E., Salerno, S., Barbieri, G., De Bartolo, L., Drioli, E. and Bader, A. (2007), "Mass transfer and metabolic reactions in hepatocyte spheroids cultured in rotating wall gas-permeable membrane system", *Biomaterials*, Vol. 28 No. 36, pp. 5487–5497.

Curk, T., Dobnikar, J. and Frenkel, D. (2016), "Design principles for super selectivity using multivalent interactions", *Multivalency: Concepts, Research & Application*, Wiley, pp. 1–30.

Daignan-Fornier, B. and Sagot, I. (2011), "Proliferation/Quiescence: When to start? Where to stop? What to stock?", *Cell Division*, Vol. 6, pp. 1–5.

Danish, L., Stöhr, D., Scheurich, P. and Pollak, N. (2017), "TRAIL-R3/R4 and Inhibition of TRAIL Signalling in Cancer", *TRAIL, Fas Ligand, TNF and TLR3 in Cancer*, Springer International Publishing, pp. 27–59.

Davidovich, I.A., Levenson, A.S. and Levenson, V. V. (2004), "Overexpression of DcR1 and survivin in genetically modified cells with pleiotropic drug resistance", *Cancer Letters*, Vol. 211 No. 2, pp. 189–197.

Degli-Esposti, M.A., Smolak, P.J., Walczak, H., Waugh, J., Huang, C.-P., DuBose, R.F., Goodwin, R.G., et al. (1997), "Cloning and Characterization of TRAIL-R3, a Novel Member of the Emerging TRAIL Receptor Family", *The Journal of Experimental Medicine*, Vol. 186 No. 7, pp. 1165–1170.

Degli-Esposti, M. a, Dougall, W.C., Smolak, P.J., Waugh, J.Y., Smith, C. a and Goodwin, R.G. (1997), "The novel receptor TRAIL-R4 induces NF-kappaB and protects against TRAIL-mediated apoptosis, yet remains an incomplete death domain", *Immunity*, Vol. 7 No. 6, pp. 813–820.

Denault, J.-B., Eckelman, B.P., Shin, H., Pop, C. and Salvesen, G.S. (2007), "Caspase 3 attenuates XIAP (X-linked inhibitor of apoptosis protein)–mediated inhibition of caspase 9", *Biochemical Journal*, Vol. 405 No. 1, pp. 11–19.

Dickens, L.S., Boyd, R.S., Jukes-Jones, R., Hughes, M.A., Robinson, G.L., Fairall, L., Schwabe, J.W.R., et al. (2012), "A Death Effector Domain Chain DISC Model Reveals a Crucial Role for Caspase-8 Chain Assembly in Mediating Apoptotic Cell Death", *Molecular Cell*, Vol. 47 No. 2, pp. 291–305.

van Dijk, M., Halpin-McCormick, A., Sessler, T., Samali, A. and Szegezdi, E. (2013), "Resistance to TRAIL in non-transformed cells is due to multiple redundant pathways", *Cell Death and Disease*, Nature Publishing Group, Vol. 4 No. 7, pp. e702-11.

Drewinko, B., Yang, L.Y., Barlogie, B. and Trujillo, J.M. (1984), "Cultured Human Tumour Cells May Be Arrested In All Stages of the Cycle During Stationary Phase: Demonstration of Quiescent Cells In G1, S and G2Phase", *Cell Proliferation*, Vol. 17 No. 5, pp. 453–463.

DrugLib.com, (2006), "www.druglib.com/druginfo/celecbrex"

Edagawa, M., Kawauchi, J., Hirata, M., Goshima, H., Inoue, M., Okamoto, T., Murakami, A., et al. (2014), "Role of Activating Transcription Factor 3 (ATF3) in Endoplasmic Reticulum (ER) stress-induced sensitization of p53-deficient human colon cancer cells to Tumor Necrosis Factor (TNF)-related apoptosis-inducing ligand (TRAIL)-mediated apoptosis through up-reulation of death receptor 5 (DR5) by Zerumbone and Celecoxib", *Journal of Biological Chemistry*, Vol. 289 No. 31, pp. 21544–21561.

Elias, A., Siegelin, M.D., Steinmüller, A., Von Deimling, A., Lass, U., Korn, B. and Mueller, W. (2009), "Epigenetic silencing of death receptor 4 mediates tumor necrosis factor-related apoptosis-inducing ligand resistance in gliomas", *Clinical Cancer Research*, Vol. 15 No. 17, pp. 5457–5465.

Eliasson, P., Rehn, M., Hammar, P., Larsson, P., Sirenko, O., Flippin, L.A., Cammenga, J., et al. (2010), "Hypoxia mediates low cell-cycle activity and increases the proportion of long-term-reconstituting hematopoietic stem cells during in vitro culture", *Experimental Hematology*, Vol. 38 No. 4, pp. 301–310.

Elvidge, G.P., Glenny, L., Appelhoff, R.J., Ratcliffe, P.J., Ragoussis, J. and Gleadle, J.M. (2006), "Concordant regulation of gene expression by hypoxia and 2-oxoglutarate-dependent dioxygenase inhibition: The role of HIF-1α, HIF-2α, and other pathways", *Journal of Biological Chemistry*, Vol. 281 No. 22, pp. 15215–15226.

Emery, J.G., Mcdonnell, P., Burke, M.B., Deen, K.C., Lyn, S., Silverman, C., Dul, E., et al. (1998), "Osteoprotegerin Is a Receptor for the Cytotoxic Ligand TRAIL", *Journal of Biological Chemistry*, Vol. 273 No. 23, pp. 14363–14367.

Fang, Y. and Yeh, C. (2017), "Inhibition of miR-302 Suppresses Hypoxia-Reoxygenation-Induced H9c2 Cardiomyocyte Death by Regulating Mcl-1 Expression", *Oxidative Medicine and Cellular Longevity*, Vol. 2017.

Feoktistova, M., Geserick, P., Kellert, B., Dimitrova, D.P., Langlais, C., Hupe, M., Cain, K., et al. (2011), "CIAPs Block Ripoptosome Formation, a RIP1/Caspase-8 Containing Intracellular Cell Death Complex Differentially Regulated by cFLIP Isoforms", *Molecular Cell*, Vol. 43 No. 3, pp. 449–463.

Finlay, D., Teriete, P., Vamos, M., Cosford, N.D.P. and Vuori, K. (2017), "Inducing death in tumor cells: roles of the inhibitor of apoptosis proteins", *F1000Research*, Vol. 6, p. 587.

Fischer, U., Jänicke, R.U. and Schulze-Osthoff, K. (2003), "Many cuts to ruin: A comprehensive update of caspase substrates", *Cell Death and Differentiation*, Vol. 10 No. 1, pp. 76–100.

Florent, D., Thibault, R., Andrei Alexandru, C., Luciana, Z., Aymeric, M., Hazem, B.M., Etienne, H., et al. (2016), "TRAIL receptor gene editing unveils TRAIL-R1 as a master player of apoptosis induced by TRAIL and ER stres", *Oncotarget*, Vol. 8 No. 6, pp. 9974–9985.

Flusberg, D.A. and Sorger, P.K. (2015), "Surviving apoptosis: Life-death signaling in single cells", *Trends in Cell Biology*, Elsevier Ltd, Vol. 25 No. 8, pp. 446–458.

Forster, J.C., Harriss-Phillips, W.M., Douglass, M.J. and Bezak, E. (2017), "A review of the development of tumor vasculature and its effects on the tumor microenvironment.", *Hypoxia (Auckland, N.Z.)*, Vol. 5, pp. 21–32.

Freyer, J.P. (1988), "Role of Necrosis in Regulating the Growth Saturation of Multicellular Spheroids", *Cancer Research*, Vol. 48 No. 9, pp. 2432–2439.

Friedrich, J., Ebner, R. and Kunz-Schughart, L.A. (2007), "Experimental anti-tumor therapy in 3-D: Spheroids - Old hat or new challenge?", *International Journal of Radiation Biology*, Vol. 83 No. 11–12, pp. 849–871.

Fu, T.M., Li, Y., Lu, A., Li, Z., Vajjhala, P.R., Cruz, A.C., Srivastava, D.B., et al. (2016), "Cryo-EM Structure of Caspase-8 Tandem DED Filament Reveals Assembly and Regulation Mechanisms of the Death-Inducing Signaling Complex", *Molecular Cell*, Elsevier Inc., Vol. 64 No. 2, pp. 236–250.

Fu, Z. and Tindall, D.J. (2008), "FOXOs, cancer and regulation of apoptosis", *Oncogene*, Vol. 27 No. 16, pp. 2312–2319.

Gallouet, A.S., Travert, M., Bresson-Bepoldin, L., Guilloton, F., Pangault, C., Caulet-Maugendre, S., Lamy, T., et al. (2014), "COX-2-independent effects of celecoxib sensitize lymphoma B cells to TRAIL-mediated apoptosis", *Clinical Cancer Research*, Vol. 20 No. 10, pp. 2663–2673.

Ganten, T.M., Koschny, R., Sykora, J., Schulze-Bergkamen, H., Büchler, P., Haas, T.L., Schader, M.B., et al. (2006), "Preclinical differentiation between apparently safe and potentially hepatotoxic applications of TRAIL either alone or in combination with chemotherapeutic drugs", *Clinical Cancer Research*, Vol. 12 No. 8, pp. 2640–2646.

Gately, S. (2000), "The contributions of cyclooxygenase-2 to tumor angiogenesis", *Cancer and Metastasis Reviews*, Vol. 19 No. 1–2, pp. 19–27.

Gimbrone, M.A., Leapman, S.B., Cotran, R.S. and Folkman, J. (1972), "Tumor dormancy in vivo by prevention of neovascularization.", *The Journal of Experimental Medicine*, Vol. 136 No. 2, pp. 261–76.

Gobbi, G., Masselli, E., Micheloni, C., Nouvenne, A., Russo, D., Santi, P., Matteucci, A., et al. (2010), "Hypoxia-induced down-modulation of PKCε promotes TRAIL-mediated apoptosis of tumor cells", *International Journal of Oncology*, Vol. 37, pp. 719–729.

Gonnissen, A., Isebaert, S. and Haustermans, K. (2015), "Targeting the Hedgehog signaling pathway in cancer: beyond Smoothened", *Oncotarget*, Vol. 6 No. 16, pp. 13899–13913.

Grantab, R., Sivananthan, S. and Tannock, I.F. (2006), "The penetration of anticancer drugs through tumor tissue as a function of cellular adhesion and packing density of tumor cells", *Cancer Research*, Vol. 66 No. 2, pp. 1033–1039.

Green, D.R. (2011), *Means to an End: Apoptosis and Other Cell Death Mechanisms*, Cold Spring Harbor (N.Y.) : Cold Spring Harbor laboratory press.

Greenhough, A., Smartt, H.J.M., Moore, A.E., Roberts, H.R., Williams, A.C., Paraskeva, C. and Kaidi, A. (2009), "The COX-2/PGE2 pathway: key roles in the hallmarks of cancer and adaptation to the tumour microenvironment", *Carcinogenesis*, Vol. 30 No. 3, pp. 377–386.

Groebe, K. and Mueller-Klieser, W. (2004), "Distributions of oxygen, nutrient, and metabolic waste concentrations in multicellular spheroids and their dependence on spheroid parameters", *European Biophysics Journal*, Vol. 19 No. 4, pp. 169–181.

Grösch, S., Tegeder, I., Niederberger, E., Brautigam, L. and Geisslinger, G. (2001), "COX-2 independent induction of cell cycle arrest and apoptosis in colon cancer cells by the selective COX-2 inhibitor celecoxib", *Faseb J*, Vol. 15 No. 14, pp. 2742–2744.

Grosser et al. (2006), "Biological basis for the cardiovascular consequences of COX-2 inhibition: therapeutic challenges and opportunities", *Journal of Clinical Investigation*, Vol. 116 No. 1, pp. 4–15.

Gupta, S., Srivastava, M., Ahmad, N., Bostwick, D.G. and Mukhtar, H. (2000), "Over-expression of cyclooxygenase-2 in human prostate adenocarcinoma", *Prostate*, Vol. 42 No. 1, pp. 73–78.

Harding, H.P., Zhang, Y., Zeng, H., Novoa, I., Lu, P.D., Calfon, M., Sadri, N., et al. (2003), "An integrated stress response regulates amino acid metabolism and resistance to oxidative stress", *Molecular Cell*, Vol. 11 No. 3, pp. 619–633.

Harper, N., Farrow, S.N., Kaptein, A., Cohen, G.M. and MacFarlane, M. (2001), "Modulation of Tumor Necrosis Factor Apoptosis-inducing Ligand-induced NF-κB Activation by Inhibition of Apical Caspases", *Journal of Biological Chemistry*, Vol. 276 No. 37, pp. 34743–34752.

Harrison, L.R.E., Micha, D., Brandenburg, M., Simpson, K.L., Morrow, C.J., Denneny, O., Hodgkinson, C., et al. (2011), "Hypoxic human cancer cells are sensitized to BH-3 mimetic-induced apoptosis via downregulation of the Bcl-2 protein Mcl-1", *Journal of Clinical Investigation*, Vol. 121 No. 3, pp. 1075–1087.

Haselmann, V., Kurz, A., Bertsch, U., Hübner, S., Olempska-Müller, M., Fritsch, J., Häsler, R., et al. (2014), "Nuclear death receptor trail-r2 inhibits maturation of let-7 and promotes proliferation of pancreatic and other tumor cells", *Gastroenterology*, Elsevier, Inc, Vol. 146 No. 1, pp. 278–290.

He, B. (2006), "Viruses, endoplasmic reciculum stress, and interferon responses", *Cell Death and Differentiation*, pp. 393–403.

He, Q., Luo, X., Jin, W., Huang, Y., Reddy, M.V.R., Reddy, E.P. and Sheikh, M.S. (2008), "Celecoxib and a novel COX-2 inhibitor ON09310 upregulate death receptor 5 expression via GADD153/CHOP", *Oncogene*, Vol. 27 No. 18, pp. 2656–2660.

Heintz, N., Sive, H.L. and Roeder, R.G. (1983), "Regulation of human histone gene expression: kinetics of accumulation and changes in the rate of synthesis and in the half-lives of individual histone mRNAs during the HeLa cell cycle.", *Molecular and Cellular Biology*, Vol. 3 No. 4, pp. 539–50.

Herbst, R.S., Eckhardt, S.G., Kurzrock, R., Ebbinghaus, S., O'Dwyer, P.J., Gordon, M.S., Novotny, W., et al. (2010), "Phase I dose-escalation study of recombinant human Apo2L/TRAIL, a dual proapoptotic receptor agonist, in patients with advanced cancer", *Journal of Clinical Oncology*, Vol. 28 No. 17, pp. 2839–2846.

Hetz, C. (2012), "The unfolded protein response: Controlling cell fate decisions under ER stress and beyond", *Nature Reviews Molecular Cell Biology*, Nature Publishing Group, Vol. 13 No. 2, pp. 89–102.

Hetz, C., Chevet, E. and Oakes, S.A. (2015), "Proteostasis control by the unfolded protein response", *Nature Cell Biology*, Nature Publishing Group, Vol. 17 No. 7, pp. 829–838.

den Hollander, M.W., Gietema, J.A., de Jong, S., Walenkamp, A.M.E., Reyners, A.K.L., Oldenhuis, C.N.A.M. and De Vries, E.G.E. (2013), "Translating TRAIL-receptor targeting agents to the clinic", *Cancer Letters*, Elsevier Ireland Ltd, Vol. 332 No. 2, pp. 194–201.

Horak, P., Pils, D., Haller, G., Pribill, I., Roessler, M., Tomek, S., Horvat, R., et al. (2005), "Contribution of epigenetic silencing of tumor necrosis factor-related apoptosis inducing ligand receptor 1 (DR4) to TRAIL resistance and ovarian cancer", *Mol Cancer Res*, Vol. 3 No. 6, pp. 335–343.

Horn, S., Hughes, M.A., Schilling, R., Sticht, C., Tenev, T., Ploesser, M., Meier, P., et al. (2017), "Caspase-10 Negatively Regulates Caspase-8-Mediated Cell Death, Switching the Response to CD95L in Favor of NF-κB Activation and Cell Survival", *Cell Reports*, ElsevierCompany., Vol. 19 No. 4, pp. 785–797.

Horree, N., Gort, E.H., van der Groep, P., Heintz, A.P.M., Vooijs, M. and Diest, P.J. (2008), "Hypoxia-inducible factor-1α is essential for hypoxic p27 induction in endometrioid endometrial carcinoma", *The Journal of Pathology*, Vol. 214, pp. 38–45.

Horsman, M.R. and Overgaard, J. (2016), "The impact of hypoxia and its modification of the outcome of radiotherapy", *Journal of Radiation Research*, Vol. 57 No. May, pp. i90–i98.

Hu, W.H., Johnson, H. and Shu, H.B. (1999), "Tumor necrosis factor-related apoptosis-inducing ligand receptors signal NF-kappaB and JNK activation and apoptosis through distinct pathways", *J Biol Chem*, Vol. 274 No. 43, p. 30603–10.

Hubbi, M.E. and Semenza, G.L. (2015), "Regulation of cell proliferation by hypoxia-inducible factors", *American Journal of Physiology - Cell Physiology*, Vol. 309 No. 12, pp. C775–C782.

Huet, H.A., Growney, J.D., Johnson, J.A., Li, J., Bilic, S., Ostrom, L., Zafari, M., et al. (2014), "Multivalent nanobodies targeting death receptor 5 elicit superior tumor cell killing through efficient caspase induction", *mAbs*, Vol. 6 No. 6, pp. 1560–1570.

Hughes, M.A., Powley, I.R., Jukes-Jones, R., Horn, S., Feoktistova, M., Fairall, L., Schwabe, J.W.R., et al. (2016), "Co-operative and Hierarchical Binding of c-FLIP and Caspase-8: A Unified Model Defines How c-FLIP Isoforms Differentially Control Cell Fate", *Molecular Cell*, The Authors, Vol. 61 No. 6, pp. 834–849.

Hutt, M. (2017), *Multivalent Antibody-scTRAIL Fusion Proteins for Tumor Therapy – Impact of Format and Targeting*, University of Stuttgart.

Hutt, M., Fellermeier-Kopf, S., Seifert, O., Schmitt, L.C., Pfizenmaier, K. and Kontermann, R.E. (2018), "Targeting scFv-Fc-scTRAIL fusion proteins to tumor cells.", *Oncotarget*, Vol. 9 No. 13, pp. 11322–11335.

Hutt, M., Marquardt, L., Seifert, O., Siegemund, M., Müller, I., Kulms, D., Pfizenmaier, K., et al. (2017), "Superior properties of Fc-comprising scTRAIL fusion proteins", *Molecular Cancer Therapeutics*, Vol. 16 No. December, p. molcanther.0551.2017.

Hüttmann, a, Liu, S.L., Boyd, a W. and Li, C.L. (2001), "Functional heterogeneity within rhodamine123(lo) Hoechst33342(lo/sp) primitive hemopoietic stem cells revealed by pyronin Y.", *Experimental Hematology*, Vol. 29 No. 9, pp. 1109–16.

Hymowitz, S.G., Christinger, H.W., Fuh, G., Ultsch, M., O'Connell, M., Kelley, R.F., Ashkenazi, A., et al. (1999), "Triggering Cell Death", *Molecular Cell*, Vol. 4 No. 4, pp. 563–571.

Hymowitz, S.G., Connell, M.P.O., Ultsch, M.H., Hurst, A., Totpal, K., Ashkenazi, A., Vos, A.M. De, et al. (2000), "A Unique Zinc-Binding Site Revealed by a High-Resolution X-ray Structure of Homotrimeric Apo2L/TRAIL", *Biochemistry*, pp. 633–640.

Ichim, G. and Tait, S.W.G. (2016), "A fate worse than death: Apoptosis as an oncogenic process", *Nature Reviews Cancer*, Nature Publishing Group, Vol. 16 No. 8, pp. 539–548.

Inoue, S., Browne, G., Melino,G., Cohen, G. M. (2009), "Ordering of caspases in cells undergoing apoptosis by the intrincisc pathway", *Cell Death and Differentiation*, Vol. 16, pp. 1053-1061

Iurlaro, R. and Muñoz-Pinedo, C. (2016), "Cell death induced by endoplasmic reticulum stress", *FEBS Journal*, Vol. 283, pp. 2640–2652.

Iurlaro, R., Püschel, F., León-Annicchiarico, C.L., O'Connor, H., Martin, S.J., Palou-Gramón, D., Lucendo, E., et al. (2017), "Glucose Deprivation Induces ATF4-Mediated Apoptosis through TRAIL Death Receptors", *Molecular and Cellular Biology*, Vol. 37 No. 10, pp. e00479-16.

Jendrossek, V. (2013), "Targeting apoptosis pathways by Celecoxib in cancer", *Cancer Letters*, Elsevier Ireland Ltd, Vol. 332 No. 2, pp. 313–324.

Johnson, A.J., Hsu, A.-L., Lin, H.-P., Song, X. and Chen, C.-S. (2002), "The cyclo-oxygenase-2 inhibitor celecoxib perturbs intracellular calcium by inhibiting endoplasmic reticulum Ca2+-ATPases: a plausible link with its anti-tumour effect Targeting apoptosis pathways by Celecoxib in cancer and cardiovascular risks.", *The Biochemical Journal*, Vol. 366 No. Pt 3, pp. 831–837.

Kaaijk, P., Troost, D., Sminia, P., Hulshof, M.C.C.M., Van Der Kracht, A.H.W., Leenstra, S. and Bosch, D.A. (1997), "Hypofractionated radiation induces a decrease in cell proliferation but no histological damage to organotypic multicellular spheroids of human glioblastomas", *European Journal of Cancer Part A*, Vol. 33 No. 4, pp. 645–651.

Kaidi, A., Qualtrough, D., Williams, A.C. and Paraskeva, C. (2006), "Direct transcriptional up-regulation of cyclooxygenase-2 by hypoxia-inducible factor (HIF)-1 promotes colorectal tumor cell survival and enhances HIF-1 transcriptional activity during hypoxia", *Cancer Research*, Vol. 66 No. 13, pp. 6683–6691.

Kallinowski, F., Vaupel, P., Runkel, S. and Berg, G. (1988), "Glucose Uptake, Lactate Release, Ketone Body Turnover, Metabolic Micromilieu, and pH Distributions in Human Breast Cancer Xenografts in Nude Rats", *Cancer Research*, Vol. 48, pp. 7264–7272.

Kang, C.H., Moon, D.O., Choi, Y.H., Choi, I.W., Moon, S.K., Kim, W.J. and Kim, G.Y. (2011), "Piceatannol enhances TRAIL-induced apoptosis in human leukemia THP-1 cells through Sp1- and ERK-dependent DR5 up-regulation", *Toxicology in Vitro*, Elsevier Ltd, Vol. 25 No. 3, pp. 605–612.

von Karstedt, S., Conti, A., Nobis, M., Montinaro, A., Hartwig, T., Lemke, J., Legler, K., et al. (2015), "Cancer cell-autonomous TRAIL-R signaling promotes KRAS-Driven cancer progression, invasion, and metastasis", *Cancer Cell*, Vol. 27 No. 4, pp. 561–573.

von Karstedt, S., Montinaro, A. and Walczak, H. (2017), "Exploring the TRAILs less travelled: TRAIL in cancer biology and therapy", *Nature Reviews Cancer*, Nature Publishing Group, Vol. 17 No. 6, pp. 352–366.

Kaufman, R.J., Scheuner, D., Schröder, M., Shen, X., Lee, K., Liu, C.Y. and Arnold, S.M. (2002), "The unfolded protein response in nutrient sensing and differentiation", *Nature Reviews Molecular Cell Biology*, Vol. 3 No. 6, pp. 411–421.

Kelley, R.F., Totpal, K., Lindstrom, S.H., Mathieu, M., Billeci, K., DeForge, L., Pai, R., et al. (2005), "Receptor-selective mutants of apoptosis-inducing ligand 2/tumor necrosis factor-related apoptosis-inducing ligand reveal a greater contribution of Death Receptor (DR) 5 than DR4 to apoptosis signaling", *Journal of Biological Chemistry*, Vol. 280 No. 3, pp. 2205–2212.

Kern, M.A., Haugg, A.M., Koch, A.F., Schilling, T., Breuhahn, K., Walczak, H., Fleischer, B., et al. (2006), "Cyclooxygenase-2 inhibition induces apoptosis signaling via death receptors and mitochondria in hepatocellular carcinoma", *Cancer Research*, Vol. 66 No. 14, pp. 7059–7066.

Kerr, J.F.R., Harmon, B. and Searle, J. (1974), "an Electron-Microscope Study of Cell Deletion in the Anuran Tadpole Tail During Spontaneous Metamorphosis With Special Reference To Apoptosis of Striated Muscle Fibres", *J. Cell Sci*, Vol. 14, pp. 571–585.

Kerr, J.F.R., Wyllie, A.H. and Currie, A.R. (1972), “Apoptosis: a Basic Biological Phenomenon With Wide- Ranging Implications in Tissue Kinetics”, *Journal of Internal Medicine*, Vol. 258 No. 6, pp. 479–517.

Kimberley, F.C. and Screaton, G.R. (2004), “Following a TRAIL: Update on a ligand and its five receptors”, *Cell Research*, Vol. 14 No. 5, pp. 359–372.

Kimura, K., Taguchi, T., Urushizaki, I., Ohno, R., Abe, O., Furue, H., Hattori, T., et al. (1987), “Phase I study of recombinant human tumor necrosis factor.”, *Cancer Chemotherapy and Pharmacology*, Vol. 20 No. 3, pp. 223–229.

Kimura, T., Takabatake, Y., Takahashi, A. and Isaka, Y. (2013), “Chloroquine in cancer therapy: A double-edged sword of autophagy”, *Cancer Research*, Vol. 73 No. 1, pp. 3–7.

Kiraz, Y., Adan, A., Kartal Yandim, M. and Baran, Y. (2016), “Major apoptotic mechanisms and genes involved in apoptosis”, *Tumor Biology*, Vol. 37 No. 7, pp. 8471–8486.

Kischkel, F.C., Lawrence, D.A., Chuntharapai, A., Schow, P., Kim, K.J. and Ashkenazi, A. (2000), “Apo2L/TRAIL-dependent recruitment of endogenous FADD and caspase-8 to death receptors 4 and 5”, *Immunity*, Vol. 12 No. 6, pp. 611–620.

Knight, E. and Przyborski, S. (2015), “Advances in 3D cell culture technologies enabling tissue-like structures to be created in vitro”, *Journal of Anatomy*, Vol. 227 No. 6, pp. 746–756.

Koh, M.Y., Darnay, B.G. and Powis, G. (2008), “Hypoxia-Associated Factor, a Novel E3-Ubiquitin Ligase, Binds and Ubiquitinates Hypoxia-Inducible Factor 1 , Leading to Its Oxygen-Independent Degradation”, *Molecular and Cellular Biology*, Vol. 28 No. 23, pp. 7081–7095.

Kojima, Y., Nakayama, M., Nishina, T., Nakano, H., Koyanagi, M., Takeda, K., Okumura, K., et al. (2011), “Importin ??1 protein-mediated nuclear localization of Death Receptor 5 (DR5) limits DR5/Tumor Necrosis Factor (TNF)-related apoptosis-inducing ligand (TRAIL)-induced cell death of human tumor cells”, *Journal of Biological Chemistry*, Vol. 286 No. 50, pp. 43383–43393.

Kontermann, R.E. (2012), “Dual targeting strategies with bispecific antibodies”, *mAbs*, Vol. 4 No. 2, pp. 182–197.

Koong, A., Che, K. and Giaccia, A. (1994), “Hypoxia causes the activation of nuclear factor kappa through the phosphorilation of I-kB on tyrosine residues”, *Cancer Res*, No. 54, pp. 1425–1430.

Koschny, R., Walczak, H. and Ganten, T.M. (2007), “The promise of TRAIL - Potential and risks of a novel anticancer therapy”, *Journal of Molecular Medicine*, Vol. 85 No. 9, pp. 923–935.

Koyasu, S., Kobayashi, M., Goto, Y., Hiraoka, M. and Harada, H. (2018), “Regulatory mechanisms of hypoxia-inducible factor 1 activity: Two decades of knowledge”, *Cancer Science*, Vol. 109 No. 3, pp. 560–571.

Kullmann, M., Göpfert, U., Siewe, B. and Hengst, L. (2002), “ELAV/Hu proteins inhibit p27 translation via an IRES element in the p27 5’UTR”, *Genes and Development*, Vol. 16 No. 23, pp. 3087–3099.

Kundu, N., Ma, X., Kochel, T., Goloubeva, O., Staats, P., Thompson, K., Martin, S., et al. (2014), “Prostaglandin e receptor EP4 is a therapeutic target in breast cancer cells with stem-like properties”, *Breast Cancer Research and Treatment*, Vol. 143 No. 1, pp. 19–31.

Kunz-Schughart, L.A., Freyer, J.P., Hofstaedter, F. and Ebner, R. (2004), “The Use of 3-D Cultures for High-Throughput Screening ”:, Vol. 9 No. 4, pp. 273–285.

Kurita, S., Mott, J.L., Almada, L.L., Bronk, S.F., Werneburg, N.W., Sun, S.Y., Roberts, L.R., et al. (2010), “GLI3-dependent repression of DR4 mediates hedgehog antagonism of TRAIL-induced apoptosis”, *Oncogene*, Nature Publishing Group, Vol. 29 No. 34, pp. 4848–4858.

Kurumbail, R.G., Stevens, A.M., Gierse, J.K., McDonald, J.J., Stegeman, R.A., Pak, J.Y., Gildehaus, D., et al. (1996), “Structural basis for selective inhibition of cyclooxygenase-2 by anti-inflammatory agents”, *Nature*, Vol. 384 No. 6610, pp. 644–648.

Kwon, Y., Cho, N., Ye, D., Baek, H. and Chun, Y. (2018), “Cytochrome P450 1B1 promotes cancer cell survival via specificity protein 1 (Sp1) -mediated suppression of death receptor 4”, *Journal of Toxicology and Environmental Health, Part A*, Taylor & Francis, Vol. 81 No. 9, pp. 278–287.

Kwon, Y.J., Baek, H.S., Ye, D.J., Shin, S., Kim, D. and Chun, Y.J. (2016), "CYP1B1 enhances cell proliferation and metastasis through induction of EMT and activation of Wnt/β-catenin signaling via Sp1 upregulation", *PLoS ONE*, Vol. 11 No. 3, available at:https://doi.org/10.1371/journal.pone.0151598.

Lafont, E., Kantari-Mimoun, C., Draber, P., De Miguel, D., Hartwig, T., Reichert, M., Kupka, S., et al. (2017), "The linear ubiquitin chain assembly complex regulates TRAIL-induced gene activation and cell death", *The EMBO Journal*, Vol. 36 No. 9, pp. 1147–1166.

Lalaoui, N., Morlé, A., Mérino, D., Jacquemin, G., Iessi, E., Morizot, A., Shirley, S., et al. (2011), "TRAIL-R4 promotes tumor growth and resistance to apoptosis in cervical carcinoma HeLa cells through AKT", *PLoS ONE*, Vol. 6 No. 5, pp. 2–9.

Lane, D., Matte, I., Rancourt, C. and Piché, A. (2012), "Osteoprotegerin (OPG) protects ovarian cancer cells from TRAIL-induced apoptosis but does not contribute to malignant ascites-mediated attenuation of TRAIL-induced apoptosis", *Journal of Ovarian Research*, Vol. 5 No. 1, pp. 1–9.

Laporte, D., Lebaudy, A., Sahin, A., Pinson, B., Ceschin, J., Daignan-Fornier, B. and Sagot, I. (2011), "Metabolic status rather than cell cycle signals control quiescence entry and exit", *Journal of Cell Biology*, Vol. 192 No. 6, pp. 949–957.

Lawrence, D., Shahrokh, Z., Marsters, S., Mounho, B., Hillan, K., Totpal, K., DeForge, L., et al. (2001), "Differential hepatocyte toxicity of recombinant Apo2L / TRAIL versions.", *Nat. Med.*, Vol. 7 No. 4, pp. 2000–2002.

Leclerc, G.J., DeSalvo, J., Du, J., Gao, N., Leclerc, G.M., Lehrman, M.A., Lampidis, T.J., et al. (2015), "Mcl-1 downregulation leads to the heightened sensitivity exhibited by BCR-ABL positive ALL to induction of energy and ER-stress", *Leukemia Research*, Elsevier Ltd, Vol. 39 No. 11, pp. 1246–1254.

Lee, C.M. and Tannock, I.F. (2006), "Inhibition of endosomal sequestration of basic anticancer drugs: Influence on cytotoxicity and tissue penetration", *British Journal of Cancer*, Vol. 94 No. 6, pp. 863–869.

Lee, H., Park, M.T., Choi, B.H., Oh, E.T., Song, M.J., Lee, J., Kim, C., et al. (2011), "Endoplasmic reticulum stress-induced JNK activation is a critical event leading to mitochondria-mediated cell death caused by β-lapachone treatment.", *PloS One*, Vol. 6 No. 6, pp. 1–12.

Lee, H.W., Lee, S.H., Lee, H.W., Ryu, Y.W., Kwon, M.H. and Kim, Y.S. (2005), "Homomeric and heteromeric interactions of the extracellular domains of death receptors and death decoy receptors", *Biochemical and Biophysical Research Communications*, Vol. 330 No. 4, pp. 1205–1212.

Lee, J.Y., Huerta-Yepez, S., Vega, M., Baritaki, S., Spandidos, D.A. and Bonavida, B. (2007), "The NO TRAIL to YES TRAIL in cancer therapy (review)", *International Journal of Oncology*, Vol. 31 No. 4, pp. 685–691.

Lee, S.M., Lee, C.T., Kim, Y.W., Han, S.K., Shim, Y.S. and Yoo, C.G. (2006), "Hypoxia confers protection against apoptosis via PI3K/Akt and ERK pathways in lung cancer cells", *Cancer Letters*, Vol. 242 No. 2, pp. 231–238.

Leithner, K., Stacher, E., Wurm, R., Ploner, F., Quehenberger, F., Wohlkoenig, C., Bálint, Z., et al. (2009), "Nuclear and cytoplasmic death receptor 5 as prognostic factors in patients with non-small cell lung cancer treated with chemotherapy", *Lung Cancer*, Vol. 65 No. 1, pp. 98–104.

Leone, V., di Palma, A., Ricchi, P., Acquaviva, F., Giannouli, M., Di Prisco, A.M., Iuliano, F., et al. (2007), "PGE2 inhibits apoptosis in human adenocarcinoma Caco-2 cell line through Ras-PI3K association and cAMP-dependent kinase A activation", *AJP: Gastrointestinal and Liver Physiology*, Vol. 293 No. 4, pp. G673–G681.

Levy, N.S., Chung, S., Furneaux, H. and Levy, A.P. (1998), "Hypoxic stabilization of vascular endothelial growth factor mRNA by the RNA-binding protein HuR", *The Journal of Biological Chemistry*, Vol. 273 No. 11, pp. 6417–6423.

Li, F., Huang, Q., Chen, J., Peng, Y., Roop, D.R., Bedford, J.S. and Li, C.-Y. (2010), "Apoptotic cells activate the "phoenix rising" pathway to promote wound healing and tissue regeneration.", *Science Signaling*, Vol. 3 No. 110, p. ra13.

Li, S., Tian, D., Fei, P., Gao, Y., Chen, Z., Wang, Q. and Tong, Q. (2011), "A cyclooxygase-2 inhibitor NS-398-enhanced apoptosis of esophageal carcinoma cell EC9706 by adjusting expression of survivin and caspase-3", *Cancer Investigation*, Vol. 29 No. 2, pp. 102–106.

Li, T., Su, L., Lei, Y., Liu, X., Zhang, Y. and Liu, X. (2015), "DDIT3 and KAT2A proteins regulate TNFRSF10A and TNFRSF10B expression in endoplasmic reticulum stress-mediated apoptosis in human lung cancer cells", *Journal of Biological Chemistry*, Vol. 290 No. 17, pp. 11108–11118.

Liang, X., Xu, X., Wang, F., Chen, X., Li, N., Wang, C. and He, J. (2015), "E-cadherin knockdown increases β-catenin reducing colorectal cancer chemosensitivity only in three-dimensional cultures", *International Journal of Oncology*, Vol. 47 No. 4, pp. 1517–1527.

Lin, R.K., Wu, C.Y., Chang, J.W., Juan, L.J., Hsu, H.S., Chen, C.Y., Lu, Y.Y., et al. (2010), "Dysregulation of p53/Sp1 control leads to DNA methyltransferase-1 overexpression in lung cancer", *Cancer Research*, Vol. 70 No. 14, pp. 5807–5817.

Lindholm, D., Korhonen, L., Eriksson, O. and Kõks, S. (2017), "Recent Insights into the Role of Unfolded Protein Response in ER Stress in Health and Disease", *Frontiers in Cell and Developmental Biology*, Vol. 5 No. May, pp. 1–16.

Liu, H., Jiang, C.C., Lavis, C.J., Croft, A., Dong, L., Tseng, H.Y., Yang, F., et al. (2009), "2-Deoxy-D-glucose enhances TRAIL-induced apoptosis in human melanoma cells through XBP-1-mediated up-regulation of TRAIL-R2", *Molecular Cancer*, Vol. 8, pp. 1–17.

Liu, X., Yue, P., Khuri, F.R. and Sun, S.Y. (2005), "Decoy receptor 2 (DcR2) is a p53 target gene and regulates chemosensitivity", *Cancer Research*, Vol. 65 No. 20, pp. 9169–9175.

Liu, X., Yue, P., Schönthal, A.H., Khuri, F.R. and Sun, S.Y. (2006), "Cellular FLICE-inhibitory protein down-regulation contributes to celecoxib-induced apoptosis in human lung cancer cells", *Cancer Research*, Vol. 66 No. 23, pp. 11115–11119.

Liu, X., Yue, P., Zhou, Z., Khuri, F.R. and Sun, S.Y. (2004), "Death receptor regulation and celecoxib-induced apoptosis in human lung cancer cells", *Journal of the National Cancer Institute*, Vol. 96 No. 23, pp. 1769–1780.

Lu, M., Lawrence, D.A., Marsters, S., Acosta-Alvear, D., Kimmig, P., Mendez, A.S., Paton, A.W., et al. (2014), "Opposing unfolded-protein-response signals converge on death receptor 5 to control apoptosis", *Science*, Vol. 345 No. 6192, pp. 98–101.

MacFarlane, M., Ahmad, M., Srinivasula, S.M., Fernandes-Alnemri, T., Cohen, G.M. and Alnemri, E.S. (1997), "Identification and molecular cloning of two novel receptors for the cytotoxic ligand TRAIL.", *The Journal of Biological Chemistry*, Vol. 272, pp. 25417–25420.

MacFarlane, M., Kohlhaas, S.L., Sutcliffe, M.J., Dyer, M.J.S. and Cohen, G.M. (2005), "TRAIL receptor-selective mutants signal to apoptosis via TRAIL-R1 in primary lymphoid malignancies", *Cancer Research*, Vol. 65 No. 24, pp. 11265–11270.

Maier, T.J., Schiffmann, S., Wobst, I., Birod, K., Angioni, C., Hoffmann, M., Lopez, J.J., et al. (2009), "Cellular membranes function as a storage compartment for celecoxib.", *Journal of Molecular Medicine (Berlin, Germany)*, Vol. 87 No. 10, pp. 981–993.

Majima, M., Hayashi, I., Muramatsu, M., Katada, J., Yamashina, S. and Katori, M. (2000), "Cyclo-oxygenase-2 enhances basic fibroblast growth factor-induced angiogenesis through induction of vascular endothelial growth factor in rat sponge implants.", *British Journal of Pharmacology*, Vol. 130 No. 3, pp. 641–649.

Majkut, J., Sgobba, M., Holohan, C., Crawford, N., Logan, A.E., Kerr, E., Higgins, C.A., et al. (2014), "Differential affinity of FLIP and procaspase 8 for FADD's DED binding surfaces regulates DISC assembly", *Nature Communications*, Vol. 5, available at:https://doi.org/10.1038/ncomms4350.

Mak, I.W.Y., Evaniew, N. and Ghert, M. (2014), "Lost in translation: Animal models and clinical trials in cancer treatment", *American Journal of Translational Research*, Vol. 6 No. 2, pp. 114–118.

Marsters, S.A., Sheridan, J.P., Pitti, R.M., Huang, A., Skubatch, M., Baldwin, D., Yuan, J., et al. (1997), "A novel receptor for Apo2L / TRAIL contains a truncated death domain", *Current Biology*, Vol. 7, pp. 1003–1006.

Martín-Pérez, R., Niwa, M. and López-Rivas, A. (2012), "ER stress sensitizes cells to TRAIL through down-regulation of FLIP and Mcl-1 and PERK-dependent up-regulation of TRAIL-R2", *Apoptosis*, Vol. 17 No. 4, pp. 349–363.

Martin, W.M. and McNally, N.J. (1980), “Cytotoxicity of adriamycin to tumour cells in vivo and in vitro.”, *British Journal of Cancer*, Vol. 42, pp. 881–889.

Martinou, J.C. and Youle, R.J. (2011), “Mitochondria in Apoptosis: Bcl-2 Family Members and Mitochondrial Dynamics”, *Developmental Cell*, Elsevier Inc., Vol. 21 No. 1, pp. 92–101.

Maurel, M., Chevet, E., Tavernier, J. and Gerlo, S. (2014), “Getting RIDD of RNA: IRE1 in cell fate regulation”, *Trends in Biochemical Sciences*, Elsevier Ltd, Vol. 39 No. 5, pp. 245–254.

Mc Cullough, K.D., Martindale, J.L., Aw, T., Holbrook, N.J., Cullough, K.D.M.C. and Klotz, L. (2001), “Gadd153 Sensitizes Cells to Endoplasmic Reticulum Stress by Down-Regulating Bcl2 and Perturbing the Cellular Redox State”, *Molecular and Cellular Biology*, Vol. 21 No. 4, pp. 1249–1259.

McCarthy, E.F. (2006), “The toxins of William B. Coley and the treatment of bone and soft-tissue sarcomas.”, *The Iowa Orthopaedic Journal*, Vol. 26, pp. 154–8.

Mehta, G., Hsiao, A.Y., Ingram, M., Luker, G.D. and Takayama, S. (2012), “Opportunities and challenges for use of tumor spheroids as models to test drug delivery and efficacy”, *Journal of Controlled Release*, Elsevier B.V., Vol. 164 No. 2, pp. 192–204.

Merino, D., Lalaoui, N., Morizot, A., Schneider, P., Solary, E. and Micheau, O. (2006), “Differential Inhibition of TRAIL-Mediated DR5-DISC Formation by Decoy Receptors 1 and 2”, *Molecular and Cellular Biology*, Vol. 26 No. 19, pp. 7046–7055.

Mert, U. and Sanlioglu, A.D. (2016), “Intracellular localization of DR5 and related regulatory pathways as a mechanism of resistance to TRAIL in cancer”, *Cellular and Molecular Life Sciences*, Springer International Publishing, Vol. 74 No. 2, pp. 245–255.

Michaelson, J.S., Demarest, S.J., Miller, B., Amatucci, A., Snyder, W.B., Wu, X., Huang, F., et al. (2009), “Anti-tumor activity of stability-engineered IgG-like bispecific antibodies targeting TRAIL-R2 and LTβR”, *mAbs*, Vol. 1 No. 2, pp. 128–141.

Micheau, O. (2018), “Regulation of TNF-related apoptosis-inducing ligand signaling by glycosylation”, *International Journal of Molecular Sciences*, Vol. 19 No. 3, available at:https://doi.org/10.3390/ijms19030715.

de Miguel, D., Lemke, J., Anel, A., Walczak, H. and Martinez-Lostao, L. (2016), “Onto better TRAILs for cancer treatment”, *Cell Death and Differentiation*, Nature Publishing Group, Vol. 23 No. 5, pp. 733–747.

Millard, M., Yakavets, I., Zorin, V., Kulmukhamedova, A., Marchal, S. and Bezdetnaya, L. (2017), “Drug delivery to solid tumors: The predictive value of the multicellular tumor spheroid model for nanomedicine screening”, *International Journal of Nanomedicine*, Vol. 12, pp. 7993–8007.

Minchinton, A.I. and Tannock, I.F. (2006), “Drug penetration in solid tumours”, *Nature Reviews Cancer*, Vol. 6 No. 8, pp. 583–592.

Misra, A., Pandey, C., Sze, S.K. and Thanabalu, T. (2012), “Hypoxia Activated EGFR Signaling Induces Epithelial to Mesenchymal Transition (EMT)”, *PLoS ONE*, Vol. 7 No. 11, available at:https://doi.org/10.1371/journal.pone.0049766.

Mizrahi, K. and Askenasy, N. (2014), “Physiological functions of TNF family receptor/ligand interactions in hematopoiesis and transplantation”, *Blood*, Vol. 124 No. 2, pp. 176–183.

Mizushima, N. and Yoshimori, T. (2007), “How to interpret LC3 immunoblotting”, *Autophagy*, Vol. 3 No. 6, pp. 542–545.

Möller, Y., Siegemund, M., Beyes, S., Herr, R., Lecis, D., Delia, D., Kontermann, R., et al. (2014), “EGFR-targeted TRAIL and a Smac mimetic synergize to overcome apoptosis resistance in KRAS mutant colorectal cancer cells”, *PLoS ONE*, Vol. 9 No. 9, available at:https://doi.org/10.1371/journal.pone.0107165.

Mongkolsapaya, J., Cowper, A.E., Xu, X.N., Morris, G., McMichael, A.J., Bell, J.I. and Screaton, G.R. (1998), “Lymphocyte inhibitor of TRAIL (TNF-related apoptosis-inducing ligand): a new receptor protecting lymphocytes from the death ligand TRAIL.”, *Journal of Immunology (Baltimore, Md. : 1950)*, Vol. 160 No. 1, pp. 3–6.

Moon, D.-O., Kim, M.-O., Choi, Y.H. and Kim, G.-Y. (2010), “Butein sensitizes human hepatoma cells to TRAIL-induced apoptosis via extracellular signal-regulated kinase/Sp1-dependent DR5 upregulation and NF-kappaB inactivation.”, *Molecular Cancer Therapeutics*, Vol. 9 No. 6, pp. 1583–95.

Moretti, M., Bennett, J., Tornatore, L., Thotakura, A.K. and Franzoso, G. (2012), “Cancer: NF-κB regulates energy metabolism”, *International Journal of Biochemistry and Cell Biology*, Elsevier Ltd, Vol. 44 No. 12, pp. 2238–2243.

Mori, C., Nakamura, N., Kimura, S., Irie, H., Takigawa, T. and Shiota, K. (1995), “Programmed cell death in the interdigital tissue of the fetal mouse limb is apoptosis with DNA fragmentation”, *The Anatomical Record*, Vol. 242 No. 1, pp. 103–110.

Murphy, K.C., Hung, B.P., Browne-Bourne, S., Zhou, D., Yeung, J., Genetos, D.C. and Leach, J.K. (2017), “Measurement of oxygen tension within mesenchymal stem cell spheroids”, *Journal of the Royal Society Interface*, Vol. 14 No. 127, available at:https://doi.org/10.1098/rsif.2016.0851.

Nagata, S. (2000), “Apoptotic DNA fragmentation”, *Experimental Cell Research*, Vol. 256 No. 1, pp. 12–18.

Nakanishi, Y., Kamijo, R., Takizawa, K., Hatori, M. and Nagumo, M. (2001), “Inhibitors of cyclooxygenase-2 (COX-2) suppressed the proliferation and differentiation of human leukaemia cell lines”, *European Journal of Cancer*, Vol. 37 No. 12, pp. 1570–1578.

Narayanan, B. a, Narayanan, N.K., Pittman, B. and Reddy, B.S. (2004), “Regression of Mouse Prostatic Intraepithelial Neoplasia by Nonsteroidal Anti-inflammatory Drugs in the Transgenic Adenocarcinoma Mouse Prostate Model”, *Clinical Cancer Research*, Vol. 10, pp. 7727–7737.

National Cancer Institute, "https://www.cancer.gov/about-cacner/treatment/clinical trials/intervention/celecoxib

Neumann, S., Hasenauer, J., Pollak, N. and Scheurich, P. (2014), “Dominant negative effects of tumor necrosis factor (tnf)-related apoptosis-inducing ligand (TRAIL) receptor 4 on TRAIL receptor 1 signaling by Formation of heteromeric complexes”, *Journal of Biological Chemistry*, Vol. 289 No. 23, pp. 16576–16587.

Nexcelom, Nexcelom Bioscience table, (2003), "www.nexcelom.com/applications/cellometer/bright-field/nci-60-cancer-cell-lines/"

Ogasawara, J., Watanabe-Fukunaga, R., Adachi, M., Matsuzawa, A., Kasugai, T., Kitamura, Y., Itoh, N., et al. (1993), “Lethal effect of the anti-Fas antibody in mice”, *Nature*, Vol. 364 No. 6440, pp. 806–809.

Oh, Y.T., Liu, X., Yue, P., Kang, S., Chen, J., Taunton, J., Khuri, F.R., et al. (2010), “ERK/ribosomal S6 kinase (RSK) signaling positively regulates death receptor 5 expression through co-activation of CHOP and Elk1”, *Journal of Biological Chemistry*, Vol. 285 No. 53, pp. 41310–41319.

Pai, R., Soreghan, B., Szabo, I.L., Pavelka, M., Baatar, D. and Tarnawski, A.S. (2002), “Prostaglandin E2, transactivates EGF receptor: A novel mechanism for promoting colon cancer growth and gastrointestinal hypertrophy”, *Nature Medicine*, Vol. 8 No. 3, pp. 289–293.

Pan, G., Ni, J., Wei, Y.F., Yu, G.I., Gentz, R. and Dixit, V.M. (1997), “An antagonist decoy receptor and a death domain-containing receptor for TRAIL”, *Science*, Vol. 277 No. 5327, pp. 815–818.

Pan, G., Ni, J., Yu, G.L., Wei, Y.F. and Dixit, V.M. (1998), “TRUNDD, a new member of thr TRAIL receptor family that antagonizes TRAIL signalling”, *FEBS Letters*, Vol. 424 No. 1–2, pp. 41–45.

Pan, G., O’Rourke, K., Chinnaiyan, A.M., Gentz, R., Ebner, R., Ni, J. and Dixit, V.M. (1997), “The receptor for the cytotoxic ligand TRAIL”, *Science*, Vol. 276 No. 5309, pp. 111–113.

Papadopoulos, K.P., Isaacs, R., Bilic, S., Kentsch, K., Huet, H.A., Hofmann, M., Rasco, D., et al. (2015), “Unexpected hepatotoxicity in a phase I study of TAS266, a novel tetravalent agonistic Nanobody®targeting the DR5 receptor”, *Cancer Chemotherapy and Pharmacology*, Springer Berlin Heidelberg, Vol. 75 No. 5, pp. 887–895.

Park, M.C., Jeong, H., Son, S.H., Kim, Y.H., Han, D., Goughnour, P.C., Kang, T., et al. (2016), “Novel morphologic and genetic analysis of cancer cells in a 3D microenvironment identifies STAT3 as a regulator of tumor permeability barrier function”, *Cancer Research*, Vol. 76 No. 5, pp. 1044–1054.

Park, S.Y., Billiar, T.R. and Seol, D.W. (2002), "Hypoxia inhibition of apoptosis induced by tumor necrosis factor-related apoptosis-inducing ligand (TRAIL)", *Biochemical and Biophysical Research Communications*, Vol. 291 No. 1, pp. 150–153.

Patel, M.I., Subbaramaiah, K., Du, B., Chang, M., Yang, P., Newman, R. a, Cordon-Cardo, C., et al. (2007), "Celecoxib inhibits prostate cancer growth: evidence of a cyclooxygenase-2-independent mechanism", *Clin Cancer Res.*, Vol. 11 No. 5, pp. 1999–2007.

Patrignani, P. and Patrono, C. (2015), "Cyclooxygenase inhibitors: From pharmacology to clinical read-outs", *Biochimica et Biophysica Acta - Molecular and Cell Biology of Lipids*, Elsevier B.V., Vol. 1851 No. 4, pp. 422–432.

Pei, G.T., Wu, C.W. and Lin, W.W. (2010), "Hypoxia-induced decoy receptor 2 gene expression is regulated via a hypoxia-inducible factor 1α-mediated mechanism", *Biochemical and Biophysical Research Communications*, Elsevier Inc., Vol. 391 No. 2, pp. 1274–1279.

Pennarun, B., Meijer, A., de Vries, E.G.E., Kleibeuker, J.H., Kruyt, F. and de Jong, S. (2010), "Playing the DISC: Turning on TRAIL death receptor-mediated apoptosis in cancer", *Biochimica et Biophysica Acta - Reviews on Cancer*, Elsevier B.V., Vol. 1805 No. 2, pp. 123–140.

Pereira, P.D., Serra-Caetano, A., Cabrita, M., Bekman, E., Braga, J., Rino, J., Santus, R., et al. (2017), "Quantification of cell cycle kinetics by EdU (5-ethynyl-2'-deoxyuridine)-coupled-fluorescence-intensity analysis", *Oncotarget*, Vol. 8 No. 25, pp. 40514–40532.

Pineda, D.M., Rittenhouse, D.W., Valley, C.C., Cozzitorto, J.A., Burkhart, R.A., Leiby, B., Winter, J.M., et al. (2012), "HuR's post-transcriptional regulation of death receptor 5 in pancreatic cancer cells", *Cancer Biology & Therapy*, Vol. 13 No. 10, pp. 946–955.

Pitti, R.M., Marsters, S.A., Ruppert, S., Donahue, C.J., Moore, A. and Ashkenazi, A. (1996), "Induction of apoptosis by Apo-2 ligand, a new member of the tumor necrosis factor cytokine family", *Journal of Biological Chemistry*, Vol. 271 No. 22, pp. 12687–12690.

Pop, C., Oberst, A., Drag, M., Van Raam, B.J., Riedl, S.J., Green, D.R. and Salvesen, G.S. (2011), "FLIP $_{L}$ induces caspase 8 activity in the absence of interdomain caspase 8 cleavage and alters substrate specificity", *Biochemical Journal*, Vol. 433 No. 3, pp. 447–457.

Portanova, P., Notaro, A., Pellerito, O., Sabella, S., Giuliano, M. and Calvarus, G. (2013), "Notch inhibition restores TRAIL-mediated apoptosis via AP1-dependent upregulation of DR4 and DR5 TRAIL receptors in MDA-MB-231 breast cancer cells", *International Journal of Oncology*, Vol. 43 No. 1, pp. 121–130.

Pozzi, A., Yan, X., Macias-Perez, I., Wei, S., Hata, A.N., Breyer, R.M., Morrow, J.D., et al. (2004), "Colon carcinoma cell growth is associated with prostaglandin E2/EP4 receptor-evoked ERK activation", *Journal of Biological Chemistry*, Vol. 279 No. 28, pp. 29797–29804.

Preisler, H.D., Walczak, I., Renick, J. and Rustum, Y.M. (1977), "Separation of Leukemic Cells into Proliferative and Quiescent Subpopulations by Centrifugal Elutriation", *Cancer Research*, Vol. 37 No. 11, pp. 3876–3880.

Pyrko, P., Kardosh, A., Liu, Y.-T., Soriano, N., Xiong, W., Chow, R.H., Uddin, J., et al. (2007), "Calcium-activated endoplasmic reticulum stress as a major component of tumor cell death induced by 2,5-dimethyl-celecoxib, a non-coxib analogue of celecoxib", *Molecular Cancer Therapeutics*, Vol. 6 No. 4, pp. 1262–1275.

Pyrko, P., Soriano, N., Kardosh, A., Liu, Y.T., Uddin, J., Petasis, N.A., Hofman, F.M., et al. (2006), "Downregulation of survivin expression and concomitant induction of apoptosis by celecoxib and its non-cyclooxygenase-2-inhibitory analog, dimethyl-celecoxib (DMC), in tumor cells in vitro and in vivo", *Molecular Cancer*, Vol. 5, pp. 1–16.

Qiu, R., Chen, J., Sima, J., Shen, X., Liu, D. and Shen, J. (2012), "NS398 induces apoptosis in non-small cell lung cancer cells", *Journal of Cancer Research and Clinical Oncology*, Vol. 138 No. 1, pp. 119–124.

Querido, E., Dekakra-Bellili, L. and Chartrand, P. (2017), "RNA fluorescence in situ hybridization for high-content screening", *Methods*, Elsevier Inc., Vol. 126, pp. 149–155.

Ramamurthy, V., Yamniuk, A.P., Lawrence, E.J., Yong, W., Schneeweis, L.A., Cheng, L., Murdock, M., et al. (2015), "The structure of the death receptor 4-TNF-related apoptosis-inducing ligand (DR4-TRAIL) complex", *Acta Crystallographica Section:F Structural Biology Communications*, International Union of Crystallography, Vol. 71, pp. 1273–1281.

Razumilava, N., Bronk, S.F., Smoot, R.L., Fingas, C.D., Werneburg, N.W., Roberts, L.R. and Mott, J.L. (2012), "miR-25 targets TNF-related apoptosis inducing ligand (TRAIL) death receptor-4 and promotes apoptosis resistance in cholangiocarcinoma", *Hepatology*, Vol. 55 No. 2, pp. 465–475.

Redza-Dutordoir, M. and Averill-Bates, D.A. (2016), "Activation of apoptosis signalling pathways by reactive oxygen species", *Biochimica et Biophysica Acta - Molecular Cell Research*, Elsevier B.V., Vol. 1863 No. 12, pp. 2977–2992.

Rey, S., Schito, L., Koritzinsky, M. and Wouters, B.G. (2017), "Molecular targeting of hypoxia in radiotherapy", *Advanced Drug Delivery Reviews*, Elsevier B.V., Vol. 109, pp. 45–62.

Riccioni, R., Pasquini, L., Mariani, G., Saulle, E., Rossini, A., Diverio, D., Pelosi, E., et al. (2005), "TRAIL decoy receptors mediate resistance of acute myeloid leukemia cells to TRAIL", *Haematologica*, Vol. 90 No. 5, pp. 612–624.

Ricciotti, E. and Fitzgerald, G.A. (2011), "Prostaglandins and inflammation", *Arteriosclerosis, Thrombosis, and Vascular Biology*, Vol. 31 No. 5, pp. 986–1000.

Riobó, N.A., Lu, K., Ai, X., Haines, G.M. and Emerson, C.P. (2006), "Phosphoinositide 3-kinase and Akt are essential for Sonic Hedgehog signaling.", *Proceedings of the National Academy of Sciences of the United States of America*, Vol. 103 No. 12, pp. 4505–10.

Rodgers, J.T., King, K.Y., Brett, J.O., Cromie, M.J., Charville, G.W., Maguire, K.K., Brunson, C., et al. (2014), "MTORC1 controls the adaptive transition of quiescent stem cells from G0to GAlert", *Nature*, Nature Publishing Group, Vol. 510 No. 7505, pp. 393–396.

Romeo, C., Weber, M.C., Zarei, M., DeCicco, D., Chand, S.N., Lobo, A.D., Winter, J.M., et al. (2016), "HuR Contributes to TRAIL Resistance by Restricting Death Receptor 4 Expression in Pancreatic Cancer Cells", *Molecular Cancer Research*, Vol. 14 No. 7, pp. 599–611.

Roos, W.P. and Kaina, B. (2006), "DNA damage-induced cell death by apoptosis", *Trends in Molecular Medicine*, Vol. 12 No. 9, pp. 440–450.

van Roosmalen, I.A.M., Reis, C.R., Setroikromo, R., Yuvaraj, S., Joseph, J. V., Tepper, P.G., Kruyt, F.A.E., et al. (2014), "The ER stress inducer DMC enhances TRAIL-induced apoptosis in glioblastoma", *SpringerPlus*, Vol. 3 No. 1, pp. 1–12.

Salmenperä, P., Kankuri, E., Bizik, J., Sirén, V., Virtanen, I., Takahashi, S., Leiss, M., et al. (2008), "Formation and activation of fibroblast spheroids depend on fibronectin–integrin interaction", *Experimental Cell Research*, Elsevier Inc., Vol. 314 No. 19, pp. 3444–3452.

Santini, M.T. and Rainaldi, G. (1999), "Three-dimensional spheroid model in tumor biology", *Pathobiology*, Vol. 67 No. 3, pp. 148–157.

Scaffidi, C., Fulda, S., Srinivasan, A., Friesen, C., Li, F., Tomaselli, K.J., Debatin, K.M., et al. (1998), "Two CD95 (APO-1/Fas) signaling pathways", *EMBO Journal*, Vol. 17 No. 6, pp. 1675–1687.

Schindelin, J., Arganda-Carreras, I., Frise, E., Kaynig, V., Longair, M., Pietzsch, T., Preibisch, S., et al. (2012), "Fiji: An open source platform for biological image analysis.", *Nature Methods*, Vol. 9 No. 7, pp. 676–682.

Schleich, K., Buchbinder, J.H., Pietkiewicz, S., Kähne, T., Warnken, U., Öztürk, S., Schnölzer, M., et al. (2016), "Molecular architecture of the DED chains at the DISC: Regulation of procaspase-8 activation by short DED proteins c-FLIP and procaspase-8 prodomain", *Cell Death and Differentiation*, Vol. 23 No. 4, pp. 681–694.

Schneider, P., Bodmer, J.L., Thome, M., Hofmann, K., Holler, N. and Tschopp, J. (1997), "Characterization of two receptors for TRAIL", *FEBS Letters*, Federation of European Biochemical Societies, Vol. 416 No. 3, pp. 329–334.

Schönenberger, M.J. (2015), "Hypoxia signaling pathways: modulators of oxygen-related organelles", *Frontiers in Cell and Developmental Biology*, Vol. 3 No. July, available at:https://doi.org/10.3389/fcell.2015.00042.

Schönthal, A.H. (2012), “Endoplasmic Reticulum Stress: Its Role in Disease and Novel Prospects for Therapy”, *Scientifica*, Vol. 2012, pp. 1–26.

Schuh, J.C.L. (2004), “Trials, Tribulations, and Trends in Tumor Modeling in Mice”, *Toxicologic Pathology*, Vol. 32 No. SUPPL. 1, pp. 53–66.

van Scott, E.J., Ekel, T.M. and Auerbach, R. (1963), “Determinants of Rate and Kinetics of Cell Division in Scalp Hair”, *Journal of Investigative Dermatology*, Elsevier Masson SAS, Vol. 41 No. 5, pp. 269–273.

Screaton, G.R., Mongkolsapaya, J., Xu, X.N., Cowper, A.E., McMichael, A.J. and Bell, J.I. (1997), “TRICK2, a new alternatively spliced receptor that transduces the cytotoxic signal from TRAIL”, *Current Biology*, Vol. 7 No. 9, pp. 693–696.

Semenza, G.L. (2017), “Hypoxia-inducible factors: coupling glucose metabolism and redox regulation with induction of the breast cancer stem cell phenotype”, *The EMBO Journal*, Vol. 36 No. 3, pp. 252–259.

Senichkin, V. V., Kopeina, G.S., Prokhorova, E.A., Zamaraev, A. V., Lavrik, I.N. and Zhivotovsky, B. (2018), “Modulation of Mcl-1 transcription by serum deprivation sensitizes cancer cells to cisplatin”, *Biochimica et Biophysica Acta - General Subjects*, Elsevier B.V, Vol. 1862 No. 3, pp. 557–566.

Sepulveda, M.A., Emelyanov, A. V and Birshtein, B.K. (2004), “NK-κB and Oct-2 synergize to activate the Human 3' Igh hs4 Enhancer in B Cells”, *J Immunol References*, Vol. 172, pp. 1054–1064.

Seshacharyulu, P., Ponnusamy, M., Haridas, D., Jain, M., Ganti, A. and Batra, S. (2013), “Targeting the EGFR signaling pathway in cancer therapy”, *Expert Opinion on Therapeutic Targets*, Vol. 16 No. 1, pp. 15–31.

Sha, W., Olesch, C., Hanaka, H., Weigert, A. and Brüne, B. (2013), “Necrosis in DU145 prostate cancer spheroids induces COX-2/mPGES-1-derived PGE2 to promote tumor growth and to inhibit T cell activation”, *International Journal of Cancer*, Vol. 133 No. 7, pp. 1578–1588.

Sharma, P., Varma, R., Sarasij, R.C., Gousset, K., Krishnamoorthy, G., Rao, M., Mayor, S., et al. (2004), “Nanoscale organization of multiple GPI-anchored proteins in living cell membranes.”, *Cell*, Vol. 116 No. 4, pp. 577–89.

Sheng, H., Shao, J., Morrow, J.D., Beauchamp, R.D. and DuBois, R.N. (1998), “Modulation of Apoptosis and Bcl-2 Expression by Prostaglandin E2 in Human Colon Cancer Cells”, *Cancer Research*, Vol. 58 No. 2, pp. 362–366.

Sheng, H., Shao, J., Washington, M.K. and DuBois, R.N. (2001), “Prostaglandin E2 Increases Growth and Motility of Colorectal Carcinoma Cells”, *Journal of Biological Chemistry*, Vol. 276 No. 21, pp. 18075–18081.

Sherar, M.D., Noss, M.B. and Foster, F.S. (1987), “Ultrasound backscatter microscopy images the internal structure of living tumour spheroids.”, *Nature*, Vol. 330 No. 6147, pp. 493–495.

Sheridan, J.P., Marsters, S.A., Pitti, R.M., Gurney, A., Skubatch, M., Baldwin, D., Ramakrishnan, L., et al. (1997), “Control of TRAIL-induced apoptosis by a family of signaling and decoy receptors”, *Science*, Vol. 277 No. 5327, pp. 818–821.

Shoeb, M., Ramana, K. V. and Srivastavan, S.K. (2013), “Aldose reductase inhibition enhances TRAIL-induced human colon cancer cell apoptosis through AKT/FOXO3a-dependent upregulation of death receptors”, *Free Radical Biology and Medicine*, Elsevier, Vol. 63, pp. 280–290.

Shrieve, D.C. and Begg, A.C. (1985), “Cell cycle kinetics of aerated , hypoxic and re-aerated cells in vitro using flow cytometric determination of cellular DNA and incorporated bromodeoxyuridine”, Cell Tissue Kinet., Vol. 18, pp.641-651.

Siegemund, M., Pollak, N., Seifert, O., Wahl, K., Hanak, K., Vogel, A., Nussler, A.K., et al. (2012), “Superior antitumoral activity of dimerized targeted single-chain TRAIL fusion proteins under retention of tumor selectivity”, *Cell Death and Disease*, Vol. 3 No. 4, available at:https://doi.org/10.1038/cddis.2012.29.

Siegemund, M., Seifert, O., Zarani, M., Džinić, T., De Leo, V., Göttsch, D., Münkel, S., et al. (2016), “An optimized antibody-single-chain TRAIL fusion protein for cancer therapy”, *mAbs*, Vol. 8 No. 5, pp. 879–891.

Sies, H. and Bruene, B. (2007), *Methods in Enymology-Oxygen Biology and Hypoxia*, 1st ed., Elsevier.

Smartt, H.J.M., Elder, D.J.E., Hicks, D.J., Williams, N.A. and Paraskeva, C. (2003), “Increased NF-κB DNA binding but not transcriptional activity during apoptosis induced by the COX-2-selective inhibitor NS-398 in colorectal carcinoma cells”, *British Journal of Cancer*, Vol. 89 No. 7, pp. 1358–1365.

Smith, M.L., Hawcroft, G. and Hull, M. a. (2000), “The effect of non-steroidal anti-inflammatory drugs on human colorectal cancer cells: evidence of different mechanisms of action.”, *European Journal of Cancer (Oxford, England : 1990)*, Vol. 36 No. 5, pp. 664–74.

Sobolewski, C., Cerella, C., Dicato, M., Ghibelli, L. and Diederich, M. (2010), “The Role of Cyclooxygenase-2 in Cell Proliferation and Cell Death in Human Malignancies”, *International Journal of Cell Biology*, Vol. 2010, pp. 1–21.

Sobolewski, C., Rhim, J., Legrand, N., Muller, F., Cerella, C., Mack, F., Chateauvieux, S., et al. (2015), “2,5-Dimethyl-Celecoxib Inhibits Cell Cycle Progression and Induces Apoptosis in Human Leukemia Cells”, *Journal of Pharmacology and Experimental Therapeutics*, Vol. 355 No. 2, pp. 322–342.

Song, J.J., Szczepanski, M.J., Kim, S.Y., Kim, J.H., An, J.Y., Kwon, Y.T., Alcala, M.A., et al. (2010), “c-Cbl-mediated degradation of TRAIL receptors is responsible for the development of the early phase of TRAIL resistance”, *Cellular Signalling*, Elsevier Inc., Vol. 22 No. 3, pp. 553–563.

Soslow, R.A., Dannenberg, A.J., Rush, D., Woerner, B.M., Nasir Khan, K., Masferrer, J. and Koki, A.T. (2000), “COX-2 is expressed in human pulmonary, colonic, and mammary tumors”, *Cancer*, Vol. 89 No. 12, pp. 2637–2645.

Spencer, J.A., Ferraro, F., Roussakis, E., Klein, A., Wu, J., Runnels, J.M., Zaher, W., et al. (2014), “Direct measurement of local oxygen concentration in the bone marrow of live animals”, *Nature*, Vol. 508 No. 7495, pp. 269–273.

Spierings, D.C.J., de Vries, E.G.E., Timens, W., Groen, H.J.M., Boezen, H.M. and de Jong, S. (2003), “Expression of TRAIL and TRAIL death receptors in stage III non-small cell lung cancer tumors.”, *Clinical Cancer Research : An Official Journal of the American Association for Cancer Research*, Vol. 9 No. 9, pp. 3397–405.

Stöhr, D. (2013), "Investigation of regulatory proteins linking TRAIL-mediated apoptosis to cell cycle phases", diploma thesis, Institute of Cell Biology and Immunology, University of Stuttgart.

Sträter, J., Hinz, U., Walczak, H., Mechtersheimer, G., Koretz, K., Herfarth, C., Möller, P., et al. (2002), “Expression of TRAIL and TRAIL receptors in colon carcinoma: TRAIL-R1 is an independent prognostic parameter”, *Clinical Cancer Research*, Vol. 8 No. 12, pp. 3734–3740.

Sutherland, R.M. and Mccredie, J.A. (1971), “Growth of Multicell Spheroids in Tissue Culture as a Model of Nodular Carcinomas”, *JNCI: Journal of the National Cancer Institute*, No. May, pp. 113–120.

Sutherland, R.M., Sordat, B., Bamat, J., Gabbert, H. and Bourrat, B. (1986), “Oxygenation and Differentiation in Multicellular Spheroids of Human Colon Carcinoma”, *Regulation*, No. October, pp. 5320–5329.

Takimoto, R. and El-Deiry, W.S. (2000), “Wild-type p53 transactivates the KILLER/DR5 gene through an intronic sequence-specific DNA-binding site”, *Oncogene*, Vol. 19 No. 14, pp. 1735–1743.

Takuma, K., Yan, S.S., Stern, D.M. and Yamada, K. (2005), “Mitochondrial dysfunction, endoplasmic reticulum stress, and apoptosis in Alzheimer’s disease”, *Journal of Pharmacological Sciences*, Vol. 97 No. 3, pp. 312–316.

Tamulevicius, P. and Streffer, C. (1995), “Metabolic imaging in tumours by means of bioluminescence”, *British Journal of Cancer*, Vol. 72 No. 5, pp. 1102–1112.

Tang, X.M., Sun, Y.J., Half, E., Kuo, M.T. and Sinicrope, F. (2002), “Cyclooxygenase-2 overexpression inhibits death receptor 5 expression and confers resistance to tumor necrosis factor-related apoptosis-inducing ligand-induced apoptosis in human colon cancer cells”, *Cancer Research*, Vol. 62 No. 17, pp. 4903–4908.

Tessner, T.G., Muhale, F., Riehl, T.E., Anant, S. and Stenson, W.F. (2004), “Prostaglandin E2 reduces radiation-induced epithelial apoptosis through a mechanism involving AKT activation and bax translocation”, *Journal of Clinical Investigation*, Vol. 114 No. 11, pp. 1676–1685.

Teutsch, H., Göllner, A. and Mueller-Klieser, W.F. (1995), “Glucose levels and succinate and lactate dehydrogenase activity in EMT6/Ro tumor spheroids.”, *European Journal of Cell Biology*.

Thoma, C.R., Zimmermann, M., Agarkova, I., Kelm, J.M. and Krek, W. (2014), "3D cell culture systems modeling tumor growth determinants in cancer target discovery", *Advanced Drug Delivery Reviews*, Elsevier B.V., Vol. 69–70, pp. 29–41.

Thomas, C.H., Collier, J.H., Sfeir, C.S. and Healy, K.E. (2002), "Engineering gene expression and protein synthesis by modulation of nuclear shape.", *Proceedings of the National Academy of Sciences of the United States of America*, Vol. 99 No. 4, pp. 1972–1977.

Thomson, B.J. (2001), "Viruses and apoptosis", *International Journal of Experimental Pathology*, Vol. 82 No. 2, pp. 65–76.

Todorova, T., Bock, F.J. and Chang, P. (2015), "PARP13 regulates cellular mRNA post-transcriptionally and functions as a pro-apoptotic factor by destabilizing TRAILR4 transcript", *Nature Communications*, Nature Publishing Group, Vol. 5, pp. 1–14.

Tolcher, A.W., Mita, M., Meropol, N.J., Von Mehren, M., Patnaik, A., Padavic, K., Hill, M., et al. (2007), "Phase I pharmacokinetic and biologic correlative study of mapatumumab, a fully human monoclonal antibody with agonist activity to tumor necrosis factor-related apoptosis-inducing ligand receptor-1", *Journal of Clinical Oncology*, Vol. 25 No. 11, pp. 1390–1395.

Tomasio, S.M., Harding, H.P., Ron, D., Cross, B.C.S. and Bond, P.J. (2013), "Selective inhibition of the unfolded protein response: Targeting catalytic sites for Schiff base modification", *Molecular BioSystems*, Vol. 9 No. 10, pp. 2408–2416.

de Toni, E.N., Thieme, S.E., Herbst, A., Behrens, A., Stieber, P., Jung, A., Blum, H., et al. (2008), "OPG is regulated by β-catenin and mediates resistance to TRAIL-induced apoptosis in colon cancer", *Clinical Cancer Research*, Vol. 14 No. 15, pp. 4713–4718.

Toscano, F., Fajoui, Z. El, Gay, F., Lalaoui, N., Parmentier, B., Chayvialle, J.A., Scoazec, J.Y., et al. (2008), "p53-Mediated upregulation of DcR1 impairs oxaliplatin/TRAIL-induced synergistic anti-tumour potential in colon cancer cells", *Oncogene*, Vol. 27 No. 30, pp. 4161–4171.

Trivedi, R. and Mishra, D.P. (2015), "Trailing TRAIL Resistance: Novel Targets for TRAIL Sensitization in Cancer Cells", *Frontiers in Oncology*, Vol. 5 No. April, available at:https://doi.org/10.3389/fonc.2015.00069.

Urano, F., Wang, X.-Z., Bertolotti, A., Zhang, Y., Chung, P., Harding, H.P. and Ron, D. (2000), "Coupling of Stress in the Endoplasmic Reticulum to Activation of JNK Protein Kinases by Transmembrane Protein Kinase IRE1", *Science (New York, N.Y.)*, Vol. 287 No. January, pp. 664–666.

Vaish, V., Rana, C., Piplani, H., Vaiphei, K. and Sanyal, S.N. (2014), "Sulindac and Celecoxib Regulate Cell Cycle Progression by p53/p21 Up Regulation to Induce Apoptosis During Initial Stages of Experimental Colorectal Cancer", *Cell Biochemistry and Biophysics*, Vol. 68 No. 2, pp. 301–319.

Valcourt, J.R., Lemons, J.M.S., Haley, E.M., Kojima, M., Demuren, O.O. and Coller, H.A. (2012), "Staying alive", *Cell Cycle*, Vol. 11 No. 9, pp. 1680–1696.

Vanamee, É.S. and Faustman, D.L. (2018), "Structural principles of tumor necrosis factor superfamily signaling", *Science Signaling*, Vol. 11 No. 511, pp. 1–12.

Varma, R. and Mayor, S. (1998), "GPI-anchored proteins are organized in submicron domains at the cell surface", *Nature*, Vol. 394 No. 6695, pp. 798–801.

Vergani, L., Grattarola, M. and Nicolini, C. (2004), "Modifications of chromatin structure and gene expression following induced alterations of cellular shape", *International Journal of Biochemistry and Cell Biology*, Vol. 36 No. 8, pp. 1447–1461.

Verjans, E.-T., Doijen, J., Luyten, W., Landuyt, B. and Schoofs, L. (2017), "Three-dimensional cell culture models for anticancer drug screening: Worth the effort?", *Journal of Cellular Physiology*, No. June 2017, pp. 2993–3003.

Vermeulen, K., Van Bockstaele, D.R. and Berneman, Z.N. (2003), "The cell cycle:a review of regulation,deregulation and therapeutic targets in cancer", *Cell Proliferation*, Vol. 36 No. 3, pp. 131–149.

Vietri, M., Bianchi, M., Ludlow, J.W., Mittnacht, S. and Villa-Moruzzi, E. (2006), "Direct interaction between the catalytic subunit of Protein Phosphatase 1 and pRb.", *Cancer Cell International*, Vol. 6, p. 3.

Vogt, C. (1842), “Untersuchungen über die Entwicklungsgeschichte der Geburtshelferkröte. (Alytes obstetricians”, *Solothurn: Jent und Gassmann*, pp.130.

Walczak, H., Degli-esposti, M.A., Johnson, R.S., Smolak, P.J., Waugh, J.Y., Boiani, N., Timour, M.S., et al. (1997), “TRAIL-R2 : a novel apoptosis-mediating receptor for TRAIL”, Vol. 16 No. 17, pp. 5386–5397.

Walenta, S., Doetsch, J., Mueller-Klieser, W. and Kunz-Schughart, L.A. (2000), “Metabolic imaging in multicellular spheroids of oncogene-transfected fibroblasts”, *Journal of Histochemistry and Cytochemistry*, Vol. 48 No. 4, pp. 509–522.

Wallace, D.I. and Guo, X. (2013), “Properties of Tumor Spheroid Growth Exhibited by Simple Mathematical Models”, *Frontiers in Oncology*, Vol. 3 No. March, pp. 1–9.

Wang, L., Shang, Z., Zhou, Y., Hu, X., Chen, Y., Fan, Y., Wei, X., et al. (2018), “Autophagy mediates glucose starvation-induced glioblastoma cell quiescence and chemoresistance through coordinating cell metabolism, cell cycle, and survival”, *Cell Death and Disease*, Springer US, Vol. 9 No. 2, available at:https://doi.org/10.1038/s41419-017-0242-x.

Wang, X.J., Feng, C.W. and Li, M. (2013), “ADAM17 mediates hypoxia-induced drug resistance in hepatocellular carcinoma cells through activation of EGFR/PI3K/Akt pathway”, *Molecular and Cellular Biochemistry*, Vol. 380 No. 1–2, pp. 57–66.

Weber, T.S., Jaehnert, I., Schichor, C., Or-Guil, M. and Carneiro, J. (2014), “Quantifying the Length and Variance of the Eukaryotic Cell Cycle Phases by a Stochastic Model and Dual Nucleoside Pulse Labelling”, *PLoS Computational Biology*, Vol. 10 No. 7, available at:https://doi.org/10.1371/journal.pcbi.1003616.

Weinmann, M., Marini, P., Jendrossek, V., Betsch, A., Goecke, B., Budach, W. and Belka, C. (2004), “Influence of hypoxia on TRAIL-induced apoptosis in tumor cells”, *International Journal of Radiation Oncology Biology Physics*, Vol. 58 No. 2, pp. 386–396.

White, E. (2015), “the role for autophagy in cancer (White, 2015).pdf”, *Journal of Clinical Investigation*, Vol. 125 No. 1, pp. 42–46.

Wiley, S.R., Schooley, K., Smolak, P.J., Din, W.S., Huang, C.P., Nicholl, J.K., Sutherland, G.R., et al. (1995), “Identification and characterization of a new member of the TNF family that induces apoptosis.”, *Immunity*, Vol. 3 No. 6, pp. 673–82.

Willems, G. (1972), “Cell renewal in the gastric mucosa.”, *Digestion*, Vol. 6 No. 1, pp. 46–63.

Williams, C.S., Mann, M. and DuBois, R.N. (1999), “The role of cyclooxygenases in inflammation, cancer, and development”, *Oncogene*, Vol. 18 No. 55, pp. 7908–7916.

Wu, C.C., Lee, S., Malladi, S., Chen, M. Der, Mastrandrea, N.J., Zhang, Z. and Bratton, S.B. (2016), “The Apaf-1 apoptosome induces formation of caspase-9 homo- and heterodimers with distinct activities”, *Nature Communications*, Nature Publishing Group, Vol. 7 No. May, pp. 1–14.

Wu, G.S., Burns, T.F., McDonald, E.R., Jiang, W., Meng, R., Krantz, I.D., Kao, G., et al. (1997), “KILLER/DR5 is a DNA damage-inducible p53-regulated death receptor gene”, *Nature Genetics*, Vol. 17 No. 2, pp. 141–143.

Wu, M.Z., Tsai, Y.P., Yang, M.H., Huang, C.H., Chang, S.Y., Chang, C.C., Teng, S.C., et al. (2011), “Interplay between HDAC3 and WDR5 Is Essential for Hypoxia-Induced Epithelial-Mesenchymal Transition”, *Molecular Cell*, Elsevier Inc., Vol. 43 No. 5, pp. 811–822.

Wu, P.-H., Chen, X.-M., Liu, X.-Q., He, J.-L., Feng, Q., Lan, X., Zhang, X., et al. (2016), “Activation of tumour necrosis factor-related apoptosis-inducing ligand (TRAIL) receptor gene expression following DNA demethylation in placental choriocarcinoma and transformed cell lines”, *Reproduction, Fertility and Development*, Vol. 28 No. 11, p. 1844.

Würstle, M.L., Laussmann, M.A. and Rehm, M. (2010), “The caspase-8 dimerization/dissociation balance is a highly potent regulator of caspase-8, -3, -6 signaling”, *Journal of Biological Chemistry*, Vol. 285 No. 43, pp. 33209–33218.

Yagami, T., Koma, H. and Yamamoto, Y. (2016), “Pathophysiological Roles of Cyclooxygenases and Prostaglandins in the Central Nervous System”, *Molecular Neurobiology*, Vol. 53 No. 7, pp. 4754–4771.

Yamaguchi, H. and Wang, H.G. (2004), “CHOP is involved in endoplasmic reticulum stress-induced apoptosis by enhancing DR5 expression in human carcinoma cells”, *Journal of Biological Chemistry*, Vol. 279 No. 44, pp. 45495–45502.

Yamanaka, Y., Shiraki, K., Inoue, T., Miyashita, K., Fuke, H., Yamaguchi, Y., Yamamoto, N., et al. (2006), “COX-2 inhibitors sensitize human hepatocellular carcinoma cells to TRAIL-induced apoptosis”, pp. 41–47.

Yan, J., Wang, L., Wang, Z., Wang, B., Zhu, R., Bi, J., Wu, J., et al. (2016), “Engineered adenovirus fiber shaft fusion homotrimer of soluble TRAIL with enhanced stability and antitumor activity”, *Cell Death & Disease*, Vol. 7 No. 6, p. e2274.

Yang, K. and Chi, H. (2015), “AMPK Helps T Cells Survive Nutrient Starvation”, *Immunity*, Elsevier Inc., Vol. 42 No. 1, pp. 4–6.

Yang, M.H., Wu, M.Z., Chiou, S.H., Chen, P.M., Chang, S.Y., Liu, C.J., Teng, S.C., et al. (2008), “Direct regulation of TWIST by HIF-1α promotes metastasis”, *Nature Cell Biology*, Vol. 10 No. 3, pp. 295–305.

Yao, G. (2014), “Modelling mammalian cellular quiescence”, *Interface Focus*, Vol. 4 No. 3, pp. 20130074–20130074.

Yao, M., Lam, E.C., Kelly, C.R., Zhou, W. and Wolfe, M.M. (2004), “Cyclooxygenase-2 selective inhibition with NS-398 suppresses proliferation and invasiveness and delays liver metastasis in colorectal cancer”, *British Journal of Cancer*, Vol. 90 No. 3, pp. 712–719.

Yoshida, H., Okada, T., Haze, K., Yanagi, H., Yura, T., Negishi, M. and Mori, K. (2000), “ATF6 Activated by Proteolysis Binds in the Presence of NF-Y (CBF) Directly to the cis-Acting Element Responsible for the Mammalian Unfolded Protein Response”, *Molecular and Cellular Biology*, Vol. 20 No. 18, pp. 6755–6767.

Yoshida, T., Shiraishi, T., Horinaka, M., Wakada, M. and Sakai, T. (2007), “Glycosylation modulates TRAIL-R1/death receptor 4 protein: Different regulations of two pro-apoptotic receptors for TRAIL by tunicamycin”, *Oncology Reports*, Vol. 18 No. 5, pp. 1239–1242.

Young-Mee, K., Hongryull, P. (2013), "Different Cell Cycle Modulation by Celecoxib at Different Concentrations", *Cancer Biotherapy and Radiopharmaceuticals*, Vol. 28.

Yu, L., Wu, W.K.K., Li, Z.J., Li, H.T., Wu, Y.C. and Cho, C.H. (2009), “Prostaglandin E_2 promotes cell proliferation *via* protein kinase C/extracellular signal regulated kinase pathway-dependent induction of c-Myc expression in human esophageal squamous cell carcinoma cells”, *International Journal of Cancer*, Vol. 125 No. 11, pp. 2540–2546.

Yuan, J. and Yanker, B.A. (2000), “Apoptosis in the Nervous System”, *Nature*, Vol. 407.

Zhang, S., Suvannasankha, A., Crean, C.D., White, V.L., Johnson, A., Chen, C.S. and Farag, S.S. (2007), “OSU-03012, a novel celecoxib derivative, is cytotoxic to myeloma cells and acts through multiple mechanisms”, *Clinical Cancer Research*, Vol. 13 No. 16, pp. 4750–4758.

Zhang, X., Fryknäs, M., Hernlund, E., Fayad, W., De Milito, A., Olofsson, M.H., Gogvadze, V., et al. (2014), “Induction of mitochondrial dysfunction as a strategy for targeting tumour cells in metabolically compromised microenvironments”, *Nature Communications*, Vol. 5, available at:https://doi.org/10.1038/ncomms4295.

Zhang, X.D., Franco, A. V., Nguyen, T., Gray, C.P. and Hersey, P. (2000), “Differential Localization and Regulation of Death and Decoy Receptors for TNF-Related Apoptosis-Inducing Ligand (TRAIL) in Human Melanoma Cells”, *The Journal of Immunology*, Vol. 164 No. 8, pp. 3961–3970.

Zhang, X.D., Nguyen, T., Thomas, W.D., Sanders, J.E. and Hersey, P. (2000), “Mechanisms of resistance of normal cells to TRAIL induced apoptosis vary between different cell types”, *FEBS Letters*, Vol. 482 No. 3, pp. 193–199.

Zhou, Y.-Y., Li, Y., Jiang, W.-Q. and Zhou, L.-F. (2015), “MAPK/JNK signaling: A potential autophagy regulation pathway”, *Bioscience Reports*, pp. 1–10.

Zou, W. (2004), “c-Jun NH2-terminal kinase-mediated up-regulation of death receptor 5 contributes to induction of apoptosis by the novel synthetic triterpenoid methyl-2-cyano-3, 12-dioxooleana-1, 9-dien-28-oate in human lung cancer cells”, *Cancer Res.*, Vol. 64, pp. 7570–7578.

Zumbrägel, F.K., Machtens, D.A., Curth, U., Lüder, C.G.K., Reubold, T.F. and Eschenburg, S. (2017), “Survivin does not influence the anti-apoptotic action of XIAP on caspase-9”, *Biochemical and Biophysical Research Communications*, Vol. 482 No. 4, pp. 530–535.

7 Appendix

7.1 TRAILR1/2 and EGFRR expression within 2D- and 3D-cultivated HT29 cells

Experiments with 2D- and 3D- (day 11) cultivated HT29 cells revealed that surface expression of TRAILR1/TRAILR2 and EGFR was significantly downregulated in spheroid-forming cells in comparison to 2D cell cultures. Furthermore, a heterogeneous surface receptor expression was found in HT29 MCTSs, including cells with receptor amounts similar to 2D-cultivated cells but also cells with extremely low or undetectable receptor expression (Figure 61).

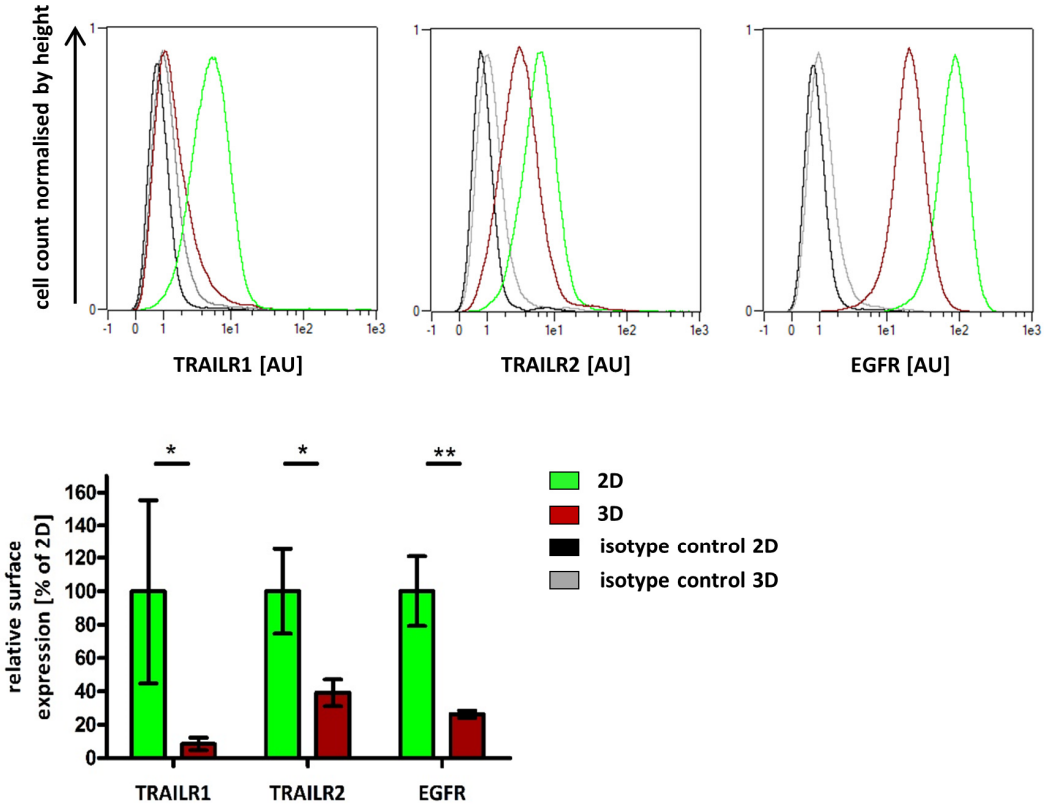

Figure 61: Differences in TRAILR1/R2 and EGFR expression between 2D- and 3D-cultivated HT29 cells

2D-cultivated HT29 cells and HT29 MCTSs (day 11) were analysed for their surface expression of the indicated proteins by flow cytometry. Shown histograms are representative of three independent experiments. Population medians were used to calculate the differences in relative surface expression between 2D- and 3D-cultivated cells. Displayed data are mean values ± SD of at least three independent experiments. Asterisks indicate statistical significance (* = $p \leq 0.05$; ** = $p \leq 0.01$; unpaired t-test).

7.2 After knockout of TRAILR2, 2D- and 3D-cultured HCT116 cells can no longer be sensitised to TRAIL treatment by celecoxib

It was investigated whether knockout of TRAILR2 would abolish the sensitisation effect of celecoxib on treatment with TRAIL in 2D- and 3D-cultivated HCT116 cells. Therefore, 2D-cultivated HCT116 T2 KO cells and HCT116 T2 KO MCTSs were stimulated first with celecoxib for 48h followed by incubation together with TRAIL for additional 24 h. Thereafter, the percentage of viable cells was determined by Annexin V-EGFP staining and flow cytometry. Performed experiments revealed that neither 2D-cultivated HCT116 T2 KO nor HCT116 T2 KO MCTSs could be sensitised to TRAIL-induced cell death by the COX II inhibitor, suggesting that celecoxib sensitises cells by upregulating TRAILR2 (Figure 62).

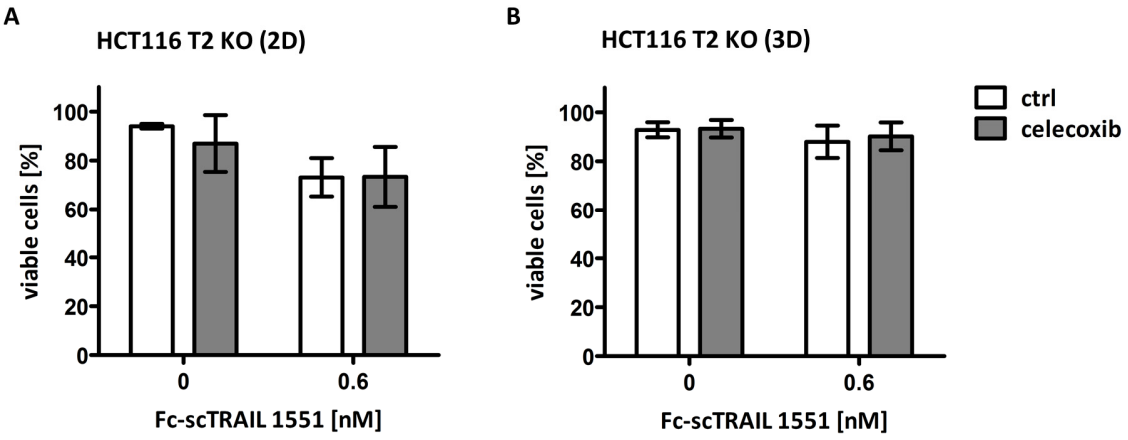

Figure 62: After knockout of TRAILR2, treatment with celecoxib no longer sensitises HCT116 cells to TRAIL

2D-cultured HCT116 T2 KO cells along with HCT116 T2 KO MCTSs were stimulated for 48 h with 50 µM celecoxib and for additional 24 h together with or without 0.6 nM Fc-scTRAIL 1551. The percentage of viable cells was determined afterwards by Annexin V-EGFP staining and flow cytometry. Data shown are mean values ± SD of three independent experiments each performed in duplicates. Experiments were done together with Alexandra Mack.

List of figures

List of tables

Danksagung

Allen voran möchte ich mich bei Peter Scheurich dafür bedanken, dass er es mir ermöglichte im Rahmen von SimTech am IZI zu promovieren. Peter, deine Tür stand immer offen und auch als du nach Innsbruck gezogen bist, konnte ich weiter auf dich zählen. Vielen Dank dafür und auch für die zahllosen anregenden Gespräche, die Ideen und die bedingungslose Unterstützung. Des Weiteren geht mein Dank an Markus Morrison, der mich sofort in seine Arbeitsgruppe integrierte und mir mit Rat und Tat, wie ein zweiter Doktorvater, die letzten 2,5 Jahre zur Seite stand. Vielen Dank Markus, für all deine Zeit, die vielen Gespräche, die mir oft eine neue Sichtweise auf die Dinge ermöglichten und vor allem für dein unerschütterliches Vertrauen in meine Fähigkeiten. Vielen Dank, dass du mir die Chance gegeben hast auch noch weiterhin an deiner Seite zu arbeiten. Zusätzlich möchte ich mich dafür bedanken, dass du mir den Kontakt zu Stephen Tait am Beatson Institut vermittelt hast. Dadurch war es mir möglich beruflich sowie privat eine tolle Zeit in Glasgow zu verbringen. An dieser Stelle geht mein Dank auch an Stephen und an meinen dortigen Betreuer Kai Cao, mit dem ich nicht nur zahllose Stunden im Labor verbracht habe, sondern der mir auch treu bei der Erforschung Schottlands zur Seite stand. Als nächstes möchte ich mich bei Nicole Radde bedanken, die als mein „second supervisor“ schon meine Milestone Prüfung abnahm und die sich nun auch bereit erklärt hat meine Doktorprüfung mitzugestalten. Des Weiteren geht mein Dank an Georg Sprenger, der den Prüfungsvorsitz übernehmen wird. Danken möchte ich auch meinen Kooperationspartnern vom IKP, Jens Schmid und Thomas Mürdter, für ihre Unterstützung beim Anfertigen der Spheroidschnitte. Außerdem danke ich auch den Kollegen von SimTech, Karsten Kuritz, Frank Allgöwer, Patrick Schröder, Wolfgang Ehlers, Timo Koch und Rainer Helmig, für die fruchtbare Zusammenarbeit. Des Weiteren möchte ich mich bei Nadine Pollak bedanken, die all die Jahre meinen Weg begleitete und die es nie müde wurde meine Fragen zu beantworten und mein Selbstvertrauen zu stärken. Besonders bedanken möchte ich mich auch bei Beate Budai, der TA meines Herzens. Vielen Dank Bea, für die wunderbare Zeit am IZI, für die tolle Organisation des Labors, deine saubere Arbeit und vor allem für deine Freundschaft. Auch vielen Dank an Nathalie Peters und Elke Gerlach, die kamen als Bea ging. Als gute Seelen des Labors werdet ihr es nie müde all unsere Fragen zu beantworten und das Labor am Laufen zu halten. Ein weiterer besonderer Dank geht an dieser Stelle an Tobias Beigl, der immer 100 % gab, sei es bei seiner Bachelorarbeit oder später als Hiwi. Vielen Dank Tobi, für deine unvergleichliche Motivation und deine herausragende Arbeit. Gleichermaßen möchte ich mich auch bei den Studenten Daniela Maichl und Alexandra Mack für ihre Mitarbeit an meinem Promotionsthema bedanken. Dani, danke für deine kritischen Fragen, die oft neue

Wege eröffnet haben. Vielen Dank auch an Roland Kontermann, Martin Siegemund und Doris Göttsch für die Bereitstellung des TRAIL Konstrukts sowie an Fabian Richter für die Produktion von Annexin V-EGFP. Außerdem Danke Fabi, für die Geduld beim Beantworten all meiner Fragen und für deine sonstige Unterstützung. Als nächstes möchte ich mich bei all den Kollegen und Freunden bedanken, die den langen Weg mit mir gingen und die Zeit am IZI unvergesslich gemacht haben. Danke ihr lieben „letzten Scheurikaner“ Aline, Claudi, Dani und Raphaela, für die schöne Zeit und die daraus entstandenen Freundschaften. Danke Cathrin, Chiara, Christian, Cristiano, Biswa, Elke, Fabi, Gabi, Gavin, Josip, Lubna, Nadine, Nats, Nivetha, Simon und Vesna für all die fachliche Unterstützung und den vielen Spaß! Danke vor allem auch dir Gabi, für all die kleinen und großen Dinge, die du für mich getan hast. Ein besonderer Dank soll hier nun auch an Gavin Fullstone gehen. Ohne dich hätte es diese Arbeit niemals gegeben. Danke für das geduldige Verbessern meines Englischs, für all die fachliche Beratung und vor allem für deine Freundschaft. Dank geht natürlich auch an die Deutsche Forschungsgemeinschaft für die Förderung des Exzellenz Clusters SimTech und damit auch meines Projekts.

Als nächtes möchte ich mich bei meinen Freunden bedanken, die zwar nicht alle etwas mit Biologie am Hut haben, die aber immer für mich da sind und deren Unterstützung in all der Zeit grenzenlos war. Danke Chrissi, Melli, Lis, Niels, Markus, Andy, Julia, Lars, Aaron, Steffi und Jan.

Vielen Dank lieber Dani, dass du da bist und mir hilfst nie aus den Augen zu verlieren, was wirklich im Leben zählt.

Zum Schluss danke ich meinen Eltern, dafür dass sie meine Liebe zur Natur weckten und für all ihre Unterstützung und Motivation, ohne die ich nicht zu dem Menschen geworden wäre, der ich heute bin.

Erklärung

Hiermit erkläre ich, dass die vorliegende Arbeit von mir persönlich ohne unrechtmäßige Hilfe angefertigt wurde. Verwendete Daten, Grafiken und Informationen, die nicht von mir stammen wurden entsprechend gekennzeichnet.

Declaration

I hereby declare, that this thesis was prepared by myself without illegal help. Where information has been derived from other sources, I confirm that this has been elucidated in the thesis.

Daniela Stöhr
Stuttgart, 28. Juni 2018

Publications, proceedings, conference contributions, secondment

Publications

Danish, L., **Stöhr, D.**, Scheurich, P., Pollak, N., (2017), "TRAIL-R3/R4 and Inhibition of TRAIL Signalling in Cancer", *In Micheau, O. (eds) TRAIL, Fas Ligand, TNF and TLR3 in Cancer. Resistance to Targeted Anti-Cancer Therapeutics vol. 12. Springer, Cham*, 27-59.

Kuritz, K., **Stöhr, D.**, Pollak, N., Allgöwer F., (2017), „On the relationship between cell cycle analysis with ergodic principles and age-structured cell population models", *Journal of Theoretical Biology, 414*, 91-102.

In preparation:
Stöhr, D., Maichl, D. S., Beigl, T. B., Budai, B. E., Schmid, J. O., Mürdter, T. E., Kontermann, R. E., Scheurich, P., Pollak, N., Rehm, M., "Spatiotemporally developing layers of TRAIL-resistant cells shield TRAIL-hypersensitive cells within multicellular tumor spheroids"

Proceedings

Schröder, P., Wagner, A., **Stöhr, D.**, Rehm, M., Ehlers, W., (2017), "Variation of different growth descriptions in a metastatic proliferation model", In M. von Scheven, M.-A. Keip & N. Karajan (eds.): *Proceedings of the 7th GACM Colloquium on Computational Mechanics*. *Institute for Structural Mechanics, University of Stuttgart, Stuttgart*, 259-262. doi: 10.18419/opus-9334.

Schröder, P., Wagner, A., **Stöhr, D.**, Rehm, M., Ehlers, W., (2017), „Data-driven simulation of metastatic processes within brain tissue", *Proceedings in Applied Mathematics and Mechanics, 17*, 221–221. doi: 10.1002/pamm.201710080.

To be submitted:
Schröder, P., Wagner, A., **Stöhr, D.**, Rehm, M., Jensch, A., Radde, N., Ehlers, W., (2018), "Modelling lung-metastases apoptosis within brain tissue", *Proceedings in Applied Mathematics and Mechanics 18*.

Conference contributions

Poster

8th Swiss Apoptosis Meeting (SAM), 10th - 12th September 2014
Institute of Pathology, University of Bern, Bern, Swiss
Title of the poster: Cell cycle-dependent activation of cell death

2nd International Conference on Simulation Technology (SimTech), 26th - 28th March 2017
University of Stuttgart, Stuttgart, Germany
Title of the poster: Spatiotemporally developing layers of TRAIL-resistant cells shield TRAIL-hypersensitive cells within multicellular tumour spheroids (finalist of the best poster award)

11th European Workshop on Cell Death (EWCD), 6th - 11th May 2018
Ambasciatori Hotel, Fiuggi, Italy
Title of the poster: Spatiotemporally developing layers of TRAIL-resistant cells shield TRAIL-hypersensitive cells within multicellular tumour spheroids

Talk

12th meeting on Cell Death (CSHL), 15th - 19th August 2017
Cold Spring Harbor Laboratory, Cold Spring Harbor, USA
Title of the talk: Spatiotemporally developing layers of TRAIL-resistant cells shield TRAIL-hypersensitive cells within multicellular tumor spheroids

Secondment

June-August 2017
Beatson Institute for Cancer Research, Glasgow, Scotland
group: **Stephen Tait** - Mitochondria and Cell Death